# MILD Combustion of Solid Fuels

**Manabendra Saha**

**A thesis submitted for the fulfilment of the requirements for the degree of PhD in Mechanical Engineering**


THE UNIVERSITY of ADELAIDE

Centre for Energy Technology
School of Mechanical Engineering
Faculty of Engineering, Computer and Mathematical Sciences

**April 2016 (Approved in July 2016)**

# DECLARATION

I certify that this work contains no material which has been accepted for the award of any other degree or diploma in my name, in any university or other tertiary institution and, to the best of my knowledge and belief, contains no material previously published or written by another person, except where due reference has been made in the text. In addition, I certify that no part of this work will, in the future, be used in a submission in my name, for any other degree or diploma in any university or other tertiary institution without the prior approval of the University of Adelaide and where applicable, any partner institution responsible for the joint-award of this degree.

I hereby give consent to this copy of my thesis, when deposited in the University Library, being made available in all form of media, throughout the world, subject to the provisions of the Copyright Act 1968.

The author acknowledges that copyright of published works contained within this thesis resides with the copyright holder(s) of those works.

I also give permission for the digital version of my thesis to be made available on the web, via the University's digital research repository, the Library Search and also through web search engines, unless permission has been granted by the University to restrict access for a period of time.

Manabendra Saha

# ACKNOWLEDGMENT

This thesis is not only a representation of my work using the keyboard, but also a milestone in more than four years of research at the University of Adelaide and in particular in the Centre for Energy Technology. Since my first day at Adelaide on 13th February 2012, I have been given unique opportunities and privileges to learn cutting edge research from the world's prominent combustion scientists. But this thesis was possible through support and contribution of many remarkable individuals, without whom I would not have been able to complete this journey.

Firstly, I would like to gratefully acknowledge the support given to me by my supervisors **Professor Bassam Dally**, **Dr Paul Medwell** and **Professor Graham (Gus) Nathan** who provided me with the guidance and training to conduct my research and to document it in this thesis. My special thanks to my principal supervisor Prof. Dally for his generous advice, patience, support and guidance through up and down times of my PhD candidature. I thank Dr Medwell for his continuous help, motivation, and outstanding technical supports during the experimental campaign and writing my thesis. I thank Prof. Nathan for his enthusiasm, immense and comprehensive knowledge in the field of combustion which were essential for my understanding, development, and designing of the MILD combustion furnace. I felt privileged to have worked with such competent combustion scientists.

Special thanks to **Dr Alfonso Chinnici** from the Centre for Energy Technology (CET) for the many fruitful discussions on various topics and teaching me numerical simulations of MILD combustion.

Many thanks also go to **Mr Marc Simpson**, Manager, Thebarton Research Laboratory of the University of Adelaide. His technical support, many interesting conversations, advice and generous help throughout the experiments will always be remembered.

I would like to acknowledge the University of Adelaide for providing me with financial support through the Adelaide Scholarship International (ASI) scheme and the School of Mechanical Engineering for the short term Scholarship in order to allow me to complete my PhD. I am also grateful to the financial support received from the Brown Coal Innovation Australia (BCIA) through a Top-Up scholarship. My special thanks go to **Dr David McManus**, Research Investment Manager, BCIA. I would also like to thank the current and former staff and technicians of the School of Mechanical Engineering and Centre for Energy Technology (CET) of the University of Adelaide.

I am deeply and forever indebted to my late father and to my lovely mother for her endless support and encouragement during the darkest days and nights of my research student life. I am also extremely grateful to my beautiful younger sister whose love and support led me to this point.

I would also like to express my special gratitude and endless thank to my office mates and friends **Dr Mehdi Jafarian**, **Dr Rabiul Islam Sarker**, **Mr Ashok Kaniyal**, **Mr Karn Schumacher**, **Ms Jingjing Ye**, **Mr Dahe Gu, Mr Chia Thong, Mr Houzhi Wang, Mr Mahyar Silakhori, Mr Raihan Rumman and Dr Md. Ayub** for their company, suggestions and support during my PhD candidature.

Last but not least, I would like to express my sincere gratitude to all the staff of the School, particularly **Associate Professor Anthony Zander**, Head of the School, **postgraduate students**, and **Ms. Patricia Anderson**, who is a manager of the International Student Centre at The University of Adelaide for their kind help during the most challenging period of my life, in particular during my major heart surgery. I will never forget your endless help and enormous encouragement during this time.

# ABSTRACT

Moderate or Intense Low-oxygen Dilution (MILD) combustion has been identified as an innovative technology that offers ultra-low pollutant emissions, high thermal efficiency, enhanced combustion stability, thermal field uniformity, and broad fuel flexibility. MILD combustion of solid fuels has received much less attention than gaseous fuels and its burning characteristics are not well understood. As solid fuels, in particular pulverised coal, form the majority of available fuel sources, there is a need to extend understanding of the application of MILD combustion to pulverised coals. The current research seeks to investigate the MILD combustion characteristics of pulverised coals via experimental and computational approaches.

In the first stage of this work, an experimental campaign was conducted to investigate the MILD combustion characteristics of pulverised coal in a laboratory-scale self-recuperative furnace. High volatile Kingston brown coal and low volatile Bowen basin black coal with a particle size in the range of 38-180 $\mu m$ were injected into the furnace using either $CO_2$ or $N_2$ as a carrier gas. The results point to major differences between the resulting 'flames' of the two coals and minor differences associated with the carrier gas in respect to pollutant emissions. Ash content analysis showed that black coal was not burnt effectively, which is thought to be due to the particle residence times being insufficient for complete combustion in the furnace.

In the next stage of this research, a comprehensive numerical investigation, using Computational Fluid Dynamics (CFD) modelling, was conducted to understand the influence of three devolatilisation models on the prediction accuracy of pulverised coal MILD combustion. It was found that the advanced chemical percolation devolatilization (CPD) devolatilization model with a three-step global kinetic mechanism gives, as expected, the best agreement with the experimental measurements for the Kingston brown coal case. While all models produced similar results for the Bowen basin black coal case.

A new vertical co-flow furnace was also designed and built for this project. The furnace contained an insulated and water-cooled central jet surrounded by a hot and

diluted co-flow. The furnace walls, as well as co-flow temperature and local oxygen concentrations, are controlled by a secondary swirling burner using non-premixed natural gas combustion. Loy-Yang brown coal from the Latrobe Valley, Victoria, Australia, with particle sizes in the range of 53-125 $\mu m$ and 250-355 $\mu m$, is injected into the furnace using $CO_2$ as a carrier gas. The bulk jet Reynolds number was varied from $Re_{jet}$ = 5,527 to $Re_{jet}$ = 20,000. In-furnace temperatures and chemical species were measured together with visual observations and CH chemiluminescence ($CH^*$) imaging at the bottom, middle and top parts of the furnace. The $CH^*$ signal intensity is found to be significantly lower at the top part of the furnace which is an indication of the slow rate of heterogeneous combustion of char particles. The largest amount of CO concentrations are measured for the highest jet velocity (i.e., $R_{jet}$ = 20,000) case which implies that with increasing turbulence there is a better mixing and a broad devolatilisation zone is formed which produces more CO. The measured NO emission for any case was less than 125 ppmv (db at 3% $O_2$) which provide evidence to the potential benefits of MILD Combustion application to Victorian brown coal towards reducing NO emission.

Complementary CFD modelling study helped in shedding light on the flow field, turbulence intensity, volatiles' release rate, combustion of volatile matters, and overall carbon consumption inside the furnace for all cases. It was found that increasing the jet Reynolds number increases the volatiles release rates and decrease the rate of overall carbon consumption. It was also found that, for both particles' size cases, stable MILD combustion is established with a similar large recirculation vortex around the centre of the furnace. Devolatilisation starts earlier for the smaller particles' case and is completed at the end of the recirculation vortex while for the larger particles' case the devolatilisation happened post the recirculation vortex. The difference is related to the particle dispersion within the jet and differences in Stokes number.

This study provided valuable systematic data for the fundamental understanding of the MILD combustion of solid fuels. The outcomes of this research are a step forward to allow the industry to have better confidence in utilising the MILD combustion technology.

# TABLE OF CONTENTS

# CHAPTER 1

# INTRODUCTION

# Chapter 1 Introduction

## 1.1. Combustion and Energy

Energy is one of the cornerstones for the development of civilisation [1]. Global energy demand increased by 26% between 2000 and 2010 and it is projected to increase by 56% relative to 2010 figures by 2040, from 553 quadrillion kilojoules (kJ) to 865 quadrillion kJ, according to the World Energy Outlook 2015 [2]. According to predictions by the United Nations (UN), the population rise of the world will rise from 6.7 billion to 8.7 billion between 2011 and 2040. As a consequence, world energy demands are expected to increase substantially over that time [2]. In addition to population growth, rapid economic development and increasing living standards in the world's developing countries (led by China and India) will be key drivers for a substantial increase in energy demands in the near future.

The world's energy demand is predominantly supplied by the combustion of fossil fuels (e.g., natural gas, oil, and coal). Although natural gas production and supply remain constant, the prices fluctuate continuously [3]. The reason behind the price fluctuation of natural gas relates to supply and demand cyclical patterns, owing to the continuous demand for power generation. Oil reserves are found in different parts of

the world and while reserves are still high [2] the utilisation of oil is mostly confined to transportation and heating purposes. In addition, the use of oil for power generation is declining for reasons related to cost, availability, and air pollution ($NO_x$, $SO_2$ and particulates). In addition, oil-burning power plants emit carbon dioxide ($CO_2$) (as well as other greenhouse gases), heavy metals such as mercury, and volatile organic compounds (which contribute to ground-level ozone). Coal is abundantly available in many parts of the world and mainly used for electricity generation. Although renewable energy is growing rapidly, its contribution is currently only 8% of the total energy consumption and is predicted to rise to just 10% by 2040 [2]. Hence, it is imperative to decrease the adverse effects of conventional energy sources on the environment, in parallel with the development of renewable and sustainable energy sources for the future.

## 1.2. Environmental Impact of Solid Fuels

Amongst all the conventional fossil fuels, solid fuels play a crucial role in the world's energy supply because they are both the cheapest fossil fuel source and abundant. Energy from solid fuels is mainly extracted through a combustion process involving one of two main technologies, namely; pulverised fuel (PF) combustion and fluidised bed combustion. The latter is mainly used for low grade fuels which are difficult to burn and highly polluting. Pulverised fuel combustion is the dominant technology for burning solid fuels because of its high combustion intensity (0.5 – 1.0 $MW \cdot m^{-3}$) and high heat transfer rates (0.1 – 1.0 $MW \cdot m^{-2}$) [4], which lead to low-cost plants. Hence pulverised fuel is considered in this research project.

Coal is an abundant fuel resource and forecasts show that it is likely to remain a dominant fuel for electricity generation for many countries for years to come. Coal is a carbon-containing rock and also consists of hydrogen, nitrogen, sulfur, oxygen and mineral matter (including compounds of silicon, aluminium, iron, calcium, magnesium) [5]. Although coal combustion contributes to a substantial number of adverse effects on the environment and public health, global warming is the most serious impact of coal combustion in terms of its universal and potentially irreversible consequences. The earth's climate is warming due to the devastating impact of greenhouse gas (GHG) emissions which result from burning fossil fuels. Amongst the three GHGs (viz., $CO_2$, $CH_4$, and $N_2O$), $CO_2$ is the major contributor to environmental pollution during the combustion of fossil fuels. According to the Environmental Protection Agency (EPA), $CO_2$ emissions represent over 99% of the total $CO_2$-equivalent GHG emissions from all commercial, industrial, and electricity generation and industrial stationary combustion sources [6]. Coal-fired power plants are the largest single source of $CO_2$ emissions in the world when compared with other forms of fossil fuel combustion [2, 7]. According to the EPA, a large coal-burning plant (~600 MW capacity) burns 3 million tons of coal and produces 11 million tons of $CO_2$ per year [6].

Beyond global warming, coal combustion using conventional technology is responsible for countless examples of environmental damage by emitting other pollutants such as $SO_2$, $NO_x$, particulate matter (PM), soot, mercury and dozens of other substances [8]. Coal-fired power plants are the major source of $SO_2$ emissions and $SO_2$ is a contributor to acid rain. Acid rain damages forests, crops, and acidifies

waterways. Nitrogen oxides ($NO_x$) are key contributors to the development of ground-level ozone and smog. Smog is one of the leading sources of air pollution, which exaggerates chronic respiratory illnesses and burns lung tissue [9]. Particulate matter, including soot, is responsible for chronic bronchitis, aggravated asthma and premature death, as well as creating haze which can obstruct visibility. Coal plants are the main source of mercury emissions. Mercury is a toxic heavy metal which seriously contaminates the environment and is responsible for brain damage and heart problems [2, 9].

In recognition of the observed adverse effects of pulverised coal combustion, the international community has become more concerned about protecting the environment and has instigated more rigorous policies to mitigate carbon emissions e.g., through the adoption of the Paris agreement in 2015 [10]. Nonetheless, the uncertainty of renewable energy and the increasing price of gaseous fuels encourage the continued usage of coal. Thus, the development of advanced coal combustion technologies is a major goal for lowering pollutant emissions. This can be achieved through research which is focused on reducing any impediments, developing accurate modelling and scaling tools and optimising these in order to improve their viability. This project is motivated by a desire to solve one of the key problems: namely the reduction of air pollutant emissions, in particular controlling of $NO_x$ emissions whilst improving the efficiency of combustion systems using pulverised coal as a fuel.

## 1.3. MILD Combustion

The preceding sections highlighted the need for more efficient and clean combustion systems to reduce the negative impact of current systems on the environment. Moderate or Intense Low-oxygen Dilution (MILD) combustion [11, 12] has been identified as an innovative technology that offers low pollutant emissions, high thermal efficiency, enhanced combustion stability, thermal field uniformity and broad fuel flexibility. MILD combustion operates on the combination of heat and combustion product recirculation. Many computational and experimental investigations have been carried out to investigate the characteristics of MILD combustion [12-23] using gaseous fuels. Although MILD combustion has been studied extensively for gaseous fuels, very few studies have been conducted for pulverised solid fuels and their burning characteristics are not well understood. Many important issues involved in MILD combustion of pulverised fuels have not been addressed fundamentally. In particular, the combustion characteristics (e.g. burning temperature, reaction zone structure and emissions) of differently ranked pulverised fuels under various conditions are not clearly understood. Furthermore, the influence of volatiles' release and reactions on the formation and destruction of pollutants under MILD combustion conditions are yet to be understood. The effect of turbulence and the impact of residence time on the char burnout rate as well as the overall carbon consumption rate, along with pollutant formations and destruction mechanisms (in particular, fuel $NO_x$ formation and reduction by reburning) on the stability of MILD combustion are still unknown. Hence, the present study aims to understand the MILD combustion characteristics of solid fuels better, in particular

for pulverised coal. This project explores the MILD combustion behaviour of a variety of coals (namely lignite and anthracite) for different particle sizes (namely 38 $\mu m$ to 250 $\mu m$), operating conditions, and carrier gases (either $CO_2$ or $N_2$). Overall, this project seeks to characterise the MILD combustion regime in a furnace environment burning pulverised coal through both experiments and numerical models.

## 1.4. Thesis Outline

The thesis reports a research study on the burning characteristics of pulverised coals under MILD combustion conditions. The work is presented in seven chapters and their contents are detailed as follows.

Chapter 2 outlines a comprehensive review of the literature including current knowledge of coal MILD combustion. This chapter also highlights the gaps in the current knowledge and the need for further research. The chapter ends with a summary of the specific research gaps and the main objectives of the research.

Chapters 3, 4, 5, and 6 are the main body of the thesis, which are an assemblage of four manuscripts that have been published, or are currently under review. The contributions of this research are presented by these publications. A detailed description of the MILD combustion characteristics of high-volatile Kingston brown coal and low-volatile Bowen basin black coal with particle sizes in the range of 38−180 $\mu m$ in a self-recuperative furnace are presented in Chapter 3. Chapter 4 describes the influence of devolatilisation models on the prediction accuracy of pulverised coal under MILD combustion conditions. The effect of particle sizes (i.e.,

for a range between $53-125\,\mu m$ and $250-355\,\mu m$) on the MILD combustion characteristics of pulverised brown coal are presented in Chapter 5. In Chapter 6, the turbulence effect on the volatiles' release and reactions under vitiated co-flow conditions, as well as the impact on the pollutants' formation and emission, is presented for Loy-Yang brown coal MILD combustion.

Finally, Chapter 7 contains a general summary of the findings and conclusions drawn from this research. The chapter ends with recommendations for future work to advance the topic of solid fuels' MILD combustion further.

## 1.5. Publications Arising from this Thesis

The following lists of publications contain all the findings of this research project, including four journal papers and six conference papers.

### Journal Papers:

1. **M. Saha**, B. B. Dally, P. R. Medwell, and E. Cleary, "Moderate or Intense Low Oxygen Dilution (MILD) Combustion Characteristics of Pulverized Coal in a Self-Recuperative Furnace", *Energy & Fuels*, (**2014**), Vol. 28(9), pp. 6046 – 6057.

2. **M. Saha**, A. Chinnici, B. B. Dally, and P. R. Medwell, "Numerical Study of Pulverized Coal MILD Combustion in a Self-Recuperative Furnace", *Energy & Fuels* (**2015**), Vol. 29 (11), pp. 7650 – 7669.

3. **M. Saha**, B. B. Dally, P. R. Medwell, and A. Chinnici, "Effect of Particle Size on the MILD Combustion Characteristics of Pulverised Brown Coal", *Fuel Processing Technology* (**2016**), DOI: 10.1016/j.fuproc.2016.04.003 (In Press).

4. **M. Saha**, B. B. Dally, P. R. Medwell, and A. Chinnici, "Burning Characteristics of Victorian Brown Coal in a MILD Combustion Furnace", *Combustion and Flame*, (**2016**) Manuscript ID. CNF-D-16-00037 (under review).

## Peer-reviewed Conference Papers:

1. **M. Saha**, B. B. Dally, P. R. Medwell, and E. Cleary, "An Experimental Study of MILD Combustion of Pulverized Coal in a Recuperative Furnace", *9th Asia-Pacific Conference on Combustion* (**2013**), Gyeongju, Korea, pp 233.

2. **M. Saha**, E. Cleary, P. R. Medwell, and B. B. Dally, "MILD Combustion of Pulverised Coal in a Recuperative Furnace", *Proceedings of the European Combustion Meeting* (**2013**), Lund, Sweden, pp 4-78.

3. **M. Saha**, B. B. Dally, P. R. Medwell, and E. Cleary, "A Study of Combustion Characteristics of Pulverised Coal under MILD Combustion Conditions", *Proceedings of the Australian Combustion Symposium* (**2013**), The University of Western Australia, Perth, WA, Australia, pp 132-135.

4. **M. Saha**, A. Chinnici, B. B. Dally, and P. R. Medwell, "Numerical Investigation of Pulverised Coal Combustion in a Self-Recuperative MILD Combustion Furnace" *10th Asia-Pacific Conference on Combustion* (**2015**), Beijing, China.

5. **M. Saha**, B. B. Dally, P. R. Medwell, and A. Chinnici, "MILD Combustion of Victorian Brown Coal", Paper no. 3127333, *International Conference on Coal Science & Technology* (**2015**), Melbourne, Australia.

6. **M. Saha**, B. B. Dally, P. R. Medwell, and A. Chinnici, "Effect of Turbulence on the MILD Combustion Characteristics of Victorian Brown Coal" *Australian Combustion Symposium* (**2015**), The University of Melbourne, Melbourne, Australia.

## 1.6. Thesis Format

The thesis has been submitted as a portfolio of the publications, according to the formatting requirements of The University of Adelaide. The printed and online versions of this thesis are completely indistinguishable. The online version of the thesis is available in portable document format (PDF). The electronic version can be viewed in its correct format with the use of software compatible with PDF version 1.7 or later.

## References

[1] V. P. Mega, *Sustainable development, energy and the city: A civilisation of concepts and actions*. Berlin, Germany: Springer Science & Business Media, 2005.

[2] U.S. Energy Information Administration. International Energy Outlook 2015; U.S. Department of Energy (DOE): Washington, DC, 2015. Available: http://www.eia.gov/forecasts/aeo/index.cfm (accessed on 10/03/2016).

[3] NASDAQ Stock Exchange. *U.S. National Average Natural Gas Price*. Available: http://www.nasdaq.com/markets/natural-gas.aspx?timeframe=1y (accessed on 29/03/2016).

[4] A. Williams, M. Pourkashanian, and J. Jones, "Combustion of pulverised coal and biomass," *Progress in Energy and Combustion Science,* vol. 27, pp. 587-610, 2001.

[5] M. Beychok and M. Perry.; *Coal*, 2007. Available: http://www.eoearth.org/view/article/151276/ (accessed on 10/03/2016).

[6] U.S. Environmental Protection Agency. Climate leaders green house gas inventory protocol, 2008, article number *EPA430-K-08-003*. Available: www.epa.gov/climateleaders (accessed on 10/03/2016).

[7] C. R. Shaddix, "Coal combustion, gasification, and beyond: Developing new technologies for a changing world," *Combustion and Flame,* vol. 159, pp. 3003-3006, 2012.

[8] D. Zhao and B. Sun, "Atmospheric pollution from coal combustion in China," *Journal of the Air Pollution Control Association,* vol. 36, pp. 371-374, 1986.

[9] J. E. Staudt, "Control technologies to reduce conventional and hazardous air pollutants from coal-fired power plants," Northeast States for Coordinated Air Use Management, USA 2011.

[10] 2015 United Nations Climate Change Conference 2015. *The Paris Agreement 2015*. Available: http://www.c2es.org/international/paris-agreement (accessed on 10/03/2016).

[11] M. A. Galbiati, A. Cavigiolo, A. Effuggi, D. Gelosa, and R. Rota, "Mild combustion for fuel-$NO_x$ reduction," *Combustion Science and Technology,* vol. 176, pp. 1035-1054, 2004.

[12] M. de Joannon, G. Langella, F. Beretta, A. Cavaliere, and C. Noviello, "Mild combustion: Process features and technological constrains," *Combustion Science and Technology,* vol. 153, pp. 33-50, 2000.

[13] R. Weber, S. Orsino, N. Lallemant, and A. Verlaan, "Combustion of natural gas with high-temperature air and large quantities of flue gas," *Proceedings of the Combustion Institute,* vol. 28, pp. 1315-1321, 2000.

[14] S. Orsino, R. Weber, and U. Bollettini, "Numerical simulation of combustion of natural gas with high-temperature air," *Combustion Science and Technology,* vol. 170, pp. 1-34, 2001.

[15] A. Cavaliere and M. de Joannon, "Mild combustion," *Progress in Energy and Combustion Science,* vol. 30, pp. 329-366, 2004.

[16] B. B. Dally, E. Riesmeier, and N. Peters, "Effect of fuel mixture on moderate and intense low oxygen dilution combustion," *Combustion and Flame,* vol. 137, pp. 418-431, 2004.

[17] R. Weber, J. P. Smart, and W. Kamp, "On the (MILD) combustion of gaseous, liquid, and solid fuels in high temperature preheated air," *Proceedings of the Combustion Institute,* vol. 30, pp. 2623-2629, 2005.

[18] P. R. Medwell, P. A. M. Kalt, and B. B. Dally, "Simultaneous imaging of OH, formaldehyde, and temperature of turbulent nonpremixed jet flames in a heated and diluted coflow," *Combustion and Flame,* vol. 148, pp. 48-61, 2007.

[19] C. Galletti, A. Parente, and L. Tognotti, "Numerical and experimental investigation of a mild combustion burner," *Combustion and Flame,* vol. 151, pp. 649-664, 2007.

[20] A. Effuggi, D. Gelosa, M. Derudi, and R. Rota, "Mild combustion of methane-derived fuel mixtures: Natural gas and biogas," *Combustion Science and Technology,* vol. 180, pp. 481-493, 2008.

[21] A. Parente, J. C. Sutherland, B. B. Dally, L. Tognotti, and P. J. Smith, "Investigation of the MILD combustion regime via Principal Component Analysis," *Proceedings of the Combustion Institute,* vol. 33, pp. 3333-3341, 2011.

[22] A. Parente, C. Galletti, and L. Tognotti, "A simplified approach for predicting NO formation in MILD combustion of $CH_4$-$H_2$ mixtures," *Proceedings of the Combustion Institute*, vol. 33, pp. 3343-3350, 2011.

[23] S. Kruse, B. Kerschgens, L. Berger, E. Varea, and H. Pitsch, "Experimental and numerical study of MILD combustion for gas turbine applications," *Applied Energy*, vol. 148, pp. 456-465, 2015.

# CHAPTER 2

# BACKGROUND LITERATURE

# Chapter 2 Background Literature

## 2.1. Combustion Overview

Combustion is one of the greatest discoveries of mankind. The energy crisis scenario of the current world has again reinforced our civilisation's strong dependency on combustion. At present, approximately 90% of our worldwide energy demands are supplied through combustion [1].

The combustion or burning process may be defined as a rapid chemical reaction between a fuel and an oxidant which produces thermal energy. The chemical reaction is also described as an oxidation process [2]. The combustion phenomenon is generally categorised into two classes: namely, "*premixed*" and "*non-premixed*" combustion, based on the mixing of the reactants. In a premixed system, the reactants (i.e., fuel and oxidizer) are mixed at the molecular level before the chemical reaction is initiated. In contrast, in the non-premixed combustion mode, the reactants are initially separated and combustion occurs in an interface/common region of fuel and oxidizer where the mixing and reaction take place. Whether premixed or non-premixed combustion is applied to the production of energy, having easy access to affordable energy sources and extracting energy efficiently from them are the major challenges. It is well established that solid fuels constitute the largest part of the

utilised fuel sources in the world, therefore attention has always been on these sources, mainly to maximise thermal efficiency and reduce the emission of pollutants.

The following sections include a review of solid fuel combustion technologies and a detailed introduction and review of a particular technology of interest to this project, namely, Moderate or Intense Low oxygen Dilution, MILD, combustion. The section incorporates a review of the literature highlighting the benefits, limitations, efficiency and pollutant emissions. It also identifies the gaps in our knowledge of these systems and how this project aims to address them.

## 2.2. Solid Fuel Combustion Systems

Solid fuels include diverse types of carbonaceous hard material that are employed as fuel for energy production through combustion. Solid fuels comprise a broad diversity of combustibles, ranging from coal to biomass and other substances (e.g., peat and charcoal).

Coal is a sedimentary rock, formed by the lithification of plant matter, which has the characteristics of being a combustible material [3, 4]. Coal is the most abundant energy source and it has been found that over 860 billion tonnes of proven coal reserves are available in different parts of the world [5]. According to the predictions for world energy demands, there is plenty of coal to continue the energy supply for around the next 118 years, at current rates of consumption [5, 6]. Almost every country in the world has some reserves of coal, while coal is economically recoverable from almost 80 countries. The biggest coal reserves are in the USA,

Australia, Russia, China and India; coal is actively mined in more than 70 countries around the world [5].

The formation of coal was originally initiated from the carboniferous period, which took place between 360 and 290 million years ago [5]. According to the World Coal Association, the quality or type of coal largely depends on the type of plants from where the coal originated, the interment depth of the coal, the pressures and temperatures at that depth, and the period of time during which coal formation has occurred. These factors contribute significantly to the degree of transformation of the original plant material to coal. The rank or quality of coal is described by its carbon content. Fundamentally, the coal that takes a longer time of its formation is associated with having a higher carbon content and named as a high-ranking coal. On the other hand, having a lower carbon content is a characteristic of low-rank coal with shorter formation time and thus called "younger coal" [7]. Low-rank coals are divided into two types, namely: lignite and sub-bituminous coal. The youngest form of coal is called lignite. Lignite is soft, brown-coloured coal, so it is also called "brown coal". Brown coal accounts for 17% of the world's coal reserves and is mainly used as a fuel for power plants [5]. The next stage of coal is sub-bituminous coal which is formed from lignite after millions of years under continuous pressure and temperature. Sub-bituminous coal accounts for 30 per cent of the world's coal reserves [5]. This type of coal combustion produces fewer pollutants than others because of its low sulfur content. High-ranking coals are also called hard coals and classified into two categories, namely: bituminous coal and anthracite. Bituminous coal accounts for the maximum portion (~52%) of the world's coal reserves [5].

Bituminous coal is blacker and harder than low-ranking coal, and also sub-divided into two types, namely: metallurgical and thermal coal. Metallurgical coal is mainly used for the iron and steel manufacturing industries, while thermal coal is used primarily for power generation and the cement manufacturing industries. The most mature coal is anthracite and it has the largest carbon content of all types of coal. Anthracite represents a very small portion (only 1%) of the world's coal reserves [5]. Anthracite is a fully black-coloured coal and thus, it is also called "black coal" [8]. This type of coal is frequently used for domestic purposes (e.g., home heating). It is also used as a "smokeless fuel" in the industrial context [4, 5].

Biomass is an organic material produced from plants and animals [9]. It is used as a fuel for combustion as well as a sustainable and renewable source of energy. The main sources of biomass energy are wood and wood wastes (~64%), municipal solid waste (~24%), agricultural crops and their waste by-products (~5%), animal wastes, waste from food processing (~5%), and aquatic plants and algae (~2%) [10-12]. Biomass has great potential to ensure a renewable fuel supply in the future. It absorbs $CO_2$ during growth, and releases it during burning, thus biomass helps the $CO_2$ recycling in the atmosphere and reduces the influence of global warming. Although biomass cannot be counted as a principal source of the world's energy supply, unlike coal, it is still the main energy source in a number of countries and regions (e.g. Bhutan 86%, Nepal 97%, Asia 16%, East Sahelian Africa 81% and Africa 39%) [13-15].

Solid fuels are used mainly for electricity generation and stationary industrial systems. While the amount of electricity generated using biomass is very small, coal

and in particular anthracite or black coal, contributed an estimated 39% of world generated energy in 2013 (75% of Australia's electricity generation), as opposed to 27% for natural gas and 13% for renewable energy [6]. Figure 2.1 illustrates that total electricity production is predicted to rise by 24% between the years 2013 to 2040 and that there is large variability among different fuels. While the electricity generated from the combustion of coal is expected to drop from 39% to 34% of total production, the absolute amount of coal consumption is predicted to remain constant at 1.75 trillion kWh. This trend is fuelled by economic drivers, as well as regulatory and global emission targets.

Energy from solid carbonaceous fuels, in particular coal, is extracted through two main combustion processes namely; fluidised bed combustion and pulverised fuel combustion.

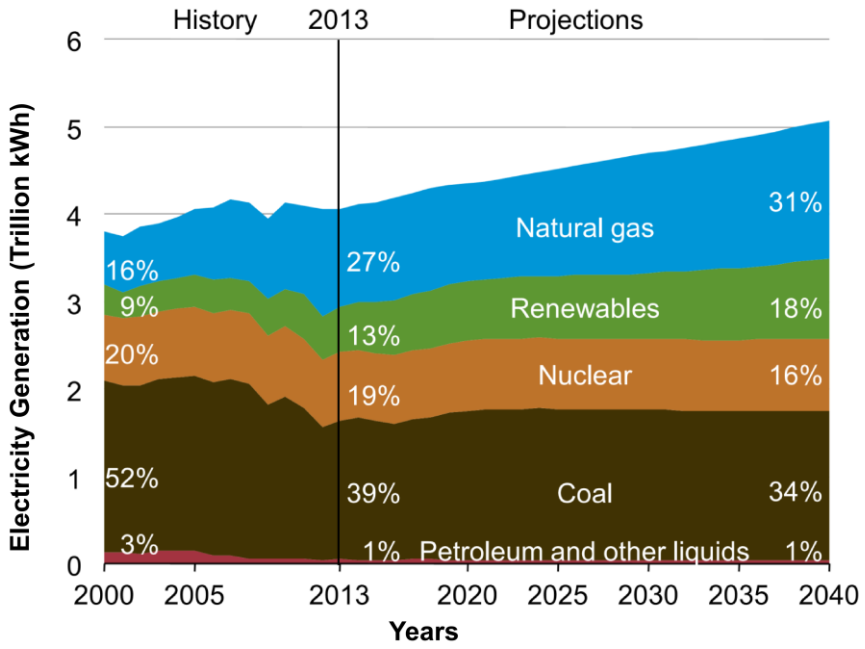


**Figure 2.1: Electricity generation by fuel 2000-2040 (Trillion kWh) [6].**

### 2.2.1. Fluidised Bed Combustion

Fluidised bed combustion (FBC) technology was developed during the 1970s [16-18] to utilise low quality solid fuels with high burning efficiency. FBC technology comprises a bed of particles in a furnace and introducing oxidising air into the mixture to disperse the solid particles, thereby inducing it to be fluidized and/or suspended in a gas stream. The particles' bed constitutes of inert materials such as sand, limestone/dolomite (for sulfur dioxide sorbent), ash, and a small portion of coal particles (3 to 5% by mass of the bed) [17]. FBC technology offers several advantages, including design simplicity, the flexibility of using different solid fuels, for example, peat, coal, biomass, waste or recycled fuels, and reasonable combustion efficiency at an extraordinarily low temperature (750 – 900 ºC) operation, which is well below the thermal $NO_x$ formation temperature. In addition, the exhaust gases come in contact with the sulfur dioxide absorbing chemicals (sorbent) due to the mixing action of the fluidised bed. Eventually, more than 95% of the produced sulfur dioxide from coal combustion is captured. However, low temperature combustion in FBC technology enhances the formation of polycyclic aromatic hydrocarbons (PAH) which lead to soot formation.

Fluidised bed combustion technology can be placed in two major categories namely; atmospheric fluidised bed combustion (AFBC) and pressurised fluidised bed combustion (PFBC). AFBC operates at a pressure close to atmospheric, where coal and limestone are continuously fed into the system and always maintain the correct amount of bed material for fluidization. The bed temperature is maintained at comparatively low levels of 750 – 850 ºC and that results in low $NO_x$ emissions.

Nonetheless, under specific operating conditions AFBC plants produce a higher level of pollutants (e.g., $CO_2$, $N_2O$, NO, and $SO_2$), when compared with other conventional coal combustion technologies [16-21]. Although AFBC plants have been commercially used for more than 30 years, the high emission intensity of AFBC plants has limited its industrial applications significantly. On the other hand, pressurised fluidised bed combustion (PFBC) technology is relatively new and recognised as the second generation of FBC technology, which operates at pressures 10 – 15 times higher than the normal atmospheric pressure of AFBC. Pressurised fluidised bed combustion technology is mainly used in combined cycle power plants where a pressurised gas stream from an PFBC plant is introduced to a steam turbine and the flue gas from the steam turbine is used to produce steam by passing through a waste heat recovery boiler. The PFBC plant efficiency is about 35 – 40% higher than the AFBC plant [18]. However, the major problem with PFBC technology is the corrosion and/or erosion of the reactor vessel and the requirement for high pumping power to maintain adequate pressure. In addition, the greenhouse gas emissions, coupled with the high capital cost, requirement for a significantly larger plant size, and the high maintenance cost of FBC plants when compared with the modern pulverised coal combustion plant, significantly reduce the application of FBC technology for commercial power plants [19].

### 2.2.2. Pulverised Fuel Combustion

Pulverised fuel combustion is the dominant technology to burn solid fuels, in particular coals, because of its high combustion intensity (0.5 – 1.0 $MW \cdot m^{-3}$) and high heat transfer rates (0.1 – 1.0 $MW \cdot m^{-2}$), which leads to low-cost plant. Pulverised

coal combustion is a well-established technology [22-26] that accounts for almost 97% of the world's coal-fired power generation capacity [3]. Those units require the reduction of large size coal particles to a powdered form and carry the particles, using a carrier gas, into the combustion chamber (i.e., furnace and/or boiler). Despite the fact that there are several advantages for pulverised fuel combustion, major challenges remain, mainly in terms of limiting pollutant (e.g., $NO_x$, $CO_2$, and $SO_2$) emissions and increasing plant efficiency.

Alternative new technologies to burning solid fuels are also under development and these include:

i. Ultra-Super Critical Combustion (USCC)
ii. Integrated Gasification Combined Cycle (IGCC)
iii. Oxy-Fuel Combustion

### *Ultra-Super Critical Combustion (USCC)*

To improve coal-fired power plant efficiency while minimising emissions of harmful species and particulates, ultra-super critical combustion (USCC) technology has been developed and implemented. USCC technology operates under elevated pressure and temperature conditions above the critical point of water (i.e. over the pressure and temperature at which the liquid and gas phases of water coexist in equilibrium). The steam pressure of USCC units can reach 350 bar and the temperatures can range up to 973 K [26]. The net efficiency of the USCC plants can be more than 45%, while the net efficiency of the conventional coal-fired power plant is less than 39% [26, 27]. From economic and pollution standpoints, USCC

technology is better than conventional coal plants. However, the major challenges of USCC technology are to maintain the necessary high temperature and pressure without inducing a sudden failure of the materials. In addition, it is expensive to retrofit the USCC technology in existing plants because of need to redesign the boilers and reconstruct most of the existing infrastructure.

### *Integrated Gasification Combined Cycle (IGCC)*

The Integrated Gasification Combined Cycle (IGCC) is an advanced gasification technology where the coal is gasified at high temperatures to produce syngas and then the high temperature syngas is fired in a gas and steam turbine combined system to generate electricity [28]. The IGCC plants operate at above 45% efficiency and $CO_2$ emissions can be decreased by up to 36%, when compared with traditional coal combustion power plants [29, 30]. It is widely accepted that IGCC technology offers low emission coal fired power generation. The key challenge of IGCC technology is its high capital cost. However, this technology is being developed further in industry; especially since the power cost per megawatt-hour for an IGCC plant is 7.5% higher than for traditional coal combustion power plants [31, 32].

### *Oxy-Coal Combustion*

Oxy-fuel combustion technology has been identified as one of the most promising technologies for carbon dioxide ($CO_2$) capture and sequestration/storage from existing plants [33, 34]. In conventional combustion, air is used as an oxidant for combustion, where the nitrogen ($N_2$) from the air (approximately 79% by volume) dilutes the $CO_2$ concentration in the flue gas. The capture of $CO_2$ from such dilute

mixtures is complex and expensive [34]. When pure oxygen ($O_2$) or the mixture of $CO_2$ and $O_2$ is used in the combustion reaction instead of standard air, then the combustion method is called oxy-fuel combustion [33, 35]. By eliminating $N_2$ from the combustion medium, the flue gas consists mainly of $CO_2$ and $H_2O$. In order to remove $H_2O$ and produce almost pure $CO_2$, a condensation process of the flue gas is utilised. Then, the $CO_2$ can be captured in pure form for commercial use like enhanced oil recovery, by inserting $CO_2$ into depleted oil and gas reservoirs [36, 37] or for sequestration. The purity of $CO_2$ has become a strict requirement for pipeline transportation and storage, to avoid corrosion and cavitation damage in the pipeline and $CO_2$ reservoir [33]. Although no quantitative limits for co-storing $NO_x$ were defined in the London Convention Protocol in 2006 [38] the feasibility of co-storing $NO_x$ with the $CO_2$ depends on the reservoir mechanics and geochemistry that are still unknown. Therefore, $NO_x$ (and other impurities') removal could be more effective for oxy-fuel combustion, considering the safety demands for transportation and storage.

Many studies [33, 34, 38-51] have been conducted on oxy-fuel combustion using pulverised coal. These studies have a common conclusion that oxy-fuel combustion is the most competitive technology option for retrofitting existing coal-fired power plants. Under oxy-fuel combustion conditions, thermal performance can be increased by raising the flame temperature and combustion intensity, which often comes at the price of high pollutant emissions (e.g., fuel $NO_x$ formation) [52]. On the other hand, a recent study [53] conducted on the effects of the endothermic $CO_2$ gasification reactions on oxy-fuel combustion of pulverised coal char via computational

approaches reported that the char oxidation rate is significantly decreased, owing to the sudden drop in char temperature required to achieve low $NO_x$ emissions in oxy-fuel combustion and consequently the thermal performance of the system dropped. Therefore, it is difficult to satisfy the requirements of high efficiency and low pollution in the oxy-fuel combustion process simultaneously. Furthermore, the oxy-fuel combustion technology still faces many challenges, as reported in a recent review [33]. Those challenges include the stabilisation of oxy-fuel flames, system integration and optimisation, scaling characteristics of oxy-combustion, advanced oxy-fuel combustor design to eliminate materials' corrosion, and numerical model development for understanding the fundamental processes (devolatilisation, char formation and agglomeration) of oxy-fuel combustion. Hence, more research is required to fathom the potential of oxy-fuel combustion technology, by addressing technological challenges to implementing its full potential.

## 2.3. Introduction to MILD Combustion

The quest to improve combustion system efficiency and reduce its impact on the environment has motivated the search for new and innovative combustion technologies over the last few decades. Although the thermal efficiency may be increased by maintaining the high temperature of the combustion by preheating the reactants [54], the immediate drawback of this technique is that the increased peak flame temperature contributes to increased $NO_x$ emissions [55]. To overcome this dilemma of high efficiency with increasing $NO_x$ formation, flue or exhaust gas recirculation into the reaction zone is the most successful scheme [56, 57]. The

recirculated exhaust gases or products of combustion lead to a diluted mixture, with low local oxygen concentration at elevated temperatures inside the combustion chamber. Dilution means that reactants (oxidiser and fuel) are mixed in the presence of 'inert' gases (such as $CO_2$, $H_2O$ and $N_2$ ) before they react [58]. The combination of the high temperature and high dilution inside the combustion chamber is the fundamental principle of MILD combustion. The environment of well-mixed and diluted reactants at temperatures above auto-ignition results in a volumetric reaction leading to a moderate furnace temperature, very low emissions of pollutants and improved thermal efficiency of combustion systems [59]. These characteristics make this technique attractive in comparison with other abatement techniques [60].

### 2.3.1. MILD Combustion Definition and Overview

Various terminologies are used to describe MILD combustion technology. From a historical point of view, combustion with high reactant temperatures, introduced with preheating regenerative systems applied to air, is called High Temperature Air Combustion (HiTAC) [61]. HiTAC, also known as highly preheated air combustion (HPAC), was reported by Katsuki and Hasegawa [62]. They focused on the effects of heat recirculating combustion under highly preheated air conditions (1200 – 1600 K). The idea of HPAC originated from the concept of the 'large excess enthalpy combustion' introduced by Weinberg [63]. MILD combustion is often called "flameless combustion" or "flameless oxidation" (FLOX®) [64] owing to the potential for no visible or audible flame to be created under specific conditions. It is also known as Fuel Direct Injection (FDI) [65], Fuel/Oxidant Direct Injection

(FODI) [66], and High temperature Combustion Technology (HiCOT) [59] in a wider sense to all the technologies which contribute high temperature reactants.

In 2004 Cavaliere and de Joannon [59, 67] attempted to define MILD combustion on the basis of the theory of a well stirred reactor. The authors explained, *"a combustion process is termed "MILD" when the inlet temperature of a reactant mixture is higher than the self-ignition temperature of the mixture, whereas the maximum allowable temperature increase with respect to the inlet temperature during combustion is lower than the self-ignition temperature."* The self-ignition or auto-ignition temperature is the lowest temperature at which the mixture spontaneously ignites and burns. They identified two regimes (Figure 2.2) wherein a high-temperature combustion regime (upper right quadrant) of the system can raise its temperature up to the stoichiometric combustion temperature of the air/fuel mixture. On the other hand, in the MILD combustion regime, the temperature increase is moderate because of the dilute conditions. In Figure 2.2 the ordinate $\Delta T$ is the temperature increase during oxidation of fuel and the abscissa $\Delta T_{inlet}$ is the temperature difference between the inlet temperature and the minimum self-ignition temperature of the reactants. Below the abscissa, the processes are identified as pyrolysis processes with a negative maximum temperature increase because of their endothermic behaviour in nature. They are subdivided in two parts *"auto incepted"* and *"assisted"* pyrolysis. Spontaneous inception of oxidation occurs via the processes in the upper-right quadrant, which are classified as auto-ignited combustion. In this case, the differential inlet temperature is positive ($\Delta T_{inlet} > 0$) and auto-ignition should occur with no external energy input. MILD combustion was

categorised under this regime, which shows great flexibility towards the use of low calorific fuels because of the initial temperature, which is higher than that of self-ignition.

An alternative approach was taken by Kumar *et al.* [68] to distinguish the MILD combustion from the classical combustion process. The quantitative definition is based on the root-mean-square (rms) temperature fluctuations in the flow field of an MILD burner. By considering a propane jet turbulent flame, they found that the normalized rms temperature variation was around 15% for MILD conditions and 51% for the conventional jet flame.

There are subtle differences between each of these combustion technologies but they all rely on the fundamental principle of the reaction taking place at a high temperature and with a high dilution level environment.

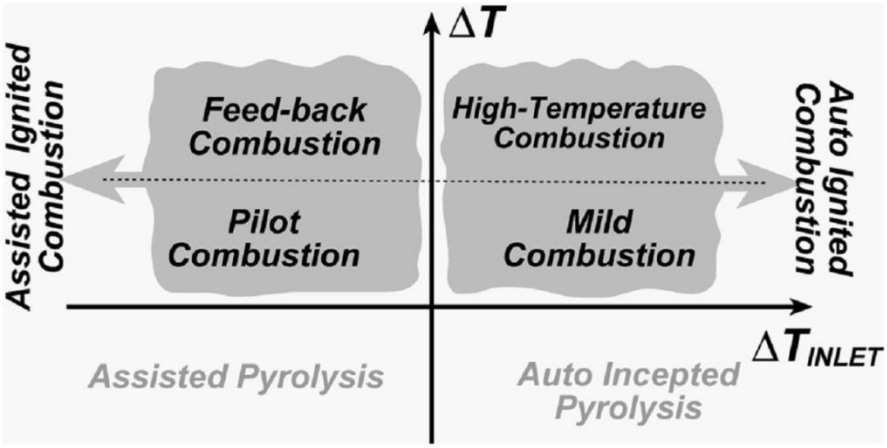


**Figure 2.2: Combustion classes as a function of $\Delta T$ and $\Delta T_{inlet}$ [67].**

### 2.3.2 Principles of MILD Combustion

MILD combustion relies on the concept of heat and exhaust gas recirculation into the reaction zone [62]. Figure 2.3 illustrates the operating principles of MILD combustion: low oxygen concentration in the reaction region while the local temperature of the combustible mixture is greater than that of the self-ignition temperature ($T_{si}$) of the reactants.

The combustion reactions occur in an environment where oxygen concentration is very low, around 2-6% [69, 70], due to the dilution of the reactants. This diluted phenomenon creates a more distributed reaction that reduces the peak temperature and pressure fluctuations of the flame front. As a result, the noise level of the combustion chamber is also reduced drastically in comparison with conventional combustion [64, 70].

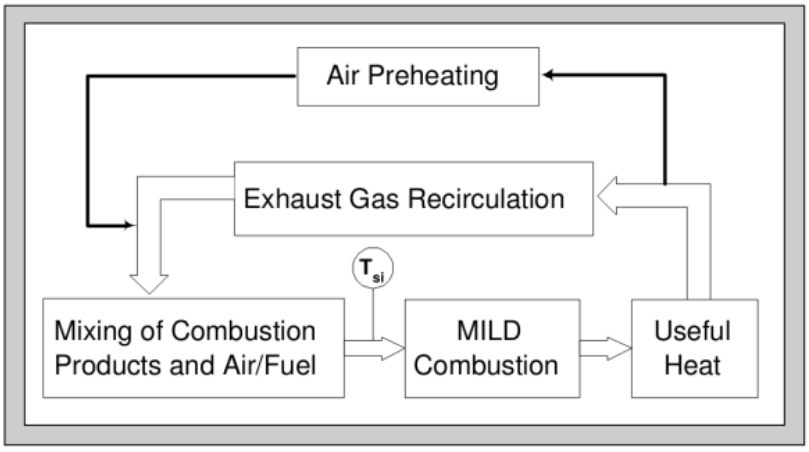


**Figure 2.3: Operation principle of MILD combustion [71]**

One of the most remarkable characteristics of MILD combustion is the low luminosity and the differences in visual appearance, compared with a conventional flame. In fact, under some conditions, there may be no visible flame during MILD combustion [59, 67, 69, 72] owing to the uniform and reduced temperature. Figure 4 shows photographs (left) and temperature distribution diagrams (right) of a test furnace operating in conventional (top) and MILD (bottom) conditions. The difference between conventional and MILD combustion is shown in Figure 2.4: a visible flame front with a high peak temperature close to the burner exit is observed in the temperature distribution diagram in the case of conventional combustion. In contrast, under MILD combustion modes the furnace is almost transparent with a distributed reaction zone and an absence of steep gradients of temperature. The uniform in-furnace thermal distribution is shown in the temperature distribution diagram of Figure 2.4.

From the above discussion, the essential characteristics of MILD combustion technology can be summarized as follows:

a) The recirculation/entrainment of the exhaust gases in the combustion reaction zone to ensure the dilution of the reactants is the key feature of this new combustion technology [73];

b) The local oxygen concentration remains between 2% - 6% in the reaction zone [69, 73], whereas the local temperature is required to be higher than the fuel's auto-ignition temperature for MILD combustion. The condition is typically achieved by the mixing of the flue gases with the reactants;

c) Typically no flame is visible during MILD combustion and the combustion reaction takes place globally, throughout the furnace;

d) The in-furnace temperatures and the radiative heat fluxes are relatively uniform [61].

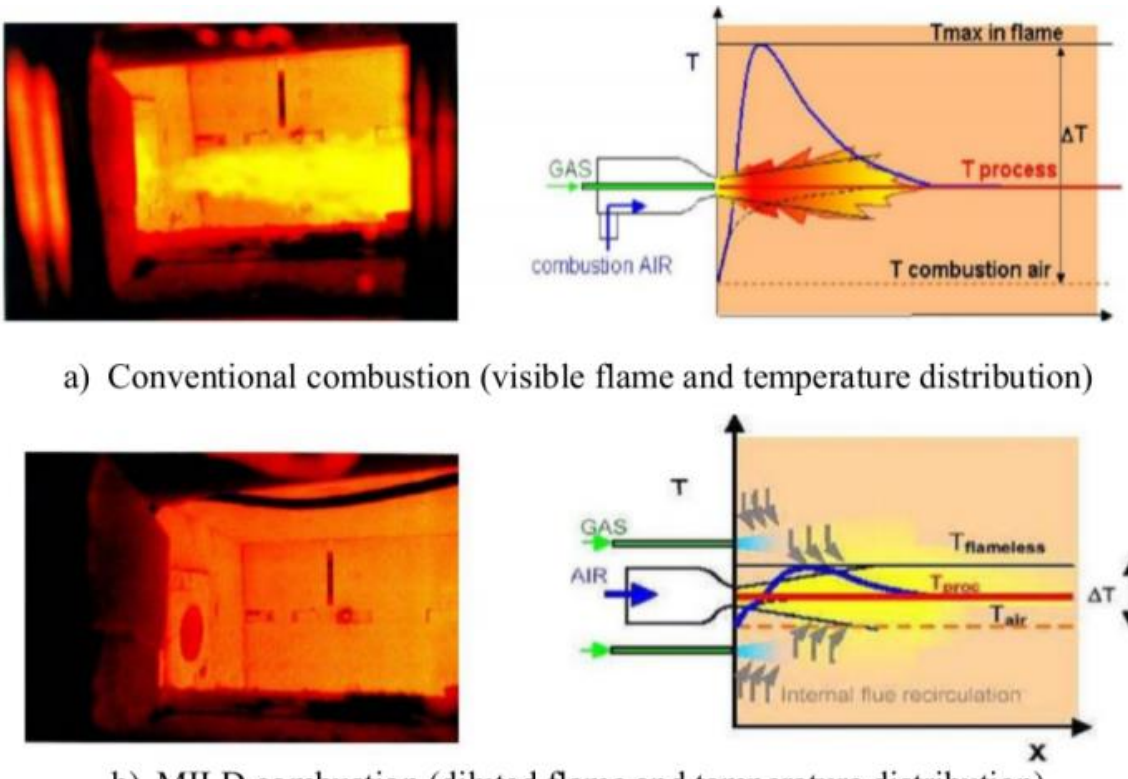


**Figure 2.4: Conventional combustion versus MILD combustion of natural gas in a 1.5 MW test furnace [58].**

The flue gas recirculation increases the content of inert gases (e.g., $N_2$, $CO_2$) in the mixture that accelerates the dilution process of the reactants. Wünning and Wünning [64] defined the exhaust gas recirculation rate ($K_V$) to measure the dilution rate of the reactants. The term $K_V$ is defined as the ratio of the mass flow rate of recirculated exhaust gases ($\dot{M}_E$) in relation to the mass flow rate of the initial fuel and air jet ($\dot{M}_F + \dot{M}_A$), mathematically:

$$K_V = \frac{\dot{M}_E}{\dot{M}_F + \dot{M}_A} \quad (1)$$

Figure 2.5(a) shows the axial evolution and radial diffusion of the air-fuel jet, which results from the recirculation of the surrounding exhaust gases and the stability limit of different combustion modes where $\dot{M}_J = \dot{M}_E + \dot{M}_F + \dot{M}_A$, is the total mass flow rate of exhaust gases with both air and fuel.

The abscissa of Figure 2.5(b) indicates the internal recirculation rate of the exhaust gas ($K_V$) and the ordinate refers to the temperature of the reactants. For a recirculation rate of less than ≈0.3, a stable conventional flame zone is found, as shown in region **A**. Region **B** shows the unstable combustion regime at increasing value of recirculation rate. When the exhaust gas recirculation rate is greater than ≈2.5 and the furnace temperature is above the self-ignition limit of fuel (about ≈750°C) a stable MILD combustion zone is established as indicated by region **C**.

The fundamental difference between MILD and conventional combustion is illustrated in Figure 2.5(b). It has been shown that entrainment of exhaust gases into the combustion zone is very important for the initiation of MILD combustion [54]. Also, that the formation of $NO_x$ and CO are directly influenced by the mixing rate, as

well as $K_V$ on the reaction temperature of MILD combustion [72]. The findings of the preceding sections show that the combustion temperature and exhaust gas recirculation rate ($K_V$) are two major parameters for the establishment of MILD combustion.

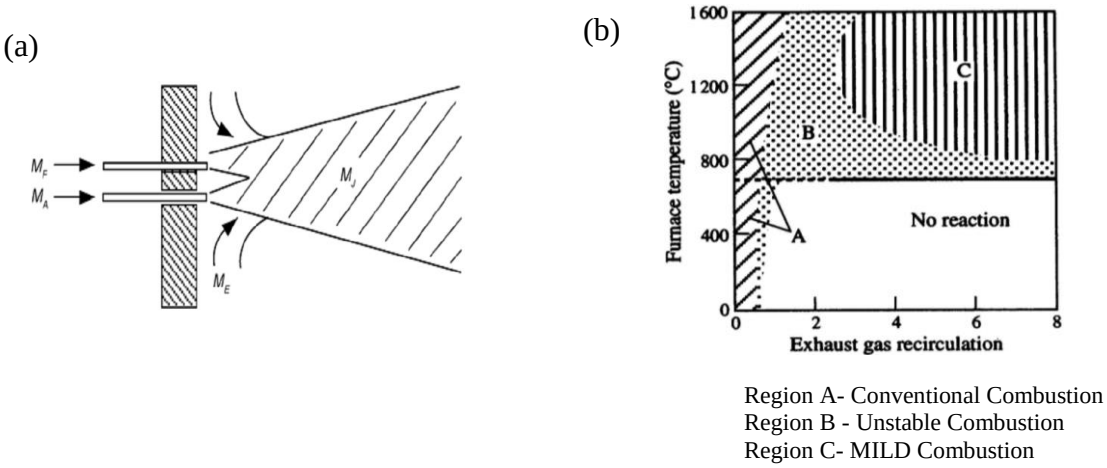


**Figure 2.5: Stability limits of the flame and the relationship between exhaust gas recirculation and temperature in the combustion of methane [64].**

## 2.3.3 Features of MILD Combustion

### *2.3.3.1 Thermal Field Uniformity*

Uniform temperature distribution along the furnace is one of the advantages of the MILD combustion technology. Figure 2.6 demonstrates the time history of the measured temperature at the bottom and top sections of the furnace, as well as the temperature of the exhaust gases and combustion air in a self-recuperative furnace using natural gas [74].

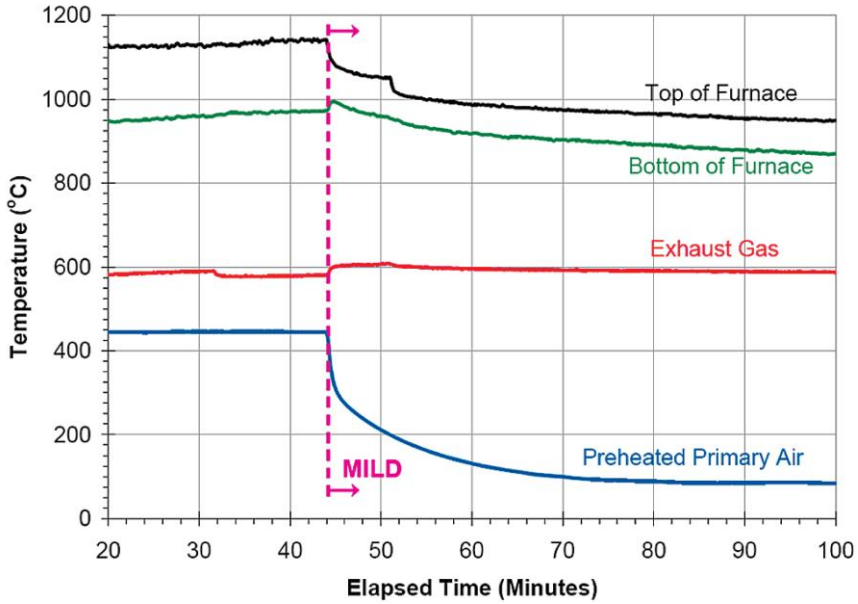


**Figure 2.6: Time history of measured furnace temperature for the MILD combustion furnace, operating on natural gas with a 10 kW heat input [74].**

The temperature difference throughout the furnace is less than 100 K which implies that a homogeneous temperature distribution is achieved in MILD coal combustion. The benefits of such features relate to better product quality due to the semi-uniform heat transfer to the product being heated by the combustion gases, reduction of $NO_x$ (as this prevents local hot spots where a higher temperature is reached where $NO_x$ is formed) and improved stability as the reaction progress and energy release are more steady and the extinction and re-ignition phenomena are avoided.

### *2.3.3.2 $NO_x$ Reduction*

One of the key advantages of MILD combustion technology is the suppression of $NO_x$ formation. Owing to the uniform temperature distribution and the low peak

flame temperature of MILD combustion technology, thermal-$NO_x$ is almost negligible for this combustion [67, 75]. This is because thermal-$NO_x$ is produced above a temperature level of 1800 K [76, 77], whereas MILD combustion operates at temperatures below that. Figure 2.7 presents a comparison of temperatures and $NO_x$ emissions for a conventional flame, a lifted flame, and a reaction in MILD mode, using an experimental burner operating on natural gas combustion [64]. The measured $NO_x$ level for the MILD combustion case is substantially lower than for the other two cases. The recorded $NO_x$ emission under MILD combustion condition is 90% lower when compared with lifted flame and is 97% lower in comparison with a conventional flame.

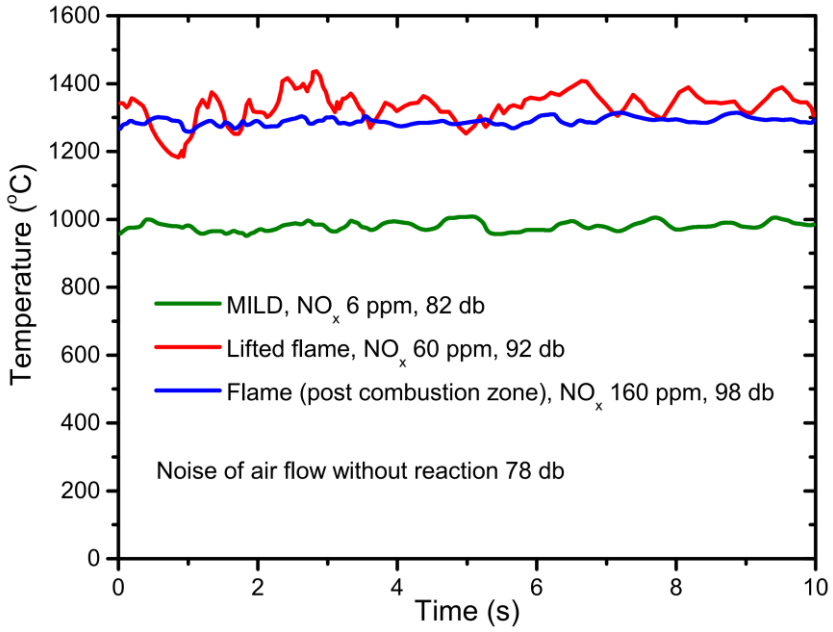


**Figure 2.7: Time history of temperature for MILD, lifted flame, and flame [64]**

#### *2.3.3.3 Fuel Saving*

MILD combustion technology recovers heat energy from the exhaust gas through the recirculation process. This energy-saving is interpreted as fuel conservation from the combustion process. Furthermore, the net radiation flux of MILD combustion technology can be ~30% higher than conventional combustion [61, 69, 73, 78, 79]. As a consequence, less fuel is needed when using MILD combustion to achieve the same energy output in a furnace system relying on radiation for heat transfer.

### 2.3.4. MILD Combustion Furnace and Burner

Due to the many advantages of MILD combustion technology, it has become more attractive to industry. Existing industrial burners operating under this combustion mode can be categorized into two classes, namely recuperative and regenerative systems. The main difference between the two systems is that recuperators transfer thermal energy directly from a steady flow of exhaust gas, where regenerators absorb the waste thermal energy into a medium from the exhaust gas, which is then transferred to heat the combustion air [52].

Regenerative MILD combustion systems have been widely implemented in industrial furnaces, in particular, in the steel and metallurgical industries [80]. Regenerators for MILD combustion were first introduced in Europe [81]. The regenerative system mainly consists of a reversing valve and regenerators [61, 62]. An example of a regenerative MILD combustion furnace which was implemented in industry is shown in Figure 2.8. It consists of two ceramic honeycomb type regenerators. During the operation of the furnace, in one cycle (typically 30 - 120 s)

the ceramic honeycomb type regenerator absorbs heat from the flue gas of the secondary burner while the other hot ceramic honeycomb is preheating the incoming air. In the second cycle, the process is reversed and the working burner is set to stand-by. A four-way switch valve is used to control the flow process. This system ensures the uniformity of temperatures of the highly preheated air during each cycle. As the temperature of the preheated air is above the auto-ignition temperature of the gaseous fuels, MILD combustion is readily achieved in the furnace [62].

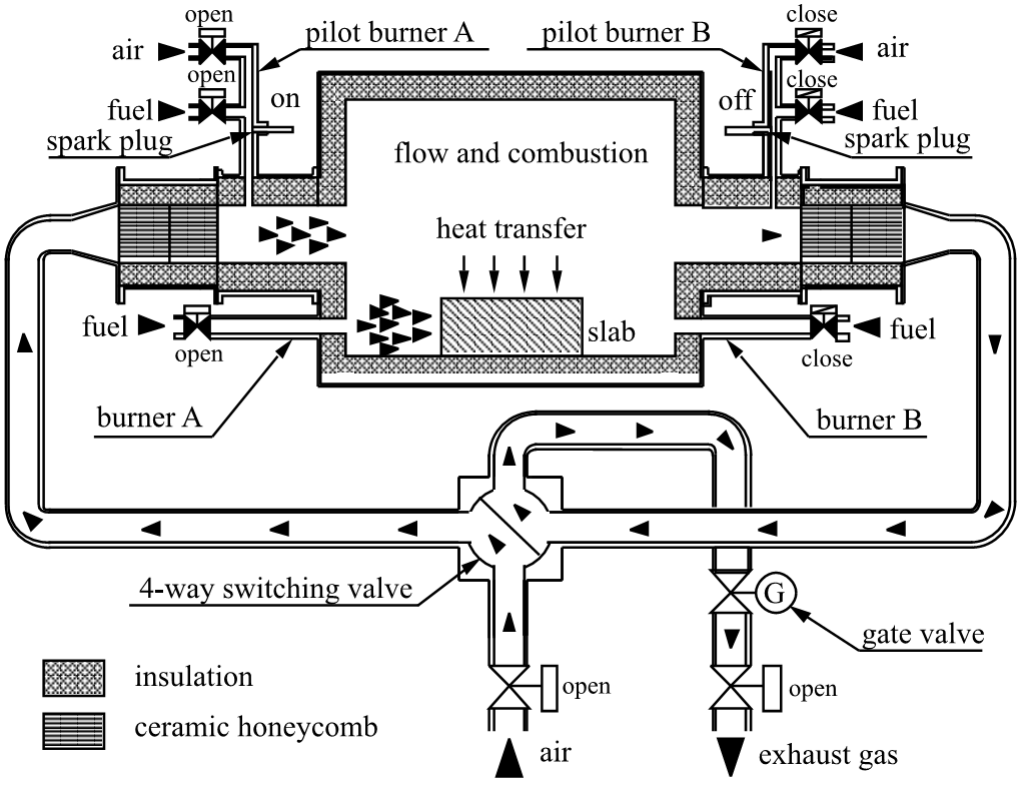


**Figure 2.8: Schematic diagram of an industrial regenerative furnace operating under MILD conditions [62].**

The second burner type was developed by Nakamachi *et al.* [82, 83]. The most prominent example for the second type of burner is the example of a Fuel Direct Injection (FDI) system [83]. This aims to increase the mixing delay between the air and the fuel by placing the air and fuel jets apart from each other. The FDI system allows air and fuel to be diluted by the hot flue gas before they mix and react. The reaction or mixing in the furnace is influenced by the number of fuel ports and the distance between the air and fuel jets [83].

The FDI method was exploited by Cain *et al.* [84] to develop the high velocity Low $NO_x$ Injection (LNI) burner [84]. Similarly, Sobiesiak *et al.* [66] introduced a new multiple jet burner for a concept called a Fuel/Oxidant Direct Injection (FODI) burner. In FODI burners, fuel and oxidant ports are placed uniformly in a circular pattern and both the fuel and the oxidant ports are at an angle in relation to the burner axis [66]. The above burner designs are focused on pollution abatement (i.e. reducing $NO_x$ emissions) and achieving a high thermal efficiency of combustion. These investigations highlighted the role of the mixing characteristics to achieve MILD combustion. In general, enhancing the high entrainment of hot combustion products inside the furnace helps to establish MILD conditions by diluting the mixture. For this purpose, most previous work has used high momentum jets and a relatively large gap between the fuel and air jets. Dilution extends the volume of the reaction zone substantially during MILD combustion. Consequently, a more uniform heat flux with lower peak temperatures can be found during this combustion. Since the peak temperature is lower, a more uniform furnace temperature is achieved during MILD

combustion [85]. Therefore, higher thermal efficiency can be achieved during MILD combustion when compared with conventional combustion [61, 69].

As mentioned in the preceding sections, most previous work on the topic of MILD combustion has been conducted for industrial requirements and the applicability of this technology is still limited to gaseous fuel combustion. Although different burner configurations have been developed for many industrial applications, MILD combustion technology is based on preheating a high level of air (because the external air preheating impacts on the system's thermal efficiency), which has restricted the application of this unique combustion technology.

Weidmann *et al.* [86, 87] reported MILD combustion of highly volatile sub-bituminous Columbian coal in a 7 m long and 500 kW down-fired furnace of 750 mm diameter cylindrical shape. The burner configuration of the combustion furnace consists of a central annulus for injecting coal carried by $CO_2$ and two symmetrically arranged nozzles for supplying combustion air. The combustion air was preheated to 423 K before being introduced into the furnace for these experiments [86, 87]. The investigations were specially focussed on the impact of carrier gas to pollutant (e.g., CO and $NO_x$) emission under coal-MILD combustion conditions. A significant increase of CO and $NO_x$ emissions was measured when $CO_2$ was replaced by air as the carrier gas of coal particles. Stadler *et al.* [76] designed and built a cylindrical, vertical, and top-fired MILD furnace which employ electrical heating for maintaining the wall temperature. The furnace is 4.2 m long and the diameter is 400 mm. The pulverised coal was carried by either air or $N_2$ and supplied through the central jet, while preheated (~575 K) air was supplied through

three jets surrounding the furnace. Szegö *et al.* [55, 88] developed a laboratory-scale recuperative MILD combustion furnace for gaseous fuel, where MILD combustion was achieved successfully without any air preheating. However, the residence time of Szegö's recuperative MILD combustion furnace, MCF, is limited for the complete combustion of the pulverised fuels [74]. To avoid the issue identified in MCF, this current study developed and used a new vertical MILD combustion furnace for pulverised fuel combustion (detail reported in Chapters 5 and 6).

## 2.4. Chemical Steps of Coal Combustion

This section highlights the chemical processes of solid fuel burning, in particular, pulverised coal under MILD combustion conditions. Pulverised fuels came into pre-eminence because of their high combustion intensity [89]. The pulverised coals, as well as pulverised biomass combustion processes, are best described through the following steps: drying, devolatilisation, volatile combustion and char burnout. These successive steps of coal combustion are depicted in Figure 2.9.

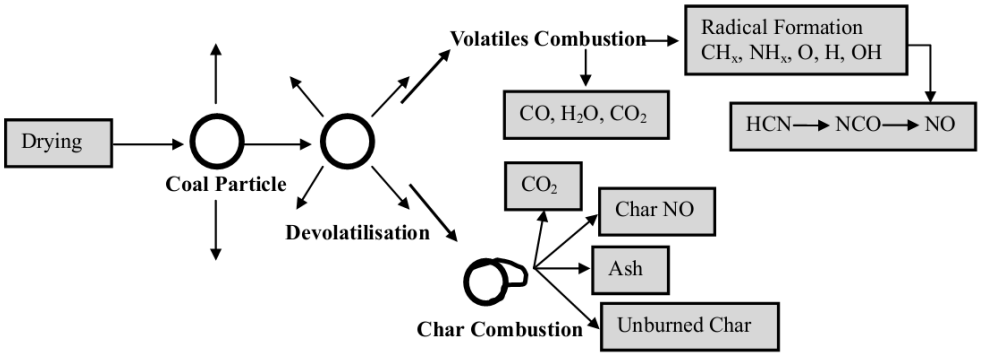


**Figure 2.9: Diagram of the coal combustion steps.**

### 2.4.1. Drying

Drying and/or water vaporisation from pulverised coal is a combination of the heat and mass transfer processes. Coal particles are heated to dry the moisture from the particles in a hot atmosphere by radiation or convection. This process usually occurs very rapidly. The pulverised coal particles are partially/fully dried by the primary hot air or recycled exhaust gas flow into the coal mill during the conventional coal combustion process. The coal particles are pre-dried to eliminate any blockage in the coal carrying pipe. The heating of the coal particles is an important step as it determines the nature of the devolatilisation products, including the char structure [89]. The higher heating effects on the volatiles' release rate that produces different char topography. However, the heating rates vary significantly with different operating conditions and various combustion environments.

### 2.4.2. Devolatilisation

Devolatilisation is the process of evolution of combustible gases from coal particles, due to the thermal decomposition at a temperature above ~580 K [90-93]. It is an endothermic physicochemical transformation of coal. Coal devolatilisation is referred to as pyrolysis when coal is devolatilised in an inert gas [94]. The terms "pyrolysis" and "devolatilisation" are usually not distinguished from one another due to the similar behaviour of coal in the two processes, in terms of char chemistry and the composition of volatile matter. During heating, coal particles are subjected to very complex physical and chemical transformations while yielding volatile matter

and generating solid residues. Coal devolatilisation can be regarded as a two-stage process [95]. The first stage is the decomposition of functional groups of coal particles to release volatile matter, composed of heavy hydrocarbons (tar), and light hydrocarbons. During the second stage of devolatilisation, tar decomposes and produces light hydrocarbons and additional gases. Devolatilisation characteristics of pulverised coals are frequently investigated and reported in the existing literature [48, 90, 96-99] under an inert gas environment, such as nitrogen ($N_2$) and argon (Ar), to avoid the interaction with ambient gases. However, devolatilisation of pulverised fuels under high temperature and a low $O_2$ concentration environment, which is typical of MILD combustion, is not well-understood and further research is required [77, 100].

### 2.4.3. Combustion of Volatiles

The combustion characteristics of volatile matter are substantially varied with particle size, coal type and surrounding temperatures, as well as the operating conditions. However, the variation of volatile combustion phenomena is mainly associated with the coal type and/or rank because the volatile and char contents of coal are significantly varied according to coal type and/or rank. For example, bituminous coal produces more tar yields (long chain hydrocarbons) than lignite and anthracite during the devolatilisation process. Consequently, more soot is formed from the combustion of bituminous coal [48]. The combustion characteristics of volatile matters are reported for conventional (i.e., $O_2/N_2$ environment) and oxy ($O_2/CO_2$) combustion modes [48, 90, 101-103]. Shaddix and Molina [48, 103] reported that oxy-coal combustion requires a longer residence time and lower

temperature than air combustion, using Black Thunder low volatile coal particles in an entrained flow reactor. The low combustion temperature and long residence time of combustion are related to the low volatile and/or $O_2$ diffusion rates in the oxy-coal environment [48]. Although some studies on the volatiles' combustion are available for air and oxy-coal combustion cases, no study has been found which reports volatiles' combustion under MILD combustion conditions.

### 2.4.4. Char Combustion

Micro-porous solids, known as char particles, are produced when the volatile matter is released from the coal particles by the devolatilisation process. The char oxidation rate is controlled by three sequential processes: namely boundary layer diffusion, chemical reaction and pore diffusion [78, 89], in a conventional coal combustion approach. While in MILD-coal combustion, char burning is influenced by the exhaust gas recirculation and heterogeneous reactions with high concentrations of $CO_2$ and $H_2O$ [100].

Few studies [76, 77, 100, 104, 105] on the heterogeneous combustion of char have been conducted using detailed surface chemistry. Heterogeneous reaction rates are governed by the diffusion of the oxidant species from the bulk phase to the particle surface [76, 100]. The overall heterogeneous reaction rate is controlled by two mechanisms: the diffusion of the oxidant through the film layer around the coal particle and the intrinsic kinetic rate of the reaction on the particle surface. However, the mechanism for char oxidation reaction is not completely understood because of a number of factors, such as the reaction due to pore growth and the mass transfer

effects [89, 106]. The char oxidation reaction is further complicated by the influence of the char mineral content, particle size, and fragmentation of the char particles.

## 2.5. Chemical Pollutants Production

A number of gaseous pollutants (e.g., $NO_x$, CO, $CO_2$, and $SO_x$) and particulate matters (e.g., soot and fly ash) are produced by the combustion of pulverised coal. The production and destruction of these pollutants are briefly described in this section.

### 2.5.1. Nitric Oxides ($NO_x$)

Nitrogen oxides ($NO_x$) form one of the predominant anthropogenic sources of air pollution and are a major concern for designers of combustion systems. Nitrogen oxides ($NO_x$) comprise both nitrogen dioxide ($NO_2$) and nitric oxide (NO). Although nitrous oxide ($N_2O$) also contributes to air pollution, $N_2O$ formation is not directly related to combustion and thus $N_2O$ is not included in the $NO_x$ [107].

In general, NO accounts for 95% of total $NO_x$ formation [89, 108] during pulverised coal combustion. Several studies [38, 39, 109-113] have been conducted to evaluate $NO_x$ emissions and their impact on the environment from pulverised coal combustion. Therefore, this sub-section briefly describes the basic NO formation and/or destruction mechanisms namely; thermal-NO, prompt-NO, and fuel-NO, as well as $NO_x$ destruction mechanisms.

### *Thermal NO*

The oxidation of atmospheric nitrogen ($N_2$) through endothermic chemical reactions produces thermal-NO. The production of thermal-NO follows the extended Zel'dovich [114] reactions mechanism:

$$N_2 + O \rightleftharpoons N + NO \quad (2)$$

$$N + O_2 \rightleftharpoons O + NO \quad (3)$$

$$N + OH \rightleftharpoons H + NO \quad (4)$$

Thermal-NO formation is highly temperature dependent. It has been reported that the effect of thermal-NO production is much lower at temperatures below the value of 1800 K [76, 77]. Since the maximum coal MILD combustion temperature is below 1600 K, it has a positive impact on the thermal-NO reduction.

### *Prompt NO*

Prompt-NO [106, 108, 115] is formed by the chemical reaction between $N_2$ and hydrocarbon radicals in fuel-rich combustion conditions. Prompt-NO typically plays a minor role in the overall NO formation under MILD combustion conditions. This is because a strongly diluted mixture of reactants is considered in MILD conditions where hydrocarbons ($C_xH_y$), hydrogen-cyanide (HCN), and nitrogen (N) concentrations decrease to low levels. Nevertheless, the prompt-NO formation occurs during following the key reactions:

$$CH + N_2 \rightleftharpoons HCN + N \quad (5)$$

$$N + O_2 \rightleftharpoons NO + O \quad (6)$$

$$HCN + OH \rightleftharpoons CN + H_2O \quad (7)$$

$$CN + O_2 \rightleftharpoons CO + NO \quad (8)$$

### *Fuel NO*

In coal MILD combustion, the main NO production is represented by the fuel-NO mechanism [77, 78, 100]. Fuel-NO is produced by the oxidation reaction of the incorporated nitrogen (N) in the coal particles. It is presumed [100] that the nitrogen (N) incorporated into the coal particles is entirely released during the devolatilization process and spread out across the volatiles and the char. Thus, there are two evolutionary paths for fuel-NO formation: (i) a share of nitrogen incorporated in the coal is converted into fuel-NO by the devolatilization process; and (ii) a share of the remaining nitrogen in the char is converted into fuel-NO by the reaction with oxygen. The conversion of nitrogen to pollutants takes place via intermediates, namely hydrogen cyanide (HCN) and ammonia ($NH_3$). Then HCN and $NH_3$ are subjected to four competitive reaction routes [116]:

$$HCN + O_2 \longrightarrow NO + products \quad (9)$$

$$NH_3 + O_2 \longrightarrow NO + products \quad (10)$$

$$HCN + NO \longrightarrow N_2 + products \quad (11)$$

$$NH_3 + NO \longrightarrow N_2 + products \quad (12)$$

### *NO-Destruction*

The recirculation of hot products of combustion in the furnace produces a positive reburning of NO and thus contributes to diminishing overall NO emissions from coal

MILD combustion [100, 116]. In the NO-reburning reaction, NO reacts with surrounding hydrocarbons and afterwards reduces, according to the following reaction [100]:

$$C_xH_y + NO \longrightarrow HCN + products \quad (13)$$

### 2.5.2. Carbon monoxide (CO)

Carbon monoxide, CO, is typically produced by the devolatilisation of coal particles, the volatiles' oxidation, and the char combustion reactions for pulverised coal-MILD combustion. The CO formation through the coal devolatilisation and oxidation process is described by a simple two-step gas phase reaction:

$$C_xH_yO_zN_lS_n + \left(\frac{x}{2} + \frac{y}{2} - \frac{z}{2} + n\right) O_2 \longrightarrow xCO + \frac{y}{2}H_2O + \frac{l}{2}N_2 + nSO_2 \quad (14)$$

$$CO + \frac{1}{2}O_2 \rightleftharpoons CO_2 \quad (15)$$

The char combustion reaction is influenced by strong exhaust gas recirculation with high concentrations of $CO_2$ and $H_2O$ under MILD combustion conditions [100]. Therefore, Boudouard (16) and gasification (17) reactions are considered in addition to the oxidation (18) reaction:

$$C_{char} + CO_2 \longrightarrow 2CO \quad (16)$$

$$C_{char} + H_2O \longrightarrow H_2 + CO \quad (17)$$

$$C_{char} + \frac{1}{2}O_2 \longrightarrow CO \quad (18)$$

Carbon monoxide (CO) is a poisonous gas, which can have a lethal effect on human health when a person is exposed to it in high concentrations. When CO is mixed with the haemoglobins of a blood cell, it forms carboxyhemoglobin in the blood. As a consequence, the tissue and cell oxygenation of the body is inhibited [117].

### 2.5.3. Fly Ash Production

Fly ash is a fine grey powder, which is produced through the combination and fragmentation of mineral contents released during coal combustion. The char burn-out rate and surrounding combustion environment, including the temperature, determine the mineral matter's transformation during pulverised coal combustion [118]. Fly ash production, along with the transformation of minerals, is displayed in a schematic diagram in Figure 2.10. The figure depicts that fly ash particles are formed through two mechanisms, namely; vaporization or condensation of heavy metals (e.g., Na, Pb, Cd, and Hg) and chemical transformation of non-volatile species (e.g., $SiO_2$) by oxidation-reduction (redox) reactions [118].

Few experimental and numerical studies [118-121] have been reported on the fly ash production from the air-coal and oxy-coal combustion processes in a furnace environment. The experiments and calculations both indicate that the production rate and composition of fly ash are not dissimilar for air-coal and oxy-coal combustion. It is concluded from the previous investigations [118-121] that the pathway of fly ash production under air/oxy-coal combustion conditions is complex and strongly influenced by the furnace operating conditions, coal rank, and the coal particle sizes. On the other hand, since the establishment of MILD combustion conditions of

pulverised coal through exhaust gas recirculation are more complicated than air/oxy-coal combustion, no studies have been found in the literature on fly ash formations and their control strategies. Therefore, major investigations are being touted to understand the particulate matter production under MILD-coal combustion [33, 47].

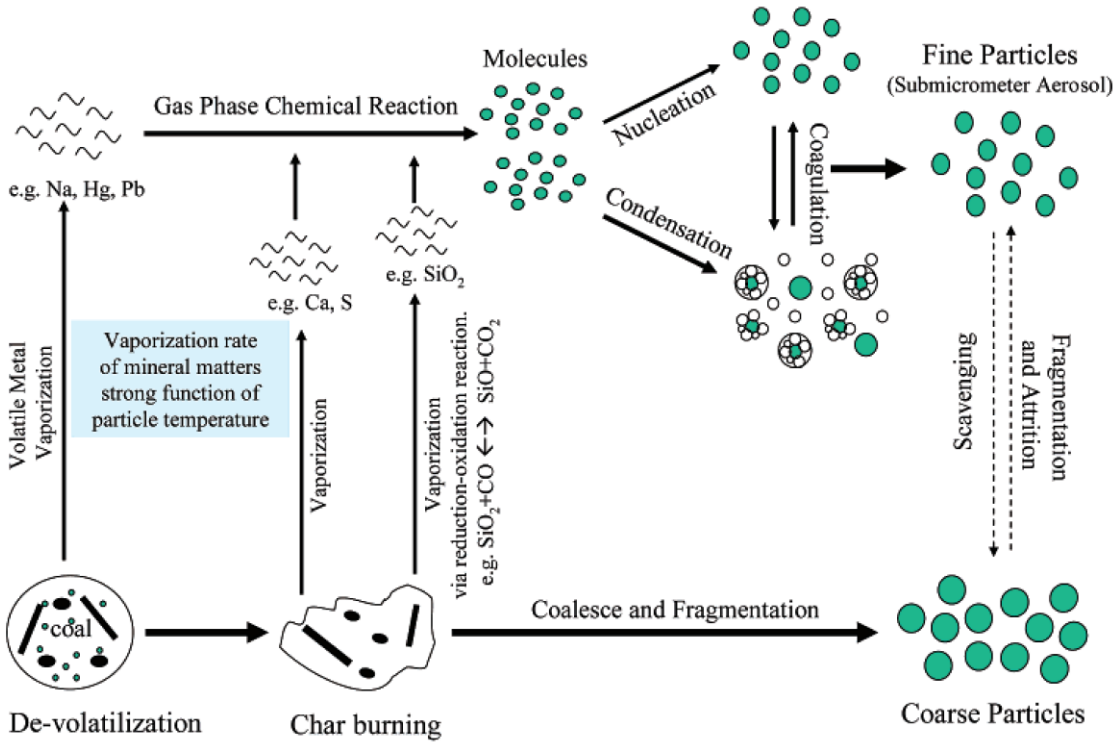


**Figure 2.10: Mineral transformation and particle formation pathways during coal combustion [118].**

## 2.6. State-of-the-art of Solid Fuels under MILD Combustion

Although MILD combustion technology is already applied commercially for gaseous fuels, research on solid fuels, including pulverised coals and biomass, using this technology has received much less attention. The previous sections of this chapter described the substantial potential of MILD combustion technology, using various kinds of fuels. Therefore, it is essential to extend this technology to solid fuels for deepening understanding of many fundamental issues (e.g., stability limits, burning characteristics, pollutant formations and destructions, carbon consumption, and ash deposition). In this section, key findings in the literature on solid fuels' combustion under MILD mode are presented and summarised.

A successful attempt at the MILD combustion of highly volatile pulverised coal of 74 μm particles was reported by Kiga *et al.* [122] using a drop tube furnace. The combustion efficiency of the furnace and $NO_x$ emissions were measured for various air preheating temperatures, excess air ratios and oxygen concentrations. Their experimental measurements suggested that increasing the air preheat resulted in a significant elevation of combustion efficiency, with a substantial reduction of $NO_x$ emissions, when compared with conventional combustion. However, they concluded that "the use of high-temperature diluted air was not suitable for stable pulverised coal combustion" because of the slow combustion rate under low-oxygen combustion conditions. Weber *et al.* [70, 73, 123] at the International Flame Research Foundation (IFRF) conducted a series of experimental investigations in a 0.58 MW furnace. The experimental findings of Weber *et al.* [70, 73, 123] are

somewhat contradictory to the conclusions of Kiga *et al.* [122] in terms of stable pulverised coal MILD combustion. The results reported a substantial $NO_x$ diminution potential for MILD combustion of highly volatile bituminous coal. However, the basic routes of $NO_x$ production/destruction were not understood from these experiments. An experimental investigation of the $NO_x$ emissions in the air, argon/oxygen, and $CO_2/O_2$ atmospheres for MILD combustion of pulverised lignite and bituminous coal was carried out by Stadler *et al.* [76]. A large reduction of NO was reported under MILD combustion conditions, which findings were similar to Weber *et al.* [73]. However, they reported the necessity for a sophisticated numerical model to analyse the $NO_x$ formation phenomenon under MILD combustion.

To investigate the impact of air preheating on the MILD combustion characteristics of anthracite and bituminous coal, Suda *et al.* [124] reported an experimental observation where it was found that the coal particles' ignition delay and $NO_x$ emissions were decreased significantly by raising the combustion air temperature. The authors concluded that further investigation is required to clarify the $NO_x$ formation/destruction mechanism for coal MILD combustion technology. He *et al.* [125] conducted a numerical investigation of the experiments carried out by Suda *et al.* [124] and found that for high rank coal (anthracite), NO is predominantly produced from the char-nitrogen, whose production/destruction mechanism is yet to be understood.

Schaffel *et al.* [78] modelled the IFRF furnace using an advanced Chemical Percolation Devolatilization (CPD) model, along with a char combustion intrinsic reactivity model, and reported the existence of strong NO-reburning mechanisms in

coal MILD combustion. However, the authors [78] reported the limitations of CFD modelling to predict CO formation and highlighted the need for a more elaborate volatile matter combustion model. Vascellari and Cau [100] reported a numerical study to probe the impact of turbulence-chemistry interactions on the prediction of pulverised coal MILD combustion. In particular, two turbulence-chemistry interaction models were investigated; namely: the conventional Eddy Dissipation Model (EDM), based on infinitely fast chemistry assumptions, and the advanced Eddy Dissipation Concept (EDC) model based on finite-rate chemistry. As expected, the EDC model reproduced the experimental results more effectively than the EDM model. The gas-phase reactions were modelled using either a detailed kinetic mechanism (consisting of 103 reactions) or a global kinetic mechanism (consisting of 2 reactions). However, no significant benefits were noticed when using the detailed kinetic mechanisms for the prediction of coal MILD combustion, when compared with the global kinetic mechanisms. In addition, detailed kinetic mechanisms require more computational time and do not seem to add any major benefits. Mei *et al.* [77] investigated the impacts of reactants' injection velocities on the stability and pollutant emissions of coal MILD combustion numerically, using the geometry and experimental conditions of IFRF furnaces [73]. They found that raising the velocity of the primary air played a significant role in decreasing the combustion temperature and overall $NO_x$ emissions. Tu *et al.* [104, 105] investigated the MILD combustion characteristics of pulverised bituminous coal under $O_2/N_2$ and $O_2/CO_2$ atmospheres using simplified combustion models numerically and reported that oxy-MILD

combustion has a great potential for reducing $NO_x$ formation and increasing heat release intensities via radiation and convection.

An experimental investigation of MILD combustion of bituminous coal, using a cylindrical bench-scale furnace, was reported by Tamura *et al.* [126], where they found overall $NO_x$ emission was reduced by increasing the residence time of the coal particles. However, they reported the difficulties of achieving MILD combustion with existing furnace start-up procedures and noted the need for new burner configurations which can operate and are able to switch between conventional and MILD modes.

An integrated air staging burner, combined with MILD combustion technology, in a cylindrical down-fired furnace, has been developed as part of a European Union supported project called FLOX-COAL [86, 87, 127, 128]. In these experiments, the high-volatile sub-bituminous coal carried either by air or $CO_2$ is injected into the furnace via a central pipe. The preheated (378 K) secondary air is supplied through a nozzle located on the circumference of the primary jet, while the tertiary air is impinged from downstream. They found an increased CO concentration in the primary combustion zone owing to the char gasification reaction caused by $CO_2$ and $H_2O$. However, a stable, attached flame did not appear during their experiments and they concluded that further optimisation of the burner geometry is necessary in order to achieve stable MILD combustion of pulverised coal.

Recently, Liu *et al.* [129] reported the optimum operating conditions of pulverised coal combustion under oxy-MILD modes in a lab-scale cylindrical furnace with

high-velocity oxygen jets. They calculated the ignition delay for Datong bituminous coal-MILD combustion with a mean particle size of 60 μm is approximately 4 ms under a coaxial jets condition, while the ignition delay is extended to 10-15 ms under co-flow jet conditions. However, they reported that extended reaction kinetics are required to capture the accurate characteristics of the oxy-MILD coal combustion process.

MILD combustion of other solid fuels like biomass and wastes has not been investigated as comprehensively as pulverised coal. Lou and Ma [130] investigated the $NO_x$ formation behaviour of biomass fuels under MILD combustion conditions using high temperature air. Rice husk and saw dust were used as biomass fuels and combusted with high temperature air (600-1200 °C) in a medium of various oxygen concentrations. The influence of the air temperature, the oxygen content in the air, and the water content of biomass fuels on the $NO_x$ emissions was investigated. Since the fixed carbon (char) in rice husk is higher than in saw dust, the $NO_x$ emission (~150 ppm) was reduced by 20% during the combustion of rice husk in comparison with sawdust fuel because of the greater de-oxidisation effect on $NO_x$. The increasing trend of $NO_x$ was observed for higher air temperatures under the same air-fuel proportions and that the water contents of biomass fuel have a positive effect on $NO_x$ reduction. The $NO_x$ concentration was decreased by up to 70% for 30% moisture contents in biomass fuel. This was explained as resulting from water vapour formation decreasing the local oxygen concentration, at the same time as the carbon reacted with water to form CO and $H_2$ and generated a reductive atmosphere, so the $NO_x$ reacted with not only with the carbon but also with CO and $H_2$. They deoxidised

$NO_x$ to $N_2$ and decreased the $NO_x$ concentration further. The authors concluded that MILD combustion of biomass fuel has a great potential to reduce $NO_x$ emissions because the biomass contains high levels of fixed carbon. However, they only considered the thermal $NO_x$ mechanism. Hence, there is a need for further investigation of absolute $NO_x$ emissions from biomass fuels considering fuel $NO_x$ mechanism, in particular for those containing higher levels of nitrogen, such as for fuels like rice husk (1.88% N).

An experimental study on the MILD combustion behaviour of wood pellets (biomass) and bituminous coal particles, with a diameter equal to 15 mm, in various oxygen concentrations, in a small scale batch reactor, was performed by Ponzio *et al.* [131, 132]. Three different ignition behaviours of fuels were found by varying the local oxygen concentrations (from 5% - 100%) and oxidizer temperatures. The three ignition mechanisms were: a) *sparking ignition* of fuels when the oxygen concentrations (21 - 100%) and oxidizer temperatures (1073 - 1273K) were both high due to the heterogeneous oxidation of non-devolatalised coal, b) *flaming ignition* of fuels when the oxygen concentration (5−30%) was low but the oxidizer temperature (1073 - 1273K) was high due to the homogeneous combustion of volatiles and c) *glowing surface ignition* with no visible flame at the condition of low oxygen concentration (5 - 10%) and low oxidiser temperature (873K) due to the heterogeneous oxidation of char. However, the ignition behaviour of solid fuels is not a material property but depends strongly on the surrounding conditions (e.g. the temperature and oxygen concentrations of the oxidiser). The transition from

heterogeneous char ignition to homogeneous volatile ignition is not understood from this study and is suggested as being worthy of further investigation.

Dally *et al.* [74, 133] have successfully achieved MILD combustion without air preheating during the burning of sawdust as a solid biomass fuel in a laboratory scale MILD combustion furnace fitted with a parallel jet burner. They found that parallel jet burner permits the initial mixing of sawdust at high jet momenta with a combustion product that dilutes the mixture very fast by reducing the residence time. However, after analysing the ash content, it was suggested that the residence time was not sufficient for complete combustion of the biomass fuel. The authors concluded that further research is required to verify the effect of residence time on carbon burnout and the resulting emissions in the recuperative furnace.

### 2.6.1 Summary

It is evident from the discussion in the preceding sections that MILD combustion offers great advantages over existing combustion modes to improve thermal efficiency and reduce pollutant emissions from solid fuels. However, for the implementation of this technology, new challenges have been identified including: the potential for $NO_x$ formation and ash deposition, improving the stabilization of solid fuel-MILD combustion due to the lower adiabatic flame temperature, delayed ignition and lower burning rates in a highly diluted environment. Therefore, more research is required to fathom the depth of MILD combustion of solid fuels by addressing these technological challenges in order to reach the full potential of this process.

## 2.7. Research Gaps

Although some studies on MILD combustion of pulverised coals and biomass have appeared in the literature, limited information is available related to the stability of MILD combustion for pulverised fuels. Also, there is a lack of a thorough understanding of fundamental aspects of solid fuel combustion using this unique technology. Moreover, the burning of low rank coal (i.e., pulverised brown coal) under MILD combustion is yet to be fully explored. In addition, since brown coal is considered the cheapest and most available energy source [6] amongst the various fuel types in the world, it is imperative to extend this technology to brown coal. Hence, the specific gaps identified from the published research on MILD combustion of solid fuels are as follows:

1. A lack of detailed experimental studies on the MILD combustion of solid fuels, including biomass and pulverised coal, to understand the combustion characteristics (e.g. temperature distribution, chemical species fields, and exhaust emissions) and facilitate a better understanding of the formation and destruction of pollutants, like CO and NO. Distinguishable combustion characteristics and the variations of devolatilisation, volatile oxidation and char combustion processes are expected to be found for differently ranked pulverised coals due to the distinctive physical properties and chemical structures. These characteristics under MILD combustion conditions need to be further investigated;

2. No systematic study has been carried out to develop understanding of the influence of the devolatilisation model on the prediction of coal combustion under MILD conditions;

3. No reliable numerical model was found for low rank Australian brown coal or high rank Australian black coal under MILD combustion. The low rank Australian brown coal (e.g., Victorian brown coal) deserves special attention because of its desirable burning characteristics, including its high reactivity owing to a high volatile content, generally low ash content, and low sulphur and heavy metals [134], while Australian black coal is a high rank coal which has a higher heating value than other solid fuels such as biomass and brown coal [8] ;

4. No study has been found in the literature that reports the impact of the surrounding flow (i.e., vitiated co-flow) and thermal fields on the volatiles' release and reaction from pulverised coal burning under MILD conditions. In particular, no systematic study has been conducted to understand the influence of the turbulence field and the effect of co-flow $O_2$ concentrations, as well as co-flow temperature on the MILD combustion characteristics of pulverised coal;

5. No study has been found in the literature to understand the impact of particle size on the burning characteristics, in particular, volatiles' release and the reactions of pulverised brown coal under MILD combustion conditions which is relevant to practical combustion systems.

6. There are very few studies on the combination of MILD combustion technology and oxy-fuel combustion technology for solid fuels. However, no study has been conducted to predict optimum $CO_2/O_2$ ratios for high volatile low rank coal combustion, in order to establish stable MILD-oxy combustion. In addition, little information is available about the phase changes, coagulation, size distribution, and element partitions of the fly ash in a high $CO_2$ environment of MILD-oxy coal combustion.

## 2.8. Research Aims

The main objective of this research is to understand the basic chemical and physical phenomena that characterise pulverised coal combustion in the MILD regime. The specific aims of this research are as follows:

1. To characterise the MILD regime in a furnace environment burning pulverised coal (low rank brown coal and high rank black coal) through a combined experimental and numerical modelling approach;

2. To analyse the role of devolatilisation models on the prediction accuracy of pulverised coal MILD combustion;

3. To develop simplified numerical models for Australian high volatile brown coal and low volatile black/hard coal, optimised for the MILD combustion conditions. In addition, to develop better understanding of $NO_x$ formation

(fuel, thermal, and prompt $NO_x$) and destruction mechanisms ($NO_x$ reburning) for pulverised coal MILD combustion;

4. To conduct a comprehensive experimental and numerical investigation to probe the influence of jet inlet velocities of pulverised brown coal on the flame stability and pollutants' formation and destruction under MILD combustion conditions;

5. To evaluate the effects of particles' size on the burning characteristics (in-furnace temperature profile, chemical species, and exhaust emissions) of pulverised brown coal under MILD combustion conditions through experimental and numerical investigations;

6. To analyse the effect of vitiated co-flow $O_2$ concentrations and co-flow temperature on the MILD combustion characteristics of the pulverised brown coal.

## References

[1] J. Warnatz, U. Maas, and R. W. Dibble, *Combustion: physical and chemical fundamentals, modeling and simulation, experiments, pollutant formation*: Springer Verlag, 2006.

[2] C. K. Law, *Combustion Physics*: Cambridge University Press, 2006.

[3] International Energy Agency, *Coal Information 2010*. University of Manchester: OECD Publishing, 2010.

[4] M. Beychok and M. Perry, *Coal*, 2007 Available: http://www.eoearth.org/view/article/151276/ (accessed on 14/03/2016)

[5] World Coal Association. *Coal Facts*, 2014 Available: http://www.worldcoal.org/coal-facts-2014 (accessed on 14/03/2016)

[6] U.S. Energy Information Administration. *International Energy Outlook 2015*; U.S. Department of Energy (DOE): Washington, DC, 2015. Available: http://www.eia.gov/forecasts/aeo/index.cfm (accessed on 10/03/2016)

[7] A. D. Ellerman, "The world price of coal," *Energy Policy*, vol. 23, pp. 499-506, 1995.

[8] Australian Government, Geoscience Australia, *Australian Black Coal*. Available:http://www.australianminesatlas.gov.au/aimr/commodity/black_coal.html (accessed on 14/03/2016)

[9] M. F. Demirbas, M. Balat, and H. Balat, "Potential contribution of biomass to the sustainable energy development," *Energy Conversion and Management*, vol. 50, pp. 1746-1760, 7// 2009.

[10] A. Demirbaş, "Biomass resource facilities and biomass conversion processing for fuels and chemicals," *Energy Conversion and Management,* vol. 42, pp. 1357-1378, 2001.

[11] A. Demirbas, "Conversion of corn stover to chemicals and fuels," *Energy Sources, Part A,* vol. 30, pp. 788-796, 2008.

[12] M. Hoogwijk, A. Faaij, B. Eickhout, B. de Vries, and W. Turkenburg, "Potential of biomass energy out to 2100, for four IPCC SRES land-use scenarios," *Biomass and Bioenergy,* vol. 29, pp. 225-257, 2005.

[13] A. Demirbaş, "Global renewable energy resources," *Energy Sources,* vol. 28, pp. 779-792, 2006.

[14] M. Balat, "Biomass energy and biochemical conversion processing for fuels and chemicals," *Energy Sources, Part A,* vol. 28, pp. 517-525, 2006.

[15] M. Balat and K. Bozbas, "Wood as an energy source: potential trends, usage of wood, and energy politics," *Energy Sources, Part A,* vol. 28, pp. 837-844, 2006.

[16] J. C. Abanades, E. J. Anthony, J. Wang, and J. E. Oakey, "Fluidized bed combustion systems integrating $CO_2$ capture with CaO," *Environmental Science & Technology,* vol. 39, pp. 2861-2866, 2005.

[17] S. Oka, *Fluidized bed combustion*: CRC Press, 2003.

[18] E. Anthony, "Fluidized bed combustion of alternative solid fuels; status, successes and problems of the technology," *Progress in Energy and Combustion Science,* vol. 21, pp. 239-268, 1995.

[19] J. Koornneef, M. Junginger, and A. Faaij, "Development of fluidized bed combustion-An overview of trends, performance and cost," *Progress in Energy and Combustion Science*, vol. 33, pp. 19-55, 2007.

[20] A. Lyngfelt, B. Leckner, and T. Mattisson, "A fluidized-bed combustion process with inherent $CO_2$ separation; application of chemical-looping combustion," *Chemical Engineering Science*, vol. 56, pp. 3101-3113, 2001.

[21] B. Leckner, "Fluidized bed combustion: mixing and pollutant limitation," *Progress in Energy and Combustion Science*, vol. 24, pp. 31-61, 1998.

[22] E. E. Khalil, *Power Plant Design*: Abacus Press/Gordon and Breach Science Publishers, 1990.

[23] S. Kakac, *Boilers, Evaporators and Condensers*: John Wiley & Sons, 1991.

[24] P. Kiameh, *Power Generation Handbook: Selection, Applications, Operation, and Maintenance*: McGraw-Hill, 2003.

[25] J. P. Longwell, E. S. Rubin, and J. Wilson, "Coal: Energy for the Future," *Progress in Energy and Combustion Science*, vol. 21, pp. 269-360, 1995.

[26] J. M. Beér, "High efficiency electric power generation: The environmental role," *Progress in Energy and Combustion Science*, vol. 33, pp. 107-134, 2007.

[27] D. Zhang, *Ultra-Supercritical Coal Power Plants: Materials, Technologies and Optimisation*: Elsevier, 2013.

[28] R. Geosits and L. Schmoe, "IGCC–The challenges of integration," presented at the Proceedings of GT2005 ASME Turbo Expo 2005: Power for Land, Sea, and Air, Nevada, USA, 2005.

[29] S. Kramer, "Gasification Plant Cost and Performance Optimization," US Department of Energy, National Energy Technology Laboratory (NETL), US DE-AC26-99FT40342, September, 2003 2003.

[30] T. Johnson, "Future options for brown coal based electricity generation–the role of IDGCC," in *ANZSES Conference: Destination Renewables*, Melbourne, Australia, 2003.

[31] J. Goodell, *Big Coal: the Dirty Secret Behind America's Energy Future*. New York: Houghton Mifflin Harcourt, 2007.

[32] J. Katzer, E. Moniz, J. Deutch, S. Ansolabehere, and J. Beer, "The future of coal: an interdisciplinary MIT study," Technical report, Massachusetts Institute of Technology, Cambridge, MA2007.

[33] L. Chen, S. Z. Yong, and A. F. Ghoniem, "Oxy-fuel combustion of pulverized coal: Characterization, fundamentals, stabilization and CFD modeling," *Progress in Energy and Combustion Science*, vol. 38, pp. 156-214, 2012.

[34] B. J. P. Buhre, L. K. Elliott, C. Sheng, R. P. Gupta, and T. F. Wall, "Oxy-fuel combustion technology for coal-fired power generation," *Progress in Energy and Combustion Science*, vol. 31, pp. 283-307, 2005.

[35] P. Sabia, G. Sorrentino, A. Chinnici, A. Cavaliere, and R. Ragucci, "Dynamic Behaviors in Methane MILD and Oxy-Fuel Combustion. Chemical Effect of $CO_2$," *Energy & Fuels*, vol. 29, pp. 1978-1986, 2015.

[36] H. J. Herzog, "Scaling up carbon dioxide capture and storage: From megatons to gigatons," *Energy Economics*, vol. 33, pp. 597-604, 2011.

[37] S. Chu, "Carbon capture and sequestration," *Science,* vol. 325, pp. 1599-1599, 2009.

[38] F. Normann, K. Andersson, B. Leckner, and F. Johnsson, "Emission control of nitrogen oxides in the oxy-fuel process," *Progress in Energy and Combustion Science,* vol. 35, pp. 385-397, 10, 2009.

[39] M. B. Toftegaard, J. Brix, P. A. Jensen, P. Glarborg, and A. D. Jensen, "Oxy-fuel combustion of solid fuels," *Progress in Energy and Combustion Science,* vol. 36, pp. 581-625, 2010.

[40] P. Glarborg and L. L. B. Bentzen, "Chemical effects of a high CO2 concentration in oxy-fuel combustion of methane," *Energy & Fuels,* vol. 22, pp. 291-296, 2007.

[41] E. Croiset, K. Thambimuthu, and A. Palmer, "Coal combustion in $O_2/CO_2$ mixtures compared with air," *The Canadian Journal of Chemical Engineering,* vol. 78, pp. 402-407, 2000.

[42] J. Zhang, B. Dai, Y. Meng, X. Wu, J. Zhang, X. Zhang, *et al.*, "Pilot-scale experimental and CFD modeling investigations of oxy-fuel combustion of Victorian brown coal," *Fuel,* 2014.

[43] J. Zhang, W. Prationo, L. Zhang, and Z. Zhang, "Computational fluid dynamics modeling on the air-firing and oxy-fuel combustion of dried Victorian brown coal," *Energy & Fuels,* vol. 27, pp. 4258-4269, 2013.

[44] B. Roy, W. L. Choo, and S. Bhattacharya, "Prediction of distribution of trace elements under oxy-fuel combustion condition using Victorian brown coals," *Fuel,* 2012.

[45] I. Bolea, L. M. Romeo, and D. Pallarés, "The role of external heat exchangers in oxy-fuel circulating fluidized bed," *Applied Energy*, vol. 94, pp. 215-223, 2012.

[46] A. H. Al-Abbas, J. Naser, and D. Dodds, "CFD modelling of air-fired and oxy-fuel combustion in a large-scale furnace at Loy Yang A brown coal power station," *Fuel*, vol. 102, pp. 646-665, 2012.

[47] S. Chen and C. Zheng, "Counterflow diffusion flame of hydrogen-enriched biogas under MILD oxy-fuel condition," *International Journal of Hydrogen Energy*, vol. 36, pp. 15403-15413, 2011.

[48] C. R. Shaddix and A. Molina, "Particle imaging of ignition and devolatilization of pulverized coal during oxy-fuel combustion," *Proceedings of the Combustion Institute*, vol. 32, pp. 2091-2098, 2009.

[49] S. Seepana and S. Jayanti, "Flame structure and NO generation in oxy-fuel combustion at high pressures," *Energy Conversion and Management*, vol. 50, pp. 1116-1123, 2009.

[50] N. Krishnamurthy, P. Paul, and W. Blasiak, "Studies on low-intensity oxy-fuel burner," *Proceedings of the Combustion Institute*, vol. 32, pp. 3139-3146, 2009.

[51] H. K. Kim, Y. Kim, S. M. Lee, and K. Y. Ahn, "NO reduction in 0.03–0.2 MW oxy-fuel combustor using flue gas recirculation technology," *Proceedings of the Combustion Institute*, vol. 31, pp. 3377-3384, 2007.

[52] S. R. Turns, *An introduction to combustion: concepts and applications*, 2nd ed. vol. 10: McGraw-Hill New York, 2000.

[53] S. Singer, L. Chen, and A. F. Ghoniem, "The influence of gasification reactions on char consumption under oxy-combustion conditions: Effects of particle trajectory and conversion," *Proceedings of the Combustion Institute,* vol. 34, 2012.

[54] I. B. Özdemir and N. Peters, "Characteristics of the reaction zone in a combustor operating at mild combustion," *Experiments in Fluids,* vol. 30, pp. 683-695, 2001.

[55] G. G. Szegö, B. B. Dally, and G. J. Nathan, "Scaling of $NO_x$ emissions from a laboratory-scale mild combustion furnace," *Combustion and Flame,* vol. 154, pp. 281-295, 2008.

[56] S. Orsino, R. Weber, and U. Bollettini, "Numerical simulation of combustion of natural gas with high-temperature air," *Combustion Science and Technology,* vol. 170, pp. 1-34, 2001.

[57] E. Mastorakos, A. Taylor, and J. Whitelaw, "Extinction of turbulent counterflow flames with reactants diluted by hot products," *Combustion and Flame,* vol. 102, pp. 101-114, 1995.

[58] A. Milani and A. Saponaro, "Diluted combustion technologies," *IFRF Combustion Journal,* vol. 1, pp. 1-32, 2001.

[59] A. Cavaliere and M. de Joannon, "Mild combustion," *Progress in Energy and Combustion Science,* vol. 30, pp. 329-366, 2004.

[60] B. B. Dally, E. Riesmeier, and N. Peters, "Effect of fuel mixture on moderate and intense low oxygen dilution combustion," *Combustion and Flame,* vol. 137, pp. 418-431, 2004.

[61] H. Tsuji, A. Gupta, T. Hasegawa, M. Katsuki, K. Kishimoto, and M. Morita, *High Temperature Air Combustion: From Energy Conservation to Pollution Reduction* vol. 4. Boca Raton, FL: CRC Press, 2003.

[62] M. Katsuki and T. Hasegawa, "The science and technology of combustion in highly preheated air," *Proceedings of the Combustion Institute,* vol. 27, pp. 3135-3146, 1998.

[63] F. J. Weinberg, "Combustion in heat-recirculating burners," *Advanced Combustion Methods,* pp. 183-236, 1986.

[64] J. Wünning and J. Wünning, "Flameless oxidation to reduce thermal NO-formation," *Progress in Energy and Combustion Science,* vol. 23, pp. 81-94, 1997.

[65] M. de Joannon, A. Matarazzo, P. Sabia, and A. Cavaliere, "Mild combustion in Homogeneous Charge Diffusion Ignition (HCDI) regime," *Proceedings of the Combustion Institute,* vol. 31 II, pp. 3409-3416, 2007.

[66] A. Sobiesiak, S. Rahbar, and H. A. Becker, "Performance characteristics of the novel low-$NO_x$ CGRI burner for use with high air preheat," *Combustion and Flame,* vol. 115, pp. 93-125, 1998.

[67] M. de Joannon, P. Sabia, and A. Cavaliere, *MILD Combustion* vol. 5. Verlag, Germany: Wiley-Vch, 2010.

[68] S. Kumar, P. Paul, and H. Mukunda, "Studies on a new high-intensity low-emission burner," *Proceedings of the Combustion Institute,* vol. 29, pp. 1131-1137, 2002.

[69] R. Weber, S. Orsino, N. Lallemant, and A. Verlaan, "Combustion of natural gas with high-temperature air and large quantities of flue gas," *Proceedings of the Combustion Institute,* vol. 28, pp. 1315-1321, 2000.

[70] R. Weber, A. Lverlaan, S. Orsino, and N. Lallemant, "On emerging furnace design methodology that provides substantial energy savings and drastic reductions in $CO_2$, CO and NOx emissions," *Journal of the Institute of Energy,* vol. 72, pp. 77-83, 1999.

[71] J. Wünning, "Method for apparatus for combusting fuel in a combustion chamber," U.S. Patent 5154599, 1992.

[72] A. Cavigiolo, M. A. Galbiati, A. Effuggi, D. Gelosa, and R. Rota, "Mild combustion in a laboratory-scale apparatus," *Combustion Science and Technology,* vol. 175, pp. 1347-1367, 2003.

[73] R. Weber, J. P. Smart, and W. Kamp, "On the (MILD) combustion of gaseous, liquid, and solid fuels in high temperature preheated air," *Proceedings of the Combustion Institute,* vol. 30, pp. 2623-2629, 2005.

[74] B. B. Dally, S. H. Shim, R. A. Craig, P. J. Ashman, and G. G. Szegö, "On the burning of sawdust in a MILD combustion furnace," *Energy and Fuels,* vol. 24, pp. 3462-3470, 2010.

[75] H. Stadler, D. Toporov, M. Förster, and R. Kneer, "On the influence of the char gasification reactions on NO formation in flameless coal combustion," *Combustion and Flame,* vol. 156, pp. 1755-1763, 2009.

[76] H. Stadler, D. Ristic, M. Förster, A. Schuster, R. Kneer, and G. Scheffknecht, "$NO_x$-emissions from flameless coal combustion in air, $Ar/O_2$ and $CO_2/O_2$," *Proceedings of the Combustion Institute,* vol. 32, pp. 3131-3138, 2009.

[77] Z. Mei, P. Li, F. Wang, J. Zhang, and J. Mi, "Influences of reactant injection velocities on moderate or intense low-oxygen dilution coal combustion," *Energy & Fuels*, vol. 28, pp. 369-384, 2013.

[78] N. Schaffel, M. Mancini, A. Szlek, and R. Weber, "Mathematical modeling of MILD combustion of pulverized coal," *Combustion and Flame*, vol. 156, pp. 1771-1784, 2009.

[79] N. Rafidi, W. Blasiak, and A. K. Gupta, "High-temperature air combustion phenomena and its thermodynamics," *Journal of Engineering for Gas Turbines and Power*, vol. 130, pp. 1-8, 2008.

[80] M. Flamme, "Low $NO_x$ combustion technologies for high temperature applications," *Energy Conversion and Management*, vol. 42, pp. 1919-1935, 2001.

[81] F. Weinberg, "Heat-recirculating burners: Principles and some recent developments," *Combustion Science and Technology*, vol. 121, pp. 3-22, 1996.

[82] M. Matsumoto, I. Nakamachi, S. Yasuoka, N. Saiki, and T. Koizumi, "Advanced fuel direct injection-FDI system," in *$11^{th}$ IFRF Members Conference*, 1995.

[83] I. Nakamachi, K. Yasuzawa, T. Miyahara, and T. Nagata, "Apparatus or method for carrying out combustion in a furnace," U.S. Patent 4945841, 1990.

[84] B. Cain, T. Robertson, and J. Newby, "The Development and Application of Direct Fuel Injection Techniques for Emissions reduction in High

Temperature Furnaces," in *2nd International Seminar on High Temperature Combustion in Industrial Furnaces*, Stockholm, Sweden, 2000.

[85] S. Som and A. Datta, "Thermodynamic irreversibilities and exergy balance in combustion processes," *Progress in Energy and Combustion Science,* vol. 34, pp. 351-376, 2008.

[86] M. Weidmann, V. Verbaere, G. Boutin, D. Honoré, S. Grathwohl, G. Goddard, *et al.*, "Detailed investigation of flameless oxidation of pulverized coal at pilot-scale (230 $kW_{th}$)," *Applied Thermal Engineering,* vol. 74, pp. 96 - 101, 2015.

[87] M. Weidmann, D. Honoré, V. Verbaere, G. Boutin, S. Grathwohl, G. Godard, *et al.*, "Experimental characterization of pulverized coal MILD flameless combustion from detailed measurements in a pilot-scale facility," *Combustion and Flame,* DOI: 10.1016/j.combustflame.2016.01.029, In Press, 2016.

[88] G. G. Szegö, B. B. Dally, and G. J. Nathan, "Operational characteristics of a parallel jet MILD combustion burner system," *Combustion and Flame,* vol. 156, pp. 429-438, 2009.

[89] A. Williams, M. Pourkashanian, and J. Jones, "Combustion of pulverised coal and biomass," *Progress in Energy and Combustion Science,* vol. 27, pp. 587-610, 2001.

[90] A. Molina and C. R. Shaddix, "Ignition and devolatilization of pulverized bituminous coal particles during oxygen/carbon dioxide coal combustion," *Proceedings of the Combustion Institute,* vol. 31, pp. 1905-1912, 2007.

[91] J. C. Chen, C. Castagnoli, and S. Niksa, "Coal devolatilization during rapid transient heating. 2. Secondary pyrolysis," *Energy & Fuels,* vol. 6, pp. 264-271, 1992.

[92] S. K. Ubhayakar, D. B. Stickler, C. W. Von Rosenberg Jr, and R. E. Gannon, "Rapid devolatilization of pulverized coal in hot combustion gases," *Symposium (International) on Combustion*, vol. 16, pp. 427-436, 1977.

[93] H. Kobayashi, J. Howard, and A. F. Sarofim, "Coal devolatilization at high temperatures," *Proceedings of the Combustion Institute,* vol. 16, pp. 411-425, 1977.

[94] J. Yu, J. A. Lucas, and T. F. Wall, "Formation of the structure of chars during devolatilization of pulverized coal and its thermoproperties: A review," *Progress in Energy and Combustion Science,* vol. 33, pp. 135-170, 2007.

[95] D. Förtsch, F. Kluger, U. Schnell, H. Spliethoff, and K. R. Hein, "A kinetic model for the prediction of NO emissions from staged combustion of pulverized coal," *Proceedings of the Combustion Institute,* vol. 27, pp. 3037-3044, 1998.

[96] E. Biagini and L. Tognotti, "A generalized procedure for the devolatilization of biomass fuels based on the chemical components," *Energy & Fuels,* vol. 28, pp. 614-623, 2014.

[97] X. Huang, J. Li, Z. Liu, M. Yang, D. Wang, and C. Zheng, "Ignition and Devolatilization of Pulverized Coals in Lower Oxygen Content $O_2/CO_2$ Atmosphere," in *Cleaner Combustion and Sustainable World*, ed Verlag: Springer, 2013, pp. 99-104.

[98] F. J. Higuera, "Numerical simulation of the devolatilization of a moving coal particle," *Combustion and Flame,* vol. 156, pp. 1023-1034, 2009.

[99] R. J. Tyler, "Flash pyrolysis of coals. 1. Devolatilization of a Victorian brown coal in a small fluidized-bed reactor," *Fuel,* vol. 58, pp. 680-686, 1979.

[100] M. Vascellari and G. Cau, "Influence of turbulence–chemical interaction on CFD pulverized coal MILD combustion modeling," *Fuel,* vol. 101, pp. 90-101, 2012.

[101] P. A. Bejarano and Y. A. Levendis, "Single-coal-particle combustion in $O_2/N_2$ and $O_2/CO_2$ environments," *Combustion and Flame,* vol. 153, pp. 270-287, 2008.

[102] C. Stivers and Y. Levendis, "Ignition of single coal particles in $O_2/N_2/CO_2$ atmospheres," in *Proceedings of the 35$^{th}$ Coal Utilization and Fuel Systems International Conference, Clearwater, Florida*, 2010.

[103] C. R. Shaddix, "Coal combustion, gasification, and beyond: Developing new technologies for a changing world," *Combustion and Flame,* vol. 159, pp. 3003-3006, 2012.

[104] Y. Tu, H. Liu, K. Su, S. Chen, Z. Liu, C. Zheng, *et al.*, "Numerical study of $H_2O$ addition effects on pulverized coal oxy-MILD combustion," *Fuel Processing Technology,* vol. 138, pp. 252-262, 2015.

[105] Y. Tu, H. Liu, S. Chen, Z. Liu, H. Zhao, and C. Zheng, "Numerical study of combustion characteristics for pulverized coal under oxy-MILD operation," *Fuel Processing Technology,* vol. 135, pp. 80-90, 2015.

[106] I. W. Smith, "The combustion rates of coal chars: a review," *Proceedings of the Combustion Institute*, vol. 19, pp. 1045-1065, 1982.

[107] C. T. Bowman, "Control of combustion-generated nitrogen oxide emissions: technology driven by regulation," in *Symposium (International) on Combustion*, 1992, pp. 859-878.

[108] S. Hill and L. Douglas Smoot, "Modeling of nitrogen oxides formation and destruction in combustion systems," *Progress in Energy and Combustion Science*, vol. 26, pp. 417-458, 2000.

[109] T. Abbas, P. Costen, F. Lockwood, and C. Romo-Millares, "The effect of particle size on NO formation in a large-scale pulverized coal-fired laboratory furnace: measurements and modeling," *Combustion and Flame*, vol. 93, pp. 316-326, 1993.

[110] D. Tian, L. Zhong, P. Tan, L. Ma, Q. Fang, C. Zhang, *et al.*, "Influence of vertical burner tilt angle on the gas temperature deviation in a 700 MW low NOx tangentially fired pulverised-coal boiler," *Fuel Processing Technology*, 2015.

[111] J. Li, X. Zhang, W. Yang, and W. Blasiak, "Effects of flue gas internal recirculation on NOx and SOx emissions in a co-firing boiler," *International Journal of Clean Coal and Energy*, pp. 13-21, 2013 2013.

[112] L. D. Smoot, S. Hill, and H. Xu, "NOx control through reburning1," *Progress in Energy and Combustion Science*, vol. 24, pp. 385-408, 1998.

[113] S. S. Daood, M. T. Javed, B. M. Gibbs, and W. Nimmo, "NOx control in coal combustion by combining biomass co-firing, oxygen enrichment and SNCR," *Fuel*, vol. 105, pp. 283-292, 2013.

[114] Y. Zeldovich, D. Frank-Kamenetskii, and P. Sadovnikov, *Oxidation of Nitrogen in Combustion*: Publishing House of the Acad of Sciences of USSR, 1947.

[115] J. P. Kim, U. Schnell, G. Scheffknecht, and A. C. Benim, "Numerical modelling of MILD combustion for coal," *Progress in Computational Fluid Dynamics*, vol. 7, pp. 337-346, 2007.

[116] B. Alganash, M. C. Paul, and I. A. Watson, "Numerical investigation of the heterogeneous combustion processes of solid fuels," *Fuel,* vol. 141, pp. 236-249, 2015.

[117] J. Raub, *Carbon monoxide*, 2nd ed. Geneva, Switzerland: International Programme on Chemical Safety (IPCS), 1999.

[118] A. Suriyawong, M. Gamble, M.-H. Lee, R. Axelbaum, and P. Biswas, "Submicrometer particle formation and mercury speciation under $O_2$-$CO_2$ coal combustion," *Energy & Fuels,* vol. 20, pp. 2357-2363, 2006.

[119] A. Stam, P. Ploumen, and G. Brem, "Ash related aspects of oxy-combustion of coal and biomass: a thermodynamic approach," in *The 34th International Technical Conference on Coal Utilization and Fuel Systems*, Clearwater, Florida, USA, 2009.

[120] C. Sheng and Y. Li, "Experimental study of ash formation during pulverized coal combustion in $O_2/CO_2$ mixtures," *Fuel,* vol. 87, pp. 1297-1305, 2008.

[121] C. Sheng, Y. Lu, X. Gao, and H. Yao, "Fine ash formation during pulverized coal combustion A comparison of $O_2/CO_2$ combustion versus air combustion," *Energy & Fuels,* vol. 21, pp. 435-440, 2007.

[122] T. Kiga, K. Yoshikawa, M. Sakai, and S. Mochida, "Characteristics of pulverized coal combustion in high-temperature preheated air," *Journal of Propulsion and Power,* vol. 16, pp. 601-605, 2000.

[123] R. Weber, Y. Poyraz, A. M. Beckmann, and S. Brinker, "Combustion of biomass in jet flames," *Proceedings of the Combustion Institute,* vol. 35, pp. 2749–2758, 2015.

[124] T. Suda, M. Takafuji, T. Hirata, M. Yoshino, and J. Sato, "A study of combustion behavior of pulverized coal in high-temperature air," *Proceedings of the Combustion Institute,* vol. 29, pp. 503-509, 2002.

[125] R. He, T. Suda, M. Takafuji, T. Hirata, and J. Sato, "Analysis of low NO emission in high temperature air combustion for pulverized coal," *Fuel,* vol. 83, pp. 1133-1141, 2004.

[126] M. Tamura, S. Watanabe, K. Komaba, and K. Okazaki, "Combustion behaviour of pulverised coal in high temperature air condition for utility boilers," *Applied Thermal Engineering,* vol. 75, pp. 445-450, 2015.

[127] D. Ristic, M. Schneider, A. Schuster, G. Scheffknecht, and J. Wünning, "Investigation of NOx formation for flameless coal combustion," in *7th High Temperature Air Combustion and Gasification International Symposium*, Phuket, Thailand, 2008.

[128] D. Ristic, A. Schuster, G. Scheffknecht, H. Stadler, M. Foerster, R. Kneer, *et al.*, "Experimental study on flameless oxidation of pulverised coal in bench and pilot scale," *Proceedings of the 23th German Flameday*, Berlin, Germany, 2007.

[129] R. Liu, E. An, K. Wu, and Z. Liu, "Numerical simulation of oxy-coal MILD combustion with high-velocity oxygen jets," *Journal of the Energy Institute*, 2016.

[130] B. Luo and X. Q. Ma, "$NO_x$ formed specialty of biomass fuel in HTAC," in *Proceedings of PWR2005, ASME Power*, Chicago, Illinois USA, 2005.

[131] A. Ponzio, S. Senthoorselvan, W. Yang, W. Blasiak, and O. Eriksson, "Ignition of single coal particles in high-temperature oxidizers with various oxygen concentrations," *Fuel*, vol. 87, pp. 974-987, 2008.

[132] A. Ponzio, W. Yang, and W. Blasiak, "Combustion of Solid Fuels under the Conditions of High Temperature and Various Oxygen Concentration," *Challenges of Power Engineering and Environment*, pp. 871-876, 2007.

[133] S. Shim, B. Dally, P. J. Ashman, G. Szegö, and R. A. Craig, "Sawdust burning under MILD combustion conditions," in *Australian Combustion Symposium*, University of Sydney, 2007, pp. 9-11.

[134] C.-Z. Li, "Some recent advances in the understanding of the pyrolysis and gasification behaviour of Victorian brown coal," *Fuel*, vol. 86, pp. 1664-1683, 2007.

# CHAPTER 3

# MILD COMBUSTION CHARACTERISTICS OF PULVERISED COAL IN A SELF-RECUPERATIVE FURNACE

# Statement of Authorship

| | |
|---|---|
| Title of Paper | Moderate or Intense Low Oxygen Dilution (MILD) Combustion Characteristics of Pulverized Coal in a Self-Recuperative Furnace |
| Publication Status | ☑ Published ☐ Accepted for Publication<br>☐ Submitted for Publication ☐ Unpublished and Unsubmitted work written in manuscript style |
| Publication Details | M. Saha, B. B. Dally, P. R. Medwell, and E. Cleary, "Moderate or Intense Low Oxygen Dilution (MILD) Combustion Characteristics of Pulverized Coal in a Self-Recuperative Furnace", *Energy & Fuels*, (2014), Vol. 28(9), pp. 6046 – 6057. |

## Principal Author

| | | | |
|---|---|---|---|
| Name of Principal Author (Candidate) | Manabendra Saha | | |
| Contribution to the Paper | Developed ideas. Conducted experiments, analysed data, wrote manuscript and acted as corresponding author. | | |
| Overall percentage (%) | 65% | | |
| Certification: | This paper reports on original research I conducted during the period of my Higher Degree by Research candidature and is not subject to any obligations or contractual agreements with a third party that would constrain its inclusion in this thesis. I am the primary author of this paper. | | |
| Signature | | Date | 6/04/2016 |

## Co-Author Contributions

By signing the Statement of Authorship, each author certifies that:

i. the candidate's stated contribution to the publication is accurate (as detailed above);

ii. permission is granted for the candidate in include the publication in the thesis; and

iii. the sum of all co-author contributions is equal to 100% less the candidate's stated contribution.

| | | | |
|---|---|---|---|
| Name of Co-Author | Bassam B. Dally | | |
| Contribution to the Paper | Supervised development of work, helped in developing ideas, data interpretation and manuscript evaluation. | | |
| Signature | | Date | 6-4-16 |

| | | | |
|---|---|---|---|
| Name of Co-Author | Paul R. Medwell | | |
| Contribution to the Paper | Supervised development of work, helped in developing ideas, data interpretation and manuscript evaluation. | | |
| Signature | | Date | 13-APR-2016 |

| | | | |
|---|---|---|---|
| Name of Co-Author | Emmet M. Cleary | | |
| Contribution to the Paper | Helped to conduct experiments, numerical simulations and manuscript evaluation. | | |
| Signature | | Date | 13-APR-2016 |

energy&fuels

Article

pubs.acs.org/EF

# Moderate or Intense Low Oxygen Dilution (MILD) Combustion Characteristics of Pulverized Coal in a Self-Recuperative Furnace

Manabendra Saha,*[,†] Bassam B. Dally,[†] Paul R. Medwell,[†] and Emmet M. Cleary[†,‡]

[†]Centre for Energy Technology, School of Mechanical Engineering, The University of Adelaide, Adelaide, SA 5005, Australia

[‡]Department of Mechanical and Aerospace Engineering, Princeton University, Princeton, New Jersey 08544, United States

**ABSTRACT:** Moderate or Intense Low oxygen Dilution (MILD) combustion is a promising technology that offers high thermal efficiency and low pollutant emissions. This study investigates the MILD combustion characteristics of pulverized coal in a laboratory-scale self-recuperative furnace. High-volatile Kingston brown coal and low-volatile Bowen basin black coal with particle sizes in the range of 38−180 $\mu$m were injected into the furnace using either $CO_2$ or $N_2$ as a carrier gas. A water-cooled sampling probe was used to conduct in-furnace gas sampling. Measurements of in-furnace gas concentration of $O_2$, CO, and NO, as well as exhaust gas emissions and in-furnace temperatures, are presented. The results suggest major differences between the two coals and minor differences associated with the carrier gas. It was found that the measured CO level of brown coal cases was 10 times higher than that of black coal cases. However, NO emission for brown coal was only 37% of that measured for black coal at an equivalence ratio of $\Phi = 0.88$. Ash content analysis showed that black coal was not burnt effectively, which is thought to be due to the particle residence times being insufficient for complete combustion in the furnace. To augment the experimental measurements, computational fluid dynamic modeling was used to investigate the effects of coal particle size and inlet air momentum on furnace dynamics and global CO emissions. It is found that coal particle size affects the coal penetration depth within the furnace and the location of the particle's stagnation point. The effects of air inlet momentum are tested in two ways: first, by raising the inlet temperature at a constant mass flow rate, and, second, by increasing the mass flow rate at a constant temperature. In both cases, increasing the air jet momentum broadens the reaction zone and facilitates MILD combustion, but also lowers reaction rates and increases CO emissions.

## 1. INTRODUCTION

From early times to the present day, energy has played a critical role in the development of civilization. The major portion of global energy needs are supplied by the combustion of fossil fuels.[1] Although renewable energy is the world's fastest growing form of energy, its share is currently only 10% of the total energy use and is predicted to increase to only 16% by 2035.[1] Hence, it is imperative to reduce the impact of traditional energy sources on the environment in parallel with the development of renewable sustainable energy sources for the future. Among all the fossil fuel sources, coal is one of the most abundant and typically the least-expensive fossil fuel in the world, and many forecasts show that this position will remain unchanged in the foreseeable future.[1] Therefore, it is important that the development of new coal combustion technologies to reduce pollutant emissions and improve thermal efficiency is continued.

In view of this, Moderate or Intense Low oxygen Dilution (MILD) combustion has been identified as an innovative approach for reducing the production of pollutants and increasing thermal efficiency from the combustion of fossil fuels. Well-documented research[2−4] has shown that burning fuels under MILD combustion conditions results in a substantial reduction in pollutant emissions (~80% in $NO_x$) and an increase in thermal efficiency (~30%). MILD combustion operates on the combination of heat and exhaust gas recirculation.[5] The recirculation of the exhaust gas decreases the local oxygen concentration and increases the temperature of the reactants. The lower oxygen concentration slows the reactions and leads to a distributed reaction zone. As a result, a distributed thermal field is established, which leads to a semi-uniform temperature distribution with a reduced peak temperature; thus, thermal $NO_x$ formation is considerably reduced. MILD combustion is often called "flameless combustion" or "flameless oxidation",[6] because, under certain conditions, the flames are both invisible and inaudible. This combustion is part of the "High Temperature Air Combustion" (HiTAC) regime, because the combustion air is usually preheated to high temperatures.[7] The term "MILD combustion" will be used throughout this paper.

There is a growing body of work on the MILD combustion regime.[2,4,8] Nevertheless, some fundamental aspects of this relatively new field are still unresolved and require further consideration. Some of these issues relate to air preheating and its impact on the system thermal efficiency. Kumar et al.[9] at the Indian Institute of Science and Dally's group at The University of Adelaide reported[10,11] that air preheating is not needed to achieve MILD combustion and that strong internal recirculation provides a simpler and effective alternative. Dally et al.[12] investigated the effect of heat and flue gas recirculation on the establishment of MILD condition in a furnace and found that initial dilution of fuel with $CO_2$ and $N_2$ affects the combustion reaction by reducing the peak temperature of the reaction zone and that contributes to reducing thermal $NO_x$ emission. On the

**Received:** March 27, 2014
**Revised:** August 26, 2014
**Published:** August 26, 2014

   dx.doi.org/10.1021/ef5006836 | *Energy Fuels* 2014, 28, 6046−6057

application side, Szegö et al.[11,13] studied MILD combustion on a furnace fitted with a parallel jet burner operating at a heating load of 15 kW. These studies reported that premixing the fuel with an inert gas, which simulates exhaust gas recirculation in the fuel jet, helps to achieve the MILD conditions without air preheating. These findings from a parallel jet furnace are being applied to pulverized coal as a solid fuel in this study.

MILD combustion has been studied extensively for gaseous and liquid fuels and has been successfully used in many industrial applications.[2] However, MILD combustion of pulverized coal has received much less attention than that of gaseous fuels and its burning characteristics are poorly understood. Some studies have recently been reported on pulverized coal combustion under MILD conditions.[14−17] An experimental study on the MILD combustion behavior of high volatile coal was conducted in a semi-industrial scale furnace with 0.58 MW thermal input by Weber et al.[16] at the International Flame Research Foundation (IFRF). High-temperature air (1573 K) was used to burn high-volatile coal and the lowest $NO_x$ emissions were recorded in the range of 160−175 ppm (at 3% $O_2$), demonstrating the high $NO_x$ reduction potential of this technology for pulverized fuels also. However, the basic mechanism of $NO_x$ formation is not clearly understood from the experiments. MILD combustion of pulverized bituminous and anthracite coal was experimentally investigated by Suda et al.[18] The inlet air was preheated to a temperature of either 623 or 1073 K in order to compare the effects of air temperature. The authors concluded that the ignition delay decreased rapidly with increasing air temperature, because of the rapid devolatilization of the coal particles, which is caused by a higher particle heating rate.

Numerical studies on MILD coal combustion were performed by He et al.,[19] using the experimental results of Suda et al.[18] to investigate $NO_x$ formation and destruction mechanisms. It was reported that 90% of the $NO_x$ emissions were formed through the fuel path and the remaining 10% were formed through the thermal route. The authors concluded that for low-volatile anthracite coal, NO is mainly formed from the nitrogen contained in char, the mechanism of which is not well-understood. An experimental investigation on the $NO_x$ emissions in air, $Ar/O_2$, and $CO_2/O_2$ atmospheres for MILD combustion of lignite and bituminous coal was carried out by Stadler et al.[20] This investigation showed a large reduction of thermal NO in the MILD mode. It also showed an increase of fuel-NO that was primarily related to the reduction of the peak flame temperature in MILD combustion. Zhang et al.[21] used a novel preheating chamber to create a two-stage hot gas recirculation in to and out of the chamber for the MILD combustion of petroleum coke and low-rank anthracite coal. These authors found that the rapid heating of the combustible mixture in the chamber facilitates pyrolysis and volatile matter release processes for the fuel particles, thereby suppressing ignition delay and increasing combustion stability. They also reported that the $NO_x$ emission was 50% lower by comparison with a conventional low $NO_x$ burner when anthracite coal was combusted. The authors concluded that this technology is a practical, efficient, and clean way to burn solid fuels. A computational fluid dynamics (CFD)-based mathematical model for MILD combustion of pulverized Guasare (high carbon bituminous) coal was developed by Schaffel et al.[17] to investigate the pollutant ($NO_x$ and CO) emission mechanism. It was found that the volatiles are released in a highly sub-stoichiometric environment and their N-containing species are preferentially converted to molecular nitrogen rather than to NO. This indicates that stronger NO-reburning mechanisms exist in the MILD combustion, when compared with conventional coal combustion technology. Recent efforts of Vascellari and Cau[14] have concentrated on numerical modeling of high-volatile bituminous pulverized coal MILD combustion using advanced turbulence-chemistry interaction models with detailed kinetic mechanisms to better understand the MILD combustion process and accurately predict the velocity, temperature, and gas concentrations. The numerical simulations were performed using the geometry and the working conditions of the IFRF furnace[16] and were validated using the experimental results of Weber et al.[16] This numerical model was able to predict the velocity field effectively but slightly overestimates the flame temperature, in comparison with the experimental data, and the NO concentration was slightly overestimated in the devolatilization zone. The authors revealed that the coal conversion mechanisms, including drying, devolatilization, and char burnout under MILD conditions, are responsible for the delayed flame lift-off and so different turbulence−chemistry models and kinetic mechanisms are needed to capture it. Therefore, the influence of these models needs to be further investigated in order to increase the overall accuracy of the numerical analysis.

The above discussion indicates that there is a need for further work on MILD combustion of pulverized coal to probe the combustion characteristics and facilitate better understanding of the formation and destruction of pollutants, such as CO and NO, under MILD conditions. Hence, this paper reports an experimental and numerical study that examines the use of high-volatile brown coal and low-volatile black coal in a self-recuperative MILD combustion furnace. On the experimental side, the effect of the carrier gas, fuel type, and the operating parameters on the characteristics of MILD combustion, in-furnace gas concentrations, and temperature, as well as pollutants emission in exhaust, are discussed and analyzed. The complementary numerical study investigates the effects of coal particle size and inlet air momentum on furnace dynamics and global CO emissions. The numerical results are also presented to shed light on the flow and structure of the thermal fields inside the furnace. First, the furnace geometry, meshing, and all numerical models used are discussed. Then, results from seven cases of simulations with different air inlet momenta and fuel particle momenta are presented and discussed.

## 2. EXPERIMENTAL AND NUMERICAL DETAILS

**2.1. Experimental Setup.** In the present study, a laboratory-scale MILD combustion furnace (MCF) is used as shown in Figure 1. Further details of the furnace have previously been reported by Szegö et al.[11] The furnace has an inner square cross-section of 280 mm × 280 mm and a height of 585 mm and is lined with a high-temperature ceramic fiber board refractory. The furnace is preheated to temperatures above that of the autoignition of the fuel, using a non-premixed natural gas flame. The switch to MILD mode is achieved once the temperature at the lower corner of the furnace, which is identified as the safety thermocouple (TC) in Figure 1 exceeds 850 °C. The burner block and jet arrangement at the bottom of the furnace is shown in Figure 2. The central fuel nozzle, with an internal diameter of 7.5 mm, is fitted with a bluff body (22 mm in diameter) and is surrounded by an air nozzle with an internal diameter of 26.4 mm. It is noteworthy that the bluff body was only used to achieve flame stability during preheating of the furnace for the experiments.

When switching to MILD mode, the inlet air through the central air nozzle is switched to the four surrounding periphery jets, which have an internal diameter of 4 mm. Pulverized coal particles replace natural


dx.doi.org/10.1021/ef5006836 | Energy Fuels 2014, 28, 6046−6057

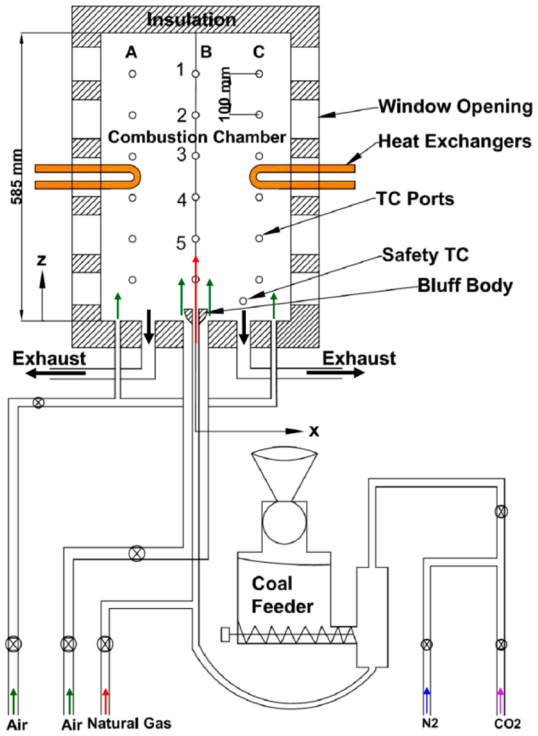


**Figure 1.** Schematic diagram of the MILD combustion furnace and supply system.

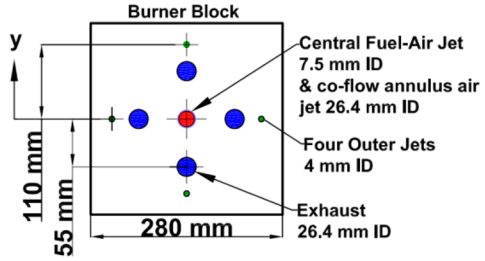


**Figure 2.** Burner block showing the arrangement of the fuel and air delivery jets and exhaust ports.

gas in the central fuel nozzle and is carried into the furnace using either $CO_2$ or $N_2$.

The furnace was equipped with two cooling-loop heat exchangers on opposite sides to each other. Water is supplied to the heat exchangers at a constant inlet temperature and flow rate. The heat exchangers were positioned at a height of 292 mm above the burner plane and had an exposed surface area of 0.03 $m^2$. When furnace operates at 15 kW, heat exchangers remove 4.5, 4.83, 4.32, and 4.04 kW of heat on average for the combustion of $CO_2$ carried brown coal, $CO_2$ carried black coal, $N_2$ carried brown coal, and, $N_2$ carried black coal, respectively.

The mole fractions of $O_2$, CO, and NO in the exhaust and within the furnace were measured using a TESTO Model 350XL portable gas analyzer. The absolute errors of these measurements, according to the manufacturer's specifications, are ±0.8% (by volume) for $O_2$, ±10 ppmv for CO, and ±5 ppmv for NO of measured value. The internal temperatures of the furnace were measured on the centerline ($x$ = 0 mm) and 100 mm left from the centerline ($x$ = −100 mm), across the height ($z$-axis) of the MCF for all experiments. The exhaust gas temperature was measured at a distance of 100 mm from the furnace outlet with a stainless steel sheathed nickel−chromium (Type K) thermocouple. The furnace reference temperature was measured flush with the inner surface using a 6 mm-diameter sheathed Nicrosil-Nisil (Type N) thermocouple, placed at 42.5 mm from the bottom of the furnace. Additional thermocouples with a 6-mm-diameter bead made of Pt/Pt 13% Rh (Type R) are inserted horizontally at heights of 142.5, 242.5, 342.5, 442.5, and 542.5 mm. All temperature measurements are logged using a personal computer (PC) and USB-TC data logger. No radiation correction of the thermocouple measurements was attempted in this study, because it was not possible to measure the temperature distribution of all walls in the furnace, which was equipped with one thermocouple that measured the wall temperature at one location. An estimate of the correction, assuming uniform surface temperature on all walls, indicates that radiation losses affect the reported thermocouple measurements by <2%.

A cyclone-based ash collector was used to separate ash from the exhaust gas stream.

A sampling probe was developed for in-furnace gas sampling during MILD combustion. The probe consisted of three stainless steel concentric pipes, enabling cold water to circulate in the probe for rapid quenching of hot combustion gases. The schematic diagram of the sampling probe is shown in Figure 3. This probe is straight and

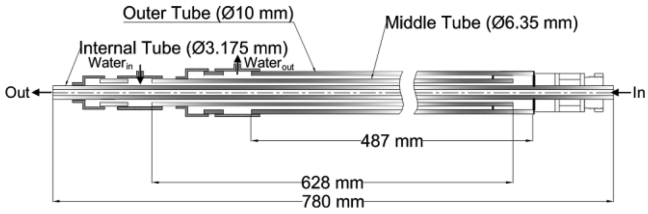


**Figure 3.** Sketch of the in-furnace sampling probe.

introduced through the thermocouple ports of the furnace toward the $y$-direction while the main direction of the flow follows in the $z$-direction. In these experiments, $O_2$, CO, and NO were measured along the centerline ($x$ = 0) and 100 mm left from the centerline ($x$ = −100) of the furnace. The sampling probe was traversed in the horizontal directions ($y$-axis) at three positions ($y$ = 0, 50, and 100 mm) across different planes at 12 holes of various vertical locations ($z$-axis) of the furnace to provide a total of 36 points of measurement.

**2.2. Characteristics of Coal.** Two different types of coal were tested in this study: Kingston brown coal, which is low-rank and high-volatile lignite, and Bowen Basin black coal, which is high-rank and low-volatile anthracite. The coal particles were milled and sieved into the 38 $\mu$m < $d$ ≤ 180 $\mu$m size range. Proximate and ultimate analyses of the coals are presented in Table 1. The gross dry calorific values of brown coal and black coal are determined to be 20.0 MJ/kg and 31.9 MJ/kg, respectively.

**Table 1. Coal Analyses**

| | Kingston brown coal (wt % db) | Bowen basin black coal (wt % db) |
|---|---|---|
| **Ultimate Analysis** | | |
| C | 52.5 | 81.2 |
| H | 3.6 | 3.6 |
| O | 17.73 | 3.47 |
| N | 0.48 | 1.35 |
| S | 4.09 | 0.58 |
| **Proximate Analysis** | | |
| fixed carbon | 35.7 | 80.7 |
| volatile matter | 42.7 | 9.5 |
| ash | 21.6 | 9.8 |

A coal feeder was specifically built for the purpose of decoupling the carrier gas flow rate from the solid particle supply rate. A small screw feeder that was operated using a stepper motor controlled the amount of coal fed into the feeding chamber. The carrier gas was set at a constant flow rate.

**2.3. Numerical Modeling.** This study uses a three-dimensional, structured, hexahedral mesh of 1.1 million cells, and models one-


dx.doi.org/10.1021/ef5006836 | Energy Fuels 2014, 28, 6046−6057

quarter of the furnace geometry. A grid-independent study was conducted, and the current mesh density was determined to be adequate. This simplification reduces computational expense and assumes symmetry. A constant surface temperature of the heat exchanger was assumed, and the heat removed was matched with the measured value.

All models presented in this work solve the steady Reynolds-averaged Navier–Stokes (RANS) equations in the ANSYS Fluent v. 14.5 code. For consistency with previous numerical studies on this furnace, the RANS equation closure uses the two-equation realizable $k$–$\varepsilon$ turbulence model[22] with the SIMPLE algorithm for pressure–velocity coupling. Particle size range from 38 $\mu$m to 180 $\mu$m in diameter and follow a Rosin-Rammler distribution. Only brown coal carried by $CO_2$ was modeled in this study. Coal devolatilization follows a single-rate model, according to Kobayashi et al.,[23] using Arrhenius coefficients of $A = 6.6 \times 10^4\ s^{-1}$ and $E_a = 1.06 \times 10^5$ J/(kg mol). Coal particles are treated as a discrete phase and are tracked using a deterministic Lagrangian approach[24] to update particle source terms. Radiation modeling uses the discrete ordinates model.[25] All spatial discretizations follow the first-order upwind scheme. Simulations were run using the Tizard supercomputer at eResearch SA on 24 cores.

*2.3.1. Chemical Mechanisms and Models.* The combustion model uses finite rate chemistry with the Eddy Dissipation Concept (EDC) model[26] for turbulence–chemistry interaction. EDC allows consideration of complex kinetic mechanisms. The multiple surface reactions combustion model is used for a six-reaction chemical mechanism, which includes volatile combustion and char burnout. Rather than track individual volatile species (e.g., $CH_4$), this work is limited to a global volatile combustion mechanism. Reactions 1 and 2 fully oxidize $C_xH_yO_zN_lS_n$. After volatile matter combustion, the char remaining in the coal particle reacts with the surrounding gas phase. Considering exhaust gas recirculation, high $CO_2$ and $H_2O$ concentrations characterize coal MILD combustion. Therefore, gasification and Boudouard reactions are considered, in addition to oxidation.

$$C_xH_yO_zN_lS_n + \left(\frac{x}{2} + \frac{y}{2} - \frac{z}{2} + n\right)O_2 \rightarrow xCO + \frac{y}{2}H_2O + \frac{l}{2}N_2 + nSO_2 \quad (1)$$

$$CO + \frac{1}{2}O_2 + H_2O \rightarrow CO_2 + H_2O \quad (2)$$

$$C_{char} + \frac{1}{2}O_2 \rightarrow CO \quad (3)$$

$$C_{char} + CO_2 \rightarrow 2CO \quad (4)$$

$$C_{char} + H_2O \rightarrow H_2 + CO \quad (5)$$

$$H_2 + \frac{1}{2}O_2 \rightarrow H_2O \quad (6)$$

Variables $x$, $y$, $z$, $l$, and $n$ are found from the ultimate analysis of the coal used (refer to Section 2.2). Refer to Table 2 for the Arrhenius coefficients.

*2.3.2. Model Parameters and Cases Considered.* For all models presented in this paper, only brown coal in a carrier gas of $CO_2$ is considered. The fuel stream has a mass flow rate of 0.236 g/s, with a carrier gas flow rate of 7.79 m/s at 300 K. The cases of interest are summarized in Table 3. Cases 1–3 examine the influence of particle diameter at a constant inlet fuel and air jet momentum ratio. Cases 1, 4, and 5 examine the influence of the inlet air jet momentum increase at constant mass flow rate through air preheating. Lastly, the inlet air jet momentum is increased at constant temperature by increasing the mass flow rate (Cases 1, 6, and 7). In all cases, the fuel inlet temperature is kept at 300 K, and the furnace wall and heat exchanger temperatures are held at constant values of 1150 and 450 K, respectively.

**Table 2. Arrhenius Coefficients for Reactions 1–6**

| reaction | $A$ | $E_a$ (J/kg mol) | reference |
|---|---|---|---|
| 1 | $4.84 \times 10^7$ | $5.1 \times 10^7$ | 27 |
| 2 | $1.3 \times 10^{11}$ | $1.26 \times 10^8$ | 28 |
| 3 | $5 \times 10^{-3}$ | $7.4 \times 10^7$ | 29 |
| 4 | $6.35 \times 10^{-3}$ | $1.62 \times 10^8$ | 30 |
| 5 | $1.92 \times 10^{-3}$ | $1.47 \times 10^8$ | 30 |
| 6 | $9.87 \times 10^8$ | $3.1 \times 10^7$ | 31 |

**Table 3. Summary of Cases of the Numerical Investigation**

| case | particle diameter ($\mu$m) | air temperature (K) | air mass flow rate (g/s) |
|---|---|---|---|
| 1 | 38–180 | 300 | 1.27 |
| 2 | 38 | 300 | 1.27 |
| 3 | 180 | 300 | 1.27 |
| 4 | 38–180 | 400 | 1.27 |
| 5 | 38–180 | 500 | 1.27 |
| 6 | 38–180 | 300 | 1.48 |
| 7 | 38–180 | 300 | 1.77 |

## 3. RESULTS AND DISCUSSION

Four different experiments were conducted using Kingston brown coal and Bowen Basin black coal with either $CO_2$ or $N_2$ as the carrier gas. The coal particles carried by either $CO_2$ or $N_2$ were supplied through the center jet, while the inlet air was supplied through the four periphery jets. A summary of the operating conditions is shown in Table 4. The results obtained from the numerical models are presented in Section 3.5 after the presentation of experimental observations. While the main objective of the numerical models in this work is to conduct a parametric study instead of directly interpret the experimental observations, the numerical model for Case 1 is validated with experimental results. The model validation is presented in Sections 3.2 and 3.3.

**3.1. Exhaust Gas Emission.** A time history of the mole fractions of $O_2$, CO, and NO in the exhaust for brown coal and black coal carried by either $CO_2$ or $N_2$ is shown in Figures 4 and 5, respectively. These figures imply that the switch of the carrier gas from $CO_2$ to $N_2$ for coal combustion under the MILD mode was associated with the major differences with respect to CO emissions and also had minor influence on the NO emissions. Minor variations in the feeding rate of the coal impacted on the equivalence ratio ($\phi$) and the $O_2$ concentration in the exhaust. This is also responsible for the change in CO concentration, especially for brown coal, because it was more "sticky" and harder to feed at a consistent rate.

Figure 4 shows that, in the case of brown coal carried by $CO_2$, the measured CO levels were 4990 ppm for an equivalence ratio of $\phi = 0.89$ but decreased to 2790 ppm at $\phi = 0.86$. However, for $N_2$ as a carrier gas of brown coal, the measured CO levels varied between 1661 ppm and 5179 ppm at $\phi = 0.86$ and 0.92, respectively. The measured NO emissions from these conditions are listed in Table 4. For brown coal carried by either $CO_2$ or $N_2$, the measured NO level is $\leq$236 ppm. In particular, for an equivalence ratio of $\phi = 0.88$, the NO measurements were 178 ppm for brown coal carried by $CO_2$ and 223 ppm for brown coal carried by $N_2$. The reason behind the increase in NO concentration, relative to changes in the carrier gas, is not well-understood. Nonetheless, it is speculated that the additional $N_2$ in the furnace from the carrier gas


dx.doi.org/10.1021/ef5006836 | Energy Fuels 2014, 28, 6046–6057

**Table 4. Operating Parameters and Resulting Emissions for MILD Combustion Using Pulverized Coals**

| parameter | $CO_2$ carried brown coal | $N_2$ carried brown coal | $CO_2$ carried black coal | $N_2$ carried black coal |
|---|---|---|---|---|
| periphery air jet velocity (m/s) | 86.2 | 86.2 | 86.2 | 86.2 |
| equivalence ratio, $\phi$ | 0.88 ± 0.02 | 0.89 ± 0.03 | 0.88 ± 0.03 | 0.89 ± 0.01 |
| central fuel jet velocity (m/s) | 7.92 | 10.43 | 7.92 | 10.43 |
| thermal input (kW) | 15 ± 0.2 | 15.2 ± 0.7 | 15.5 ± 0.5 | 15.5 ± 1 |
| CO in the exhaust (ppmv dry) | 2790−4996 | 1661−5179 | 331−547 | 300−310 |
| NO in the exhaust (ppmv dry) | 178−228 | 164−236 | 296−366 | 347−366 |

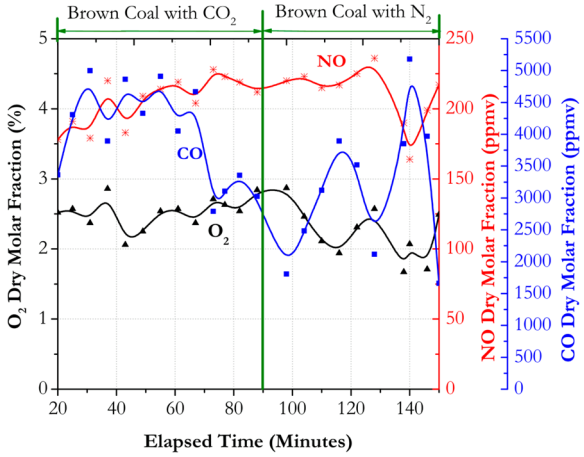


**Figure 4.** Temporal variations of $O_2$, CO, and NO measured in the exhaust for brown coal, carried by either $CO_2$ or $N_2$, under the MILD combustion mode.

increases the overall $N_2$ concentration and contributes to relatively higher NO emissions in the corresponding cases.

A similar experiment, as presented for the previous cases, was conducted for black coal carried by either $CO_2$ or $N_2$. Figure 5

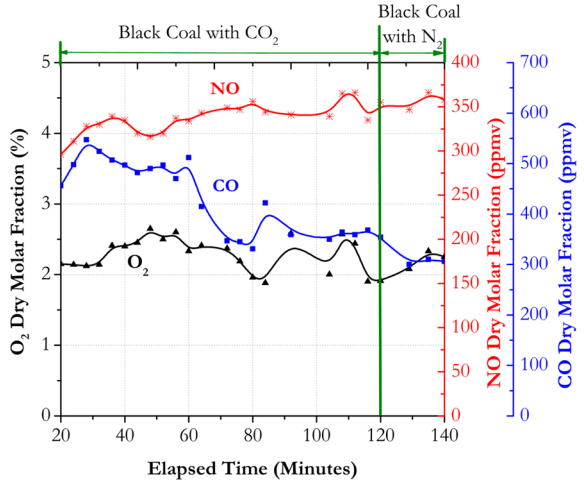


**Figure 5.** Temporal variations of $O_2$, CO, and NO measured in the exhaust for black coal, carried by either $CO_2$ or $N_2$, under the MILD combustion mode.

shows that the measured CO concentration for $N_2$ as the carrier gas is up to 2-fold lower than those measured for the case where $CO_2$ was used as the carrier gas at the equivalence ratio of $\phi$ = 0.90. The recorded NO concentration for both carrier gases with black coal, listed in Table 4, is ≤366 ppm.

The measured NO emissions from black coal combustion are observed to be higher than those of brown coal combustion. The reason behind this increase can be explained by a brief description of NO formation behavior of pulverized coal combustion. In pulverized coal combustion, NO emission is formed via three routes: fuel-NO, thermal-NO, and prompt-NO.[32−34] Fuel-NO is formed by oxidation of the nitrogen bound in the fuel, where molecular nitrogen $N_2$ is released as hydrogen cyanide (HCN) and ammonia ($NH_3$) during devolatilization and char burnout. Then, HCN and $NH_3$ react with oxygen and NO to produce NO and $N_2$, respectively. Thermal-NO formation is based on the oxidation reactions of the $N_2$ contained in the inlet air, which are favored by high flame temperature. Therefore, under MILD combustion, the reduced temperature minimizes NO production through thermal-NO pathways. Then, prompt-NO is formed by reactions of local $N_2$ with hydrocarbon radicals in fuel-rich regions of the flame.[33] It is believed that prompt-NO has a minor influence on MILD combustion, because reactants are diluted with combustion products.The fuel-NO mechanism represents the main NO formation for coal MILD combustion, while the thermal-NO mechanism is reduced by the low flame temperature and prompt-NO plays a secondary role. It is thus concluded that, for black coal combustion, the high nitrogen contents of fuel (where the nitrogen content in black coal is ∼64% higher than that of brown coal) lead to higher NO emissions that are produced through the fuel NO formation mechanism.

The measured CO levels of brown coal were generally higher in these experiments than the black coal. The higher CO emissions for brown coal are related to the more-significant char burnout of brown coal (char burnout is discussed further in Section 3.4 of this paper) by the heterogeneous reactions between char ($C_{char}$) and gaseous products according to reactions 3−5. Consequently, the furnace temperature for this case was found to be lower, because of the endothermic nature of the heterogeneous reactions.[15,35,36] It has been reported by Stadler et al.[15] that heterogeneous reactions of char with $O_2$, $CO_2$, and $H_2O$ contribute to the production of high CO concentration in coal MILD combustion. Generally, heterogeneous (also called gasification) reactions of char alter the CO/$CO_2$ balance, increasing CO concentrations and reducing particle temperature, because of their endothermic behavior.[36] Therefore, the explanation for the phenomenon of lower furnace temperature and higher CO emission for the brown coal case is the endothermic nature of the heterogeneous reactions between char and gaseous products of the combustion reactions.

**3.2. Furnace Temperature.** Figure 6 shows the time history of the furnace temperature at five different locations along the centerline inside the furnace as well as the exhaust gas temperature for brown and black coal that was carried by $CO_2$. The temperature difference across the furnace is <100 K and quite uniform, which implies that a homogeneous temperature distribution is achieved in MILD coal combustion. In the figure,


dx.doi.org/10.1021/ef5006836 | Energy Fuels 2014, 28, 6046−6057

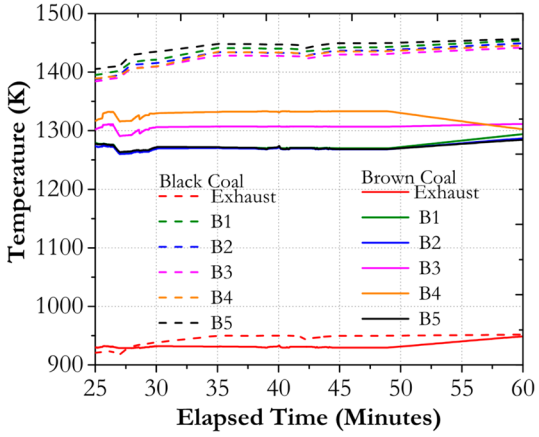


**Figure 6.** Time history of measured furnace temperature at different heights within the MILD combustion furnace operating on either brown coal or black coal carried by $CO_2$.

the furnace has a more consistent temperature profile, which implies a reasonably uniform combustion process and heat release from the black coal within the furnace. The semi-uniform furnace temperature implies strong recirculation of hot combustion products inside the furnace, which plays a key role in establishing MILD combustion. The average mixture temperature of the furnace for the brown coal case was determined to be ~1300 K, and the exhaust gas temperature was measured to be ~930 K. Whereas for black coal, the average gas temperature of the furnace was measured to be ~1450 K, with the exhaust gas temperature being ~950 K.

Figure 7a shows the computed temperature contour plot at the symmetry planes for brown coal under the MILD mode at an equivalence ratio of $\phi$ = 0.88 and with a carrier gas of $CO_2$. The plot shows that the air jets dominate the flow pattern in the furnace and create a large recirculation zone in the top part of the furnace. The periphery air jets (operating at a velocity of $U$ = 86.2 m/s) impinge on the top of the furnace and turn back to engulf the central fuel jet, reacting with its volatiles to create a mixture of hot products with a temperature of ~1350 K.

Figure 7b shows a qualitative comparison of computed and measured temperatures. The plot shows that the temperature difference of the recirculated products is within 50 K inside the furnace. From the numerical results, it is clear that the central jet penetrates further into the furnace and its temperature is lower than the measured values. It is believed that the cold zone is related to a delayed ignition of the flame, as well as the relatively poor performance of the devolatilization model. However, the numerical results reasonably capture the temperature profile from the middle to the top of the furnace with slight overestimations (~50−100 K). The performance of this model is reasonable, considering its simplicity in representing the gas phase reactions.

The comparisons between the measured mean temperatures of brown coal carried by $CO_2$, brown coal carried by $N_2$, and black coal carried by $CO_2$ cases and numerical results for the temperature of case 1 (see Table 3) are shown in Figure 8. The furnace temperatures were measured along various vertical locations (the $z$-axis) of the furnace centerline ($x$ = 0 mm) and

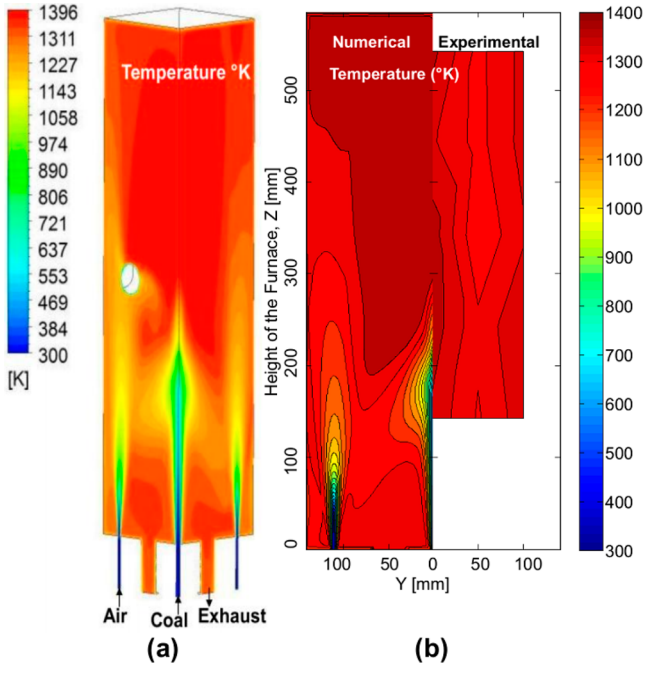


**Figure 7.** (a) Temperature distribution of numerical results along the vertical section; (b) temperature profile of numerical and experimental results at the centerline of the furnace for the combustion of brown coal carried by $CO_2$.

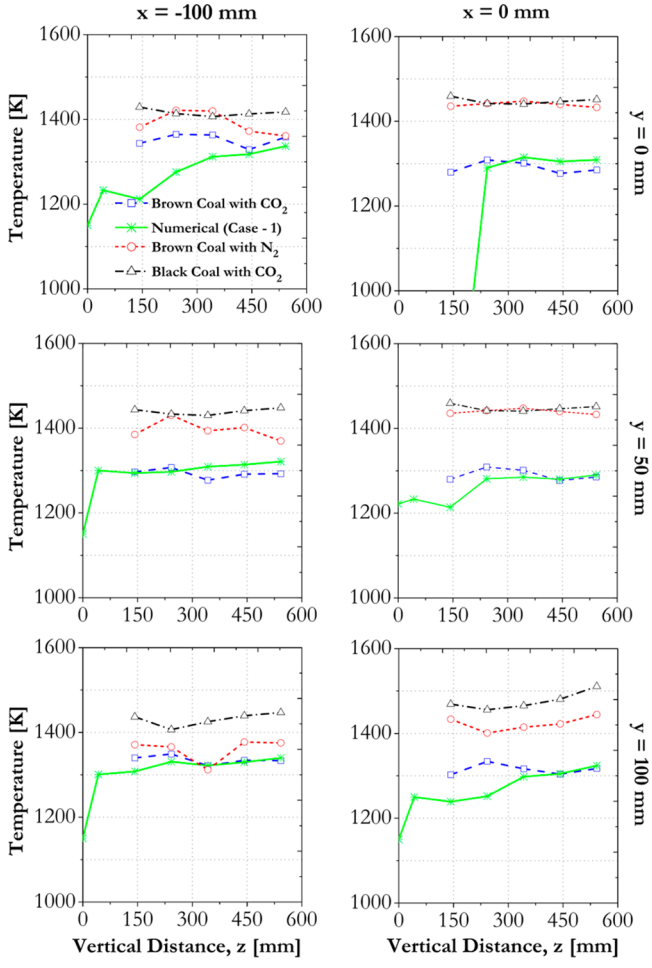


**Figure 8.** Comparison of numerical and measured temperature profiles at $x$ = −100 mm (left) and $x$ = 0 (centerline) along the vertical locations (the $z$-axis) at different horizontal distances (the $y$-axis) from the center of the furnace.


dx.doi.org/10.1021/ef5006836 | Energy Fuels 2014, 28, 6046−6057

100 mm left from the centerline ($x = -100$ mm) for each cases. For both cases, the highest temperatures were recorded at the top of the furnace ($z = 542.5$ mm), because the top position of the furnace is expected to have hot combustion products. It is clear that the temperature is quite uniform, with a difference as little as 50 K at different locations. However, a clear distinction exists between those measured temperatures of the brown and black coal combustion experiments. For instance, the maximal mean temperature of the combustion of the black coal (carried by $CO_2$) is ~200 K higher than that of maximal mean temperature of the combustion of the brown coal (carried by $CO_2$). The temperature discrepancy between these cases is related to the CO production by heterogeneous reactions of char. Such reactions are endothermic[36] and responsible for decreasing the temperature of the reaction zone.

After primary pyrolysis when volatile matter is completely released, the char remaining in the coal particles reacts with the surrounding gases. Considering the strong exhaust gas recirculation of MILD combustion, high $CO_2$ and $H_2O$ concentrations react with the char that remains in the coal particle, besides oxidation. A large amount of CO is produced from char burnout, according to reactions 3−5. CO formation inversely affects the furnace temperature. When compared to the black coal experiments, the brown coal produced a higher concentration of CO and, thus, had a lower furnace temperature. Furthermore, Figure 8 shows the distinction in the mean temperatures between that of the combustion of brown coal carried by $CO_2$ and the combustion of brown coal carried by $N_2$. The mean temperature of the furnace during the combustion of brown coal carried by $N_2$ is higher because (1) the specific heat of $CO_2$ is higher than $N_2$ (at these flow rates, the heating of $CO_2$ as a carrier gas takes 33% more energy, compared with $N_2$ as a carrier gas) and (2) a equivalence ratio of the combustion of brown coal carried by $N_2$ is relatively higher (see Table 4).

In Figure 8, no substantial difference between the model predictions and the measurements for the gaseous temperatures of brown coal carried by $CO_2$ case can be seen with exception of the fuel jet at the centerline of the furnace ($x = 0$ mm, $y = 0$ mm) and around to the air jet ($x = -100$ mm, $y = 0$ mm) positions. The numerical model underestimates the flame temperature at these ($x = 0$ mm, $y = 0$ mm and $x = -100$ mm, $y = 0$ mm) positions. The underestimation of these temperatures can be explained by the presence of a cold zone that corresponds to the adjacent jet of the model, which is not found by experimental observation. Nonetheless, the temperature level and the temperature peaks are well-reproduced by the simulations at the position of $y = 50$ mm and $y = 100$ mm. It is noteworthy that temperature profiles are flat from the middle to top of the furnace, since pointing to a homogeneous mixture and a slow reaction. This feature is well-reproduced by the numerical model. Generally, the agreement between the temperature predictions by the model and the measurements is quite reasonable.

**3.3. In-Furnace Gas Sampling.** *3.3.1. In-Furnace CO Concentration.* Figure 9 shows numerical results for Case 1 (see Table 3) and measured in-furnace CO molar fraction (dry basis) of flames with brown and black coal and under MILD conditions, along the vertical direction (the $z$-axis) of the furnace. For brown coal, a high concentration of CO was measured at the lower part of the furnace, because of the early volatile matter release. It is observed that the highest concentration of CO at 5% was found at the centerline,

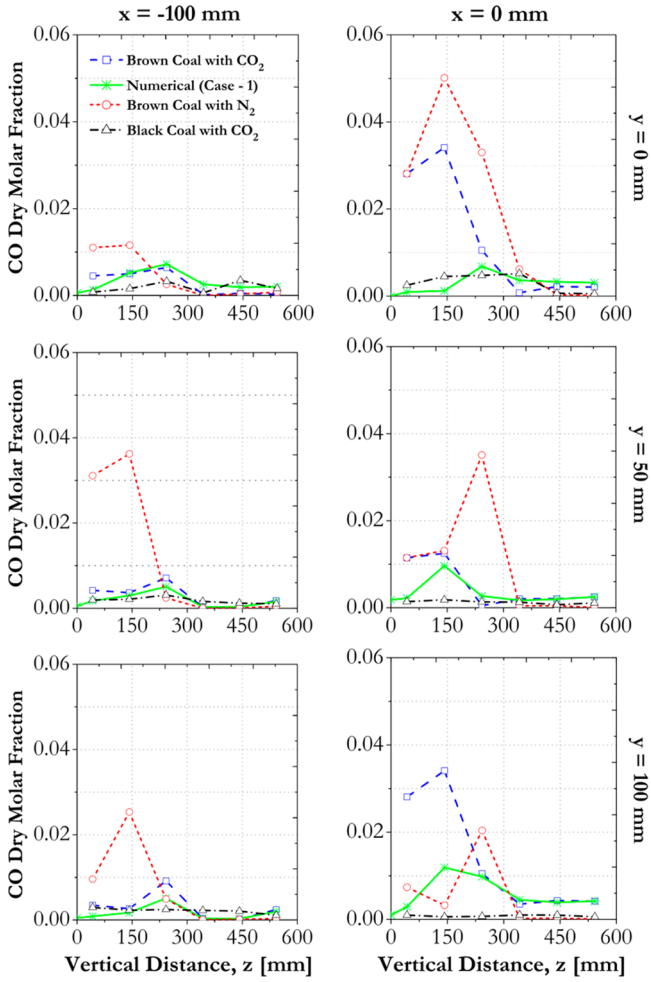


**Figure 9.** Comparison of numerical and measured in-furnace CO dry molar fraction at $x = -100$ mm (left) and $x = 0$ (centerline) along the vertical locations (the $z$-axis) at different horizontal distances (the $y$-axis) from the center of the furnace.

where ($x = 0$) and $z = 142.5$ mm in the furnace, for the case of brown coal with $N_2$. Along the centerline of the furnace, the measured CO mole fraction was highest in the coal devolatilization zone. Hence, it is believed that, for these experimental conditions, the devolatilization zone of brown coal was located at ~142.5 mm above from the fuel jet exit. It is remarkable that at the middle parts of the furnace ($z = 342.5$ mm), CO levels are found at their lowest, suggesting that gaseous volatiles are completely burned by then. The upper part of the furnace has a low concentration of CO, not dissimilar to that at the exhaust.

On the other hand, for black coal case, the release of volatiles seems to start at the $z = 342.5$ mm position of the furnace, because of the slow pyrolysis of low-volatile and high-rank black coal. Also, for the combustion of black coal, the CO mole fraction was determined to be always <0.5%. The large difference in CO production between the combustions of black and brown coal is mainly related to the char burnout, as a large part of the CO is produced from effective char burnout according to reactions 3−5. The incomplete char burnout of black coal is further discussed below, in Section 3.4.

Numerical simulation predicts smaller concentration of CO, with respect to the experimental results. This difference could be attributed to several reasons. CO is formed and oxidized in


dx.doi.org/10.1021/ef5006836 | Energy Fuels 2014, 28, 6046−6057

several parallel and sequential reactions. CO is released as a volatiles component, as a volatile oxidation product, and as a char combustion product. CO is oxidized by OH radicals and O radicals, although with a lower rate. Moreover, the water gas shift reaction ($CO + H_2O \rightarrow CO_2 + H_2$) alters CO concentrations. None of those processes were considered in the numerical simulation except volatile oxidation and char combustion. In addition, the discrepancy between measured values of CO dry molar fraction and model predictions could be related to the poor performance of the devolatilization model.

*3.3.2. In-Furnace $O_2$ Concentration.* In Figure 10, the numerical results for Case 1 (see Table 3) and measured in-

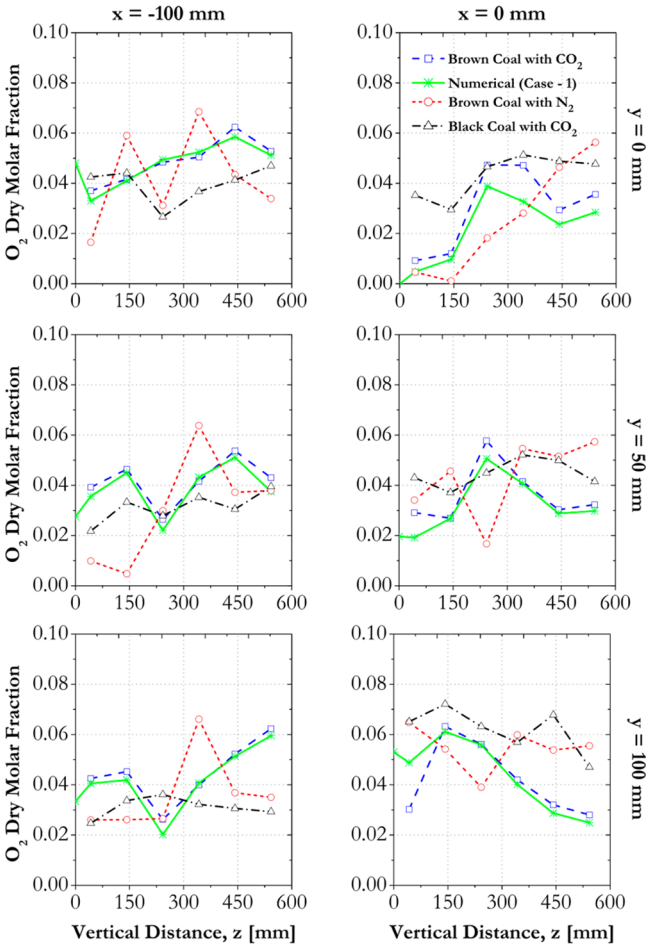


**Figure 10.** Comparison of numerical and measured in-furnace $O_2$ dry molar fraction at $x = -100$ mm (left) and $x = 0$ (centerline) along the vertical locations (the $z$-axis) at different horizontal distances (the $y$-axis) from the center of the furnace.

furnace $O_2$ molar fractions (dry basis) for brown and black coal combustion under MILD conditions along the vertical direction (the $z$-axis) of the furnace are shown. The $O_2$ concentration at 100 mm away from the centerline ($y = 100$ mm) is measured to be higher, because of the position of air jets (see Figure 2). Primary air of the combustion is introduced into the furnace through this position; as a result, the $O_2$ concentration was measured to be ~7.2%. vol Whereas, at the centerline of the furnace ($x = 0$, $y = 0$), the mean $O_2$ mole fraction was less than ~5 vol %. Because of the low oxygen concentration, chemical reactions under MILD combustion occur more slowly than in conventional combustion and the reaction zone spreads throughout the entire volume of the furnace; in turn, a volumetric reaction is established. This distributed heat release coupled with strong recirculation, leads to the semi-uniform furnace temperature under these conditions.

No major differences between the experimental results and the calculated values by the simulation for the $O_2$ concentrations can be observed from Figure 10. However, the $O_2$ concentrations are slightly underestimated from the middle to the top of the furnace along the centerline ($x = 0$ mm, $y = 0$ mm), which is consistent with the temperature predictions by the model regarding those positions. It may be related to inaccurate prediction of the entrainment of the fuel jet. Predictions of $O_2$ concentrations in other locations of the furnace are reasonably similar to the measurements. Altogether, numerical predictions of $O_2$ concentrations and the measurements are in a good agreement.

*3.3.3. In-Furnace NO Concentration.* In Figure 11, the measured in-furnace NO mole fraction (dry basis) of brown and black coal combustion under MILD conditions along the vertical direction (the $z$-axis) of the furnace, is shown. The plots show that, when burning brown coal that has been carried by $CO_2$, NO formation at the top part of the furnace is consistent

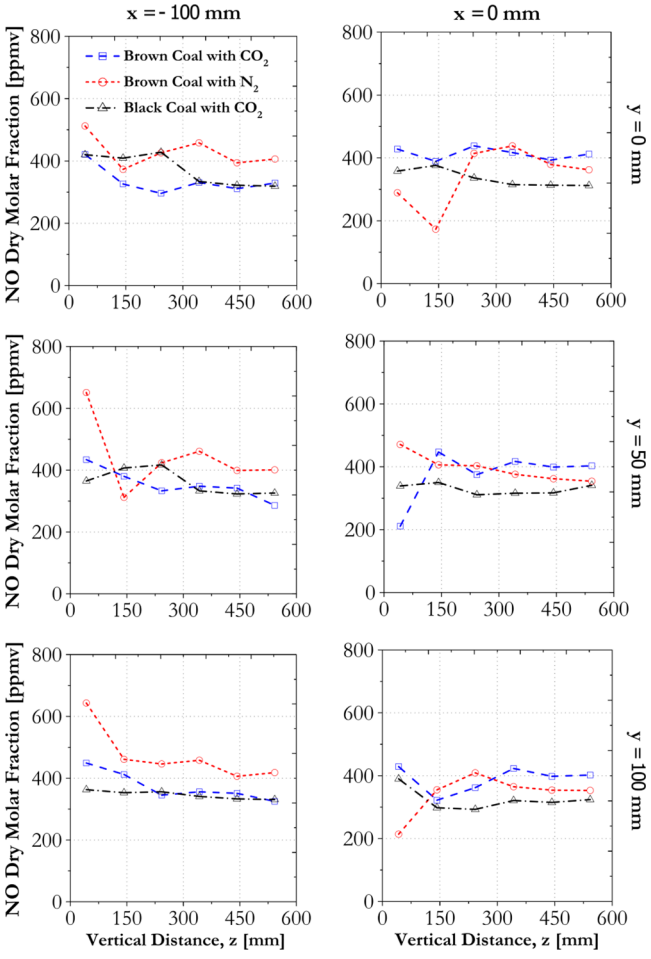


**Figure 11.** In-furnace NO dry molar fraction at $x = -100$ mm (left) and $x = 0$ (centerline) of the MILD combustion furnace operating on brown coal carried by either $CO_2$ or $N_2$, and black coal carried by $CO_2$ along the vertical locations (the $z$-axis) at different horizontal distances (the $y$-axis) from the center of the furnace.


dx.doi.org/10.1021/ef5006836 | Energy Fuels 2014, 28, 6046−6057

at ~400 ppm, while at the bottom ($z$ = 42.5 mm) of the furnace the NO mole fraction decreases to 210 ppm near to the exhaust port ($y$ = 50 mm). This result points to the reburning of NO, as the top part of the furnace is known to have recirculating products. Exhaust gas recirculation of NO produces a positive reburning consumption,[37,38] where NO reacts with hydrocarbons according to the following reaction:

$$CH_i + NO \rightarrow HCN + \text{products} \quad (7)$$

As a result, the overall NO emission is subsequently reduced.

In the case of black coal carried by $CO_2$, the level of NO is constant at furnace locations 342.5 mm and 442.5 mm away from the centerline. The NO mole fraction in the furnace changes marginally in other locations and at the bottom of the furnace is ~350 ppm, which is not dissimilar from that measured in the exhaust for the combustion of black coal.

For brown coal carried by $N_2$, the highest NO mole fraction was measured to be ~650 ppm at 100 mm left from the furnace centerline ($x$ = −100 mm) and 50 mm away from the middle of the furnace ($y$ = 50 mm) and at $z$ = 42.5 mm. The level of NO mole fraction is generally higher for this case than that of brown coal carried by $CO_2$ and black coal carried by $CO_2$ cases. The increased NO formation is caused by the additional $N_2$ in the furnace from the carrier gas, which increases the overall $N_2$ concentration and, hence, contributes to relatively higher NO production, because of the reaction between $O_2$ and the abundance of $N_2$ in the furnace. In addition, better char burnout for this case also has minor influence on higher NO formation by the combustion of $N_2$ contained in the char matrix.

**3.4. Ash Content Analysis.** The char for the three different cases (black coal with $CO_2$, brown coal with $N_2$, and $CO_2$ as carrier gases) studied in this work was collected and analyzed for ash content. The furnace ash analysis indicates that brown coal with $N_2$ as the carrier gas gives the best carbon burnout, with a loss on ignition of 17.5%, while the brown coal with $CO_2$ shows lower extents of burnout with a loss on ignition of 38.0%, while the black coal with $CO_2$ as the carrier gas gives the lowest carbon burnout, with a loss on ignition of 86.9%. Figure 12 displays the unburned carbon in ash and resultant CO emissions for these cases. By performing a carbon balance, it is estimated that only 38.9% of the fixed carbon was consumed for black coal with $CO_2$ and the rest is not combusted, which points to incomplete char burnout of black coal combustion. Conversely, the cases for brown coal with $N_2$ and $CO_2$ as a carrier gas show 91.7% and 83.04% carbon burnout in the furnace, respectively. Taking a more-detailed look at the char burnout (Figure 12), the in-furnace temperature (Figure 8), and the in-furnace $O_2$ concentration (Figure 10), it is found that higher values of temperature and $O_2$ concentration can be attributed to the higher char burnout for brown coal combustion. This observation is not dissimilar to the work of Dally et al.[10] for sawdust MILD combustion in the same furnace. However, the residence time of the coal particles in the furnace plays a vital role in the char burnout and resulting emissions. It is clear that the residence time was not sufficient in the case of black coal. The calculated residence times for these cases are summarized in Table 5. In this table, the residence time of the supplied gaseous streams was calculated using the furnace length method, given in parentheses, and the volume method. The furnace length method relies on the ratio of twice the furnace length to the fuel stream velocity, while the volume method simply relies on the ratio of the total inlet flow rate to the furnace volume. The particle residence time is difficult to estimate, because of the recirculating nature of the flow field inside the furnace. It is noteworthy that the short residence time of carrier gases seems to lead to the appearance of flame sheets and burning particles into the furnace. Moreover, char burnout is also influenced by both the volatile content and particle size. It was reported by Du et al.[39] that the char burnout is increased by ~10%−15% when the coal particle size is reduced from the 150−250 $\mu$m range to the 75−150 $\mu$m range. Weber et al.[16] reported that, for MILD combustion of high volatile coal, char was completely burned. Hence, it can be concluded that the complete combustion of coal char is dependent on the residence time, volatile contents, and/or the particle size.

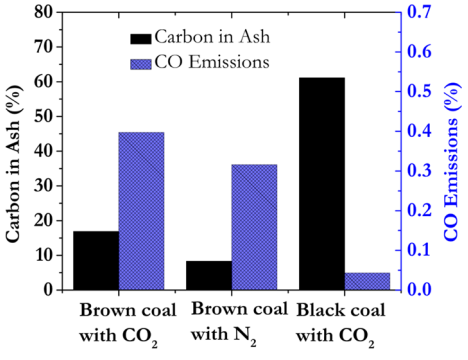


**Figure 12.** Exhaust char burnout and average CO emissions of the MILD combustion of brown coal carried by either $CO_2$ or $N_2$, and black coal carried by $CO_2$.

**Table 5. Flame Visibility, Calculated Residence Time (Using the Furnace Length Method), and Measured Carbon Consumption for the Different Cases**

| | | Residence Time (s) | | | |
|---|---|---|---|---|---|
| fuel | carrier gas | length method | volume method | flame visibility | carbon consumption (wt % db) |
| brown coal | $CO_2$ | 0.148 | 9.80 | not visible | 83.1 |
| brown coal | $N_2$ | 0.112 | 9.57 | not visible | 91.7 |
| black coal | $CO_2$ | 0.148 | 9.80 | not visible | 38.9 |

**3.5. Numerical Modeling Results.** *3.5.1. Effects of Coal Particle Diameter.* Comparison of the velocity fields for Cases 1−3 (see Table 3) show that the coal particle diameter has only a slight effect on furnace performance (results not shown for brevity). However, the particle trajectory for these cases differs noticeably, because of the higher Stokes numbers of larger (heavier) particles. In all cases, the momentum of the air jet dominates that of the fuel jet, creating a stagnation point some distance above the fuel jet, as shown pictorially in Figure 13. The height of the particles' stagnation point above the exit plane is a function of particle diameter: Case 3 produces the highest particle stagnation point with the heaviest particles, Case 2 produces the lowest with the lightest particles, and, for Case 1, the stagnation point falls between the previously cited two, because of the distribution of particle sizes. It is important to note that the overall fuel jet momentum is the same in all cases. Any differences between Cases 1, 2, and 3 are solely due to the size of the particles.


dx.doi.org/10.1021/ef5006836 | Energy Fuels 2014, 28, 6046−6057

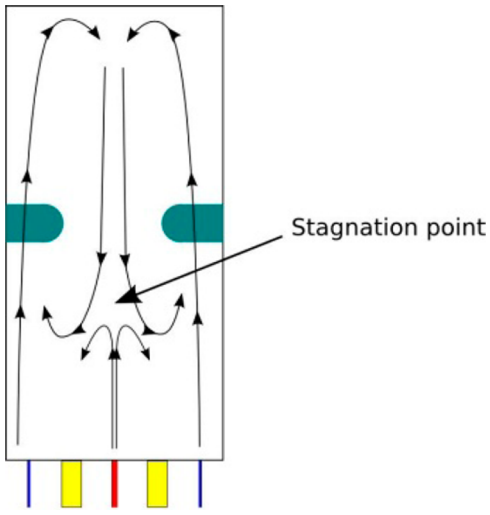


**Figure 13.** Recirculation pattern observed in the furnace.

In each case, devolatilization occurs rapidly and is completed before the particles reach the stagnation point. After devolatilization, MILD combustion proceeds in a manner similar to that of gaseous fuels with little influence from the particles: the high jet momentum of the air creates a strong vortex that entrains the gaseous volatiles which combust in a broad reaction zone, producing a nearly uniform temperature throughout the furnace. The different particle momenta among Cases 1−3 yield noticeably different temperature distributions above the fuel jet (see Figure 14). This is because heavier

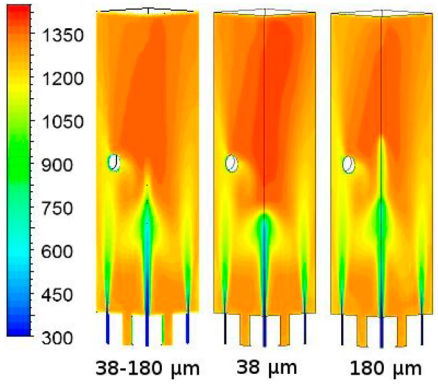


**Figure 14.** Temperature contours (temperatures given in Kelvin) on the symmetry planes for various particle diameters.

particles have more momentum and, therefore, penetrate deeper into the furnace. Consequently, volatile release and combustion will occur further downstream.

*3.5.2. Effects of Inlet Air Temperatures.* Cases 1, 4, and 5 (see Table 3) show the effect of increasing inlet air temperature has on the furnace operation. Physically, these cases correspond to an increase in jet velocity by air preheating, which adds negligible heat (≤0.5%) to the system and results in similar temperature profiles. In the same way that heavier particles have greater jet penetration, increasing the air jet momentum most noticeably lengthens the air jet cores. Figure 15 shows the mass fraction of $O_2$ for Cases 1, 4, and 5, respectively. It is clear that more $O_2$ reaches the top of the furnace in the higher momentum cases. This has several significant implications on the kinetic rates of reactions 1 and 2. As seen in Figure 16,

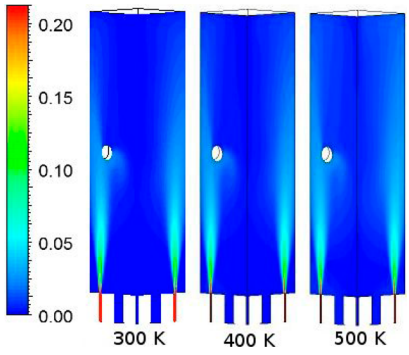


**Figure 15.** Mass fraction of $O_2$ contours on the symmetry planes.

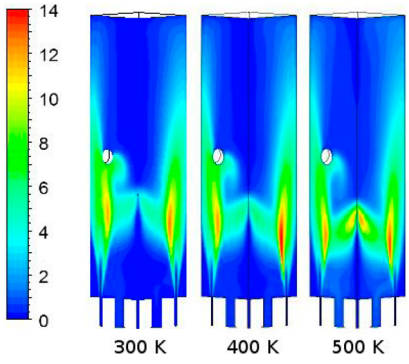


**Figure 16.** Contours of rates of reaction 1 (in units of mol/m$^3$s) on the symmetry planes.

increasing the air jet momentum increases the combustion rate of volatiles (see eq 1) in the fuel jet. Since this reaction depends on local $O_2$ concentration, this increase in reaction rates is due to the increased circulation of air and higher concentration of $O_2$ near the fuel jet. Figure 17 shows that increasing the air jet

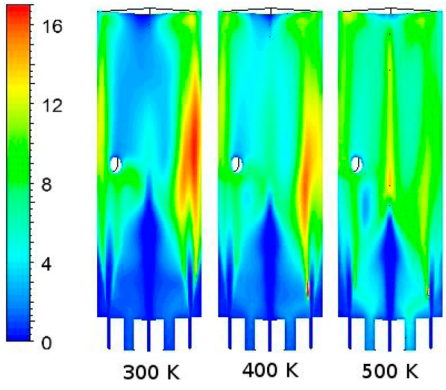


**Figure 17.** Contours of rates of reaction 2 (in units of mol/m$^3$s) on the symmetry planes.

momentum diminishes the oxidation rate of CO, but broadens its reaction zone to almost the entire furnace in Case 5. While strengthened circulation patterns and broadened reaction zones do promote MILD combustion, in this furnace, the higher inlet air jet momenta shift the reaction zone downward into the exhaust pipes. The result is incomplete combustion and higher CO emissions. For Cases 1, 4, and 5, the computed CO emissions are 1010, 1120, and 1600 ppmv, respectively.

*3.5.3. Effects of Inlet Air Mass Flow Rates.* Cases 1, 6, and 7 show an increase in air jet momentum by increasing the air


dx.doi.org/10.1021/ef5006836 | *Energy Fuels* 2014, 28, 6046−6057

mass flow rate. As with the other cases, longer air jet penetration lengths are observed. In cases 6 and 7, volatiles combust quickly upon release from the coal, because of the increased $O_2$ levels throughout the furnace, in the same way as in Case 5.

Despite operating under leaner conditions, significantly more CO exists in the furnace in Case 7. For Cases 1, 6, and 7, their respective CO emissions are 1010, 1360, and 6910 ppmv. This increase is explained by the region where reaction 2 is active, as shown in Figure 18. As with Case 5, increasing the inlet air momentum in Case 6 leads to a broader, more uniform reaction zone and a small increase in CO emissions. In Case 7, the air jet momentum is so strong that reaction 2 mostly only happens in or near the exhaust pipe, which accounts for the drastic increase in CO emissions. Although volatile species can combust properly, the momentum of the air jet is too high to entrain and oxidize CO.

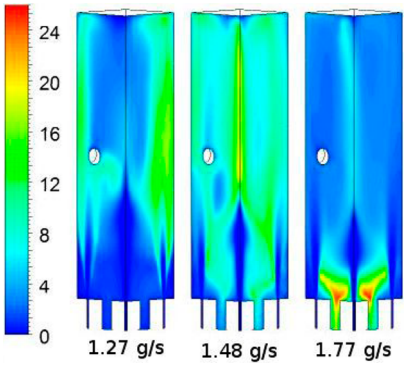


**Figure 18.** Contours of the kinetic rate of reaction 2 (in units of mol/$m^3$s) on the symmetry planes.

## 4. CONCLUSIONS

This study is conducted to advance the understanding of Moderate or Intense Low oxygen Dilution (MILD) combustion characteristics of pulverized coal through a combined experimental and numerical investigation of a parallel jet MILD combustion burner system in a self-recuperative laboratory-scale furnace. The key findings of this investigation are as follows:

(1) The MILD combustion of low-rank brown coal and high-rank black coal was successfully achieved in the present self-recuperative furnace without any external air preheating. The pulverized coal was carried into the furnace using either $CO_2$ or $N_2$ as carrier gas. MILD conditions were achieved for all cases, and no visible flame was observed for any of the test cases.

(2) Results point to a major difference between the two coals and minor differences associated with the carrier gas. It was found that, for brown coal, the NO emissions dropped to 37% of that measured for black coal at an equivalence ratio of $\phi = 0.88$. By comparing higher NO concentration at in-furnace gas with a relatively low NO emission in the exhaust, it can be concluded that there is a strong NO reburning reaction inside the furnace, because of the strong recirculation of combustion products.

(3) The temperature distribution inside the furnace was semi-uniform for all test cases investigated in this study. Computed and measured temperature results indicate that a large recirculation zone, similar to the gaseous fuel MILD combustion,[11] suggests rapid devolatilization of brown coal halfway along the furnace.

(4) Ash content analysis showed that the carbon in the ash for the black coal is quite high and suggests insufficient residence time in the furnace.

(5) It was found that the measured CO level of brown coal cases was 10 times higher than that of black coal cases. The higher CO emission is related to the more-substantial char burnout of brown coal, which is confirmed by the carbon content analysis of the ash.

(6) Numerical modeling was performed to investigate the effect of increasing the air jet momentum and coal particle momentum on furnace dynamics and global emissions for the present furnace. In all cases, volatiles are released in the fuel jet and carried by a strong vortex induced by the air jets in a manner not dissimilar to gaseous MILD combustion in this furnace. The most significant impact of increasing the air jet momentum, either by increasing the temperature or by increasing the mass flow rate, is an increased air jet penetration distance. This facilitates the reaction of the volatiles and leads to more-uniform reaction zones, except in Case 7, where the reaction zone is limited to the base of the furnace, resulting in insufficient mixing and increased CO emissions, despite leaner operating conditions.

(7) The most significant impacts of the coal particle size are on the jet penetration distance and the location of the stagnation point. This modifies the temperature distribution above the fuel jet, but has little impact on achieving MILD combustion. While the results of these simulations are specific to the present experimental furnace, it can be suggested that future experiments must pay special attention to the relative momentum of the air jets, fuel jets, and coal particles to ensure proper mixing, combustion, and circulation. The results may also be helpful in designing new, but similar, self-recuperative furnaces.

## AUTHOR INFORMATION

### Corresponding Author

*Tel.: +61 (0)8 8313 5460. E-mail: manabendra.saha@adelaide.edu.au.

### Notes

The authors declare no competing financial interest.

## ACKNOWLEDGMENTS

M.S. gratefully acknowledges the Adelaide Scholarship International (ASI) of The University of Adelaide and Brown Coal Innovation Australia (BCIA) Top-Up Scholarship for financial support. E.C. gratefully acknowledges the Australian−American Fulbright Commission for their support and eResearch SA for the use of their computational facilities. The authors would also like to thank Mr. Marc Simpson, Manager, Thebarton Laboratory, and Mr. Pedro Nel Alvarado, visiting researcher from Universidad de Antioquia, Colombia, for their help throughout the experiment.

## REFERENCES


(1) Energy Information Administration. *International Energy Outlook 2011*, Report No. DOE/EIA-0484(2011). Sept. 19, 2011; U.S. Department of Energy (DOE): Washington, DC, 2011.

(2) Li, P. F.; Mi, J. C.; Dally, B.; Wang, F. F.; Wang, L.; Liu, Z. H.; Chen, S.; Zheng, C. G. Progress and recent trend in MILD combustion. *Sci. China: Technol. Sci.* **2011**, *54* (2), 255−269.

(3) Katsuki, M.; Hasegawa, T. The science and technology of combustion in highly preheated air. *Proc. Combust. Inst.* **1998**, *27* (2), 3135−3146.

(4) Tsuji, H.; Gupta, A.; Hasegawa, T.; Katsuki, M.; Kishimoto, K.; Morita, M. *High Temperature Air Combustion: From Energy Conservation to Pollution Reduction*. CRC Press: Boca Raton, FL, 2003; Vol. *4*.

(5) Cavaliere, A.; de Joannon, M. Mild combustion. *Prog. Energy Combust. Sci.* **2004**, *30* (4), 329−366.

(6) Wünning, J.; Wünning, J. Flameless oxidation to reduce thermal NO-formation. *Prog. Energy Combust. Sci.* **1997**, *23* (1), 81−94.

(7) Kiga, T.; Yoshikawa, K.; Sakai, M.; Mochida, S. Characteristics of pulverized coal combustion in high-temperature preheated air. *J. Propul. Power* **2000**, *16* (4), 601−605.

(8) Noor, M. M.; Wandel, A. P.; Yusaf, T. A review of MILD combustion and open furnace design consideration. *Int. J. Automot. Mech. Eng.* **2012**, *6* (1), 730−754.

(9) Kumar, S.; Paul, P.; Mukunda, H. Investigations of the scaling criteria for a mild combustion burner. *Proc. Combust. Inst.* **2005**, *30* (2), 2613−2621.

(10) Dally, B. B.; Shim, S. H.; Craig, R. A.; Ashman, P. J.; Szegö, G. G. On the burning of sawdust in a MILD combustion furnace. *Energy Fuels* **2010**, *24* (6), 3462−3470.

(11) Szegö, G. G.; Dally, B. B.; Nathan, G. J. Operational characteristics of a parallel jet MILD combustion burner system. *Combust. Flame* **2009**, *156* (2), 429−438.

(12) Dally, B. B.; Riesmeier, E.; Peters, N. Effect of fuel mixture on moderate and intense low oxygen dilution combustion. *Combust. Flame* **2004**, *137* (4), 418−431.

(13) Szegö, G. G.; Dally, B. B.; Nathan, G. J. Scaling of NOx emissions from a laboratory-scale mild combustion furnace. *Combust. Flame* **2008**, *154* (1−2), 281−295.

(14) Vascellari, M.; Cau, G. Influence of turbulence−chemical interaction on CFD pulverized coal MILD combustion modeling. *Fuel* **2012**, *101*, 90−101.

(15) Stadler, H.; Toporov, D.; Förster, M.; Kneer, R. On the influence of the char gasification reactions on NO formation in flameless coal combustion. *Combust. Flame* **2009**, *156* (9), 1755−1763.

(16) Weber, R.; Smart, J. P.; Kamp, W. On the (MILD) combustion of gaseous, liquid, and solid fuels in high temperature preheated air. *Proc. Combust. Inst.* **2005**, *30* (2), 2623−2629.

(17) Schaffel, N.; Mancini, M.; Szlek, A.; Weber, R. Mathematical modeling of MILD combustion of pulverized coal. *Combust. Flame* **2009**, *156* (9), 1771−1784.

(18) Suda, T.; Takafuji, M.; Hirata, T.; Yoshino, M.; Sato, J. A study of combustion behavior of pulverized coal in high-temperature air. *Proc. Combust. Inst.* **2002**, *29* (1), 503−509.

(19) He, R.; Suda, T.; Takafuji, M.; Hirata, T.; Sato, J. Analysis of low NO emission in high temperature air combustion for pulverized coal. *Fuel* **2004**, *83* (9), 1133−1141.

(20) Stadler, H.; Ristic, D.; Förster, M.; Schuster, A.; Kneer, R.; Scheffknecht, G. $NO_x$-emissions from flameless coal combustion in air, $Ar/O_2$ and $CO_2/O_2$. *Proc. Combust. Inst.* **2009**, *32* (2), 3131−3138.

(21) Zhang, H.; Yue, G.; Lu, J.; Jia, Z.; Mao, J.; Fujimori, T.; Suko, T.; Kiga, T. Development of high temperature air combustion technology in pulverized fossil fuel fired boilers. *Proc. Combust. Inst.* **2007**, *31* (2), 2779−2785.

(22) Shih, T.-H.; Liou, W. W.; Shabbir, A.; Yang, Z.; Zhu, J. A new $k-\varepsilon$ eddy viscosity model for high reynolds number turbulent flows. *Comput. Fluids* **1995**, *24* (3), 227−238.

(23) Kobayashi, H.; Howard, J.; Sarofim, A. F. Coal devolatilization at high temperatures. *Proc. Combust. Inst.* **1977**, *16* (1), 411−425.

(24) Popoff, B.; Braun, M. A Lagrangian approach to dense particulate flows. Presented at the *International Conference on Multiphase Flow*, Leipzig, Germany, 2007.

(25) Chui, E.; Raithby, G. Computation of radiant heat transfer on a nonorthogonal mesh using the finite-volume method. *Numer. Heat Transfer, Part B* **1993**, *23* (3), 269−288.

(26) Magnussen, B. On the structure of turbulence and a generalized eddy dissipation concept for chemical reaction in turbulent flow. Presented at the *Nineteenth AIAA Meeting*, St. Louis, MO, 1981.

(27) Shaw, D. W.; Zhu, X.; Misra, M. K.; Essenhigh, R. H. Determination of global kinetics of coal volatiles combustion. *Proc. Combust. Inst.* **1991**, 1155−1162.

(28) Howard, J.; Williams, G.; Fine, D. Kinetics of carbon monoxide oxidation in postflame gases. *Proc. Combust. Inst.* **1973**, *14* (1), 975−986.

(29) Field, M. Measurements of the effect of rank on combustion rates of pulverized coal. *Combust. Flame* **1970**, *14* (2), 237−248.

(30) Smoot, D.; Pratt, D. *Pulverized-Coal Combustion and Gasification: Theory and Applications for Continuous Flow Processes*; Plenum Press: New York, 1979.

(31) Hsu, K.; Jemcov, A. *Numerical Investigation of Detonation in Premixed Hydrogen−Air Mixture—Assessment of Simplified Chemical Mechanisms*, AIAA Paper 00-2478, AIAA, Denver, CO, 2000.

(32) Smith, I. W. The combustion rates of coal chars: A review. *Proc. Combust. Inst.* **1982**, *19* (1), 1045−1065.

(33) Hill, S.; Douglas Smoot, L. Modeling of nitrogen oxides formation and destruction in combustion systems. *Prog. Energy Combust. Sci.* **2000**, *26* (4), 417−458.

(34) Kim, J. P.; Schnell, U.; Scheffknecht, G.; Benim, A. C. Numerical modelling of MILD combustion for coal. *Prog. Comput. Fluid Dyn.* **2007**, *7* (6), 337−346.

(35) Shaddix, C. R.; Molina, A. Particle imaging of ignition and devolatilization of pulverized coal during oxy-fuel combustion. *Proc. Combust. Inst.* **2009**, *32* (2), 2091−2098.

(36) Hecht, E. S.; Shaddix, C. R.; Molina, A.; Haynes, B. S. Effect of $CO_2$ gasification reaction on oxy-combustion of pulverized coal char. *Proc. Combust. Inst.* **2011**, *33* (2), 1699−1706.

(37) Chen, W.; Smoot, L.; Hill, S.; Fletcher, T. Global rate expression for nitric oxide reburning. Part 2. *Energy Fuels* **1996**, *10* (5), 1046−1052.

(38) Chen, W.; Smoot, L.; Fletcher, T.; Boardman, R. A computational method for determining global fuel-NO rate expressions. Part 1. *Energy Fuels* **1996**, *10* (5), 1036−1045.

(39) Du, S.-W.; Chen, W.-H.; Lucas, J. A. Pulverized coal burnout in blast furnace simulated by a drop tube furnace. *Energy* **2010**, *35* (2), 576−581.

# CHAPTER 4

# NUMERICAL STUDY OF PULVERISED COAL MILD COMBUSTION IN A SELF-RECUPERATIVE FURNACE

# Statement of Authorship

| | |
|---|---|
| Title of Paper | Numerical Study of Pulverized Coal MILD Combustion in a Self-Recuperative Furnace |
| Publication Status | ☑ Published ☐ Accepted for Publication<br>☐ Submitted for Publication ☐ Unpublished and Unsubmitted w ork w ritten in manuscript style |
| Publication Details | **M. Saha**, A. Chinnici, B. B. Dally, and P. R. Medwell, "Numerical Study of Pulverized Coal MILD Combustion in a Self-Recuperative Furnace", *Energy & Fuels* (**2015**), Vol. 29 (11), pp. 7650 – 7669. |

## Principal Author

| | | | |
|---|---|---|---|
| Name of Principal Author (Candidate) | Manabendra Saha | | |
| Contribution to the Paper | Developed ideas. Performed CFD modelling, analysed data, wrote manuscript and acted as corresponding author. | | |
| Overall percentage (%) | 70% | | |
| Certification: | This paper reports on original research I conducted during the period of my Higher Degree by Research candidature and is not subject to any obligations or contractual agreements with a third party that would constrain its inclusion in this thesis. I am the primary author of this paper. | | |
| Signature | | Date | 6/04/2016 |

## Co-Author Contributions

By signing the Statement of Authorship, each author certifies that:

i. the candidate's stated contribution to the publication is accurate (as detailed above);

ii. permission is granted for the candidate in include the publication in the thesis; and

iii. the sum of all co-author contributions is equal to 100% less the candidate's stated contribution.

| | | | |
|---|---|---|---|
| Name of Co-Author | Alfonso Chinnici | | |
| Contribution to the Paper | Helped in developing ideas, performing CFD modelling, data interpretation and manuscript evaluation. | | |
| Signature | | Date | 07/04/2016 |

| | | | |
|---|---|---|---|
| Name of Co-Author | Bassam B. Dally | | |
| Contribution to the Paper | Supervised development of work, helped in developing ideas, data interpretation and manuscript evaluation. | | |
| Signature | | Date | 6-4-16 |

| | | | |
|---|---|---|---|
| Name of Co-Author | Paul R. Medwell | | |
| Contribution to the Paper | Supervised development of work, helped in developing ideas, data interpretation and manuscript evaluation. | | |
| Signature | | Date | 13-APR-2016 |

energy&fuels

Article

pubs.acs.org/EF

# Numerical Study of Pulverized Coal MILD Combustion in a Self-Recuperative Furnace

Manabendra Saha,* Alfonso Chinnici, Bassam B. Dally, and Paul R. Medwell

Centre for Energy Technology, School of Mechanical Engineering, The University of Adelaide, Adelaide SA 5005, Australia

**ABSTRACT:** A numerical study of pulverized coal combustion under Moderate or Intense Low oxygen Dilution (MILD) combustion conditions is presented in a parallel jet self-recuperative MILD combustion furnace. The Reynolds-Averaged Navier−Stokes equations, in a three-dimensional axisymmetric furnace domain, were solved using the Eddy Dissipation Concept model for the turbulence−chemistry interaction. The main aim of this study is to understand the influence of devolatilization models on the prediction accuracy of pulverized coal combustion under MILD combustion conditions. In particular, three devolatilization models are analyzed: a conventional single-rate model, a two-competing-rates model, and an advanced chemical percolation devolatilization (CPD) model based upon structural networks of the coal with a global kinetics mechanism. In addition, a new simplified numerical model is developed for Australian black and/or hard coal and optimized for the MILD combustion conditions. The modeling cases are validated with the experimental results of MILD combustion of high volatile Australian brown coal from Kingston using $N_2$ as a carrier gas and low volatile Australian black coal from the Bowen basin using $CO_2$ as a carrier gas in a MILD combustion furnace. From the comparison, the advanced CPD devolatilization model with a three-step global kinetic mechanism gives, as expected, the best agreement with the experimental measurements for the Kingston brown coal case, while all the models tested provide similar results for the Bowen basin black coal case. The heterogeneous reactions on the char burnout rate for pulverized coal combustion under MILD combustion conditions are presented and discussed. The characteristics of three NO formation mechanisms, namely, thermal-NO, prompt-NO, and fuel-NO, together with the NO reduction mechanism, named NO-reburning, are evaluated using the postprocessing modeling approach. The results reveal that the sum of contributions from the thermal-NO and prompt-NO routes only accounts for less than 3.8% to the total NO emissions, while the fuel-NO route dominates the NO emissions under MILD combustion conditions. It is also found that the total NO emission is reduced by up to 47% for the brown coal case and up to 39% for the black coal case via the reburning mechanisms.

## 1. INTRODUCTION

It is well-established that renewable energy adaptations alone will not address the predicted increase in energy demand around the world. Hence, the use of fossil fuels will remain the predominant source of energy for the foreseeable future. Among the available fossil fuels, coal is the cheapest and is an abundant resource in many parts of the world. While combustion of pulverized coal is linked to global warming and environmental pollution, it supplies 30% of the total global energy demands and is forecast to remain as such until 2035.[1]

Pulverized coal combustion influences the environment through its $CO_2$ emission as well as through emissions of nitrogen oxides ($NO_x$), sulfur dioxide ($SO_2$), soot, mercury, particulate matter (PM), and dozens of other substances released to the atmosphere.[2] Because of the abundant availability of coal as well as economic reasons and more strict legislation against pollutant emissions, major attempts are being touted to make pulverized coal combustion more efficient and environmentally adoptable. Thus, the improvement of advanced pulverized coal combustion technologies is a major goal toward increasing efficiency and lowering pollutant emissions, in particular controlling $NO_x$ emission. In light of this, Moderate or Intense Low oxygen Dilution (MILD) combustion has been identified as an advanced combustion technology to decrease combustion-produced pollutants and improving thermal efficiency.[3] This novel concept is based on exhaust gas and heat recirculation to create a volumetric reaction zone at reduced combustion temperatures. Therefore, the emission of pollutants such as $NO_x$ via the thermal route will sharply decrease due to the reduced temperature and reduced fluctuation found in MILD combustion. Consequently, MILD combustion technology is different from conventional combustion technology because of the nonexistence of any visible or audible flame at optimized conditions. As a result, MILD combustion is also called "flameless combustion" or "flameless oxidation, FLOX".[4] In some cases of MILD combustion technology, high temperature combustion air is used, and thus, this combustion regime is also named "high temperature air combustion" (HiTAC).[5] The word "MILD combustion" will be used in this article.

There is a substantial volume of literature on gaseous[6−11] MILD combustion, which has been successfully implemented in various industrial sectors. Nevertheless, solid fuels, in particular pulverized coal, under MILD combustion conditions have received much less attention than that of gaseous fuels. Thus far, some numerical and experimental investigations have been performed on pulverized coal under MILD combustion conditions.[5,12−25]

**Received:** July 20, 2015
**Revised:** October 9, 2015
**Published:** October 12, 2015





DOI: 10.1021/acs.energyfuels.5b01644
*Energy Fuels* 2015, 29, 7650−7669

On the experimental side, the first significant attempt to apply MILD combustion technology to pulverized coal was conducted by Kiga et al.[5] by burning a high volatile pulverized coal with high temperature preheated air in a drop-tube furnace. Although their experimental measurements suggested that increasing air preheat resulted in reduced $NO_x$ emissions and increased combustion efficiency, they concluded that "the use of high-temperature diluted air was not suitable for pulverized coal combustion". The MILD combustion behavior of high volatile pulverized coal was investigated by Weber et al.[12] using high temperature air (1300 °C) in a furnace, and the measured values of the $NO_x$ emissions at the furnace exit were found to be in the range of 160−175 ppm (at 3% $O_2$ concentrations), which demonstrated the high $NO_x$ reduction potential of this technology. The results reported by Weber et al.[12] were somewhat contradictory with the conclusions reported by Kiga et al.[5] Suda et al.[13] experimentally investigated the MILD combustion characteristics of pulverized bituminous and anthracite coal. Combustion stability, ignition delay, $NO_x$ emission, and char burnout rate were analyzed using a 250 kW furnace. To probe the effect of preheated combustion air temperature on the MILD combustion characteristics, the air temperature was raised to either 350 or 800 °C before entering into the combustion chamber. They found that increased air temperature drastically decreased the ignition delay owing to the fast devolatilization of the coal. He et al.[15] numerically investigated the $NO_x$ production and destruction mechanisms of pulverized coal combustion in a drop-tube furnace operated in MILD mode and validated their models using the experimental results of Suda et al.[13] They reported that, for coal with less volatiles, such as anthracite, NO is predominantly produced from the nitrogen bound in char, whose formation mechanism is yet to be fully understood. Schaffel et al.[22] proposed a computational fluid dynamics (CFD) based model for pulverized Guasare (bituminous) coal MILD combustion to explore the pollutant formation mechanism. They used both the chemical percolation devolatilization (CPD) model and the char combustion intrinsic reactivity model to predict the flow field as well as the temperature and the gas composition ($CO_2$, $O_2$, CO, NO) fields. The results revealed that the volatile contents of the coal particles are liberated in an extremely sub-stoichiometric condition and their N-containing species are predominantly altered to molecular nitrogen instead of forming NO. The outcomes of the study revealed that MILD coal combustion technology consists of potential NO-reburning mechanisms in comparison with conventional technology. The $NO_x$ concentrations were slightly under-predicted, as compared to the measured values, while the CO concentrations varied considerably from the experimental data. They concluded that more elaborate schemes of volatile matter combustion are desired. Vascellari and Cau[24] conducted a numerical study utilizing advanced turbulence−chemistry interaction models to better understand the MILD combustion characteristics of highly volatile bituminous pulverized coal. The numerical study considered the working conditions and the geometry of IFRF furnace No. 1. The numerical results were validated using experimental outcomes of Weber et al.[12] The velocity field was well-predicted by the computational model; however, flame temperatures were slightly overestimated than the measured values, while the NO concentration value was highly over predicted in the devolatilization regime. This study highlighted the need for further investigation, in particular the influence of devolatilization model on coal MILD combustion in order to improve the validity of the prediction of this mode of combustion. Furthermore, detailed kinetic mechanisms (consisting of 103 reactions) and global kinetic mechanisms (consisting of 2 reactions) for gas-phase reactions were investigated in the study of Vascellari and Cau,[24] while no substantial success was reported for the prediction of MILD coal combustion by the detail kinetic mechanisms in comparison with global kinetic mechanisms. In addition, global kinetic mechanisms are efficient in terms of computational cost and CPU working hours. Therefore, global kinetic mechanisms are considered to describe gas-phase reactions in our investigation.

Generally, coal combustion modeling represents an ensemble of sub-models to describe four physical steps, namely, particle heating, devolatilization, volatile combustion, and combustion of char. The most important sub-model of coal combustion modeling is the devolatilization model, which can be expressed as either a simple reaction rate formulation or formulations based upon structural networks of the coal. It is well-established that the devolatilization mode of coal combustion, and especially the release position and rate of volatiles, are the main controlling parameters which regulate the flame shape, and the length and shape of the internal recirculation zone.[26] However, no systematic study has been carried-out to develop an understanding of the influence of the devolatilization model on the prediction of coal combustion under MILD conditions. In addition, no numerical modeling has been found in the literature for Australian black and/or hard coal combustion under MILD combustion conditions. The reason for extending the numerical study of MILD combustion to Australian black is that Australian black coal is a high rank coal which has a higher heating value than other solid fuels such as biomass and brown coal.[27] A previous study[18] has begun to address the aforementioned gaps, but some specific issues remain unresolved, in particular (a) $NO_x$ formation and destruction behavior of low and/or high volatile coal under MILD combustion conditions, (b) flow-field characteristics inside the furnace, and (c) char burnout rate by the heterogeneous reactions, in a self-recuperative furnace.

The present work is to address the stated gaps by solving the Reynolds-averaged Navier−Stokes (RANS) equations using CFD modeling, rather than expensive experimental measurements, which are not viable or even possible for many cases. The main aim is to investigate the prediction accuracy of three devolatilization models; a conventional single-rate devolatilization, a two-competing-rates model,[34] and an advanced CPD model based upon structural networks of the coal. The numerical results are validated using experimental measurements.[18] An additional aim is to develop a simplified model for Australian black coal combustion under MILD combustion conditions. This paper extends previous studies[18,28−30] by adding further information on MILD coal combustion in a self-recuperative furnace through reporting the characteristics of thermal-NO, prompt-NO, fuel-NO, and NO-reburning mechanisms for the MILD combustion of high volatile, low rank Kingston brown coal, and/or low volatile, high rank Bowen basin black coal. Furthermore, numerical results concerning the influence of heterogeneous reactions on char burnout rate for the MILD coal combustion and the flow field inside the furnace are presented and discussed.



DOI: 10.1021/acs.energyfuels.5b01644
Energy Fuels 2015, 29, 7650−7669

## 2. EXPERIMENTAL SUMMARY

**2.1. Furnace Geometry.** The geometry of the self-recuperative MILD combustion furnace[7] is shown in Figure 1. The combustion

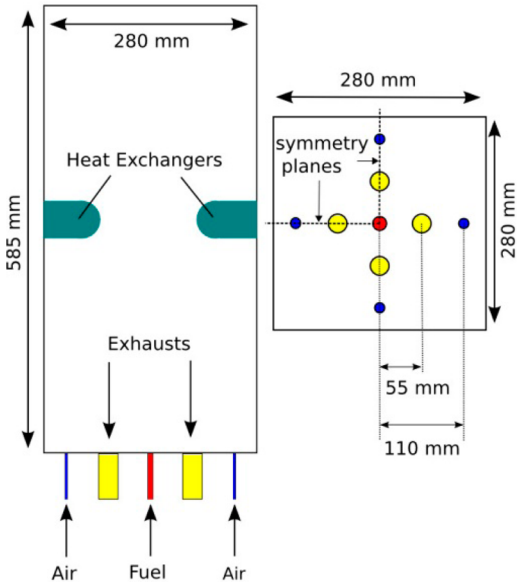


**Figure 1.** Side view (left) and top view (right) of the furnace modeled.

chamber of the furnace has a square cross section of 280 × 280 $mm^2$ and a height of 585 mm. This recuperative furnace includes a central fuel jet (7.5 mm diameter) parallel to four air jets (each 4 mm diameter) and four exhaust ports (each 26.4 mm diameter). Two U-shaped cooling-loop heat exchangers were inserted at a height of 292 mm above the burner exit plane in the furnace on opposite sides to each other. The cooling-loop heat exchangers, with an outer diameter of 33.4 mm, had an exposed surface area of 0.03 $m^2$ within the furnace.

The combustion furnace is preheated with a natural gas flame that is switched off when the furnace temperature is 850 °C. Pulverized coal particles are injected through the central fuel jet into the furnace using either $CO_2$ or $N_2$ as a carrier gas. The supplied water into the heat exchangers had a fixed inlet temperature and flow rate. The heat exchangers transferred on-average 4.32 and 4.83 kW of heat for the combustion of brown coal using $N_2$ as a carrier gas and black coal using $CO_2$ as a carrier gas, respectively, while the furnace was fired at 15 kW.

**2.2. Coal Characterization.** Two types of coal were used in the experiments, namely, high volatile and low rank brown coal from Kingston and low volatile and high rank black coal from the Bowen basin. The coal particles were finely pulverized and sieved into the 38 $\mu m < d \leq 180$ $\mu m$ size range. The gross heating value of Kingston brown coal and Bowen basin black coal is measured to be 20.0 and 31.9 MJ/kg, respectively. Proximate and ultimate analyses of the coals are given in Table 1.

**2.3. Experimental Measurements and Operating Parameters.** The furnace temperatures were measured on the centerline and 100 mm left from the centerline, along the height ($z$ axis) of the furnace. The time-averaged exhaust temperature was measured at a distance of 100 mm from the furnace exit. In these experiments, dry-basis $O_2$, $CO_2$, CO, and NO gas concentrations were measured along the centerline and 100 mm left from the centerline of the furnace. The water-cooled sampling probe was traversed in the straight direction ($y$ direction) at three different locations ($y$ = 0, $y$ = 50, $y$ = 100 mm) across distinct planes of various perpendicular positions ($z$ axis) of the furnace, which provides in total of 36 points of measurement. The coal particles were carried through the central jet by either $CO_2$ or $N_2$ while the four periphery jets were used to inject the combustion air into the furnace. A summary of the operating conditions is shown in Table 2.

**Table 1. Coal Analyses**

| ultimate analysis | | |
|---|---|---|
| | Kingston brown coal (wt % db) | Bowen basin black coal (wt % db) |
| C | 52.5 | 81.2 |
| H | 3.6 | 3.6 |
| O | 17.73 | 3.47 |
| N | 0.48 | 1.35 |
| S | 4.09 | 0.58 |
| **proximate analysis** | | |
| | Kingston brown coal (wt % db) | Bowen basin black coal (wt % db) |
| fixed carbon | 35.7 | 80.7 |
| volatile matter | 42.7 | 9.5 |
| ash | 21.6 | 9.8 |

**Table 2. Operating Parameters for MILD Combustion of Pulverized Coals**

| parameter | $N_2$-carried brown coal | $CO_2$-carried black coal |
|---|---|---|
| periphery air jet velocity (m/s) | 86.2 | 86.2 |
| equivalence ratio, $\phi$ | 0.89 | 0.88 |
| central fuel jet velocity (m/s) | 10.43 | 7.92 |
| thermal input (kW) | 15.2 | 15.5 |
| inlet air temperature (K) | 300 | 300 |

## 3. COMPUTATIONAL MODELS

Coal MILD combustion simulations were performed using ANSYS Fluent version 14.5. A quarter of the furnace was modeled to take advantages of the symmetry. A three-dimensional (3D) structured, hexahedral mesh of 1.1 million cells is constructed (shown in Figure 2).


**Figure 2.** Computational grid used for numerical simulations.

The steady RANS equations are solved by all presented models in this investigation. The SIMPLE (Semi-Implicit Method for Pressure Linked Equations) algorithm method is used for the pressure−velocity coupling. The second-order upwind scheme is employed for momentum, energy, turbulent kinetic energy, species transport, turbulent dissipation, and pressure discretization.

Previous numerical modeling[18] has found that the two-equation realizable $k$-$\varepsilon$ turbulence model[31] is the best for this furnace. The radiation heat transfer equation is solved by using the Discrete Ordinates (DO)[32] radiation model because the DO radiation model is considered more suitable for the


DOI: 10.1021/acs.energyfuels.5b01644
Energy Fuels 2015, 29, 7650−7669

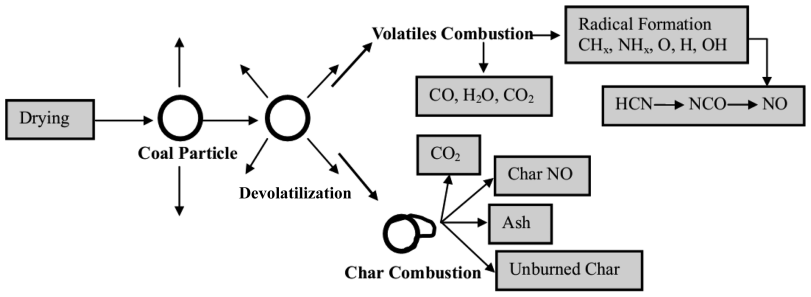


**Figure 3.** Diagram of the coal combustion steps.

laboratory-scale furnace.[33] The Rosin−Rammler distribution is used with the particles' mean diameter of 109 $\mu$m and the particle size range from 38 to 180 $\mu$m in diameter to describe particle size distribution.

The coal particles are treated as a discrete phase, whereas, for updating particle source terms, the coal particles are tracked using a deterministic Lagrangian method.[34] The simulations were run with 48 cores on the Tizard supercomputer facilities of eResearch SA.

Pulverized coal combustion is modeled using four well-defined steps, namely, drying, devolatilization, volatile combustion, and char oxidation. The successive steps are illustrated in Figure 3.

**3.1. Drying.** Coal particles are heated for drying the moisture from the particles' surface in a hot atmosphere by radiation or convection. This process usually occurs very rapidly. It is noteworthy that the pulverized coal used in these experiments was predried using an electric furnace at 105 °C for 4 h (as shown in Table 1), and thus, the computational models do not incorporate the drying process.

**3.2. Devolatilization.** Coal devolatilization is referred to as pyrolysis when coal is devolatilized in an inert gas.[35] The terms "pyrolysis" and "devolatilization" are generally not differentiated from each other owing to the similar behavior of coal in the two processes considering the volatile matter composition and char chemistry. The process of evolution of combustible gases due to the thermal decomposition of the coal is referred to as pyrolysis/devolatilization. Coal devolatilization can be considered as a two-stage process.[36] The first stage is the decomposition of functional groups of coal particles to release volatile matters, composed by heavy hydrocarbons (tar), light hydrocarbons, and gases. During the second stage of devolatilization, tar decomposes and produces soot, light hydrocarbons, and additional gases.

It has been reported that the devolatilization process has great impact on ignition and $NO_x$ emissions in pulverized coal combustion.[26] Three devolatilization models are considered in the present study. The first model is a single-step reaction model where the kinetic rate ($k_v$) is calculated in an Arrhenius form; $k_v = A\cdot\exp(-E_a/RT)$. Here, "$A$" and "$E_a$" represent the pre-exponential factor and activation energy, respectively. The single-step model is based on the assumption that the devolatilization process is first-order dependent on the total volatile contents in the coal particle and employs global kinetics by the following reaction:

$$\text{coal} \rightarrow \text{volatile}\ (\alpha) + \text{char}\ (1-\alpha)$$

Here, "$\alpha$" is the distribution coefficient. The kinetic data such as pre-exponential factor, $A = 6.6 \times 10^4\ s^{-1}$, and activation energy, $E_a = 1.0463 \times 10^5$ J/kg mol, were used for the brown coal combustion case following Kobayashi et al.[37] For the black coal combustion case, the kinetic parameters were set to $A = 4.5 \times 10^5\ s^{-1}$ and $E_a = 8.1 \times 10^7$ J/kg mol. These values have been measured experimentally for Australian black coal and/or calibrated for the single-rate model, employing an advanced devolatilization model (chemical percolation devolatilization, CPD) by Sheng et al.[33]

The second model is the well-established two-competing-rates (2CR) model.[37] The model comprises two overall reactions, i.e., a low temperature step, $r_1$, and a high temperature step, $r_2$, as follows:

$$\text{coal} \xrightarrow{r_1} \text{volatile}\ (\alpha 1) + \text{char}\ (1-\alpha 1)$$

$$\text{coal} \xrightarrow{r_2} \text{volatile}\ (\alpha 2) + \text{char}\ (1-\alpha 2)$$

The kinetic rates that control the devolatilization over different temperature ranges are given by

$$r_1 = A_1 \exp^{-\left(\frac{E_1}{RT}\right)}$$

$$r_2 = A_2 \exp^{-\left(\frac{E_2}{RT}\right)}$$

For the brown coal case, the pre-exponential factors ($A_1$, $A_2$) and the activation energies ($E_1$, $E_2$) were set to $A_1 = 2 \times 10^5\ s^{-1}$, $E_1 = 1.046 \times 10^8$ J/kg mol, $A_2 = 1.3 \times 10^7\ s^{-1}$, and $E_2 = 1.674 \times 10^8$ J/kg mol, according to Kobayashi et al.[37] Only the brown coal case was modeled employing the two-competing-rates (2CR) model since no kinetic parameters for the Bowen basin black coal are available in the literature for this model.

The third model which is considered in this study to evaluate coal devolatilization is the chemical percolation devolatilization (CPD) model.[38−40] In contrast to the simple global kinetic models that are based on empirical rate relations, the CPD coal devolatilization model characterizes the devolatilization behavior of rapidly heated coal based on the physical and chemical transformation of the coal structure. The CPD model considers the coal structure as a network of chemical bridges with linking the atomic clusters or a simplified lattice to describe the physical and chemical processes. This model is able to predict accurately[41] the volatile rates and composition in terms of light gases and tar (heavier hydrocarbons).

The five coal-specific parameters used in the CPD model inputs are the average molecular weight per aromatic cluster ($M_{cl}$), the average side-chain molecular weight ($M_\delta$), the fraction of in-tact bridges ($p_0$), the average number of attachments per cluster ($\sigma + 1$), and initial fraction of char bridges ($c_0$). The CPD model uses nuclear magnetic resonance (NMR) data to determine the physical structure of the coal as a form of aromatic carbons per cluster and the number of attachments per aromatic cluster, which provide the model


DOI: 10.1021/acs.energyfuels.5b01644
Energy Fuels 2015, 29, 7650−7669

input parameters. However, such kinds of experimental data are not easily available for specific types of coal. Hence, a mathematical expression was required to estimate the input parameters for the CPD model. Genetti et al.[42] formulated a correlation to obtain the input parameters for the CPD model from proximate and ultimate analyses of the coal. The CPD parameters used for coal devolatilization in this study are obtained from the proximate and ultimate analyses of Australian brown coal and black coal following the correlation of Genetti et al.[42] and are shown in Table 3.

**Table 3. Parameters Used for CPD Model**

| parameter | Kingston brown coal | Bowen basin black coal |
|---|---|---|
| $M_\delta$ | 51.8 | 14.1 |
| $M_{cl}$ | 351.9 | 239.8 |
| $p_0$ | 0.60 | 0.83 |
| $\sigma + 1$ | 4.30 | 4.33 |
| $c_0$ | 0 | 0 |

**3.3. Combustion of Volatiles.** The volatile matter is assumed to be composed of elements (i.e., C, H, O, N, S), which enter the gas phase through the devolatilization reaction. In this study, a global volatile combustion mechanism is used, instead of tracking individual volatile species:

$$C_xH_yO_zN_lS_n + \left(\frac{x}{2} + \frac{y}{2} - \frac{z}{2} + n\right)O_2 \rightarrow xCO + \frac{y}{2}H_2O + \frac{l}{2}N_2 + nSO_2 \quad \text{(R1)}$$

The values of the variables $x$, $y$, $z$, $l$, and $n$ are obtained from the ultimate analysis of the coal used (refer to Table 1). The kinetic constants of this reaction R1 are $A = 4.84 \times 10^7$ and $E_a = 5.1 \times 10^7$ J/kg mol for the brown coal case according to previous studies,[18] whereas, for the black coal case, these parameters are $A = 5.03 \times 10^{11}$ and $E_a = 2 \times 10^8$ J/kg mol following Álvarez et al.[43]

The present work uses two gas-phase reaction models. The first case considers a two-step homogeneous reaction model:

$$CO + 0.5O_2 \rightarrow CO_2 \quad \text{(R2)}$$

$$H_2 + 0.5O_2 \rightarrow H_2O \quad \text{(R3)}$$

In the two-step gas-phase reaction model, CO and $H_2$ are completely oxidized and thus produce $CO_2$ and $H_2O$.

The second case considers a three-step gas-phase reaction model. The three-step global mechanism was originally proposed by Westbrook and Dryer[44] for premixed and non-premixed flames of hydrocarbons. Wang et al.[45] optimized the three-step gas-phase reactions using a modified mechanism of Westbrook and Dryer for MILD combustion of methane in a turbulent flow reactor. In the present work, a simplified model for MILD combustion of pulverized coal is developed by applying the three-step gas-phase reaction model and validated with the results from previous experimental measurements.[18]

The three-step gas-phase reaction model involves the following steps:

$$CO + 0.5O_2 + H_2O \rightleftharpoons CO_2 + H_2O \quad \text{(R4)}$$

$$H_2 + 0.5O_2 \rightleftharpoons H_2O \quad \text{(R5)}$$

$$CO + H_2O \rightarrow CO_2 + H_2 \quad \text{(R6)}$$

The first two reactions (i.e., R4 and R5) of the three-step gas-phase reactions are reversible reactions. The kinetic constants for reactions R2–R6 are listed in Table 4.

**3.4. Char Combustion.** Char particles are microporous solids produced when volatile matter is released from the coal particles by rapid devolatilization. Three sequential processes, namely, boundary layer diffusion, chemical reaction, and pore diffusion,[22,26] control the char oxidation rate in the conventional coal combustion approach. However, in MILD combustion of coal, char burning is influenced by strong exhaust gas recirculation and heterogeneous reactions with high concentrations of $CO_2$ and $H_2O$.[24] Therefore, Boudouard (R8) and gasification (R9) reactions are considered in addition to the oxidation (R7) reaction:

$$C_{char} + \frac{1}{2}O_2 \rightarrow CO \quad \text{(R7)}$$

$$C_{char} + CO_2 \rightarrow 2CO \quad \text{(R8)}$$

$$C_{char} + H_2O \rightarrow H_2 + CO \quad \text{(R9)}$$

In Table 5, the kinetic constants of the heterogeneous reactions R7–R9 are listed.

**3.5. Turbulence–Chemistry Interaction Model.** The interaction between turbulent flow and chemical reaction plays a vital role in MILD combustion modeling.[24] Vascellari and Cau[24] reported that infinitely fast chemistry–turbulence models, such as the Eddy Dissipation Model (EDM), cannot correctly predict experimental results for MILD combustion conditions. This is because, in the MILD combustion case, the chemical time scale is of the same order to the turbulence time scale and the reactions take place volumetrically rather than a narrow reaction zone as found in conventional combustion. Therefore, a more sophisticated turbulence–chemistry interaction model is necessary for the accurate prediction of MILD combustion. Hence, the combustion model in the present study uses the Eddy Dissipation Concept (EDC) model[54] with finite-rate chemistry. The volatile combustion and char burnout are characterized by using the multiple-surface-reactions combustion model.

**Table 4. Kinetic Constants for Homogeneous Gas-Phase Reactions R2–R6**

| gas-phase model | reaction | $A$ | $E_a$ (J/kg mol) | reference |
|---|---|---|---|---|
| two-step | R2 | $1.3 \times 10^{11}$ | $1.26 \times 10^8$ | 46 |
| | R3 | $9.87 \times 10^8$ | $3.1 \times 10^7$ | 47 |
| three-step | R4 forward | $2.24 \times 10^6$ | $4.18 \times 10^7$ | 45 |
| | backward | $1.1 \times 10^{13}$ | $3.28 \times 10^8$ | |
| | R5 forward | $7.9 \times 10^{10}$ | $1.46 \times 10^8$ | 45 |
| | backward | $3.48 \times 10^{13}$ | $3.98 \times 10^8$ | |
| | R6 | $2.75 \times 10^9$ | $8.36 \times 10^7$ | 45, 48, 49 |



DOI: 10.1021/acs.energyfuels.5b01644
Energy Fuels 2015, 29, 7650–7669

Table 5. Kinetic Constants for Heterogeneous Reactions R7−R9

| | Kingston brown coal | | | Bowen basin black coal | | |
|---|---|---|---|---|---|---|
| reaction | $A$ | $E_a$ (J/kg mol) | reference | $A$ | $E_a$ (J/kg mol) | reference |
| R7 | 0.005 | $7.4 \times 10^7$ | 50 | $1.97 \times 10^2$ | $1.53 \times 10^5$ | 51 |
| R8 | 0.00635 | $1.62 \times 10^8$ | 52 | 5.69 | $2.42 \times 10^5$ | 53 |
| R9 | 0.00192 | $1.47 \times 10^8$ | 52 | $2.41 \times 10^2$ | $2.63 \times 10^5$ | 53 |

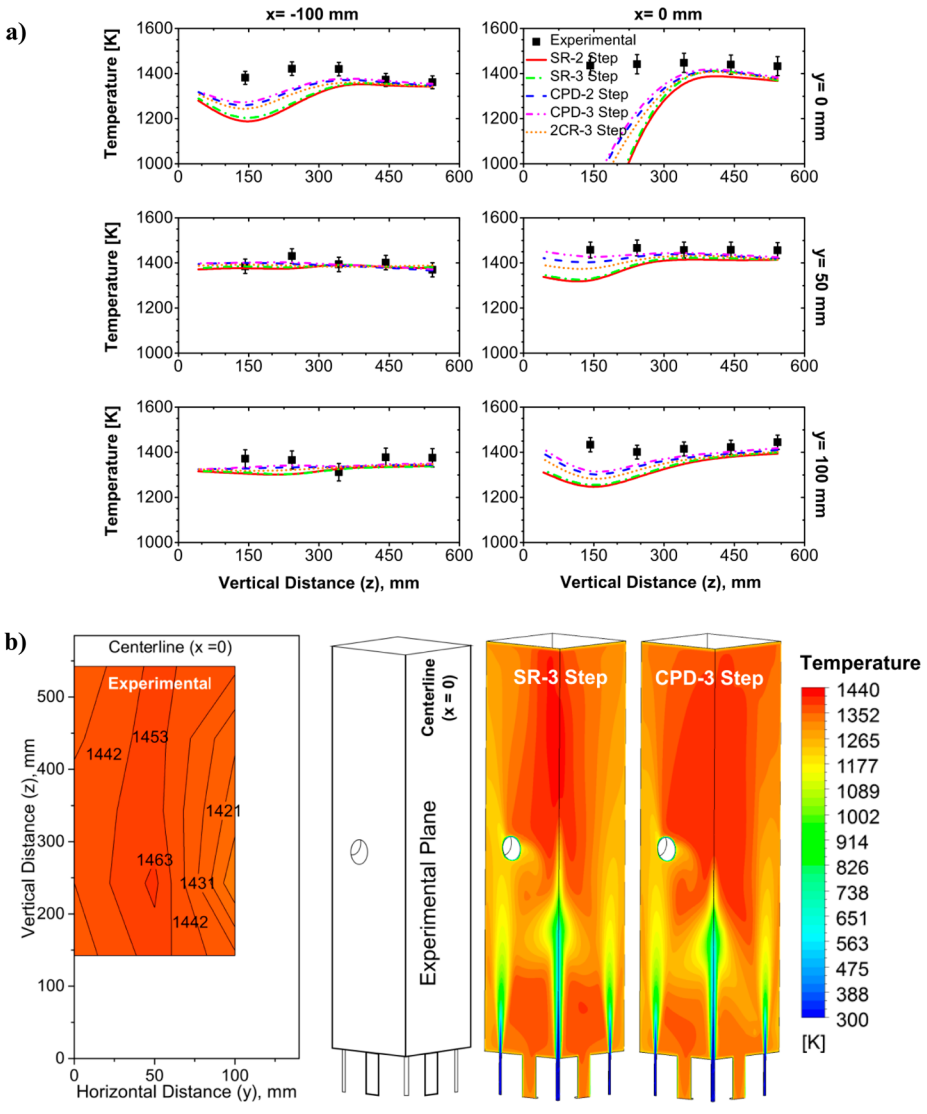


Figure 4. Temperature of brown coal using $N_2$ as a carrier gas case: (a) Calculated and measured profiles of the furnace. The standard deviations are given as error bars. (b) Contour plots of experimental results at the centerline and numerical results (single-rate three-step and CPD three-step) on the symmetry planes of the furnace.

## 4. RESULTS AND DISCUSSION

The numerical modeling results of pulverized coal combustion in a self-recuperative furnace operated in MILD mode are revealed and validated against the experimental outcomes.[18] In total, seven different numerical simulations are performed. Five simulations are conducted for Kingston brown coal using $N_2$ as a carrier gas, namely, single-rate devolatilization with two-step gas-phase reactions (SR-2 Step), single-rate devolatilization with three-step gas-phase reactions (SR-3 Step), CPD with two-step gas-phase reactions (CPD-2 Step), CPD with three-step gas-phase reactions (CPD-3 Step), and the two-competing-rates devolatilization model with three-step gas-phase reactions (2CR-3 Step). For Bowen basin black coal, two simulations are conducted using $CO_2$ as a carrier gas, namely, the SR-3 Step and CPD-3 Step models.

**4.1. Furnace Temperature.** The comparison between the numerical results and the measured mean temperatures for the $N_2$ carried brown coal and $CO_2$ carried black coal cases are shown in Figures 4a and 5a, respectively. The calculated and measured temperatures are presented for different perpendicular locations ($z$ direction) of the furnace centerline ($x$ = 0 mm) and 100 mm left ($x$ = −100 mm) from the centerline for each of the cases.

A relatively good agreement can be found between the model predictions and the measured temperatures in Figures 4a and



DOI: 10.1021/acs.energyfuels.5b01644
Energy Fuels 2015, 29, 7650−7669

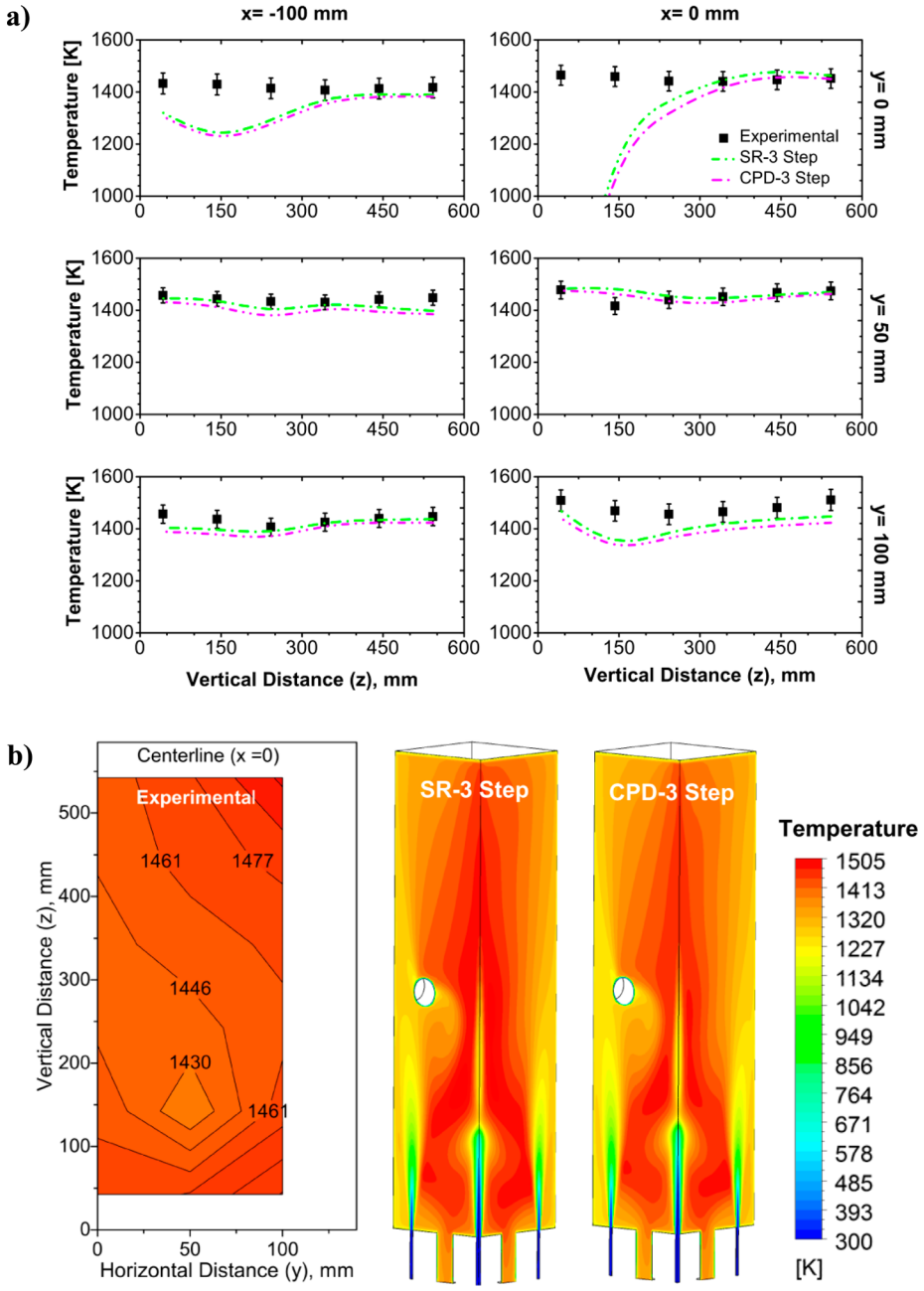


**Figure 5.** Temperature of black coal using $CO_2$ as a carrier gas case: (a) Calculated and measured profiles of the furnace. The standard deviations are given as error bars. (b) Contour plots of experimental results at the centerline and numerical results (single-rate three-step and CPD three-step) on the symmetry planes of the furnace.

5a. The exception is the temperatures close to the fuel jet exit at the centerline ($x$ = 0 mm, $y$ = 0 mm) of the furnace, where all models predict a much lower temperature. This discrepancy disappears 50 mm away from these locations, as seen in other plots of these figures. In general, numerical predictions for all cases in this study largely underestimate the furnace temperature at the location of the fuel jet. The numerical simulations do not predict heat release and consequently produce a cold zone near the exit of the fuel jet, which is not found in the experimental data. This cold zone is responsible for the underestimation of temperatures in this region. It is speculated that the cold zone is associated with a delayed flame ignition and the comparatively poor performance of the coal devolatilization model, in particular for the MILD combustion condition where $O_2$ is strongly diluted to a lower value by the recirculation of the products of combustion. Nevertheless, the temperature levels, as well as the temperature peaks, are regenerated well by the numerical simulations at 50 mm and 100 mm away from the center of the furnace.

With regard to the brown coal case, it can be observed in Figure 4a that the CPD model is characterized by a better agreement with the experimental measurements, although the single-rate and the two-competing-rates devolatilization models predict the basic trend of the temperature profile. Nonetheless, it can be seen that the two-competing-rates model shows slightly better performance in comparison with the single-rate model, suggesting that the effect of competing rates on coal devolatilization influences the overall reliability of simplified



DOI: 10.1021/acs.energyfuels.5b01644
*Energy Fuels* 2015, 29, 7650−7669

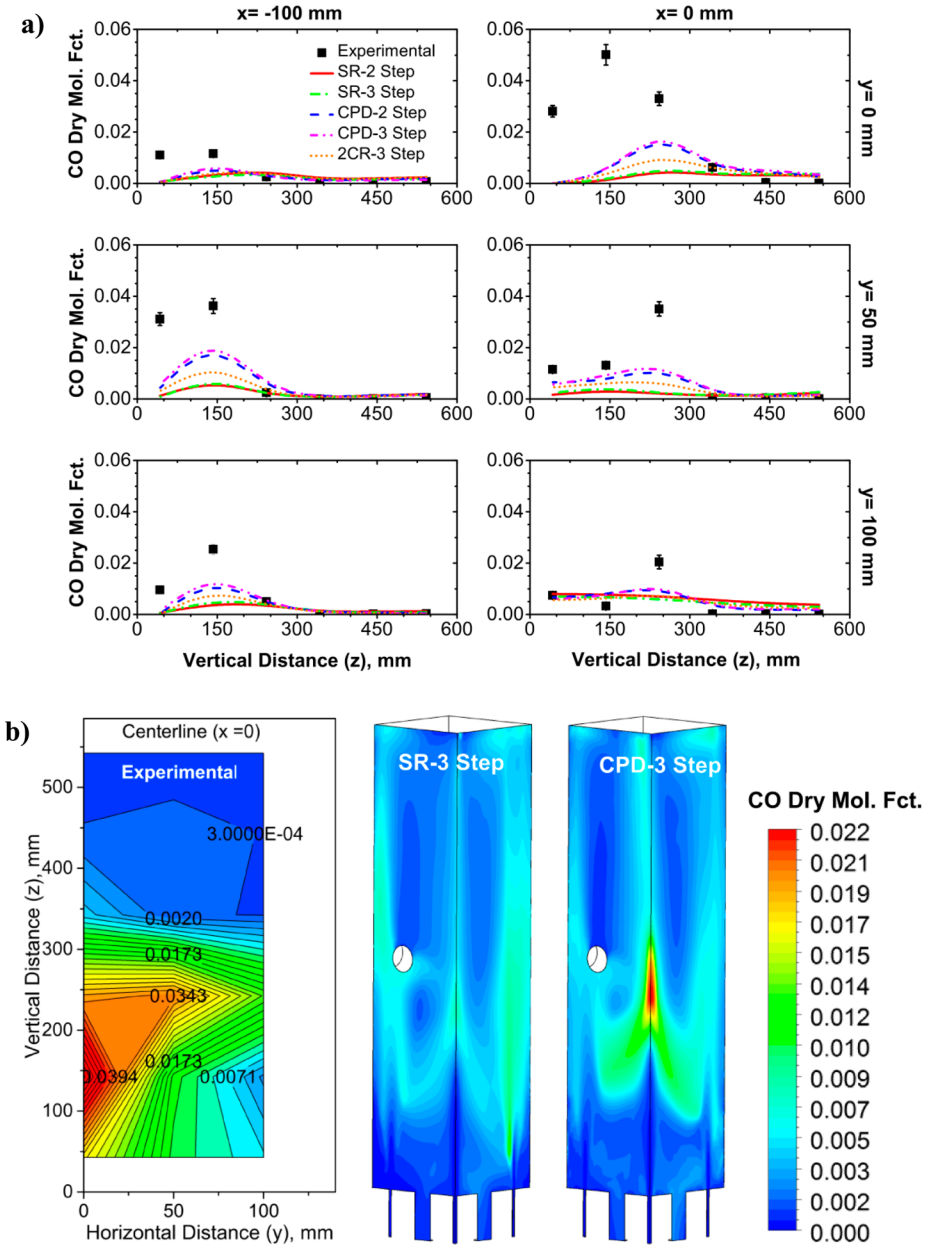


**Figure 6.** In-furnace CO dry molar fraction of brown coal using $N_2$ as a carrier gas case: (a) Calculated and measured profiles of the furnace. The standard deviations are given as error bars. (b) Contour plots of experimental results at the centerline and distributions of numerical results (single-rate three-step and CPD three-step) on the symmetry planes of the furnace.

devolatilization models. For either devolatilization model, the two-step and three-step gas-phase reactions show very similar behavior regarding the prediction of furnace temperatures.

For the black coal case, no remarkable difference was observed between the modeling results obtained by single-rate and CPD models. In this view, the different accuracy obtained in the brown and black coals simulations employing the single-rate model can be attributed to the relative difference with which the activation energy and pre-exponential factor were calibrated/chosen in the simulations. In particular, as reported in section 3.2, the kinetic parameters of the single-rate model employed for the Bowen basin black coal were obtained experimentally for Australian black coals and/or calibrated using the CPD model as external tool by Sheng et al.[33] For the Kingston brown coal case, instead, the kinetic data of the single-rate model were set to those obtained experimentally obtained in an early work of Kobayashi et al.,[37] investigating brown coals with similar characteristics of the coal analyzed in this study (thus, the kinetic data were not calibrated employing the CPD model). This difference could also explain the similar performances of the single-rate and the CPD models in predicting the measured in-furnace temperature profiles for the black coal case.

Figures 4b and 5b illustrate the comparison of temperature contour plots between experimental results at the centerline and numerical results of single-rate three-step and CPD three-step modeling on the symmetry planes of the furnace for the brown coal and black coal cases, respectively. The figures clearly revealed that the furnace temperature is almost homogeneous with as low as 30 K difference at various positions. Nonetheless, an obvious distinction subsists for those calculated and measured temperatures between both cases. It is



DOI: 10.1021/acs.energyfuels.5b01644
Energy Fuels 2015, 29, 7650−7669

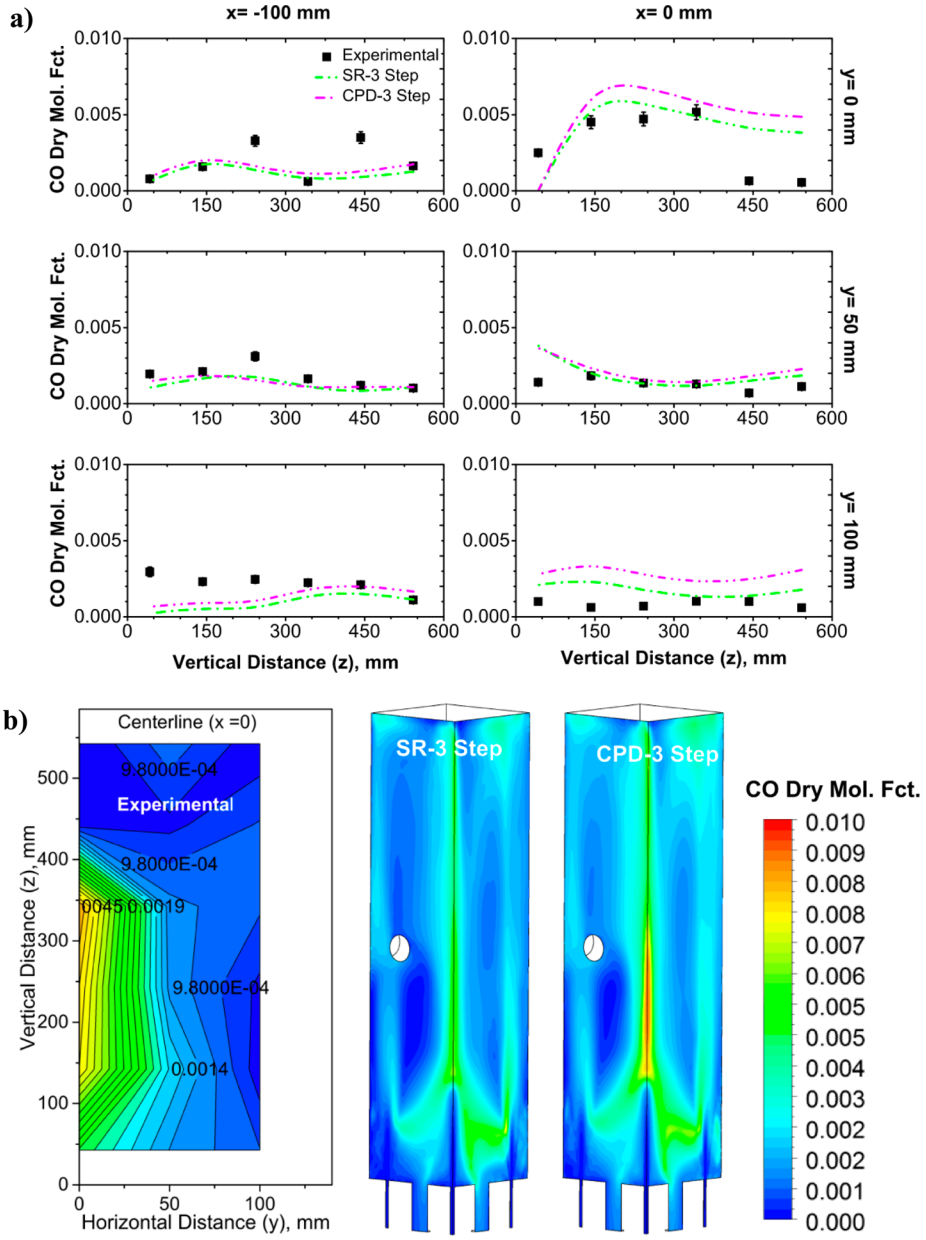


**Figure 7.** In-furnace CO dry molar fraction of black coal using $CO_2$ as a carrier gas case: (a) Calculated and measured profiles of the furnace. The standard deviations are given as error bars. (b) Contour plots of experimental results at the centerline and distributions of numerical results (single-rate three-step and CPD three-step) on the symmetry planes of the furnace.

shown in Figures 4b and 5b that a big recirculation zone is produced in the top portion of the furnace. The contour plots (Figures 4b and 5b) of numerical data imply that the fuel jet penetrates further within the MILD combustion furnace and its calculated temperature is less than the experimental measurements.

**4.2. In-Furnace Gas Composition.** *4.2.1. In-Furnace CO Concentration.* The comparison between the numerical results and measured in-furnace CO concentration (dry basis) for the brown coal carried by $N_2$ and black coal carried by $CO_2$ cases is shown in Figures 6a and 7a, respectively. The measured and calculated in-furnace CO dry molar fractions are presented for different vertical positions ($z$ direction) of the furnace centerline and 100 mm left from the centerline for all cases. Figures 6b and 7b illustrate the comparison of CO dry molar fraction contour plots between experimental results at the centerline and numerical results of single-rate three-step and CPD three-step modeling on the symmetry planes of the furnace for the brown coal and black coal cases, respectively.

For the brown coal combustion case, a large volume of CO concentration was measured at the bottom portion of the furnace. The highest measured concentration of CO was 5% along the centerline at $z$ = 142.5 mm in the furnace, for the MILD combustion of brown coal. However, considering the black coal case, the volatiles release seems to start at the $z$ = 342.5 mm position of the furnace, which is due to the slow pyrolysis of low volatile black coal. It can also be seen that a low concentration of CO was measured in the top part of the furnace, suggesting that no unburned gaseous volatiles exist in this zone.

With respect to the experimental measurements for the brown coal case, a large difference in CO production can be



DOI: 10.1021/acs.energyfuels.5b01644
*Energy Fuels* 2015, 29, 7650−7669

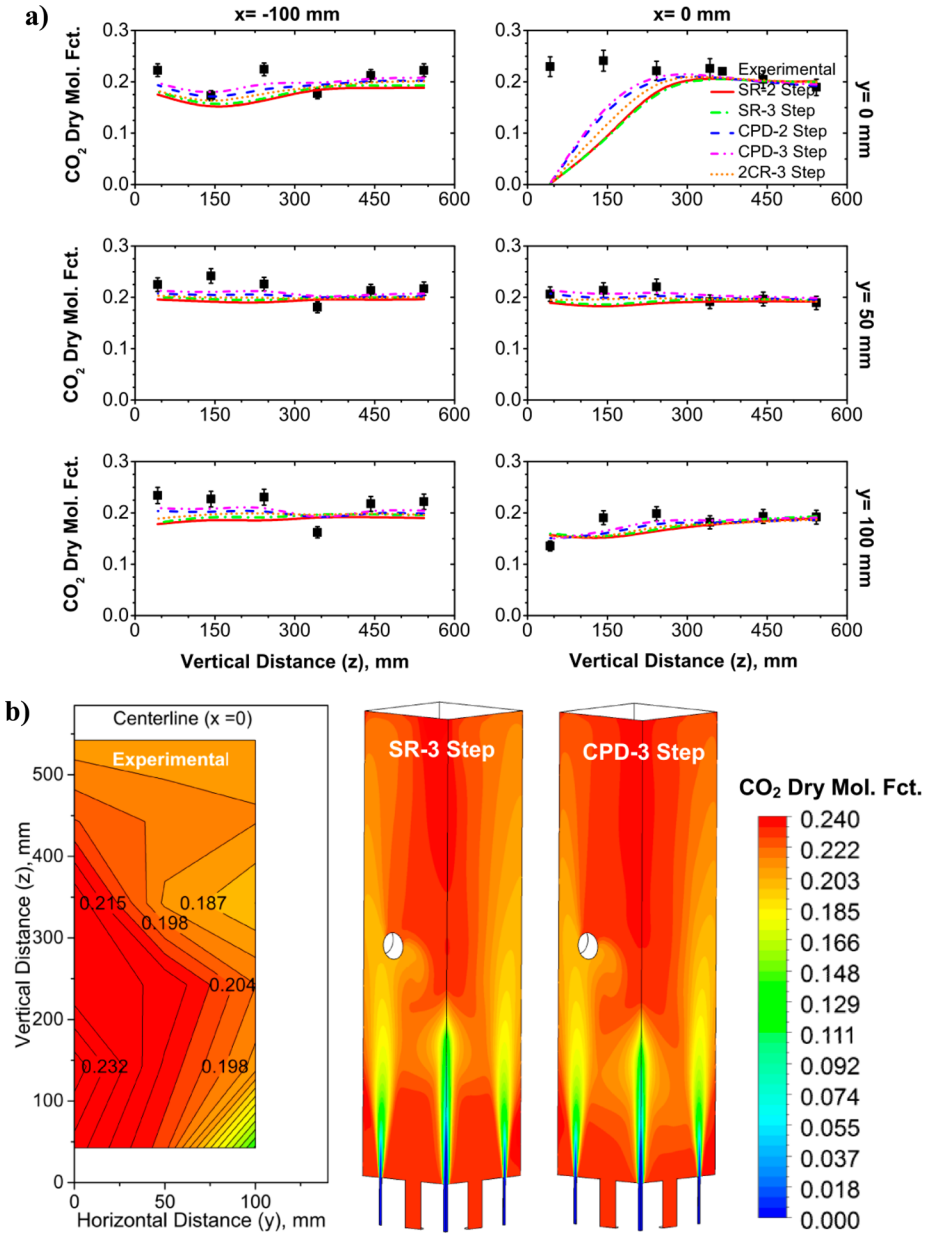


**Figure 8.** In-furnace $CO_2$ dry molar fraction of brown coal using $N_2$ as a carrier gas case: (a) Calculated and measured profiles of the furnace. The standard deviations are given as error bars. (b) Contour plots of experimental results at the centerline and distributions of numerical results (single-rate three-step and CPD three-step) on the symmetry planes of the furnace.

observed among the numerical predictions from the contour plots and the vertical CO concentration profiles, particularly around the middle of the furnace. Overall, numerical models predict a lower concentration of CO as compared to the experiments. CO is produced and oxidized in a number of parallel and sequential reactions. CO is escaped as a volatile component, as a volatile oxidation product, and as a char combustion product. CO is oxidized by OH radicals and O radicals. In addition, the water gas shift reaction ($CO + H_2O \rightarrow CO_2 + H_2$) alters CO concentrations. In our numerical simulations, CO is generated only from the oxidation of volatiles and char combustion reactions. Furthermore, the CO concentrations near the fuel jet are low in comparison with the measured values, consistent with the temperature predictions in this region (see Figures 4b and 5b). Indeed, this region corresponds to the cold zone and relates to the ignition delay in the computational models. The devolatilization models are believed to be responsible for the difference, where, in the experiment, the devolatilization process was faster than the simulations. Nevertheless, the CPD model gives a better prediction than the single-rate and the two-competing-rates devolatilization models. In particular, numerical simulations showed that, for the CPD case, the volatile release process occurs earlier and faster, thus producing a higher release of volatile contents in comparison with the other devolatilization models analyzed. As a consequence, the CPD devolatilization model also leads to a higher CO concentration. With regard to the performance of the simplified models tested, the two-competing-step model shows a better agreement with the experimental data in comparison with the single-rate model.

For the black coal case, the single-rate and the CPD models predict a similar CO concentration. In particular, good



DOI: 10.1021/acs.energyfuels.5b01644
Energy Fuels 2015, 29, 7650−7669

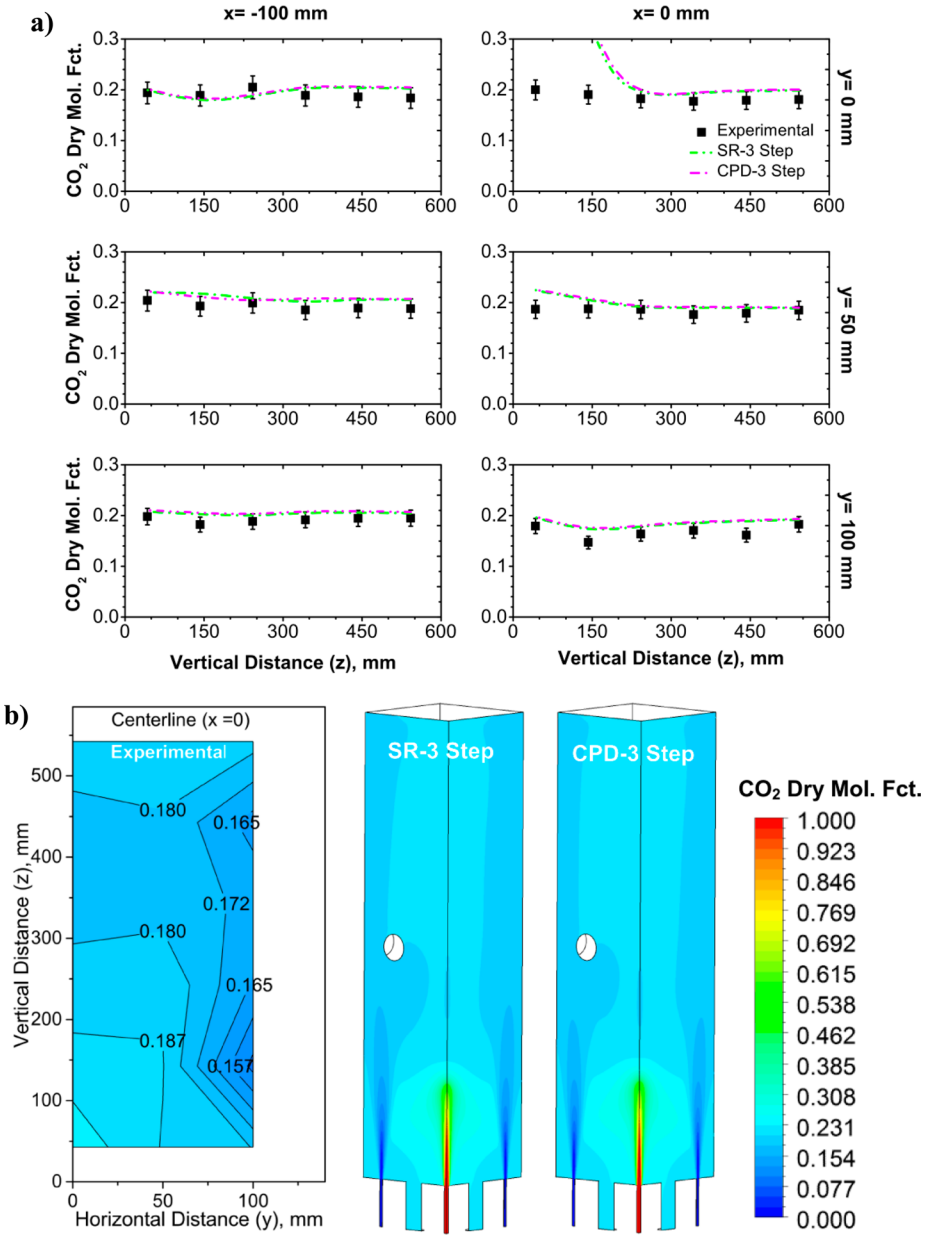


**Figure 9.** In-furnace $CO_2$ dry molar fraction of black coal using $N_2$ as a carrier gas case: (a) Calculated and measured profiles of the furnace. The standard deviations are given as error bars. (b) Contour plots of experimental results at the centerline and distributions of numerical results (single-rate three-step and CPD three-step) on the symmetry planes of the furnace.

agreement with the experimental data was found, although a larger difference in CO production can be observed between the computational and experimental results along the furnace centerline (Figure 7a). Furthermore, a slightly better agreement with the measured data was found in comparison with the brown coal case.

*4.2.2. In-Furnace $CO_2$ Concentration.* Figures 8a and 9a show the comparison between the numerical results and measured in-furnace $CO_2$ concentration for the brown coal and black coal cases, respectively. The calculated and measured $CO_2$ dry molar fractions are presented for different vertical positions ($z$ direction) of the furnace centerline and 100 mm left from the centerline for all cases. Figures 8b and 9b illustrate the comparison of $CO_2$ dry molar fraction contour plots between the experimental results at the centerline and numerical results of single-rate three-step and CPD three-step modeling on the symmetry planes of the furnace for the brown coal and black coal cases, respectively.

Numerical models predict a similar trend of $CO_2$ concentration to those obtained experimentally, except along the centerline ($x$ = 0 mm, $y$ = 0 mm) of the furnace. Computational models of all cases predict a lower $CO_2$ concentration when compared with the measured data along the centerline of the furnace for the $N_2$ carried brown coal case, which is related to the slower chemistry and delay of ignition, as described previously. On the other hand, considering the $CO_2$ carried black coal case, numerical models overestimate $CO_2$ concentrations in this region ($x$ = 0 mm, $y$ = 0 mm), because of poor mixing of carrier gas ($CO_2$) with combustion products and injected air (note that, in Figure 9b, the models predict the $CO_2$ concentration to be in the range of 90−100% at the furnace centerline, up to 50 mm height of the furnace from the



DOI: 10.1021/acs.energyfuels.5b01644
Energy Fuels 2015, 29, 7650−7669

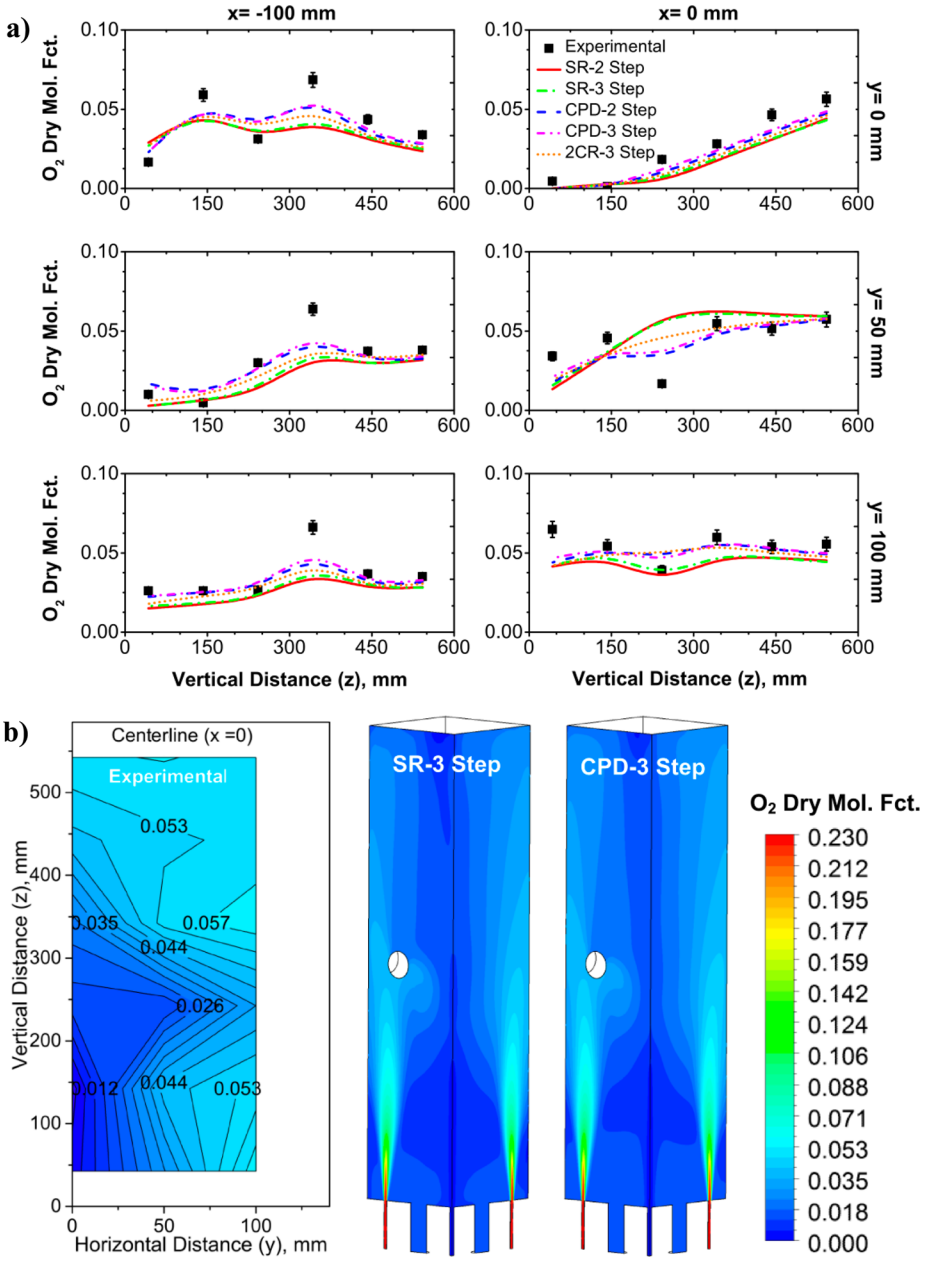


**Figure 10.** In-furnace $O_2$ dry molar fraction of brown coal using $N_2$ as a carrier gas case: (a) Calculated and measured profiles of the furnace. The standard deviations are given as error bars. (b) Contour plots of experimental results at the centerline and distributions of numerical results (single-rate three-step and CPD three-step) on the symmetry planes of the furnace.

bottom). It is interesting to note that no significant difference is observed between the CPD and single-rate devolatilization models regarding estimation of $CO_2$ concentrations. Altogether, the numerical predictions of $CO_2$ concentrations and the experimental measurements are in good agreement.

*4.2.3. In-Furnace $O_2$ Concentration.* The comparison between the numerical results and the measured in-furnace $O_2$ concentrations (dry basis) for the brown coal and black coal cases is shown in Figures 10a and 11a, respectively. Figures 10b and 11b illustrate the comparison of $O_2$ dry molar fraction contour plots between experimental results at the centerline and numerical results of the single-rate three-step and CPD three-step modeling on the symmetry planes of the furnace for the brown coal and black coal cases, respectively. No major differences between the experimental results and the numerical predictions can be found. However, the $O_2$ concentrations are somewhat underestimated between the middle and the top portion of the furnace, particularly along the centerline of the furnace. This might be associated with inaccurate calculation of the entrainment of the fuel jet. The numerical predictions of the $O_2$ mole fraction at other furnace locations are similar to the experimental results.

**4.3. NO Concentration Analysis.** In the present investigation, the postprocessing approach is used to evaluate the nitric oxide (NO) formation and reduction. The NO concentration is low compared with the major species, and hence, the NO formation and reduction mechanisms have a minor influence on the mass, momentum, and energy balances. Furthermore, the postprocessing approach is advantageous in terms of computational efficiency, and thus, the nitrogen pollutants models are dissociated from the combustion model



DOI: 10.1021/acs.energyfuels.5b01644
*Energy Fuels* 2015, 29, 7650−7669

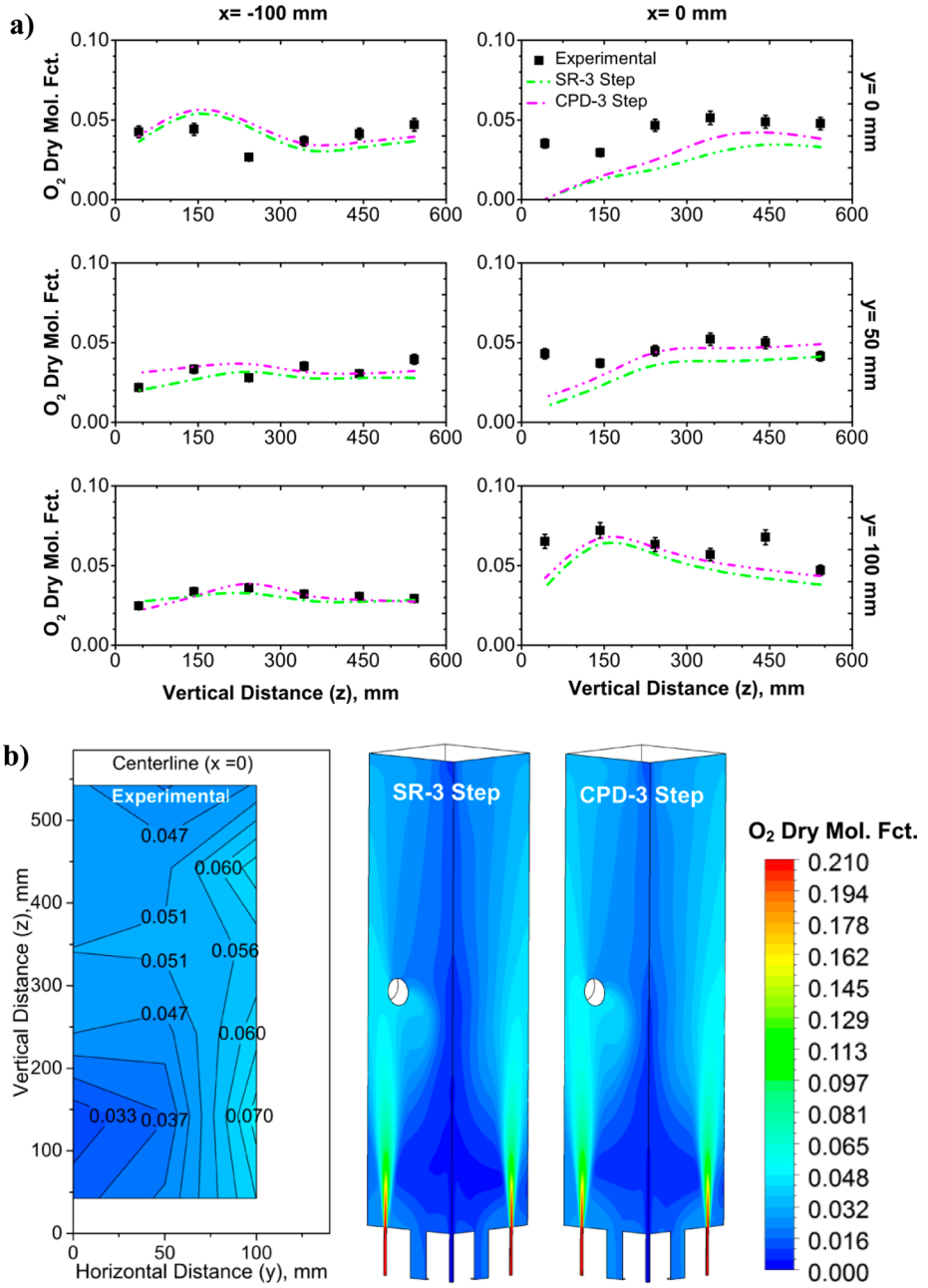


**Figure 11.** In-furnace $O_2$ dry molar fraction of black coal using $CO_2$ as a carrier gas case: (a) Calculated and measured profiles of the furnace. The standard deviations are given as error bars. (b) Contour plots of experimental results at the centerline and distributions of numerical results (single-rate three-step and CPD three-step) on the symmetry planes of the furnace.

and performed after the prediction of the flame structure by the NO modeling in RANS simulations in ANSYS Fluent.

It is noteworthy that $NO_2$ was below detection limits in the experimental measurements. In the numerical study, only NO is considered, which is well-known to account for at least 95% of the total $NO_x$ formation in most typical coal combustion processes.[26,55]

Three NO production mechanisms, namely, thermal-NO, prompt-NO, and fuel-NO, together with the NO reduction mechanism, named the NO-reburning mechanism, are considered in the present work. Turbulence effect on the temperature fluctuations is modeled by considering probability density function (PDF). The NO calculation is performed by solving the mass transport equation and by considering diffusion, convection, production, and consumption of NO and related chemical species

At first, the formation of thermal-NO follows the well-known Zel'dovich[56] reactions mechanism:

$$N_2 + O \rightarrow N + NO \quad \text{(R10)}$$

$$N + O_2 \rightarrow O + NO \quad \text{(R11)}$$

$$N + OH \rightarrow H + NO \quad \text{(R12)}$$

The thermal-NO formation is highly temperature-dependent and based on the oxidation of molecular nitrogen ($N_2$) in the combustion air. It has been reported that the effect of thermal-NO production is negligible below the temperature values of 1800 K.[14,49] Since, the maximum temperature of the present



DOI: 10.1021/acs.energyfuels.5b01644
Energy Fuels 2015, 29, 7650−7669

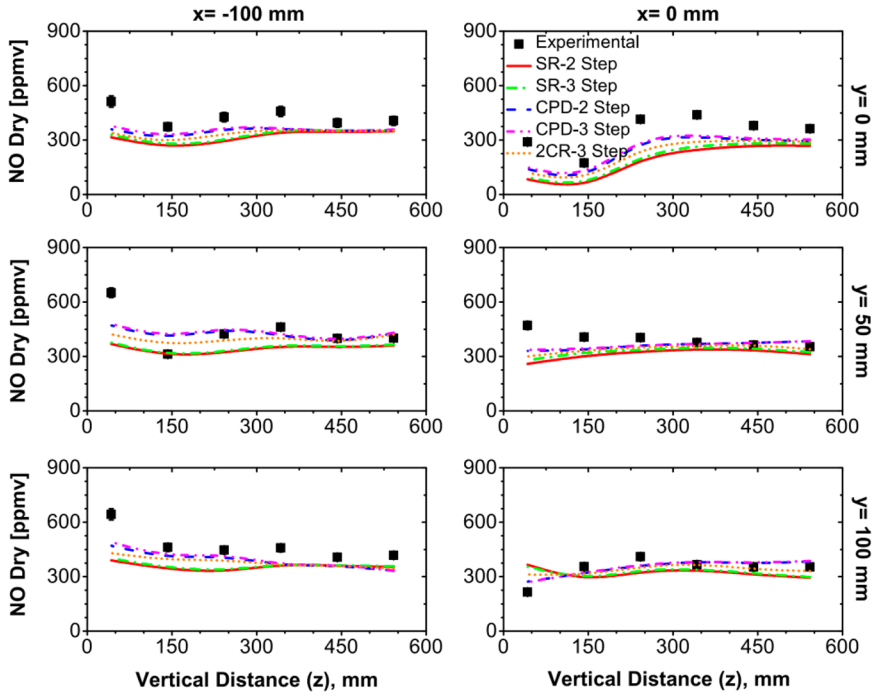


**Figure 12.** Calculated and measured profiles of in-furnace NO dry molar fraction for the brown coal using $N_2$ as a carrier gas case.

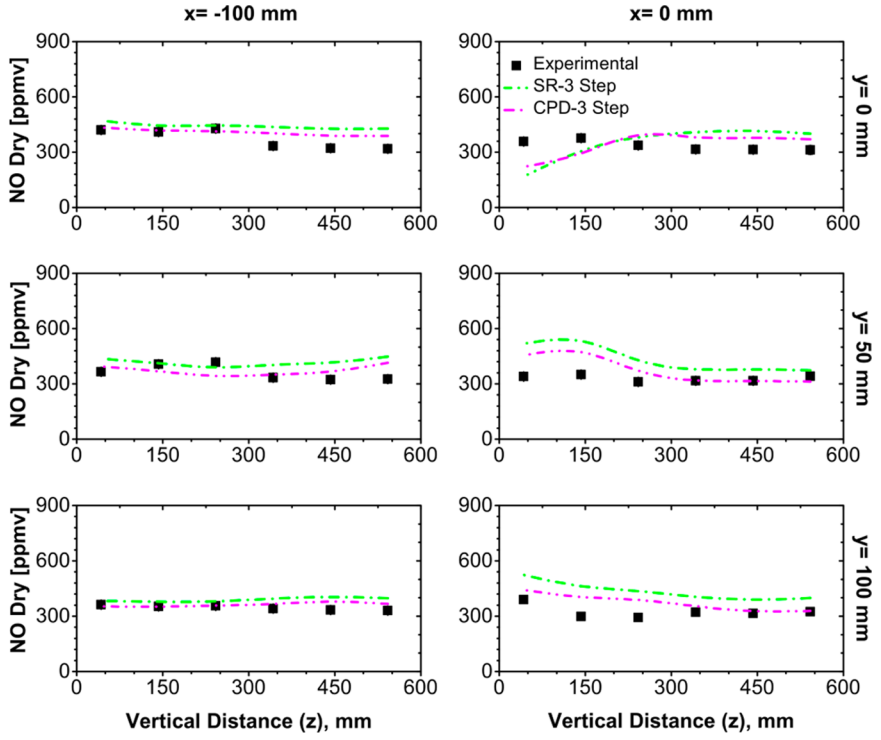


**Figure 13.** Calculated and measured profiles of in-furnace NO dry molar fraction for the black coal using $CO_2$ as a carrier gas case.

coal MILD combustion is found to be below 1550 K, it has a positive impact on the thermal-NO reduction.

The prompt-NO formation is produced by the reaction of atmospheric $N_2$ with hydrocarbon fuels in fuel-rich and low temperature combustion conditions. This study adopted the proposed reactions of Mei et al.[49] for prompt-NO formation in the MILD combustion of pulverized coal:

$$CH + N_2 \rightleftharpoons HCN + N \quad \text{(R13)}$$

$$N + O_2 \rightleftharpoons NO + O \quad \text{(R14)}$$

$$HCN + OH \rightleftharpoons CN + H_2O \quad \text{(R15)}$$

$$CN + O_2 \rightleftharpoons CO + NO \quad \text{(R16)}$$

Usually, prompt-NO plays a secondary role in the overall NO formation in MILD combustion conditions. This is because a strong diluted mixture of reactants is considered in MILD conditions where hydrocarbons ($C_xH_y$), hydrogen-cyanide



DOI: 10.1021/acs.energyfuels.5b01644
*Energy Fuels* 2015, 29, 7650−7669

(HCN), and nitrogen (N) concentrations decrease to low levels.

Fuel NO is produced by the oxidation reaction of the incorporated nitrogen (N) in the coal particles. It is presumed that the nitrogen (N) incorporated into the coal particle is entirely released during the devolatilization process and spread out between the volatiles and the char. Thus, there are two evolution paths for the fuel-NO formation: (i) a share of nitrogen incorporated in the coal is converted into fuel-NO, by the devolatilization process, and (ii) a share of the remaining nitrogen in the char is converted into fuel-NO, by the reaction with oxygen. The conversion of nitrogen to pollutants takes place via intermediates HCN and ammonia ($NH_3$). Then, HCN and $NH_3$ are subjected to four competitive reactions routes, as proposed by Alganash et al:[57]

$$HCN + O_2 \rightarrow NO + \text{products} \quad \text{(R17)}$$

$$NH_3 + O_2 \rightarrow NO + \text{products} \quad \text{(R18)}$$

$$HCN + NO \rightarrow N_2 + \text{products} \quad \text{(R19)}$$

$$NH_3 + NO \rightarrow N_2 + \text{products} \quad \text{(R20)}$$

Generally speaking, in coal MILD combustion, the main NO production is represented by the fuel-NO mechanism, whereas the thermal-NO is minimized by the reduced peak combustion temperature.

Finally, the recirculation of hot products of combustion in the furnace produces a positive reburning of NO and thus contributes to diminish the overall NO emission from coal MILD combustion. In the NO-reburning reaction, NO reacts with surrounding hydrocarbons and afterward reduced according to the following reaction:

$$C_xH_y + NO \rightarrow HCN + \text{products} \quad \text{(R21)}$$

Figures 12 and 13 represent the comparison between numerical results and measured in-furnace NO dry molar fraction along the vertical direction of the furnace for the MILD combustion of brown and black coals, respectively. The maximum value of NO mole fraction for the $N_2$ carried brown coal case is measured to be ~650 ppm, which is significantly larger than that of the black coal carried by $CO_2$ case. The reason behind the increase in the overall NO formation for the $N_2$ carried brown coal case is the presence of additional $N_2$ into the furnace from the carrier gas. The additional $N_2$ raises the overall $N_2$ concentration into the furnace and consequently leads to the relatively higher NO formation. For both the black and brown coal combustion cases, the NO concentration is found to be lowest at the bottom of the furnace centerline. The reason behind the decrease in NO concentration in the bottom portion (near the exhaust ports) of the furnace can be explained by the NO-reburning reaction R21, where hydrocarbons react with NO and subsequently reduce overall NO formation. The calculated NO mole fraction for all cases considered agrees very well with the measured NO mole fractions. The CPD model predicts NO concentrations more accurately than the single-rate and the two-competing-step devolatilization models for the brown coal case. On the other hand, no significant difference was observed between the predictions of CPD and single-rate models in the black coal simulations. Furthermore, for all the cases analyzed, the two-step and three-step gas-phase reactions exhibit similar accuracy in predicting the in-furnace NO concentrations.

Figure 14a,b shows the NO formation and reduction according to the main mechanisms considered: thermal-NO,

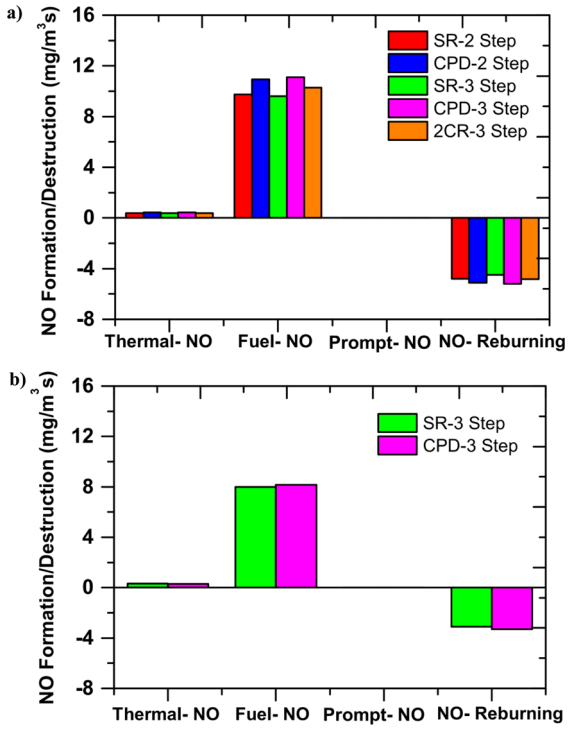


**Figure 14.** NO formation and destruction rates according to the main mechanisms: (a) brown coal carried by $N_2$ case; (b) black coal carried by $CO_2$ case.

fuel-NO, prompt-NO, and NO-reburning. Panels (a) and (b) in Figure 14 imply that fuel-NO is the main mechanism of NO production and about 96% of the total NO is produced through this route. Furthermore, the rate of NO production through the fuel-NO routes gives almost a similar value for both the two-step and three-step gas-phase reaction models. However, for the brown coal case, it can be observed that the CPD model predicts more fuel-NO than the single-rate and two-competing-rates devolatilization models. This is because fuel-NO formation mainly depends on the nature of the devolatilization model to form volatile contents. As highlighted in section 4.2.1 (in-furnace CO analysis), the CPD model produces a higher release of volatile contents than the single-rate and two-competing-rates devolatilization models, thus, leading to a larger fuel-NO production. Furthermore, the numerical carbon consumption analysis (refer to section 4.6 for details) provides an indication of the higher volatiles release for the CPD model. In particular, it was found that the CPD model predicts larger overall carbon consumption in comparison with the other analyzed models.

For the black coal case, only a minor difference between the predictions of the single-rate and CPD models can be seen. In particular, the fuel-NO productions are calculated to be 7.98 and 8.16 $mg/m^3$ s for the single-rate model and CPD, respectively.

Under MILD combustion conditions, the temperatures are lower than that of conventional combustion, and thus, thermal-NO plays a secondary role. For all simulation cases, the value of prompt-NO is found to be extremely low (maximum value was calculated to be ≤0.005 ppm) and cannot be sighted in Figures 14a,b. It is believed that the negligible value of prompt-NO



DOI: 10.1021/acs.energyfuels.5b01644
Energy Fuels 2015, 29, 7650−7669

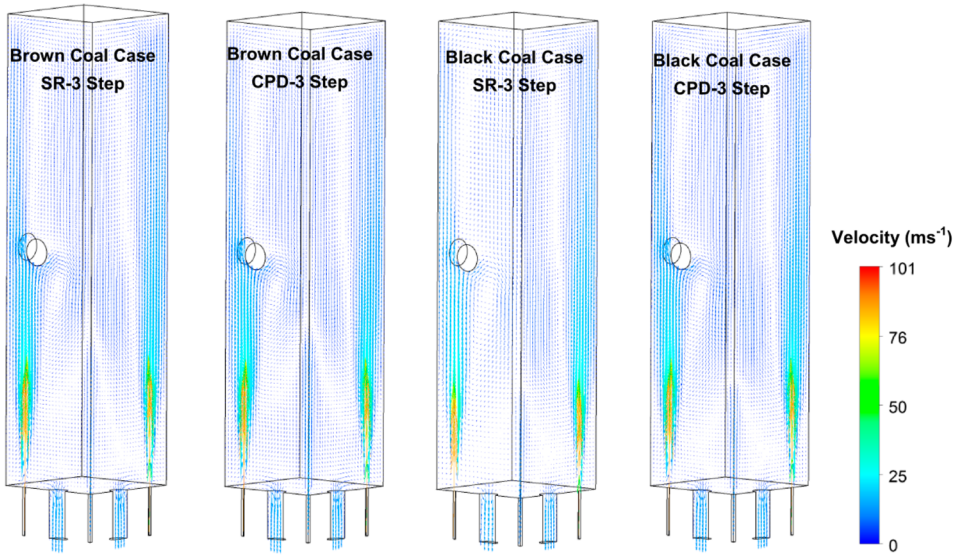


**Figure 15.** Hot combustion products velocity vector fields for different cases on the symmetry planes of the furnace.

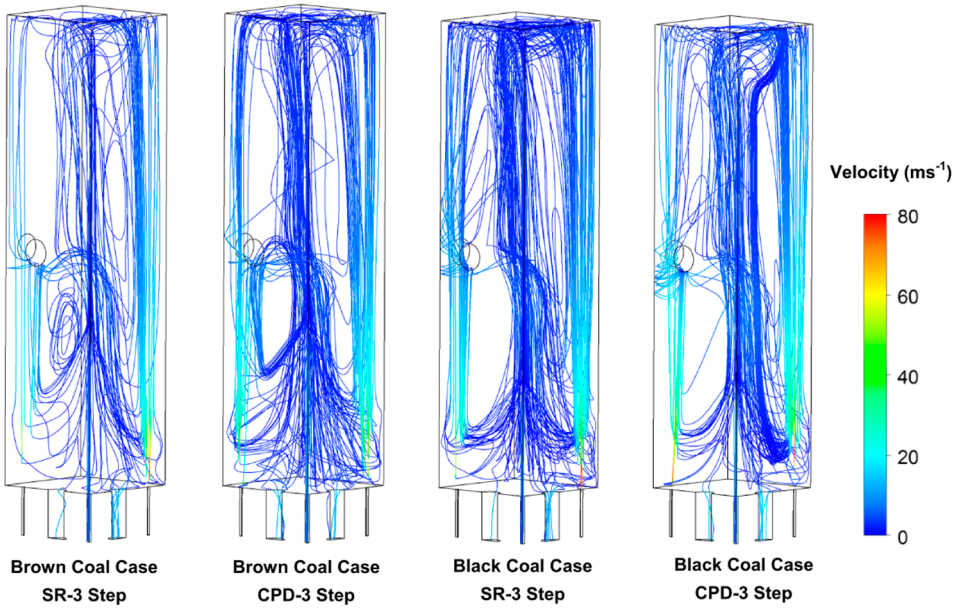


**Figure 16.** Coal particle concentration distributions in terms of velocity on the symmetry planes in the furnace for different cases.

formation is caused by a combination of (i) the decreased concentration of species (i.e., $C_xH_y$, HCN, and N), owing to the strong dilution by the flue gases in MILD combustion condition, and (ii) the low level of $O_2$ in the combustion region, because $O_2$ plays a vital role for the prompt-NO formation process through reactions R14 ($N + O_2 \rightleftharpoons NO + O$) and R16 ($CN + O_2 \rightleftharpoons CO + NO$). Moreover, the $O_2$ concentration is mostly diluted to a low level by the strong recirculation of hot combustion products in the MILD combustion. On the contrary, panels (a) and (b) in Figure 14 imply that the NO emission is reduced by up to 47% for the brown coal case and up to 39% for the black coal case via the reburning mechanism. This depends primarily on the NO recombination with hydrocarbons according to reaction R21 ($C_xH_y + NO \rightarrow HCN + products$) and to the reduction of NO on the char surface. This pronounced effect of the reburning mechanism is in agreement with previous work[24] for coal MILD combustion, and it is mainly related to the use of a simplified kinetic scheme for the gas-phase reactions.

From comparison of the numerical simulations with the experimental measurements, numerical models accurately predict NO concentrations along the vertical direction of the furnace, especially considering the CPD devolatilization model. However, no significant difference is observed in the cases of two-step and three-step gas-phase reactions for the prediction of NO concentrations.

**4.4. Flow-Field Analysis (Gas-Particle Flow Predictions).** To understand the combustion characteristics as well as the ratio of unburnt carbon in the fly ash, it is necessary to realize the actual aerodynamic fields within the furnace.[58] Figure 15 illustrates the comparison of the gas-phase velocity vector fields between the single-rate three-step and CPD three-step models for both the brown coal and the black coal cases. The gas velocity field contours imply the recirculation of the products of combustion in the furnace that plays a vital role in



DOI: 10.1021/acs.energyfuels.5b01644
Energy Fuels 2015, 29, 7650−7669

establishing MILD combustion conditions and, therefore, influences the local oxygen concentration and furnace temperature. The results also show that the high velocity air jets are injected into the confined combustion chamber to induce and create a recirculating flow region in the middle of the furnace. In all cases, the fuel jet momentum is dominated by the air jet momentum.

Figure 16 illustrates the coal particle concentration distribution as well as trajectories of coal particle streams in terms of velocity using the single-rate three-step and CPD three-step models for both the brown coal and the black coal cases. The simulation results indicate that strong recirculation of the products of combustion inside the furnace affect the coal particles to be entrained into the combustion region and dispersed into the furnace volume.

It is shown in Figure 16 that there is only a slight difference between the two devolatilization models to predict the particle velocity distribution because the same realizable $k$-$\varepsilon$ turbulence model is used. However, it is noticeable that the particle trajectory produces a swirling vortex in the midway of the furnace for the $N_2$-carried brown coal case. As a result, a majority of the coal particles concentrate in the middle of the furnace for this case. On the other hand, the swirling vortex is produced further downstream for the $CO_2$ carried black coal case. This is because the black coal particles are larger than brown coal particles and, as usual, larger particles have more momentum and consequently penetrate further into the furnace.

For all cases, the modeling results illustrate that there is an obvious distinction between the gas-phase and particle-phase velocities, in both their magnitude and their direction. The gas velocity is found to be larger than the particle velocity.

**4.5. Furnace Exhaust Gas Composition.** The comparison between measured and computed exhaust gas concentrations (nitric oxide (NO), oxygen ($O_2$), carbon monoxide (CO), and carbon dioxide ($CO_2$)) is illustrated in Figure 17. There is a moderate discrepancy between the model predictions and the measured values of exhaust gas concentrations, in particular for CO and NO emissions. This could be mainly attributed to the poor performances of all the devolatilization models tested in predicting correctly the in-furnace temperature and species profiles near the exit of the fuel jet and in the bottom part of the furnace ($z$ = 42.5 mm). It is worth mentioning that the exhaust gas concentrations were measured at a distance of 100 mm from the furnace outlet in the experiment, while the numerical models calculate the exhaust gas concentrations at the end of the furnace outlets. However, this difference can be assumed to not have a significant impact on the comparison. In particular, the exhaust tube in the experiment is insulated and the temperature change of the exhaust gases over this short distance is very small. Furthermore, the exhaust gases are at a temperature which is quite low for any reaction to proceed within this 100 mm, and hence, it is expected that the composition of the exhaust gases at the inlet of the exhaust port and 100 mm after will be very much the same.

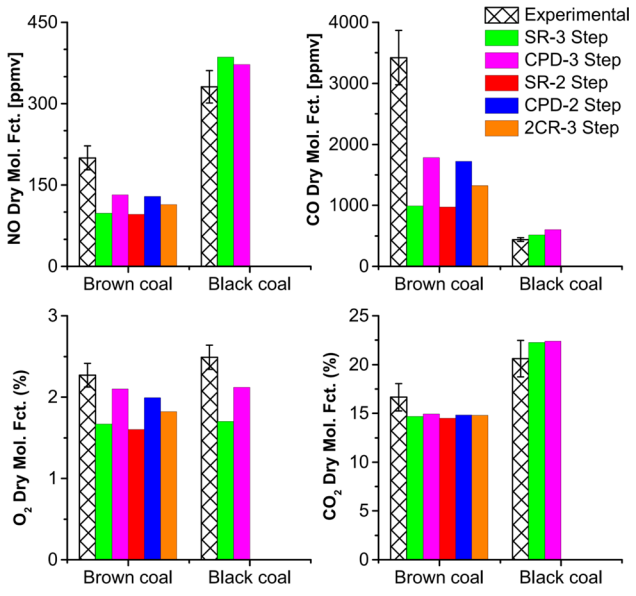


**Figure 17.** Computed and measured values of exhaust gas concentrations of the MILD combustion of brown coal using $N_2$ as a carrier gas and black coal using $CO_2$ as a carrier gas. The standard deviations are given as error bars.

The CPD devolatilization model more accurately predicts the exhaust gas concentrations in comparison to the other devolatilization models. Furthermore, no significant difference has been observed between two-step and three-step gas-phase reaction models for the prediction of exhaust gas concentrations. Moreover, it can be observed, from Figure 17, that a larger amount of overall NO emission was found for the black coal case than the brown coal case. As described in section 4.3, for coal MILD combustion, the main NO formation mechanism is represented by the fuel-NO route, whereas the thermal-NO production is minimized by the low flame temperature and a secondary role is played by the prompt-NO. It is thus quite understandable that the reason behind the increased NO concentrations for the black coal combustion case is due to the higher N contents of the fuel (it is notable that the black coal contains about a 64% higher value of N contents than that of the brown coal), leading to higher NO emission due to the fuel-NO production mechanism.

**4.6. Char Burnout.** Figure 18a,b depicts the partitioning of the char burnout rate considering the heterogeneous reactions (R7−R9), respectively, with $O_2$, $CO_2$, and $H_2O$. The bar graphs show that the char conversion rates as well as the direct formation of CO from the char are about 70% for the brown coal case and around 83% for the black coal case by considering reaction R7 ($C_{char} + {}^1/_2O_2 \rightarrow CO$); similar findings were reported by Vascellari and Cau[24] for the MILD combustion simulations of bituminous coal in the IFRF furnace. From the comparison between the $CO_2$ concentration (Figures 8 and 9) and $O_2$ concentration (Figures 10 and 11), it is seen that the amount of $CO_2$ is significantly larger than $O_2$, which contributes to an increase in the char conversion rate through the gasification reactions. Generally, gasification reactions (also termed heterogeneous reactions) of char alter the $CO/CO_2$ balance and increase CO concentration in the reaction zone.[24] The effects of heterogeneous reactions are especially observed in MILD combustion because of the presence of large amounts of $CO_2$ and $H_2O$ inside the furnace, owing to the recirculation of the hot combustion products. In contrast, the impacts of these reactions are mostly negligible in conventional combustion systems.

Figure 19 displays the comparison between the measured and the calculated values of overall carbon consumptions for the two different cases ($N_2$ carried brown coal and $CO_2$ carried black coal) studied in this work. For the CFD modeling, all the



DOI: 10.1021/acs.energyfuels.5b01644
Energy Fuels 2015, 29, 7650−7669

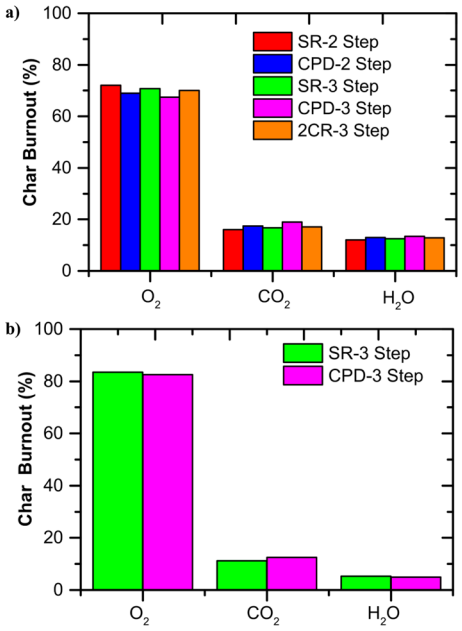


**Figure 18.** Influence of the heterogeneous reactions (R7–R9) on char burnout for (a) brown coal using $N_2$ as a carrier gas case and (b) black coal using $CO_2$ as a carrier gas case.

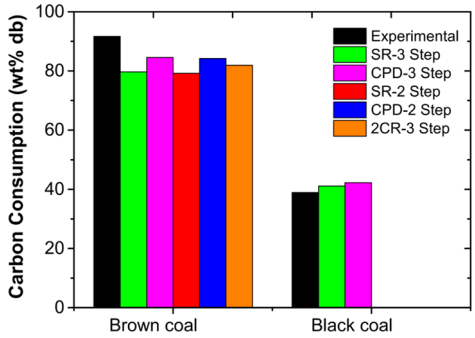


**Figure 19.** Overall carbon consumption of the MILD combustion for brown coal using $N_2$ as a carrier gas case and black coal using $CO_2$ as a carrier gas case.

models predict very similar results. The calculated carbon consumption percentages are in good agreement with the measured values. Nonetheless, it can be seen in Figure 19 that the carbon consumption was under-predicted by the simulations for the brown coal case. The fact that, for the brown coal case, the predicted carbon consumption is lower than that of the measured value is confirmed by the lower CO production and CO exhaust emissions by the numerical simulations in comparison with the experimental measurement for both CPD, single-rate, and two-competing-rates devolatilization models. However, the CPD model improves the prediction, in this case. On the other hand, it can be seen that, for the black coal case, the agreement with the experiment is quite good for both CPD and single-rate models.

It is noteworthy to mention that the overall equivalence ratio ($\phi$), as shown in Table 2, was calculated on the basis of the measured oxygen concentration in exhaust gases (a posteriori calculation), rather than based on the inlet conditions. The reason for reverse/posteriori calculation is that the inlet mass flow rate of coal was not uniform owing to the limitation of the coal feeder while the inlet mass flow rate of air as well as inlet oxygen concentration and outlet excess oxygen concentration was measured accurately. Similar values of oxygen concentration at the furnace outlet were measured for brown and black coals (2.3% and 2.5% by volume, respectively), and thus, the overall equivalence ratio was almost the same for both coals. The char burnout rate is considerably influenced by the particles' residence time inside the furnace. It is clearly understandable from the black coal combustion case that the residence time was not adequate for complete combustion. Furthermore, the volatile contents of the fuel play a significant impact on the overall char burnout rate. Hence, the lower rate of aggregate carbon consumption for the black coal case can be explained by (i) the lower volatile contents and (ii) the short residence time for the complete combustion of the black coal particles.

## 5. CONCLUSIONS

This work is conducted to investigate the influence of devolatilization models to more accurately predict pulverized coal combustion under MILD combustion conditions. In particular, three devolatilization models, namely, a simple single-step reaction model, a two-competing-rates model, and an advanced CPD model, are examined. The modeling cases are validated with previous experimental measurements of MILD combustion of high volatile Kingston brown coal using $N_2$ as a carrier gas and low volatile Bowen basin black coal using $CO_2$ as a carrier gas in a self-recuperative furnace. Moreover, a simplified model has been adopted and optimized for the MILD combustion of Australian black coal, for the first time. In addition, this numerical study is carried out to advance the understanding of $NO_x$ formation and destruction mechanisms, flow-field characteristics, and the effect of heterogeneous reactions on char burnout of the pulverized brown and black coal combustion in a self-recuperative furnace.

The key findings of this investigation are as follows:

1. From the comparison of the experimental measurements with the numerical simulations, the CPD devolatilization model better reproduces the temperature and species concentrations of pulverized coal MILD combustion in comparison to the simplified models tested in this study, for the brown coal case. On the other hand, the single-rate model and the CPD show similar accuracy in reproducing the experimental data for the black coal case. The different accuracy of the single-rate model in predicting the combustion characteristics of the two different coals investigated in this study is mainly attributed to how the chemical kinetic parameters are selected.
2. No significant differences are observed between the two-step and three-step gas-phase reaction models regarding the reproduction of temperature and chemical species.
3. All models fail to predict the rate of devolatilization and reaction close to the jet exit.
4. A new simplified numerical model is suggested for the combustion of Australian black/hard/low volatile coal and optimized, for the MILD combustion conditions, for the first time. Overall, the model agrees well with experimental measurements.
5. The modeling results indicate that the NO emissions are dominantly formed by the fuel-NO path, whereas the sum of the contribution of the total NO emissions from the thermal-NO and prompt-NO is less than 3.8% for


DOI: 10.1021/acs.energyfuels.5b01644
Energy Fuels 2015, 29, 7650−7669

any of the cases. Moreover, there exists a strong NO-reburning reaction inside the furnace, which leads to relatively low NO emissions in the exhaust. It is found that total NO emissions are reduced by up to 47% for the brown coal case and up to 39% for the black coal case via the reburning mechanisms. It can be concluded that a strong NO-reburning mechanism exists in the MILD combustion of pulverized coal in a self-recuperative furnace.

6. A semi-uniform temperature distribution in the furnace, which is observed by the models and experiments, indicates that a big recirculation zone is formed in the top portion of the furnace, which is similar to the case with gaseous fuel[7] under MILD combustion conditions. Nonetheless, a cold zone is formed around halfway along the fuel jet of the furnace, which suggests rapid devolatilization of pulverized coal in this region.
7. Although the overall carbon consumption predictions happen to be in very good agreement with the experimental values, this agreement may be coincidental because only simplified char reaction models are used in the present study. Therefore, further study is recommended with more elaborated char reaction models considering the complex deactivation mechanisms during char combustion.

## AUTHOR INFORMATION


### Corresponding Author

*E-mail: manabendra.saha@adelaide.edu.au. Phone: +61 (0)8 8313 5460.


### Notes

The authors declare no competing financial interest.

## ACKNOWLEDGMENTS

The support of the University of Adelaide is gratefully acknowledged; in particular, M.S. acknowledges the Adelaide Scholarship International (ASI) of The University of Adelaide and Brown Coal Innovation Australia (BCIA) Top-Up scholarship for financial support. The authors would also like to acknowledge eResearch SA for the use of their computational facilities. The assistance provided by Mr. Marc Simpson in collecting the experimental measurements is gratefully acknowledged.

## REFERENCES


(1) U.S. Energy Information Administration. *International Energy Outlook 2011*; Report No. DOE/EIA-0484(2011); U.S. Department of Energy (DOE): Washington, DC, Sept. 19, 2011.

(2) Zhao, D.; Sun, B. Atmospheric pollution from coal combustion in China. *J. Air Pollut. Control Assoc.* **1986**, *36* (4), 371−374.

(3) de Joannon, M.; Langella, G.; Beretta, F.; Cavaliere, A.; Noviello, C. Mild combustion: Process features and technological constrains. *Combust. Sci. Technol.* **2000**, *153* (1), 33−50.

(4) Wünning, J. A.; Wünning, J. G. Flameless oxidation to reduce thermal NO-formation. *Prog. Energy Combust. Sci.* **1997**, *23* (1), 81−94.

(5) Kiga, T.; Yoshikawa, K.; Sakai, M.; Mochida, S. Characteristics of pulverized coal combustion in high-temperature preheated air. *J. Propul. Power* **2000**, *16* (4), 601−605.

(6) de Joannon, M.; Chinnici, A.; Sabia, P.; Ragucci, R. Optimal post-combustion conditions for the purification of $CO_2$-rich exhaust streams from non-condensable reactive species. *Chem. Eng. J.* **2012**, *211-212*, 318−326.

(7) Szegö, G. G.; Dally, B. B.; Nathan, G. J. Operational characteristics of a parallel jet MILD combustion burner system. *Combust. Flame* **2009**, *156* (2), 429−438.

(8) Kruse, S.; Kerschgens, B.; Berger, L.; Varea, E.; Pitsch, H. Experimental and numerical study of MILD combustion for gas turbine applications. *Appl. Energy* **2015**, *148*, 456−465.

(9) Mi, J.; Wang, F.; Li, P.; Dally, B. B. Modified vitiation in a moderate or intense low-oxygen dilution (MILD) combustion furnace. *Energy Fuels* **2012**, *26* (1), 265−277.

(10) de Joannon, M.; Sorrentino, G.; Cavaliere, A. MILD combustion in diffusion-controlled regimes of Hot Diluted Fuel. *Combust. Flame* **2012**, *159* (5), 1832−1839.

(11) Sabia, P.; Sorrentino, G.; Chinnici, A.; Cavaliere, A.; Ragucci, R. Dynamic behaviors in methane MILD and oxy-fuel combustion. Chemical effect of $CO_2$. *Energy Fuels* **2015**, *29* (3), 1978−1986.

(12) Weber, R.; Smart, J. P.; Kamp, W. On the (MILD) combustion of gaseous, liquid, and solid fuels in high temperature preheated air. *Proc. Combust. Inst.* **2005**, *30* (2), 2623−2629.

(13) Suda, T.; Takafuji, M.; Hirata, T.; Yoshino, M.; Sato, J. A study of combustion behavior of pulverized coal in high-temperature air. *Proc. Combust. Inst.* **2002**, *29* (1), 503−509.

(14) Stadler, H.; Ristic, D.; Förster, M.; Schuster, A.; Kneer, R.; Scheffknecht, G. $NO_x$-emissions from flameless coal combustion in air, $Ar/O_2$ and $CO_2/O_2$. *Proc. Combust. Inst.* **2009**, *32* (2), 3131−3138.

(15) He, R.; Suda, T.; Takafuji, M.; Hirata, T.; Sato, J. Analysis of low NO emission in high temperature air combustion for pulverized coal. *Fuel* **2004**, *83* (9), 1133−1141.

(16) Zhang, H.; Yue, G.; Lu, J.; Jia, Z.; Mao, J.; Fujimori, T.; Suko, T.; Kiga, T. Development of high temperature air combustion technology in pulverized fossil fuel fired boilers. *Proc. Combust. Inst.* **2007**, *31* (2), 2779−2785.

(17) Tu, Y.; Liu, H.; Chen, S.; Liu, Z.; Zhao, H.; Zheng, C. Numerical study of combustion characteristics for pulverized coal under oxy-MILD operation. *Fuel Process. Technol.* **2015**, *135*, 80−90.

(18) Saha, M.; Dally, B. B.; Medwell, P. R.; Cleary, E. M. Moderate or Intense Low Oxygen Dilution (MILD) Combustion Characteristics of Pulverized Coal in a Self-Recuperative Furnace. *Energy Fuels* **2014**, *28* (9), 6046−6057.

(19) Li, P.; Wang, F.; Tu, Y.; Mei, Z.; Zhang, J.; Zheng, Y.; Liu, H.; Liu, Z.; Mi, J.; Zheng, C. Moderate or Intense Low-Oxygen Dilution Oxy-combustion Characteristics of Light Oil and Pulverized Coal in a Pilot-Scale Furnace. *Energy Fuels* **2014**, *28* (2), 1524−1535.

(20) Vascellari, M.; Xu, H.; Hasse, C. Flamelet modeling of coal particle ignition. *Proc. Combust. Inst.* **2013**, *34* (2), 2445−2452.

(21) Stadler, H.; Toporov, D.; Förster, M.; Kneer, R. On the influence of the char gasification reactions on NO formation in flameless coal combustion. *Combust. Flame* **2009**, *156* (9), 1755−1763.

(22) Schaffel, N.; Mancini, M.; Szlek, A.; Weber, R. Mathematical modeling of MILD combustion of pulverized coal. *Combust. Flame* **2009**, *156* (9), 1771−1784.

(23) Kim, J. P.; Schnell, U.; Scheffknecht, G.; Benim, A. C. Numerical modelling of MILD combustion for coal. *Prog. Comput. Fluid Dyn.* **2007**, *7* (6), 337−346.

(24) Vascellari, M.; Cau, G. Influence of turbulence−chemical interaction on CFD pulverized coal MILD combustion modeling. *Fuel* **2012**, *101*, 90−101.

(25) Jin, X.; Zhou, Y. Numerical Analysis on Microscopic Characteristics of Pulverized Coal Moderate and Intense Low-Oxygen Dilution Combustion. *Energy Fuels* **2015**, *29* (5), 3456−3466.

(26) Williams, A.; Pourkashanian, M.; Jones, J. Combustion of pulverised coal and biomass. *Prog. Energy Combust. Sci.* **2001**, *27* (6), 587−610.

(27) Australian Government, Geoscience Australia. Black Coal. Commonwealth of Australia: Canberra, Australia.http://www.australianminesatlas.gov.au/aimr/commodity/black_coal.html (accessed 13/07/2015).

(28) Saha, M.; Dally, B. B.; Medwell, P. R.; Cleary, E. MILD Combustion of Pulverised Coal in a Recuperative Furnace. In




DOI: 10.1021/acs.energyfuels.5b01644
*Energy Fuels* 2015, 29, 7650−7669

*Proceedings of the European Combustion Meeting 2013*, Lund, Sweden, June 25−28, 2013.
(29) Saha, M.; Dally, B. B.; Medwell, P. R.; Cleary, E. A Study of Combustion Characteristics of Pulverised Coal under MILD Combustion Conditions. In *Proceedings of the Australian Combustion Symposium 2013*, The University of Western Australia, Perth, Australia, Nov 6−8, 2013; pp 132−135.
(30) Saha, M.; Dally, B. B.; Medwell, P. R.; Cleary, E. An Experimental Study of MILD Combustion of Pulverized Coal in a Recuperative Furnace. In *Proceedings of the 9th Asia-Pacific Conference on Combustion*, Gyeongju Hilton, Gyeongju, Korea, 2013; p 223.
(31) Shih, T.-H.; Liou, W. W.; Shabbir, A.; Yang, Z.; Zhu, J. A new *k*-e eddy viscosity model for high reynolds number turbulent flows. *Comput. Fluids* **1995**, *24* (3), 227−238.
(32) Chui, E.; Raithby, G. Computation of radiant heat transfer on a nonorthogonal mesh using the finite-volume method. *Numer. Heat Transfer, Part B* **1993**, *23* (3), 269−288.
(33) Sheng, C.; Moghtaderi, B.; Gupta, R.; Wall, T. F. A computational fluid dynamics based study of the combustion characteristics of coal blends in pulverised coal-fired furnace. *Fuel* **2004**, *83* (11), 1543−1552.
(34) Popoff, B.; Braun, M. A Lagrangian Approach to Dense Particulate Flows. In *Proceedings of the 6th International Conference on Multiphase Flow*, Leipzig, Germany, 2007.
(35) Yu, J.; Lucas, J. A.; Wall, T. F. Formation of the structure of chars during devolatilization of pulverized coal and its thermoproperties: A review. *Prog. Energy Combust. Sci.* **2007**, *33* (2), 135−170.
(36) Förtsch, D.; Kluger, F.; Schnell, U.; Spliethoff, H.; Hein, K. R. A kinetic model for the prediction of NO emissions from staged combustion of pulverized coal. *Symp. Combust., [Proc.]* **1998**, *27* (2), 3037−3044.
(37) Kobayashi, H.; Howard, J.; Sarofim, A. F. Coal devolatilization at high temperatures. *Symp. Combust., [Proc.]* **1977**, *16* (1), 411−425.
(38) Fletcher, T. H.; Kerstein, A. R.; Pugmire, R. J.; Solum, M. S.; Grant, D. M. Chemical percolation model for devolatilization. 3. Direct use of carbon-13 NMR data to predict effects of coal type. *Energy Fuels* **1992**, *6* (4), 414−431.
(39) Fletcher, T. H.; Kerstein, A. R.; Pugmire, R. J.; Grant, D. M. Chemical percolation model for devolatilization. 2. Temperature and heating rate effects on product yields. *Energy Fuels* **1990**, *4* (1), 54−60.
(40) Solum, M. S.; Pugmire, R. J.; Grant, D. M. Carbon-13 solid-state NMR of Argonne-premium coals. *Energy Fuels* **1989**, *3* (2), 187−193.
(41) Fletcher, T. H.; Kerstein, R.; Pugmire, R.; Grant, D. A Chemical Percolation Model for Devolatilization: Temperature and Heating Rate Effects'. *Am. Chem. Soc., Div. Fuel Chem. Prepr. Pap.* **1989**, *34* (4), 1272−1279.
(42) Genetti, D.; Fletcher, T. H.; Pugmire, R. J. Development and Application of a Correlation of 13C NMR Chemical Structural Analyses of Coal Based on Elemental Composition and Volatile Matter Content. *Energy Fuels* **1999**, *13* (1), 60−68.
(43) Álvarez, L.; Gharebaghi, M.; Jones, J.; Pourkashanian, M.; Williams, A.; Riaza, J.; Pevida, C.; Pis, J.; Rubiera, F. CFD modeling of oxy-coal combustion: prediction of burnout, volatile and NO precursors release. *Appl. Energy* **2013**, *104*, 653−665.
(44) Westbrook, C. K.; Dryer, F. L. Simplified reaction mechanisms for the oxidation of hydrocarbon fuels in flames. *Combust. Sci. Technol.* **1981**, *27* (1−2), 31−43.
(45) Wang, L.; Liu, Z.; Chen, S.; Zheng, C. Comparison of different global combustion mechanisms under hot and diluted oxidation conditions. *Combust. Sci. Technol.* **2012**, *184* (2), 259−276.
(46) Howard, J.; Williams, G.; Fine, D. Kinetics of carbon monoxide oxidation in postflame gases. *Symp. Combust., [Proc.]* **1973**, *14* (1), 975−986.
(47) Hsu, K.; Jemcov, A. *Numerical Investigation of Detonation in Premixed Hydrogen-Air Mixture - Assessment of Simplified Chemical Mechanisms*; AIAA Paper 00-2478; AAIA: Denver, CO, 2000.
(48) Kumar, M.; Ghoniem, A. F. Multiphysics simulations of entrained flow gasification. Part II: Constructing and validating the overall model. *Energy Fuels* **2012**, *26* (1), 464−479.
(49) Mei, Z.; Li, P.; Wang, F.; Zhang, J.; Mi, J. Influences of reactant injection velocities on moderate or intense low-oxygen dilution coal combustion. *Energy Fuels* **2014**, *28* (1), 369−384.
(50) Field, M. Measurements of the effect of rank on combustion rates of pulverized coal. *Combust. Flame* **1970**, *14* (2), 237−248.
(51) Roberts, D.; Harris, D. Char gasification with O2, CO2, and H2O: Effects of pressure on intrinsic reaction kinetics. *Energy Fuels* **2000**, *14* (2), 483−489.
(52) Smoot, D.; Pratt, D. *Pulverized-Coal Combustion and Gasification: Theory and Applications for Continuous Flow Processes*; Plenum Press: New York, 1979.
(53) Hodge, E. M. The coal char−$CO_2$ reaction at high temperature and high pressure. PhD Thesis, University of New South Wales, Australia, 2009.
(54) Magnussen, B. On the Structure of Turbulence and a Generalized Eddy Dissipation Concept for Chemical Reaction in Turbulent Flow. In *Proceedings of the 19th AIAA Meeting*, St. Louis, MO, 1981.
(55) Hill, S.; Douglas Smoot, L. Modeling of nitrogen oxides formation and destruction in combustion systems. *Prog. Energy Combust. Sci.* **2000**, *26* (4), 417−458.
(56) Zeldovich, Y.; Frank-Kamenetskii, D.; Sadovnikov, P. *Oxidation of Nitrogen in Combustion*; Publishing House of the Academy of Sciences of USSR: Moscow, 1947.
(57) Alganash, B.; Paul, M. C.; Watson, I. A. Numerical investigation of the heterogeneous combustion processes of solid fuels. *Fuel* **2015**, *141*, 236−249.
(58) Ren, F.; Li, Z.; Liu, G.; Chen, Z.; Zhu, Q. Numerical simulation of flow and combustion characteristics in a 300 MWe down-fired boiler with different overfire air angles. *Energy Fuels* **2011**, *25* (4), 1457−1464.


DOI: 10.1021/acs.energyfuels.5b01644
*Energy Fuels* 2015, 29, 7650−7669

# CHAPTER 5

# EFFECT OF PARTICLE SIZE ON THE MILD COMBUSTION CHARACTERISTICS OF PULVERISED BROWN COAL

# Statement of Authorship

| | |
|---|---|
| Title of Paper | Effect of Particle Size on the MILD Combustion Characteristics of Pulverised Brown Coal |
| Publication Status | ☐ Published ☑ Accepted for Publication<br>☐ Submitted for Publication ☐ Unpublished and Unsubmitted w ork w ritten in manuscript style |
| Publication Details | **M. Saha,** B. B. Dally, P. R. Medwell, and A. Chinnici, "Effect of Particle Size on the MILD Combustion Characteristics of Pulverised Brown Coal", *Fuel Processing Technology*, DOI: 10.1016/j.fuproc.2016.04.003, 2016 (In Press). |

## Principal Author

| | | | |
|---|---|---|---|
| Name of Principal Author (Candidate) | Manabendra Saha | | |
| Contribution to the Paper | Designed, built and commissioned furnace. Conducted experiments, analysed data, wrote manuscript and acted as corresponding author. | | |
| Overall percentage (%) | 75% | | |
| Certification: | This paper reports on original research I conducted during the period of my Higher Degree by Research candidature and is not subject to any obligations or contractual agreements with a third party that would constrain its inclusion in this thesis. I am the primary author of this paper. | | |
| Signature | | Date | 6/04/2016 |

## Co-Author Contributions

By signing the Statement of Authorship, each author certifies that:

i. the candidate's stated contribution to the publication is accurate (as detailed above);

ii. permission is granted for the candidate in include the publication in the thesis; and

iii. the sum of all co-author contributions is equal to 100% less the candidate's stated contribution.

| | | | |
|---|---|---|---|
| Name of Co-Author | Bassam B. Dally | | |
| Contribution to the Paper | Supervised development of work, helped in developing ideas, data interpretation and manuscript evaluation. | | |
| Signature | | Date | 6-4-16 |

| | | | |
|---|---|---|---|
| Name of Co-Author | Paul R. Medwell | | |
| Contribution to the Paper | Supervised development of work, helped in developing ideas, data interpretation and manuscript evaluation. | | |
| Signature | | Date | 13-APR-2016 |

| | | | |
|---|---|---|---|
| Name of Co-Author | Alfonso Chinnici | | |
| Contribution to the Paper | Helped in performing CFD modelling, data interpretation and manuscript evaluation. | | |
| Signature | | Date | 07/04/2016 |

Fuel Processing Technology xxx (2015) xxx–xxx

Contents lists available at ScienceDirect

Fuel Processing Technology

journal homepage: www.elsevier.com/locate/fuproc

Research article

# Effect of particle size on the MILD combustion characteristics of pulverised brown coal

Manabendra Saha *, Bassam B. Dally, Paul R. Medwell, Alfonso Chinnici

*Centre for Energy Technology, School of Mechanical Engineering, The University of Adelaide, SA 5005, Australia*

ARTICLE INFO

*Article history:*
Received 13 January 2016
Received in revised form 28 March 2016
Accepted 3 April 2016
Available online xxxx

*Keywords:*
Pulverised Victorian brown coal
MILD combustion
Particles size
Temperature
CO
NO

ABSTRACT

This paper reports a combined experimental and numerical investigation on the impact of particle size on the MILD combustion characteristics of pulverised brown coal. In particular, the work investigates the volatiles release and reactions from the coal particles with a vitiated co-flow and its impact on the formation and emission of CO, $CO_2$, and $NO_x$. The experimental vertical furnace is 1200 mm long with an internal cross-section of 260 × 260 $mm^2$. High volatile brown coal from the Latrobe Valley, Victoria, with particle sizes in the range of 53–125 μm and 250–355 μm is injected into the furnace using $CO_2$ as a carrier gas through an insulated water-cooled central jet. The complementary numerical results are in good agreement with the experimental measurements. It is found that, for both cases, a stable MILD combustion is established with a similar large recirculation vortex around the centre of the furnace. Devolatilisation starts earlier for the smaller particles' case and is completed at the end of the recirculation vortex, while for the larger particles' case the devolatilisation happened post the recirculation vortex. The difference is related to the particle dispersion within the jet and differences in Stokes number. The particle flow path and difference in residence time had influence on char burn-out and emission levels. The formation/destruction of NO is measured to be subtly varied by the combination of the physical and chemical nature of the MILD combustion characteristics related to both particle sizes. The measured NO emission of the larger particle case is 15% higher than that of smaller particle case. The model calculated about 95.5% of total NO is produced via the fuel-NO route. A strong NO-reburning mechanism is found for both cases, where ≈55% of total NO is reduced for the small particle case and ≈39% of total NO is reduced for the large particle case.


## 1. Introduction

Amongst the various fuel types in the world, brown coal is considered the cheapest and most available energy source [1]. The state of Victoria in Australia has the fourth-largest share of vindicated brown coal reserves in the world [2]. The huge brown coal reserve in the Latrobe Valley, Victoria, Australia which is named as Loy-Yang brown coal provides one-third of electricity in Victoria [3] and predictions show that it will continue to be a leading source of reliable and affordable electricity for the foreseeable future. The downside of Victorian brown coal is its high moisture content (about 60–70 wt%) [4] that affects thermal efficiency. Nonetheless, Loy-Yang brown coal deserves special attention because of its desirable burning characteristics, including; high reactivity owing to a high volatile content, generally low ash content, and low sulphur and heavy metals [3]. Therefore, more research and application of new technologies are necessary for more efficient and environmentally-friendly utilisation of Victorian brown coal.

Moderate or Intense Low-oxygen Dilution (MILD) combustion [5–10] has been identified as an innovative technology that offers ultra-low pollutant emissions, high thermal efficiency, enhanced combustion stability, thermal field uniformity, and broad fuel flexibility. Although MILD combustion technology has been successfully implemented in various industrial sectors for gaseous fuels, this technology is still in an infancy stage for solid fuels, in particular for pulverised brown coal. Thus far, some studies have been conducted on MILD combustion of pulverised fuels [11–34]. The first successful attempt on the MILD combustion of high volatile pulverised coal of 74 μm particles size was reported by Kiga et al. [11] using a drop tube furnace. They reported that this technology is useful for the elevation of combustion efficiency with a substantial $NO_x$ reduction compared with conventional combustion. To investigate the impact of air preheating on the MILD combustion characteristics of anthracite and bituminous coal, Suda et al. [12] reported an experimental observation where it was found that the coal particles' ignition delay decreased significantly by rising the combustion air temperature. He et al. [13] conducted a numerical investigation of the experiments carried out by Suda et al. [12] and found that for high rank coal (anthracite), NO is predominantly produced from the char-nitrogen, whose production/destruction mechanism is yet to be fully understood. Mei et al. [14] numerically investigated the impacts of reactants injection velocities on coal MILD combustion and found that rising velocity of primary air played a significant role to decrease combustion temperature and overall $NO_x$ emission. Tu et al. [15,16] numerically investigated the MILD combustion characteristics of pulverised bituminous coal under $O_2/N_2$ and $O_2/CO_2$ atmospheres using simplified combustion models and reported that

* Corresponding author.
*E-mail address:* manabendra.saha@adelaide.edu.au (M. Saha).

http://dx.doi.org/10.1016/j.fuproc.2016.04.003
0378-3820/

oxy-MILD combustion has a great potential of reducing $NO_x$ formation. Weber et al. [17–19] at the International Flame Research Foundation (IFRF) conducted a series of experimental investigations in a 0.58 MW furnace and reported large $NO_x$ diminution potential of the MILD combustion of high volatile bituminous coal. However, the basic routes of $NO_x$ production/destruction were not understood from these experiments. Schaffel et al. [20] modelled the IFRF furnace using an advanced Chemical Percolation Devolatilisation (CPD) model along with char combustion intrinsic reactivity model and reported the existence of strong NO-reburning mechanisms in coal MILD combustion. However, the authors [20] reported the limitations of CFD modelling to predict CO formation and highlighted the need for a more elaborate volatile matter combustion model. A numerical study to probe the impact of turbulence-chemistry interaction on the prediction of pulverised coal MILD combustion was reported by Vascellari and Cau [21]. They modelled gas phase reactions using either a detailed kinetic mechanisms (consisting of 103 reactions) or a global kinetic mechanisms (consisting of 2 reactions). However, no significant benefits were noticed when using the detail kinetic mechanisms for the prediction of coal MILD combustion when compared with global kinetic mechanisms. As global kinetic mechanisms require less computational time and it does not seem to add any major benefits, the current investigation considered only global kinetics mechanism to model gas phase homogeneous reactions. Recently, an experimental investigation on the MILD combustion of bituminous coal using a cylindrical bench-scale furnace is reported by Tamura et al. [22] where they found overall $NO_x$ emission was reduced by increasing the residence time of the coal particles.

It has previously been found that a long residence time is essential for efficient burning of coal particles under MILD combustion conditions in a recuperative furnace [24,25]. However, the influence of volatiles' release and reactions on the formation and destruction of pollutants was not understood from the previous studies because of the uncontrolled complex flow pattern inside the recuperative furnace. In addition, no study has been found in the literature to understand the impact of particle size on the burning characteristics, in particular, volatiles' release and the reaction of pulverised brown coal under MILD combustion conditions which is relevant to practical combustion systems. Moreover, different particle sizes react in a different manner after injection into the furnace, which is influenced by the dominant furnace aerodynamics. As a result, various particle sizes undergo different chemical processes and particle size impacts on the devolatilisation and volatiles oxidation. In this way, the particle size influences on the NO formation and the relationship between particle size and NO formation/destruction is not readily available for pulverised brown coal. Therefore, it is necessary to develop such fundamental-level understanding on the physical phenomena related to the combustion of pulverised brown coal under MILD combustion regime through a comprehensive experimental and numerical study.

This article reports an evaluation of the effects of particle size on the burning characteristics (in-furnace temperature profile, chemical species, i.e., CO, $CO_2$, $O_2$, and $NO_x$ profiles and exhaust emissions) of pulverised Victorian brown coal under MILD combustion conditions. To this end, the particle size is varied between the range of 53–125 μm and 250–355 μm under the same operating conditions (5.9% co-flow $O_2$ concentration, $Re_{jet} = 20{,}000$, and coal mass flow rate of 1.47 kg/h) of pulverised coal was kept constant. To augment the experimental measurements, computational fluid dynamic (CFD) modelling is used to investigate the effect of coal particle size on the NO emissions by partitioning the NO formation/destruction behaviour via thermal-NO, prompt-NO, fuel-NO, and NO-reburning routes. In-addition the presented and discussed CFD modelling results highlights the flow field inside the furnace, devolatilisation zone, volatile combustion, and the influence of heterogeneous reactions on the char burnout rate.

## 2. Experimental and modelling details

### 2.1. Experimental details

A brief description of the experimental set-up is provided here whilst the details of the experimental rig have been described previously [35,36]. A schematic diagram of the vertical MILD combustion furnace used in this study is shown in Fig. 1. The furnace has a height of 1200 mm and an inner cross-section of 260 × 260 $mm^2$. The furnace is well insulated, with 100-mm-thick high-temperature ceramic fibreboard refractory that allows only around ~9% of total heat lost through the furnace walls. The maximum designed capacity of the furnace is 60 kW where 40 kW heat can be added from the secondary burner. The secondary burner is used to control furnace wall and co-flow temperature as well as the co-flow $O_2$ concentration. The secondary burner is a swirl burner which operates in a non-premixed combustion mode and supplies hot combustion products under different stoichiometry. The swirl burner is capable of operating between the equivalence ratio of 0.5 to stoichiometric combustion conditions with a stable and attached non-sooty flame. Air at room temperature was used as an oxidant and natural gas was used as fuel for the non-premixed combustion of the swirling burner. The co-flow conditions were kept constant for this work. An insulated duct configuration is built to transport the hot products of combustion from secondary burner to the furnace at a uniform flow speed. The water cooled and well insulated central jet with an internal diameter ($D_{jet}$) of 19 mm is used to inject pulverised coal into the furnace. When the thermocouple temperature at the point 9 in Fig. 1, exceeded a set threshold (≈1100 K) which is above the self-ignition temperature of pulverised brown coal, the coal particles are introduced into the furnace through the central fuel jet using carbon dioxide ($CO_2$) as a carrier gas. Stable combustion was achieved and thermal equilibrium was confirmed for all cases. A summary of the experimental conditions on the stable combustion of pulverised brown coal is shown in Table 1.

The flow temperature and gas composition inside the furnace was measured on the centreline (X = 0 mm) at nine different axial locations (Y-axis) namely; at 70, 170, 270, 370, 470, 570, 670, 770, and 870 mm from the fuel jet exit plane in the furnace. Further measurements

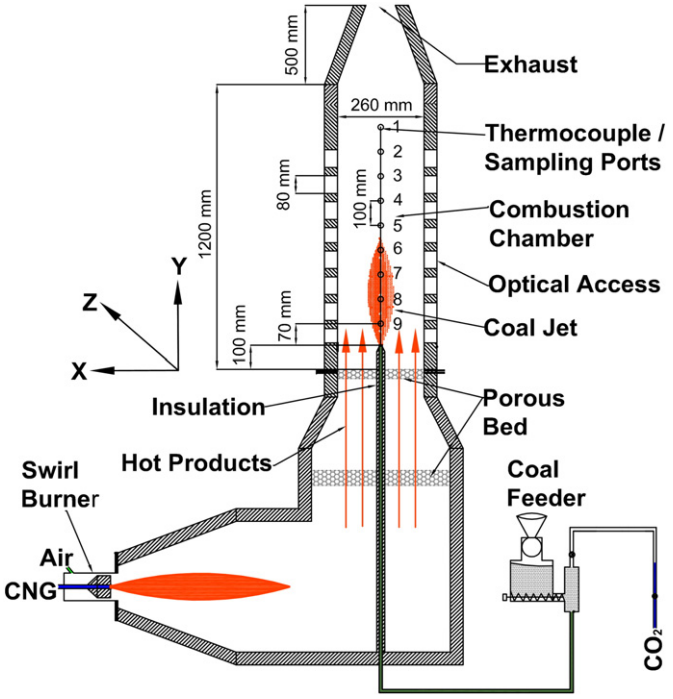


**Fig. 1.** Schematic diagram of the MILD combustion furnace and supply system.

Please cite this article as: M. Saha, et al., Effect of particle size on the MILD combustion characteristics of pulverised brown coal, Fuel Processing Technology (2015), http://dx.doi.org/10.1016/j.fuproc.2016.04.003

**Table 1**
Furnace operating parameters for the stable combustion of Loy-Yang brown coal.

| Experimental cases | Case 1 | Case 2 |
|---|---|---|
| Fuel jet inlet temperature (K) | 325 | 325 |
| Fuel jet velocity (m/s) | 8.84 | 8.84 |
| Jet Reynolds number | 20,000 | 20,000 |
| Furnace wall temperature (K) | 1112–1236 | 1112–1236 |
| Particle sizes (μm) | 53–125 | 250–355 |
| Global equivalence ratio, Φ | 0.96 ± 0.02 | 0.96 ± 0.02 |
| Co-flow velocity (m/s) | 1.56 | 1.56 |
| Co-flow temperature (K) | 1284 | 1284 |
| Co-flow $O_2$ (v/v% db) | 5.9 | 5.9 |
| Co-flow excess air coefficient, λ | 1.39 | 1.39 |

were also conducted at Z = 50, and Z = 100 mm from the centreline and along the furnace axis (Y-direction) providing a total of 27 points of measurement. A steady-state energy balance equation is used on the thermocouples' bead surface for radiation temperature corrections, which indicates that the radiation correction is within 4.5% of the thermocouples' measurement.

The temperatures were measured simultaneously using 6-mm-diameter sheathed Pt/Pt 13%Rh (R-Type) thermocouples. All temperature measurements were logged continuously using a PC and USB-TC data logger. The thermocouples are ceramics sheathed and the effect of any surface reaction is believed to be negligible and un-likely to affect the temperature and the reaction rate in any tangible way.

A portable gas analyser, TESTO Model 350XL is used to measure the in-furnace gas concentrations and global emissions. A water cooled sampling probe [24] is used and introduced through the sampling ports to measure in-furnace $O_2$, CO, $CO_2$ and NO mole fraction. According to the manufacturer's specifications, the absolute errors of these measurements are ±0.8% (by volume) for $O_2$, ±10 ppmv for CO, and ±5 ppmv for NO of measured value.

### 2.2. Coal characteristics

A Victorian brown coal was milled and sieved into two different size ranges, namely; 53 μm < d ≤ 125 μm and 250 μm < d ≤ 355 μm. The pulverised coal was dried in an electric oven at 105 °C for 4–5 h to remove moisture and then stored in a sealed container under ambient conditions. Proximate and ultimate analyses of the coal are presented in Table 2. The gross dry calorific value is measured to be 24.5 MJ/kg. A volumetric coal feeder operating with a twin-screw was used to decouple the carrier gas flow rate from the solid particle supply rate. The coal feeder is operated using a variable speed motor to control the amount of coal fed into the furnace. The coal feeding rate was constant and set to 1.47 kg/h for ≈10 kW heat input by the pulverised coal for all the experiments.

It is worth noting that the absolute error of the coal mass flowrate was measured to be ±1.5%, while the absolute errors of the gas flowrate measurements were ±2% according to the manufacturer's specifications.

**Table 2**
Loy-Yang brown coal analyses.

| Ultimate analysis (wt% dry ash free) | |
|---|---|
| C | 66.8 |
| H | 4.8 |
| O (by difference) | 28.0 |
| N | 0.4 |
| S | – |
| *Proximate analysis (wt% dry basis)* | |
| Fixed carbon | 47.3 |
| Volatile matter | 51.3 |
| Ash | 1.4 |

### 2.3. Computational modelling details

Numerical modelling of MILD combustion of pulverised brown coal was preformed using the CFD software ANSYS Fluent version 14.5. Specific numerical models including the phenomena of multiphase flow, turbulence-chemistry interactions, thermal radiation, homogeneous gas phase reactions, heterogeneous char combustion reactions, are considered for the present computational study. A finite volume discretisation approach is used to generate a hexahedral mesh consisting of 1 million cells for modelling half of the furnace geometry. The current mesh density was found to be adequate after conducting a grid independence study. The Reynolds-Averaged Navier-Stokes (RANS) equations are solved for all models. The Semi-Implicit Method for Pressure Linked Equations (SIMPLE) algorithm [37] is utilised to solve pressure-velocity coupling. All models used the second-order upwind discretisation scheme for increase accuracy and reducing numerical diffusion of the solution.

The two-equation realisable k-ε turbulence model [38] is used to simulate turbulent flow characteristics. The radiation heat transfer equation is solved using a Discrete Ordinates (DO) [39] radiation model.

The coal particle sizes are distributed following the Rosin-Rammler distribution approach. The discrete phase of coal particles is tracked using a deterministic Lagrangian approach [40]. The Lagrangian frame of reference is considered to solve the discrete solid phase of coal particles while an Eulerian frame is employed to solve the continuous gas phase transport equations. The modellings were conducted using Tizard supercomputer facilities of eResearch SA.

The present modelling study followed the sequence of pulverised coal combustion phenomena such as devolatilisation, volatile reactions and char combustion.

#### 2.3.1. Devolatilisation/pyrolysis

Coal devolatilisation/pyrolysis refers to the process of combustible gas evolution from the coal particles owing to thermal decomposition. A two-stage process [41] is considered to describe coal devolatilisation, where volatile matters including light hydrocarbons and gases (CO, $CO_2$, $CH_4$, $H_2O$, etc.) are released in the first stage and heavy hydrocarbons are decomposed during the second stage to form additional gases and hydrocarbons.

Pyrolysis/devolatilisation plays a very crucial role in a combustion process, controlling the yields of volatiles, tars and char, in addition to the ratio of fuel-N in the volatiles and char. Several different devolatilisation models exist, including; single-rate model, two competing rates model, chemical percolation devolatilisation (CPD) model, and the functional group – depolymerisation vaporisation cross-linking (FG-DVC) model. The single-rate devolatilisation model [42] acts on the first-order dependence of the entire volatile matters in the coal particle. The global kinetics of single-rate devolatilisation model is calculated according to the reaction as follows:

$$\text{coal} \rightarrow \text{volatile}\ (\alpha) + \text{char}\ (1-\alpha).$$

Here "α" is the distribution co-efficient.

The second model is a two competing-rates model [42] which includes two reactions, i.e. a high temperature reaction and a low temperature reaction, as follows:

$$\text{coal} \rightarrow \text{volatile}\ (\alpha 1) + \text{char}\ (1-\alpha 1)$$

$$\text{coal} \rightarrow \text{volatile}\ (\alpha 2) + \text{char}\ (1-\alpha 2).$$

The CPD devolatilisation model [43–45] identifies the physical and chemical processes of the coal structure as a chemical bridge network linking with the atomic clusters. Nuclear Magnetic Resonance (NMR) data is used to identify the physical structure of the coal which provides

Please cite this article as: M. Saha, et al., Effect of particle size on the MILD combustion characteristics of pulverised brown coal, Fuel Processing Technology (2015), http://dx.doi.org/10.1016/j.fuproc.2016.04.003

the CPD model input parameters. However, such kinds of experimental data are not available in the literature for Victorian brown coal.

The fourth devolatilisation model, i.e., advanced FG-DVC model determines the molecular constitution of the solid fuel and its impact on the light gases and tar decomposition. The FG-DVC model is not dissimilar to the CPD model [46]. However, FG-DVC model is not readily available in FLUENT and thus user-defined functions (UDFs) are required to implement the FG-DVC in FLUENT [46]. However, UDFs data is obtained from experimental observations of a specific coal. Nonetheless, to the authors' knowledge, there is a lack of adequate kinetic data in the literature to embed FG-DVC into FLUENT, for Victorian brown coal. This is why the FG-DVC model is not considered in this work. Furthermore, in the CFD analyses, the advanced models are generally used for calibration purposes of simpler devolatilisation models (e.g. single rate), thus being applied as an external tool [47]. A recent study [25] regarding the effect of the devolatilisation models on Australian brown and black coals under MILD combustion conditions concluded that the single-rate model, although being a simplistic model, has been found adequate in predicting several key burning characteristics of the coals analysed under MILD conditions. Therefore, in this study, coal devolatilisation process is modelled using single-rate reaction model for the specific Victorian brown coal following Zhang et al. [48].

### 2.3.2. Volatile reactions

The devolatilisation process releases the volatile contents as a combination of gaseous elements of C, H, O, N, and S as the pseudo-volatile species. The volatile oxidation is described using a global volatile combustion mechanism as follows:

$$C_xH_yO_zN_lS_n + \left(\frac{x}{2}+\frac{y}{2}-\frac{z}{2}+n\right)O_2 \longrightarrow xCO + \frac{y}{2}H_2O + \frac{l}{2}N_2 + nSO_2. \quad (R1)$$

The values of the variables $x$, $y$, $z$, $l$, and $n$ are obtained from the ultimate analysis of the coal used (refer to Table 2). After the combustion of pseudo-volatile species, the $H_2$ and CO is further oxidised following two-step homogeneous reactions:

$$CO + 0.5O_2 + H_2O \rightleftharpoons CO_2 + H_2O \quad (R2)$$

$$H_2 + 0.5O_2 \rightleftharpoons H_2O. \quad (R3)$$

Table 3 represented the kinetic constants of reactions (R1)–(R3).

### 2.3.3. Char combustion

The solid char particles are formed after complete decomposition of volatile contents from the coal particles. The microporous solid char particles react with the surrounding co-flow gases following heterogeneous chemical reactions such as oxidation, Boudouard and gasification reactions:

$$C_{char} + \frac{1}{2}O_2 \longrightarrow CO \quad (R4)$$

$$C_{char} + CO_2 \longrightarrow 2CO \quad (R5)$$

$$C_{char} + H_2O \longrightarrow H_2 + CO. \quad (R6)$$

The char combustion reactions' rate is controlled by two mechanisms such as the oxidant's diffusion via the film layer surrounding the coal particle and the intrinsic kinetic rate of the reaction on the particle surface [21]. The kinetic constants of reactions (R4)–(R6) are listed in Table 4.

### 2.3.4. Turbulence-chemistry interaction

MILD combustion modelling is greatly influenced by the interaction between turbulent flow and chemical reactions. Vascellari and Cau [21] reported that Eddy Dissipation Concept (EDC) can accurately predict the MILD combustion characteristics of solid fuels. Hence, the combustion model in the present study uses the EDC model [51] with finite-rate chemistry to describe turbulence-chemistry interaction.

### 2.3.5. Nitrogen oxides ($NO_x$) formation/destruction

Nitrogen oxides ($NO_x$) comprise both nitrogen dioxide ($NO_2$) and nitric oxide (NO). However, for pulverised coal combustion, NO accounts for 95% of total $NO_x$ formation [52,53]. In addition, during the experimental campaign, the measured value of $NO_2$ was below detection limits of the gas analyser. Therefore, only NO formation and/or destruction are considered in the computational modelling. The post-processing approach is considered to calculate NO in this study because the NO formation and/or destruction mechanisms have little impact on the flow properties or on the momentum and energy balances. The probability density function (PDF) is considered to model the turbulence effects.

Three well-known $NO_x$ formation mechanisms, thermal-$NO_x$, prompt-$NO_x$, and fuel-$NO_x$ combined with the $NO_x$ destruction mechanisms, i.e., $NO_x$-reburning mechanisms are considered in the current study.

The thermal-$NO_x$ is produced by the oxidation of atmospheric nitrogen ($N_2$) through endothermic chemical reactions. As a result, thermal-$NO_x$ production mainly depends on high temperature. Previous studies reported that a negligible amount of $NO_x$ is produced through thermal-route under the temperature level of 1800 K [14,33]. The highest temperature of the present study is measured to be below 1400 K, and thus, it has a positive impact on mitigation of thermal-$NO_x$ formation.

The thermal-$NO_x$ production follows the well-known Zel'dovich [54] reactions mechanism as follows:

$$N_2 + O \longrightarrow N + NO \quad (R7)$$

$$N + O_2 \longrightarrow O + NO \quad (R8)$$

$$N + OH \longrightarrow H + NO. \quad (R9)$$

$NO_x$ can be produced from the oxidation of atmospheric nitrogen ($N_2$) in combustion air via distinct reaction mechanism from the thermal-$NO_x$ which called prompt-$NO_x$ mechanism. The prompt-$NO_x$ formation occurs at fuel-rich environments, low temperature, and short residence time conditions. Generally, prompt-$NO_x$ does not influence the overall $NO_x$ production under MILD combustion conditions, because reactants are strongly diluted in the MILD case.

**Table 3**
Kinetic constants of gas phase reactions (R1)–(R3).

| Reaction | | $A$ | $E_a$ (J/kg mol) | Reference |
|---|---|---|---|---|
| (R1) | | $4.84 \times 10^7$ | $5.1 \times 10^7$ | [49] |
| (R2) | Forward | $2.24 \times 10^6$ | $4.18 \times 10^7$ | [50] |
| | Backward | $1.1 \times 10^{13}$ | $3.28 \times 10^8$ | |
| (R3) | Forward | $7.9 \times 10^{10}$ | $1.46 \times 10^8$ | [50] |
| | Backward | $3.48 \times 10^{13}$ | $3.98 \times 10^8$ | |

**Table 4**
Kinetic constants of heterogeneous reactions (R4)–(R6).

| Reaction | $A$ | $E_a$ (J/kg mol) | Reference |
|---|---|---|---|
| (R4) | $2.4 \times 10^{-3}$ | $6.906 \times 10^1$ | [48] |
| (R5) | $5.3 \times 10^{-3}$ | $1.255 \times 10^3$ | [48] |
| (R6) | $6.35 \times 10^{-3}$ | $1.62 \times 10^2$ | [48] |

Please cite this article as: M. Saha, et al., Effect of particle size on the MILD combustion characteristics of pulverised brown coal, Fuel Processing Technology (2015), http://dx.doi.org/10.1016/j.fuproc.2016.04.003

This study followed the proposed reactions of Saha et al. [25] for prompt- $NO_x$ formation in the MILD combustion of Australian brown coal:

$$CH + N_2 \rightleftharpoons HCN + N \quad (R10)$$

$$N + O_2 \rightleftharpoons NO + O \quad (R11)$$

$$HCN + OH \rightleftharpoons CN + H_2O \quad (R12)$$

$$CN + O_2 \rightleftharpoons CO + NO. \quad (R13)$$

The major $NO_x$ formation is described by the fuel $NO_x$ mechanism in pulverised coal combustion. Fuel $NO_x$ is formed by the oxidation of the organically bound nitrogen (N) in the coal particles. During the coal devolatilisation process, nitrogen is distributed between the volatiles and the char in the form of intermediates HCN and $NH_3$. While, HCN and $NH_3$ are subjected to four competitive reactions routes as proposed by Alganash et al. [55]:

$$HCN + O_2 \longrightarrow NO + \text{products} \quad (R14)$$

$$NH_3 + O_2 \longrightarrow NO + \text{products} \quad (R15)$$

$$HCN + NO \longrightarrow N_2 + \text{products} \quad (R16)$$

$$NH_3 + NO \longrightarrow N_2 + \text{products}. \quad (R17)$$

At the final stage of $NO_x$ mechanism, the interaction of turbulent fuel jet and hot co-flow gases in the furnace creates a positive reburning of $NO_x$ and leads to decrease overall $NO_x$ formation. The pathway of reaction between $NO_x$ and surrounding hydrocarbons ($C_xH_y$) is described as $NO_x$-reburning as follows:

$$C_xH_y + NO \longrightarrow HCN + \text{products} \quad (R18)$$

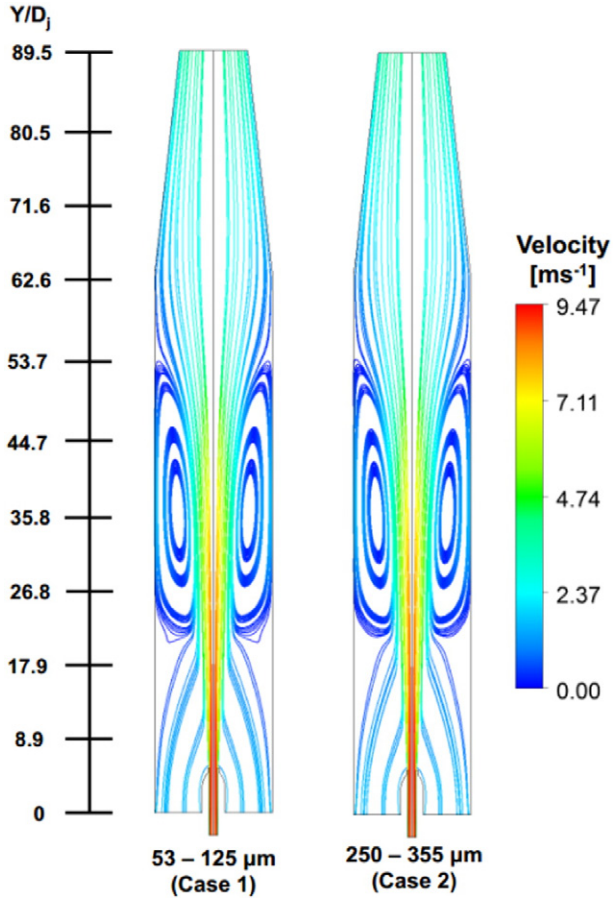


**Fig. 2.** Predicted velocity streamline for cases 1 and 2.

## 3. Results and discussion

To probe the impact of particle size on the burning characteristics of pulverised Loy-Yang brown coal with $CO_2$ as a carrier gas under MILD combustion conditions two different experimental and numerical investigations are conducted using a medium-scale laboratory furnace. For this comparative study, two ranges of particles' size are considered, namely; 53 μm–125 μm range and 250 μm–355 μm range. Other operating conditions such as the co-flow temperature and composition (i.e., 1284 K and 5.9% $O_2$), jet Reynolds number (i.e., $Re_{jet} = 20.000$), and the pulverised coal mass flow rate (i.e., 1.47 kg/h) were kept constant.

### 3.1. Flow patterns inside the furnace

Fig. 2 illustrates the velocity streamline contours for the two cases investigated in this study. For both cases, the velocity contours reveal the existence of recirculation vortices in the middle of the furnace. Recirculation inside the furnace, in general, plays a vital role in establishing MILD combustion and it appears to be contributing to the establishment of MILD combustion in this furnace as well. The figure reveals that there are no substantial differences between the two recirculation vortices in terms of flow path-lines distribution, size and location. Noteworthy is that the carrier gas flowrate is the same for both cases owing to the constant jet Reynolds number, i.e., $Re_{jet} = 20{,}000$. This suggests that the flow pattern inside the furnace is dominated by the carrier gas injection velocity rather than the coal particles' size.

### 3.2. Volatiles release and combustion

Fig. 3 shows the predicted volatiles mole fraction contours for cases 1 and 2. The value was calculated as the ratio of released gaseous volatiles from the coal particles to the total moles of gas in the furnace. The plots show that the location of volatiles release is significantly different for the different particle size cases. The volatiles are released earlier, close to the jet exit plane for the smaller particles' case while for the larger particles case the volatile matters release began further downstream in the upper section of the furnace and happened within a shorter period. Although the coal mass flow rate was fixed for both cases, the smaller particle case produced the maximum volatiles mole fraction at the centreline. On the other side, the shape of volatiles mole fraction zone is much wider and broader for large particle size in comparison with small particle size where volatiles are released along the furnace centreline and starts much earlier.

The predicted combustion rate of volatiles is shown in Fig. 4. The contour plots compare the rate of volatiles oxidation reaction (R1) between cases 1 and 2. The distribution of the volatiles reaction rates is consistent with the calculated distribution of the volatiles release. The volatiles of small size particles react earlier, away from the centreline, and happen along the furnace length. On the other hand, for the large particles' case the reaction seems to be concentrated on a bubble-like zone above the recirculation zone, shown earlier in Fig. 2.

The difference between the two cases is believed to be related to two main inter-related reasons. The first is to do with heat transfer to the particles to initiate the devolatilisation via convection and radiation.

Please cite this article as: M. Saha, et al., Effect of particle size on the MILD combustion characteristics of pulverised brown coal, Fuel Processing Technology (2015), http://dx.doi.org/10.1016/j.fuproc.2016.04.003

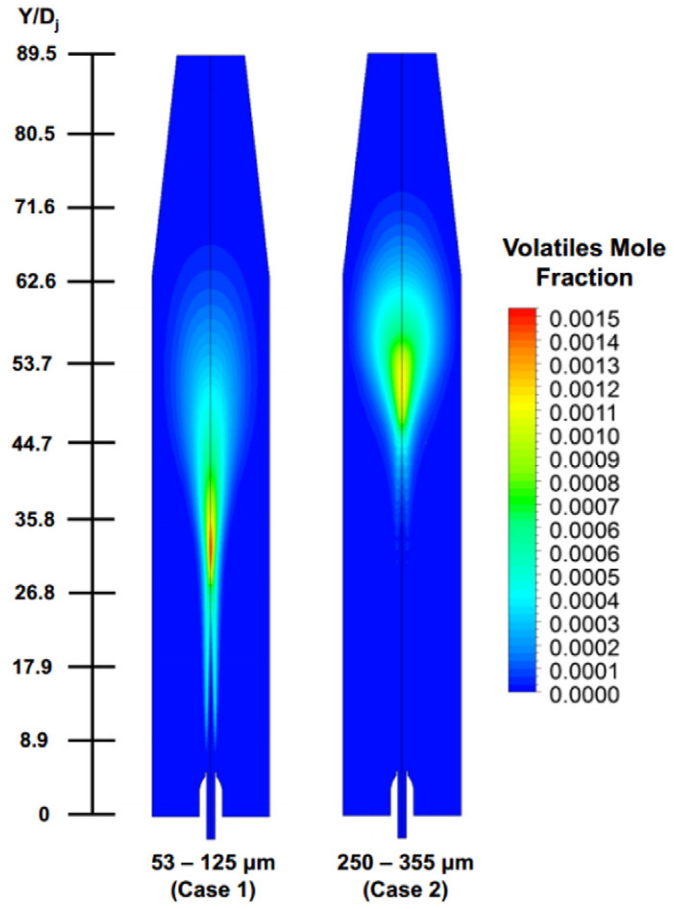


**Fig. 3.** Predicted contours of volatiles mole fraction.

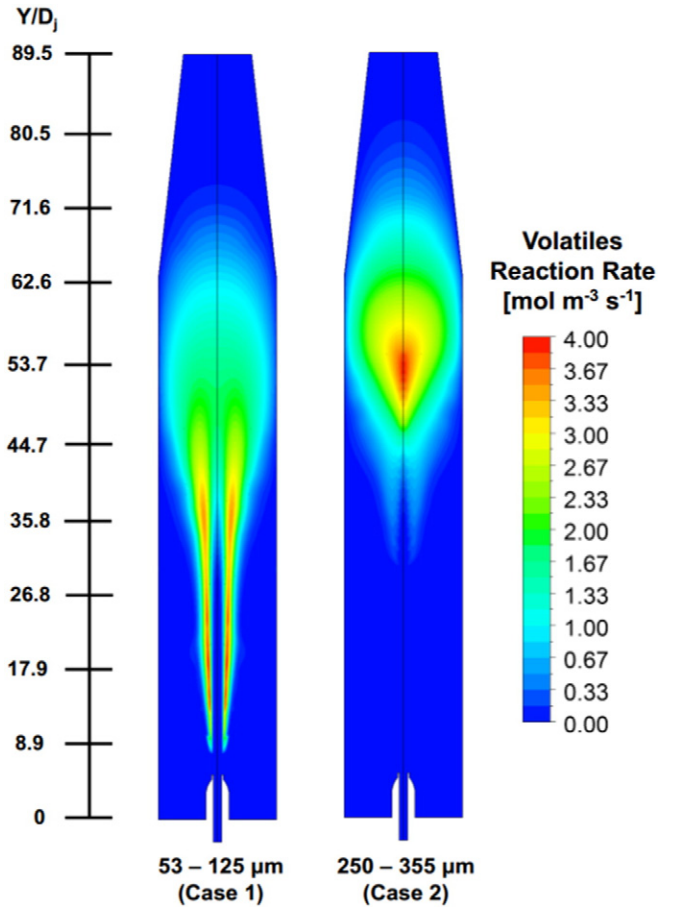


**Fig. 4.** Predicted contours of volatiles reaction (R1) rate.

While radiation from the walls to this dense medium plays a smaller role the convection part is likely to dominate. It is clear that larger particles are not interacting with the vitiated co-flow the same way smaller particles are and that results in the delayed release of volatiles as seen in Fig. 3. One of the key factors that influence the interaction of the particles with the flow is the Stokes number, $S_{tk}$. It is calculated using the ratio of the particle response time to a time characteristic of the flow, which is expressed [56,57] as:

$$S_{tk} = \frac{\rho_p d_p^2 U_{in}}{18 \mu D_j} \tag{19}$$

where, $\rho_p$, $d_p$, $U_{in}$, $\mu$ and $D_j$ represent the particle density, particle diameter, jet inlet velocity, gas viscosity, and jet diameter, respectively. It is well established that particles with smaller Stokes number more closely follow the fluid flow path-line, while particles with higher Stokes number detach from the fluid flow and are only weakly influenced by the fluid motion. Table 5 lists the particles' residence time and the Stokes number for different particle size cases. It is noticeable that Stokes number is calculated to be higher than 1 for both experimental cases. However, for the large particle case Stokes number is significantly higher and this may explain the delayed volatiles release. Also apparent is that release and reaction for case 2 happen above the recirculation zone while for case 1 the highest release and reaction occur within the recirculation zone. This difference implies that smaller particles are being circulated and mixed with the hot co-flow while the majority of the larger particles would have gone past the recirculation zone. This observation is further explained by the particle concentration distribution as well as trajectories of particle streams in terms of velocity contours as shown in Fig. 5. The plot provides the further evidence that for case 1, there is a strong recirculation vortex at the middle of the furnace which affects the coal particles to be entrained into the combustion region and dispersed into the furnace volume. While for case 2, the particle trajectory creates a straight path-line and tends to penetrate further downstream into the flow.

It is well established that in jets with poly-disperse particles, the small particles tend to move outwards towards the edge while larger particles stay close to the jet center [58]. This phenomenon may also explain the observed differences in the path-lines for case 1 as compared to case 2, where more dispersion and devolatilisation is apparent for the smaller particles case. While the larger particles tend to shoot through the centre and be less impacted by the recirculation vortex.

To better understand the Stokes number effect a standalone simulation is conducted considering mono-sized particles (1 μm) injected through the central jet. The Stokes number for 1 μm size particle is calculated to be much smaller than 1 and it is found that the particle acts as a tracer following the fluid flow perfectly. The difference in particles flow pattern is evident in the calculated residence time shown in Table 5 where the residence time for the small particle case is longer

**Table 5**
Calculated mean particles residence time and Stokes number.

| Particle size (μm) | Mean particle residence time (ms) | Stokes number |
|---|---|---|
| 1 | 468 | 0.001 |
| 53–125 | 371 | 3.9–21.75 |
| 250–355 | 285 | 87–175.5 |

Please cite this article as: M. Saha, et al., Effect of particle size on the MILD combustion characteristics of pulverised brown coal, Fuel Processing Technology (2015), http://dx.doi.org/10.1016/j.fuproc.2016.04.003

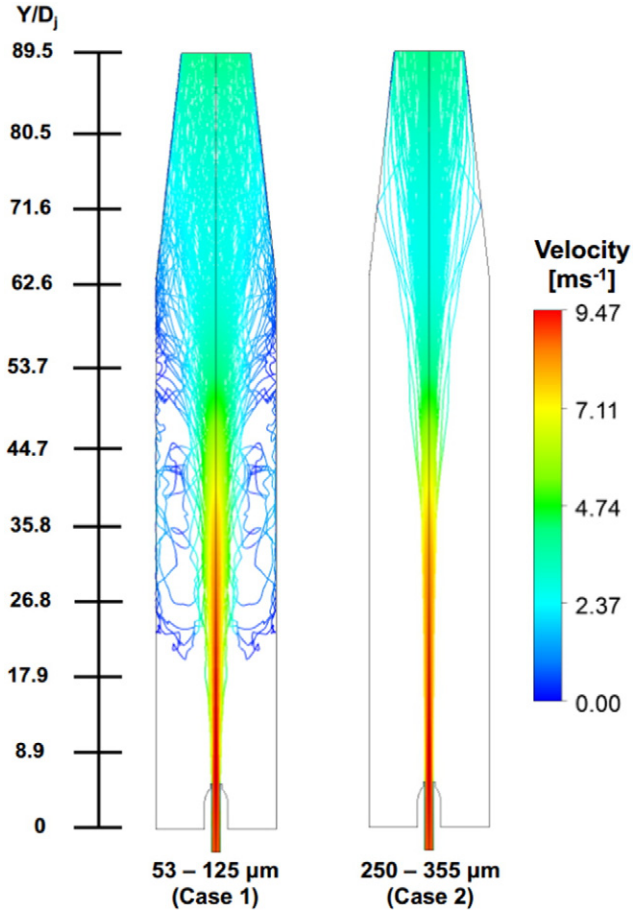


**Fig. 5.** Coal particle concentration distributions in terms of velocity for cases 1–2.

due to the recirculation as compared to the large particle case. As expected, the mean particle residence time for 1 μm size particle is higher than case 1 and case 2. This is because 1 μm sized particles are more likely to be entrained in the vortex region. In this way, the particle residence time for 1 μm size case represents also the gas residence time as well as the maximum possible particle residence time in the furnace for the specific conditions. Noteworthy, is that the jet velocity and momentum is the same for all cases.

### 3.3. Visual observations

Displayed in Fig. 6 are photographs taken from a side window close to the bottom (Y = 80 mm), middle (Y = 500 mm), and top (Y = 995 mm) of the furnace for both particles cases. The photographs were taken with the same camera settings (F/4.6–16 ms – ISO 250). It is clear that there is no visible flame apparent inside the furnace for either case. The photos at the bottom window show that a broader luminous image close to the jet exit plane is more clearly visible for smaller particles case than larger particles' case. This seems to be consistent with calculated earlier volatile release for the smaller particles' case. Although visual inspection through the middle and top windows of the furnace could not detect any substantial differences in terms of particles' ignition, the smaller particles' combustion is far more luminous in comparison with the combustion of larger particles' case. The comparatively higher combustion temperature of smaller particles' case (as will be shown later) might influence or be influenced by this high radiant effect.

### 3.4. Thermal fields

Presented in Fig. 7 are the measured and predicted furnace temperature profiles at several vertical axial locations (Y-direction) along the furnace centreline (X = 0 mm); and 50 mm (X = 0 mm, Z = 50 mm) and 100 mm (X = 0 mm, Z = 100 mm) away from the furnace centreline. The vertical locations are expressed in terms of the dimensionless ratio ($Y/D_j$) of vertical distance from the jet exit plane and the jet diameter ($D_j$ = 19 mm). The measured profiles of in-furnace temperatures are compared between the cases 1 and 2. The plot shows that smaller particles produce distinctly higher furnace temperature than larger particles. This of course relates to the position and manner that volatile are released and reacted in the smaller particles' case.

It is clear from Fig. 7, that there are no significant discrepancies between the predicted and the measured temperatures of either cases at locations Z = 50 mm and Z = 100 mm. For the centreline profile both models are predicting lower temperatures at the exit plane of 360 K for case 1 and 350 K for case 2. These values are much lower than the experimental value of 1230 K and 1131 K measured for case 1 and case 2, respectively. The models agree very well with measured temperatures at location $Y/D_j > 28$. This discrepancy is not well understood and is believed to be related to delayed volatilisation and or mixing rate by the model. It is also plausible that at least for case 1 the measurements spatial resolution (6 mm diameter thermocouple) and/or the accuracy of positioning may have contributed to the higher temperatures at these upstream locations. However, the differences are quite large (>780 K) and are unlikely to all be explained by the inaccuracy of the measurements, especially considering the very good agreement for the other two profiles.

Fig. 8 shows the measured temperature contours for the two cases. It is clear that temperature inside the furnace is semi-uniform for both cases and that a thermal boundary layer appears next to the furnace wall. For case 1 the temperature is higher closer to the jet exit while a homogenous temperature appears for the rest of the furnace, perhaps helped by the recirculation vortex shown in Fig. 2. For case 2 the temperature is lower close to the jet exit and lower temperatures appear in the rest of the furnace. Unfortunately no data are available for higher locations where the model has shown that most volatiles have burned and heat was released in case 2.

### 3.5. In-furnace chemical species

Figs. 9, 10 and 11 present the measured profiles of in-furnace gas composition, including; CO, $CO_2$ and $O_2$ mole fractions, respectively, at each of the 27 measurement locations. In general, the in-furnace CO formation trends for case 1 are significantly higher than for case 2. The higher CO production for smaller particles' case is consistent with finding that the rate of volatiles' release and reactions of smaller particles at upstream locations are substantially higher than larger particles. In addition, the highest CO concentration peak for smaller particles is found to be between $\approx Y/D_j = 30$–35.3 above the jet exit plane, while for the larger/heavier particles the CO peak was extended to $Y/D_j$ = 40.5 above the jet exit plane. This is because larger particles penetrate deeper into the furnace owing to the higher value of Stokes number (refer to Table 5). Therefore, volatiles release, as well as combustion of volatile matters takes place further downstream. It is also shown from Fig. 9 that higher value of CO mole fraction is found along the centreline of the furnace (X = 0 mm, Z = 0 mm) for both cases. This is because both combustion cases have a fuel-rich streamline in the central region where volatile matters are released by the particles. It is noticeable that CO levels are found at their lowest concentration at the top part of the furnace for smaller particles' case which points to the complete burning of gaseous volatiles, whereas for bigger particles' case a ~0.3% CO mole fraction (dry) is measured at the furnace exit which indicates that for the larger particles case longer residence time is required to burn all the volatiles and char.

Please cite this article as: M. Saha, et al., Effect of particle size on the MILD combustion characteristics of pulverised brown coal, Fuel Processing Technology (2015), http://dx.doi.org/10.1016/j.fuproc.2016.04.003

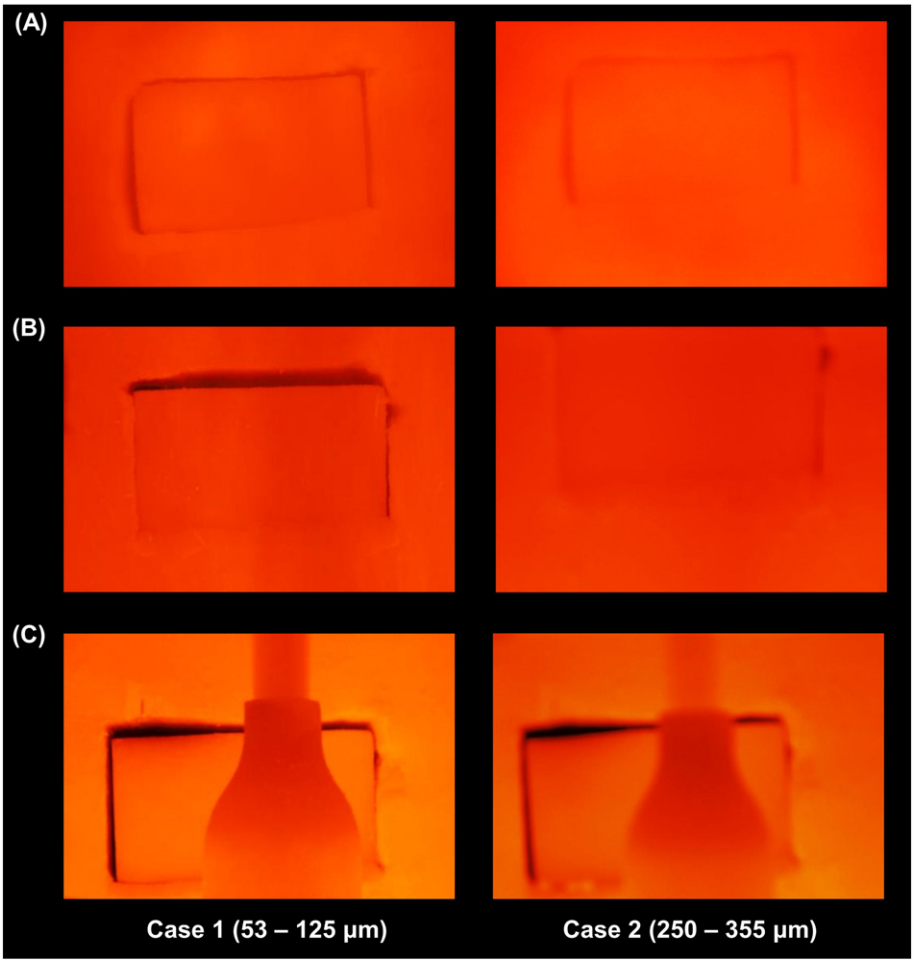


**Fig. 6.** Photographs of the inside of the furnace; (A) top (Y = 995 mm), (B) middle (Y = 500 mm), and (C) bottom (Y = 80 mm) part of the furnace.

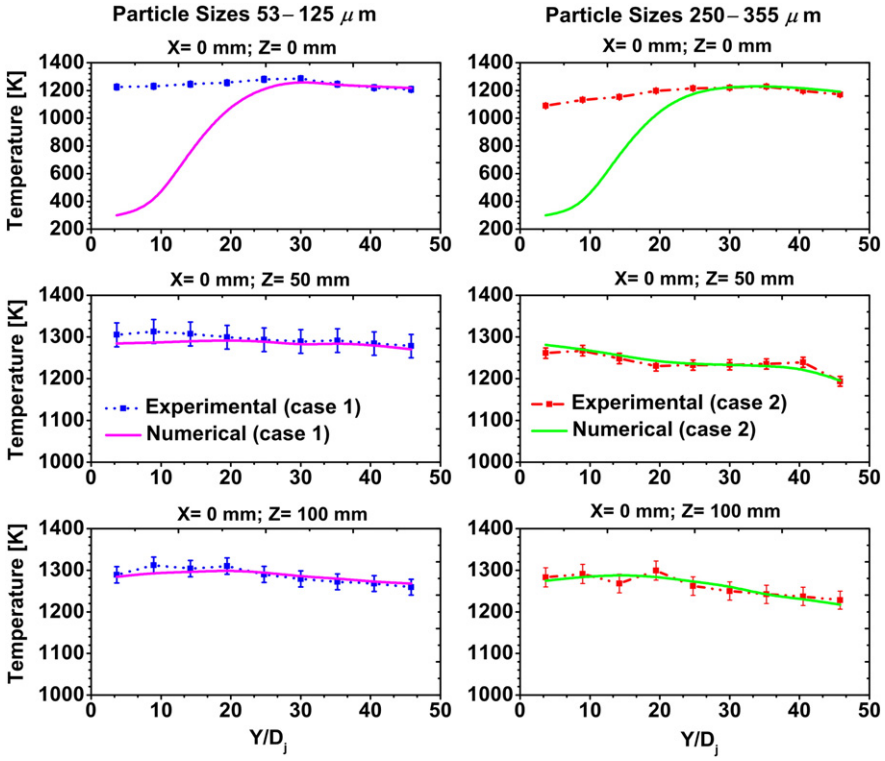


**Fig. 7.** In-furnace temperature profiles.

Please cite this article as: M. Saha, et al., Effect of particle size on the MILD combustion characteristics of pulverised brown coal, Fuel Processing Technology (2015), http://dx.doi.org/10.1016/j.fuproc.2016.04.003

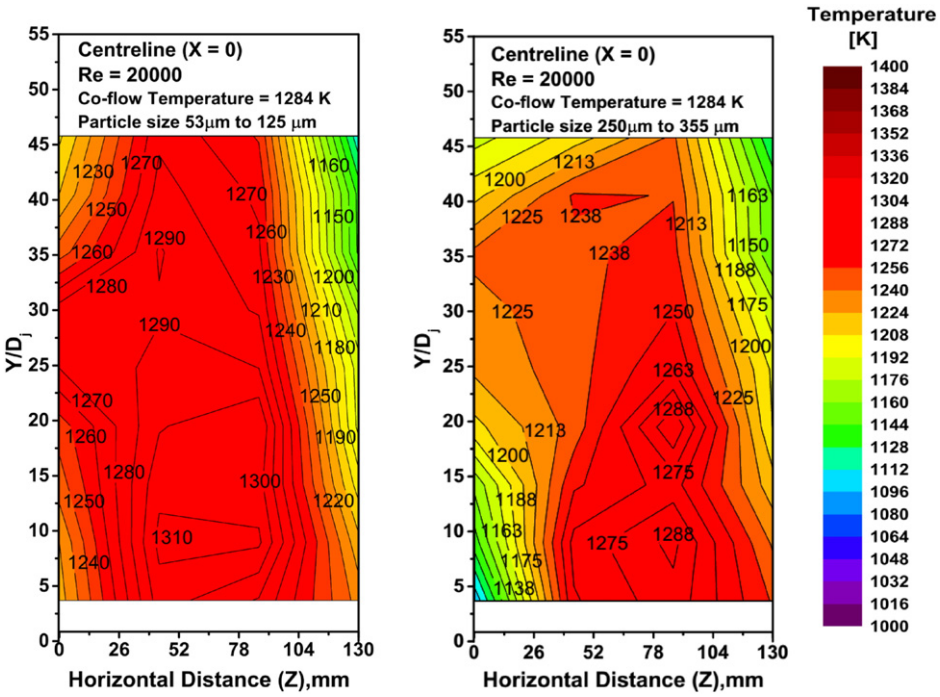


**Fig. 8.** Measured temperature distribution at the furnace centreline for the cases with different particles' size.

Fig. 9 also demonstrates the comparison between computed and measured CO mole fraction. The modelled CO mole fraction for the case 2 shows much lower values at upstream positions for all cases (up to 0.3% difference) and at location $Y/D_j = 30$ a gradual increase is observed. The predicted value close to the exit plane is much closer to that measured from the experiments. However, the low CO mole fraction prediction is quite similar with previous works [14,21,24,25] for the coal MILD combustion. This discrepancy could be associated with several causes. A sequential number of reactions are involved in producing CO. Coal devolatilisation process releases CO as a volatile matter. In addition, CO is formed by the oxidation of volatile contents and char. Furthermore, CO concentration is altered by the water gas shift reaction ($CO + H_2O \rightleftharpoons CO_2 + H_2$). It appears that the model is under-predicting the rate of CO production. The present numerical

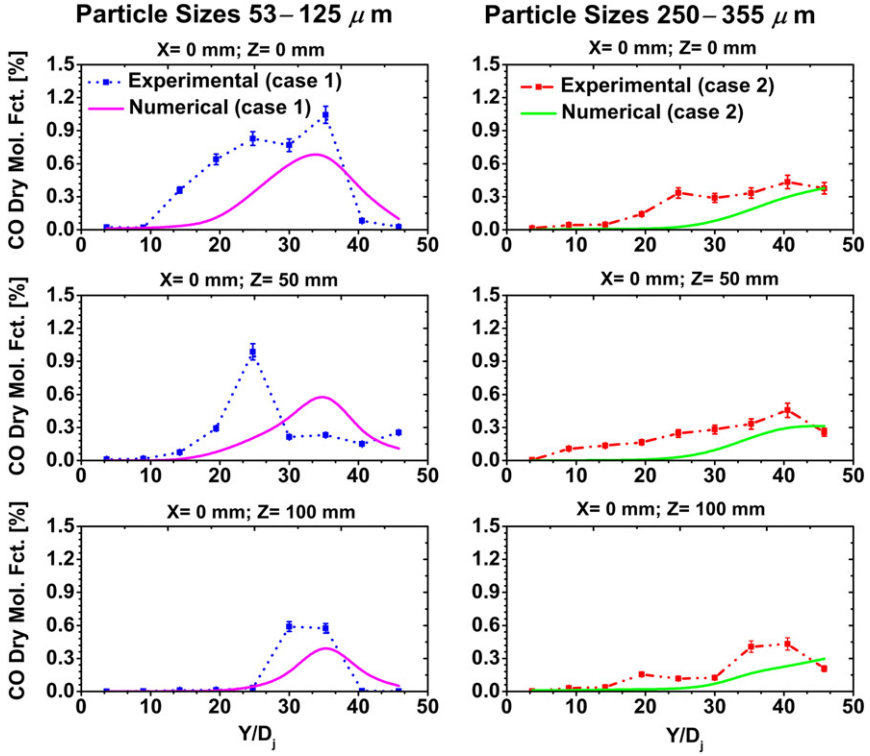


**Fig. 9.** In-furnace CO dry molar fraction.

Please cite this article as: M. Saha, et al., Effect of particle size on the MILD combustion characteristics of pulverised brown coal, Fuel Processing Technology (2015), http://dx.doi.org/10.1016/j.fuproc.2016.04.003

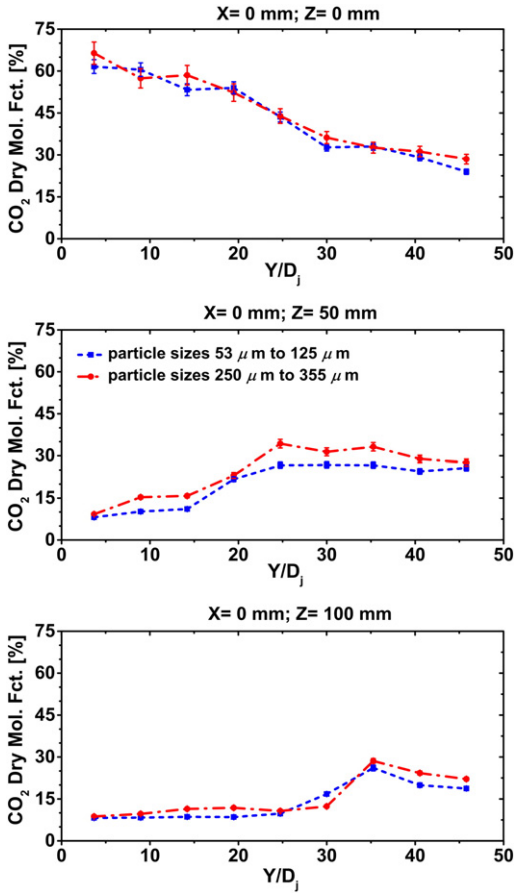


**Fig. 10.** Measured profiles of in-furnace $CO_2$ dry molar fraction for the cases of different particles' size.

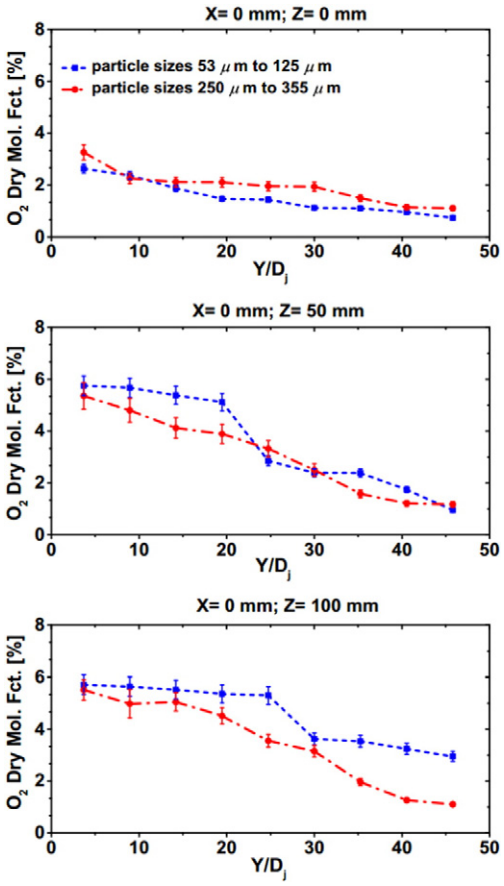


**Fig. 11.** Measured profiles of in-furnace $O_2$ dry molar fraction for the cases of different particles' size.

modellings considered only simplified volatile and char combustion reactions and thus replicated CO concentration was lower than measured values. The delayed release of calculated CO for both cases as compared to the measured value is consistent with the differences in the centreline temperature seen earlier in Fig. 6 and point to a model deficiency rather than an experimental error.

In Fig. 10, the mole fraction of $CO_2$ is shown. The figure shows that the highest levels of $CO_2$ mole fraction are measured to be ≈61.7% for the smaller particles' case and the value is found to be ≈64% for the larger particles' case. The maxima appear at the nearest location of jet exit plane, $Y/D_j = 3.68$, along the centreline (X = 0 mm, Z = 0 mm) of the furnace. Those values are predominantly represented by the input $CO_2$ concentrations. It is apparent that a diminishing trend of $CO_2$ concentration is found for both cases along the height of the furnace. The results indicate that the devolatilisation of coal particles has started at the jet exit plane but volatile matters' reactions commenced at a certain height of the furnace and then volatile matters/gases are effectively mixed and diluted with incoming $CO_2$. On the other hand, the $CO_2$ formation trends are found almost similar for both cases for 50 mm (X = 0 mm, Z = 50 mm) and 100 mm (X = 0 mm, Z = 100 mm) away from the furnace centreline which suggest that the combustion reaction started slowly because of longer ignition delay due to the high dilution of reactants.

Fig. 11 shows a decreasing trend of $O_2$ dry molar fraction along the furnace due to dilution and reaction. At the centreline, $O_2$ level are higher for case 2 up to $Y/D_j = 8.9$ and is lower for other locations. It is clear that for case 1 the reaction starts earlier as seen in the CO profile shown earlier. From the Z = 50 mm the $O_2$ mole fraction for case 1 remains almost constant up to $Y/D_j = 20$ before it is diluted and consumed by the identified recirculation vortex at this location. Further reduction happens at $Y/D_j = 35$ were char burnout is likely to have happened. While for case 2 the trends are gradually reduce along the furnace pointing to a reduced effect of the recirculation vortex in this case. At Z = 100 mm, similar trends to the profile at Z = 50 mm is observed for both cases.

The lowest values of $O_2$ concentration was measured at the furnace top, $Y/D_j = 45.8$, along the centreline (X = 0 mm, Z = 0 mm) of the furnace which is measured to be ≈1.1% for larger particles' case and ≈0.73% for smaller particles. The difference in $O_2$ level is attributed to the delayed devolatilisation in case 2 and more char burn out for case 1 leading to higher oxygen consumption and lower $O_2$ emission.

### 3.6. Nitric oxide (NO) concentration

Fig. 12 compares the measured in-furnace NO dry molar fraction between the particle sizes of 53–125 μm (case 1) and 250–355 μm (case 2). The NO mole fraction at the centreline for both cases are similar up to $Y/D_j = 20$ with values similar to that measured in the co-flow (~53 ppm). At higher locations the NO mole fraction, in case 1, increases to 170 ppm before reducing to an exhaust level of ~160 ppm. For case 2 the NO increases linearly and peaks at the exhaust level value to ~160 ppm. The difference relates to the location of volatiles release and reaction and the reduction seem to relate to a reburning mechanism. In quintessence, the volatile-N release is controlled by the variation of the particle size. The production of fuel-NO relies on the dominating environment of the re-circulating vortex where the trajectory of the coal particle sizes meets/encounters.

Considering NO profiles at the locations of 50 mm and 100 mm away from the centreline, a reduction is apparent at $Y/D_j = 25$ and 20, respectively, for case 2, which is associated with the mixing pattern and its

Please cite this article as: M. Saha, et al., Effect of particle size on the MILD combustion characteristics of pulverised brown coal, Fuel Processing Technology (2015), http://dx.doi.org/10.1016/j.fuproc.2016.04.003

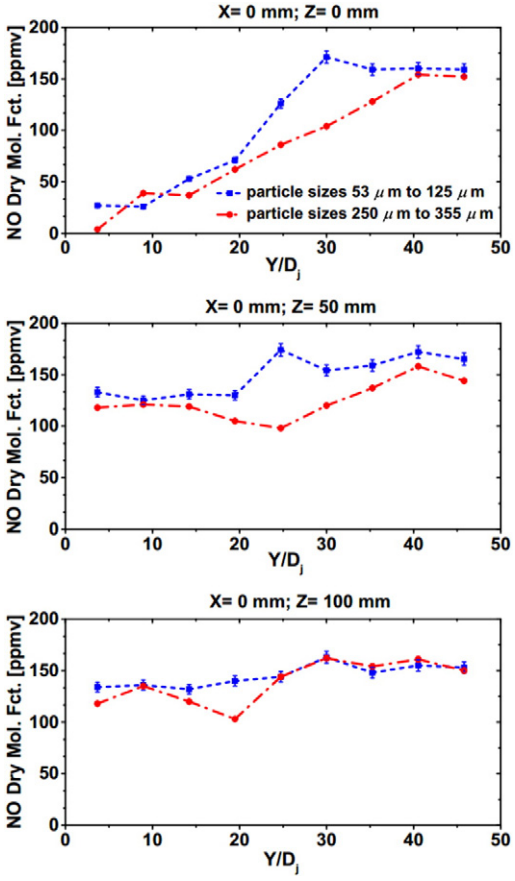


**Fig. 12.** Measured profiles of in-furnace NO dry molar fraction for the cases of different particles' size.

known effect on the reburning mechanism. For case 1 an increase is apparent at $Y/D_j = 20$, before a plateau close to the exit plane.

Presented in Fig. 13 are the predicted rates of NO formation and destruction, based on the main known mechanisms; thermal, fuel, prompt, and re-burn. There is an apparent difference in the NO formation rate, via the fuel-NO path, between case 1 and case 2. In particular, the predicted values of fuel-NO formation are 8.1 and 6.5 mg/m$^3$ s for case 1 and case 2, respectively. This is because the fuel-NO formation largely depends on the devolatilisation rate. As discussed in Section 3.2, the volatile release rate and reaction are more intense for the small size particle; it is not surprising for this case to lead to higher fuel-NO formation. However, both particle cases produce an almost similar rate of NO through the thermal-NO route albeit at very small amount accounting for <4.5% of the total NO. It is well-known that MILD combustion furnace temperatures are significantly lower than that of traditional combustion, and therefore thermal-NO does not have any significant impact on the overall NO emission.

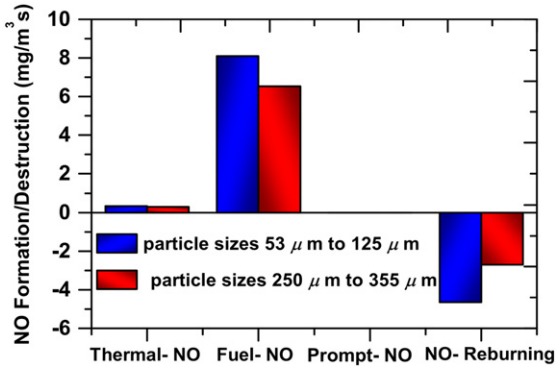


**Fig. 13.** NO production and destruction rate according to the main mechanisms.

For both cases, the value of prompt-NO is calculated to be almost nil, and cannot be sighted in Fig. 13. The MILD combustion conditions with a strong dilution of $CO_2$, as a carrier gas affects the formation of a negligible amount of prompt-NO.

Fig. 13 implies that the overall NO emission is decreased by up to 55% for case 1 and up to 40% for case 2 through the NO-reburning mechanism. The impact of reburning mechanism on the NO reduction is well-known from previous studies [14,21,25] for the MILD combustion of pulverised coal. The NO reduction is largely influenced by the volatiles production and combustion phenomena, because $C_xH_y$, HCN, and $NH_3$ are the primary species to lead homogeneous NO reduction reaction ($C_xH_y + NO \rightarrow HCN + products$). Therefore, case 1 reduces more NO than large particle case. As a consequence, the net NO emission is measured to be higher at the furnace exit for the large particle case.

### 3.7. Exhaust emissions

The comparison of measured and predicted NO, CO, $O_2$, and $CO_2$ mole fractions (dry basis) in the exhaust, between case 1 and case 2 are illustrated in Fig. 14.

The largest NO emission was measured for case 2 which is ≤124 ppmv and the value is about 15% higher than that of case 1 for the same experimental conditions. Nonetheless, the global NO emission is significantly lower than the measured local NO mole fraction in the furnace for both cases, due to the influence of NO-reburning reactions. The CO emission for case 2 is substantially, ~52%, lower than case 1, which is not dissimilar to the trend of in-furnace CO mole fraction (see Fig. 9). The exhaust CO level was measured to be 750–892 ppmv for case 2 while for case 1 the CO level was 1650–1780 ppmv. The lower CO emission for larger particles' case is related to the low volatile matters release rate which is attributed by the shorter residence time as was show earlier.

The $O_2$ mole fraction in the exhaust is almost ≈54% higher for case 2 than case 1; although for both cases global equivalence ratio was close to the stoichiometry combustion conditions. For the same boundary conditions, the higher value of $O_2$ concentration indicates that combustion is not completed for the large particles' case.

Fig. 14 shows a minor discrepancy between the measured values and computational results of exhaust gas emissions. The under-prediction of the CO and NO emissions indicate that the simplified devolatilisation model, reduction mechanism of gaseous species, and simplistic char combustion reactions, which play such a crucial role, are as yet not adequate to completely reproduce the experimental measurements.

### 3.8. Char burnout and overall carbon consumption rate

Fig. 15 shows the char burnout rate analyses according to the heterogeneous reactions ((R4)–(R6)) of char ($C_{char}$) with $O_2$, $CO_2$, and $H_2O$, respectively. The column graph illustrates that the char oxidation rate is about ≈65% for both cases by considering the chemical reaction of R4 ($C_{char} + \frac{1}{2}O_2 \rightarrow CO$). Almost similar findings are reported by other researchers [21,25] for the MILD combustion simulations considering low rank pulverised coal. As highlighted in Section 3.5, the amount of $CO_2$ mole fraction (Fig. 10) is substantially larger than $O_2$ mole fraction (Fig. 11). The higher $CO_2$ concentration leads to an increase in the char burnout rate following the gasification reaction.

Fig. 16 illustrates the overall carbon consumption rate of case 1 and case 2. The plot implies that around 71% carbon was burnt for the smaller particle size, while the amount of carbon consumption is around 57% for the larger particle size. The lower carbon consumption rate for the larger

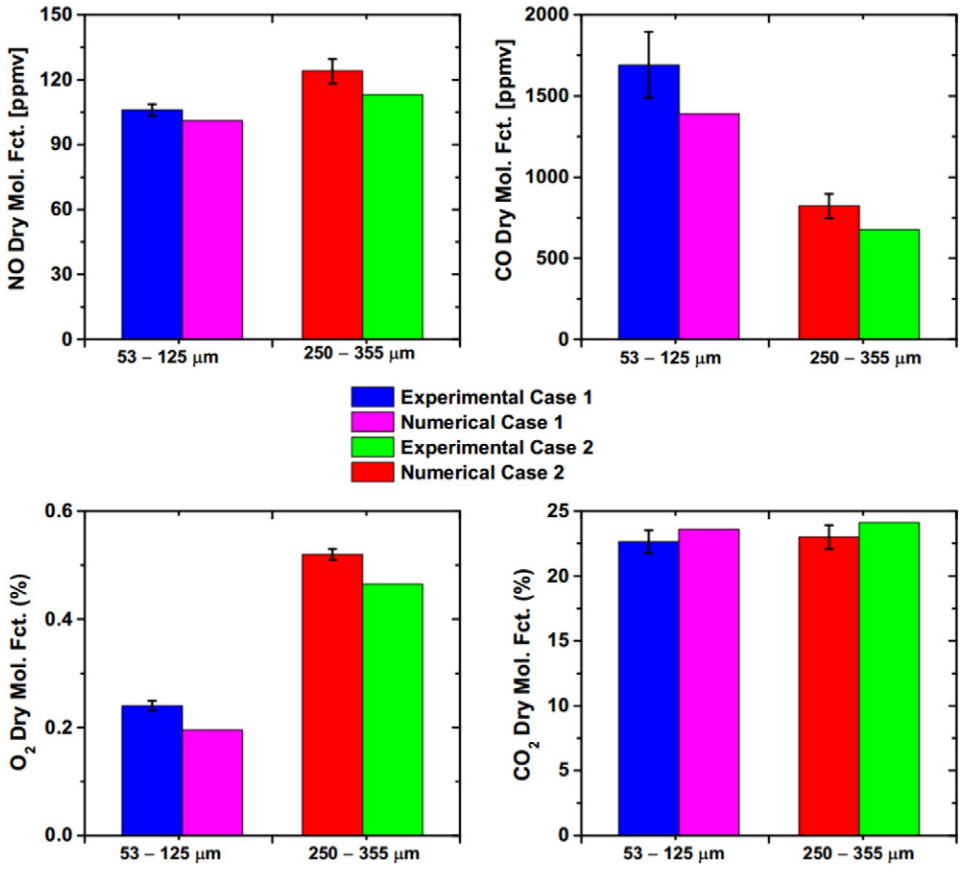


**Fig. 14.** Exhaust gas concentrations at the furnace exit.

particle size is related to the insufficient residence time of combustion. The larger particles are heavier than smaller particles and consequently the larger particles require more residence time to burn substantially in comparing with the smaller particles. Future experiments will verify these results.

## 4. Conclusions

The present experimental and numerical study demonstrates the impact of particle size on the MILD combustion characteristics of pulverised brown coal. In particular, this work investigates the impact of high temperature vitiated co-flow on the volatiles release and reaction from different sized particles. In addition, this paper reports the particle size impact on the NO formation/destruction along with volatile combustion rates and heterogeneous reactions on char burnout.

The major findings of this study are as follows:

1. A stable MILD combustion of pulverised brown coal is achieved for both particle size cases. No visible flame is found in the furnace for any case. Higher luminosity and interior furnace radiation is observed for the small particles' case than the large particles' case.
2. The small particle case produces higher furnace temperature than the large particle case. The high temperature production is influenced by more intense volatile combustion of smaller particles' case. In addition, the increasing Stokes number of the larger particles' case has a negative impact on the mixing with the hot co-flow as well as on the volatile release rate and reactions and consequently decreases the combustion temperature.

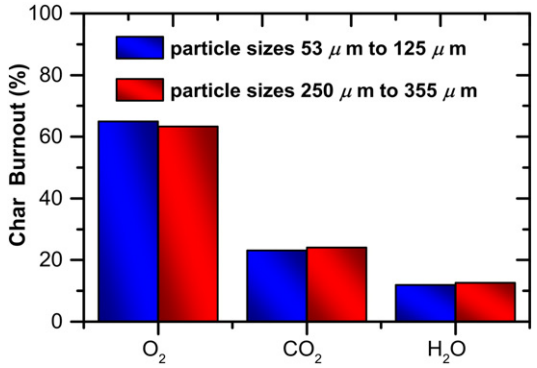


**Fig. 15.** Char burnout by the influence of heterogeneous reactions ((R4)–(R6)).

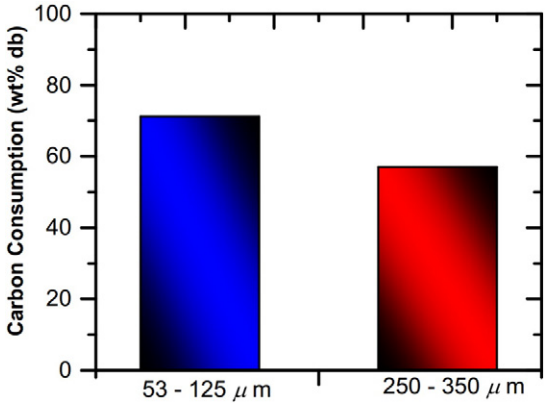


**Fig. 16.** Overall carbon consumption for cases 1–2.

Please cite this article as: M. Saha, et al., Effect of particle size on the MILD combustion characteristics of pulverised brown coal, Fuel Processing Technology (2015), http://dx.doi.org/10.1016/j.fuproc.2016.04.003

3. A semi-uniform temperature distribution is measured inside the furnace with <100 K difference from the bottom to the top of the furnace for both cases.
4. The CO emission for the large particle case is substantially, around 52%, lower than the small particle case. This indicates volatile release rate is significantly lower for the large particles' case in comparison with the small particles' case.
5. The NO formation trend is considerably higher for smaller particle case than bigger particle case. The small size particles released volatiles earlier and combustion initiated shortly. As a consequence, the succeeding NO production is high. On the other hand, the large particles take a longer time to dissociate for volatile evolution and volatile combustion takes long residence time to initiate.
6. The numerical models predict similar flow path-line in the furnace for both small and large particle cases. The flow pattern inside the furnace is dominated by the carrier gas injection velocity rather than the coal particle size. The smaller particles are being circulated and mixed with the hot co-flow following the flow pattern, while the larger particles did not follow the flow path-line.
7. In general, the models are well replicated the experimental data. However, numerical simulation slightly under-predicts CO and NO emissions. This under-prediction indicates that the simplified devolatilisation model, reduction mechanism of gaseous species, and simplistic char combustion reactions, which play such a crucial role, are as yet not adequate to completely reproduce the experimental measurements.
8. The numerical simulations predict that 95.5% of total NO produced via the fuel-NO route for both cases. However, NO formation through the fuel-NO route for the small particle case is significantly higher than large particle case. Furthermore, it is calculated that the small particle case reduced ≈55% of total NO, while the large particle case decreased ≈39% of total NO through the NO-reburning mechanism. As a consequence, the overall NO emission is measured to be higher at the furnace exit for the large particle case.

## Acknowledgments

The support of the University of Adelaide is gratefully acknowledged; in particular M. Saha acknowledges the Adelaide Scholarship International (ASI) of The University of Adelaide and Brown Coal Innovation Australia (BCIA) Top-Up scholarship for the financial support. The authors would like to thank Mr Marc Simpson, Manager, Thebarton Laboratory, for his help throughout the experiments. The authors would also like to acknowledge eResearch SA for the use of their computational facilities.

## References

[1] U.S. Energy Information Administration, International Energy Outlook 2015, U.S. Department of Energy (DOE), Washington, DC, 2015.
[2] Department of Economic Development, Transport and Resources, Victoria, Australia, Energy and Earth Resources, http://www.energyandresources.vic.gov.au/earth-resources/victorias-earth-resources/coal (Australia) 2015.
[3] C.-Z. Li, Some recent advances in the understanding of the pyrolysis and gasification behaviour of Victorian brown coal, Fuel 86 (2007) 1664–1683.
[4] E. Binner, L. Zhang, C.-Z. Li, S. Bhattacharya, In-situ observation of the combustion of air-dried and wet Victorian brown coal, Proc. Combust. Inst. 33 (2011) 1739–1746.
[5] M. de Joannon, A. Matarazzo, P. Sabia, A. Cavaliere, Mild combustion in homogeneous charge diffusion ignition (HCDI) regime, Proc. Combust. Inst. 31 (2007) 3409–3416.
[6] M.A. Galbiati, A. Cavigiolo, A. Effuggi, D. Gelosa, R. Rota, Mild combustion for fuel-NOx reduction, Combust. Sci. Technol. 176 (2004) 1035–1054.
[7] M. de Joannon, G. Langella, F. Beretta, A. Cavaliere, C. Noviello, Mild combustion: process features and technological constrains, Combust. Sci. Technol. 153 (2000) 33–50.
[8] P. Sabia, G. Sorrentino, A. Chinnici, A. Cavaliere, R. Ragucci, Dynamic behaviors in methane MILD and oxy-fuel combustion. Chemical effect of $CO_2$, Energy Fuel 29 (2015) 1978–1986.
[9] P. Sabia, M. de Joannon, A. Picarelli, A. Chinnici, R. Ragucci, Modeling negative temperature coefficient region in methane oxidation, Fuel 91 (2012) 238–245.
[10] M. de Joannon, A. Chinnici, P. Sabia, R. Ragucci, Optimal post-combustion conditions for the purification of $CO_2$-rich exhaust streams from non-condensable reactive species, Chem. Eng. J. 211 (2012) 318–326.
[11] T. Kiga, K. Yoshikawa, M. Sakai, S. Mochida, Characteristics of pulverized coal combustion in high-temperature preheated air, J. Propuls. Power 16 (2000) 601–605.
[12] T. Suda, M. Takafuji, T. Hirata, M. Yoshino, J. Sato, A study of combustion behavior of pulverized coal in high-temperature air, Proc. Combust. Inst. 29 (2002) 503–509.
[13] R. He, T. Suda, M. Takafuji, T. Hirata, J. Sato, Analysis of low NO emission in high temperature air combustion for pulverized coal, Fuel 83 (2004) 1133–1141.
[14] Z. Mei, P. Li, F. Wang, J. Zhang, J. Mi, Influences of reactant injection velocities on moderate or intense low-oxygen dilution coal combustion, Energy Fuel 28 (2013) 369–384.
[15] Y. Tu, H. Liu, K. Su, S. Chen, Z. Liu, C. Zheng, W. Li, Numerical study of $H_2O$ addition effects on pulverized coal oxy-MILD combustion, Fuel Process. Technol. 138 (2015) 252–262.
[16] Y. Tu, H. Liu, S. Chen, Z. Liu, H. Zhao, C. Zheng, Numerical study of combustion characteristics for pulverized coal under oxy-MILD operation, Fuel Process. Technol. 135 (2015) 80–90.
[17] R. Weber, Y. Poyraz, A.M. Beckmann, S. Brinker, Combustion of biomass in jet flames, Proc. Combust. Inst. 35 (2015) 2749–2758.
[18] R. Weber, J.P. Smart, W. Kamp, On the (MILD) combustion of gaseous, liquid, and solid fuels in high temperature preheated air, Proc. Combust. Inst. 30 (2005) 2623–2629.
[19] R. Weber, A. Lverlaan, S. Orsino, N. Lallemant, On emerging furnace design methodology that provides substantial energy savings and drastic reductions in $CO_2$, CO and NOx emissions, J. Inst. Energy 72 (1999) 77–83.
[20] N. Schaffel, M. Mancini, A. Szlek, R. Weber, Mathematical modeling of MILD combustion of pulverized coal, Combust. Flame 156 (2009) 1771–1784.
[21] M. Vascellari, G. Cau, Influence of turbulence–chemical interaction on CFD pulverized coal MILD combustion modeling, Fuel 101 (2012) 90–101.
[22] M. Tamura, S. Watanabe, K. Komaba, K. Okazaki, Combustion behaviour of pulverised coal in high temperature air condition for utility boilers, Appl. Therm. Eng. 75 (2015) 445–450.
[23] P. Li, F. Wang, Y. Tu, Z. Mei, J. Zhang, Y. Zheng, H. Liu, Z. Liu, J. Mi, C. Zheng, Moderate or intense low-oxygen dilution oxy-combustion characteristics of light oil and pulverized coal in a pilot-scale furnace, Energy Fuel 28 (2014) 1524–1535.
[24] M. Saha, B.B. Dally, P.R. Medwell, E.M. Cleary, Moderate or intense low oxygen dilution (MILD) combustion characteristics of pulverized coal in a self-recuperative furnace, Energy Fuel 28 (2014) 6046–6057.
[25] M. Saha, A. Chinnici, B.B. Dally, P.R. Medwell, Numerical study of pulverized coal MILD combustion in a self-recuperative furnace, Energy Fuel 29 (2015) 7650–7669.
[26] B.B. Dally, S.H. Shim, R.A. Craig, P.J. Ashman, G.G. Szegö, On the burning of sawdust in a MILD combustion furnace, Energy Fuel 24 (2010) 3462–3470.
[27] H. Zhang, G. Yue, J. Lu, Z. Jia, J. Mao, T. Fujimori, T. Suko, T. Kiga, Development of high temperature air combustion technology in pulverized fossil fuel fired boilers, Proc. Combust. Inst. 31 (2007) 2779–2785.
[28] M. Saha, B.B. Dally, P.R. Medwell, E. Cleary, MILD combustion of pulverised coal in a recuperative furnace, Proceedings of the European Combustion Meeting 2013, Lund, Sweden, June 25–28, 2013.
[29] M. Saha; B. B. Dally; P. R. Medwell; E. Cleary, An experimental study of MILD combustion of pulverized coal in a recuperative furnace, In Proceedings of the 9th Asia-Pacific Conference on Combustion 2013, Gyeongju Hilton, Gyeongju, Korea; p 223.
[30] M. Saha, B.B. Dally, P.R. Medwell, E. Cleary, A study of combustion characteristics of pulverised coal under MILD combustion conditions, Proceedings of the Australian Combustion Symposium 2013, The University of Western Australia, Perth, Australia 2013, pp. 132–135.
[31] N. Schaffel-Mancini, Ecological Evaluation of the Pulverized Coal Combustion in HTAC Technology(a PhD thesis) Silesian University of Technology and Clausthal University of Technology, Poland, 2009.
[32] H. Stadler, D. Toporov, M. Förster, R. Kneer, On the influence of the char gasification reactions on NO formation in flameless coal combustion, Combust. Flame 156 (2009) 1755–1763.
[33] H. Stadler, D. Ristic, M. Förster, A. Schuster, R. Kneer, G. Scheffknecht, $NO_x$-emissions from flameless coal combustion in air, $Ar/O_2$ and $CO_2/O_2$, Proc. Combust. Inst. 32 (2009) 3131–3138.
[34] M. Saha, A. Chinnici, P.R. Medwell, B.B. Dally, Numerical investigation of pulverised coal combustion in a self-recuperative MILD combustion Furnace, Proceedings of the 10th Asia-Pacific Conference on Combustion, Beijing, China, 2015.
[35] M. Saha, B.B. Dally, P.R. Medwell, A. Chinnici, MILD combustion of Victorian brown coal, Proceedings of the International Conference on Coal Science & Technology 2015, Melbourne, Australia, 2015.
[36] M. Saha, B.B. Dally, P.R. Medwell, A. Chinnici, Effect of turbulence on the MILD combustion characteristics of Victorian brown coal, Proceedings of the Australian Combustion Symposium 2015, The University of Melbourne, Australia 2015, pp. 92–95.
[37] S.V. Patankar, D.B. Spalding, A calculation procedure for heat, mass and momentum transfer in three-dimensional parabolic flows, Int. J. Heat Mass Transf. 15 (1972) 1787–1806.
[38] T.-H. Shih, W.W. Liou, A. Shabbir, Z. Yang, J. Zhu, A new k-ε eddy viscosity model for high Reynolds number turbulent flows, Comput. Fluids 24 (1995) 227–238.
[39] E. Chui, G. Raithby, Computation of radiant heat transfer on a nonorthogonal mesh using the finite-volume method, Numer. Heat Transfer 23 (1993) 269–288.
[40] B. Popoff, M. Braun, A Lagrangian approach to dense particulate flows, International Conference on Multiphase Flow, Leipzig, Germany, 2007.
[41] D. Förtsch, F. Kluger, U. Schnell, H. Spliethoff, K.R. Hein, A kinetic model for the prediction of NO emissions from staged combustion of pulverized coal, Proc. Combust. Inst. 27 (1998) 3037–3044.
[42] H. Kobayashi, J. Howard, A.F. Sarofim, Coal devolatilization at high temperatures, Proc. Combust. Inst. 16 (1977) 411–425.
[43] T.H. Fletcher, A.R. Kerstein, R.J. Pugmire, M.S. Solum, D.M. Grant, Chemical percolation model for devolatilization. 3. Direct use of carbon-13 NMR data to predict effects of coal type, Energy Fuel 6 (1992) 414–431.

Please cite this article as: M. Saha, et al., Effect of particle size on the MILD combustion characteristics of pulverised brown coal, Fuel Processing Technology (2015), http://dx.doi.org/10.1016/j.fuproc.2016.04.003

[44] T.H. Fletcher, A.R. Kerstein, R.J. Pugmire, D.M. Grant, Chemical percolation model for devolatilization. 2. Temperature and heating rate effects on product yields, Energy Fuel 4 (1990) 54–60.
[45] M.S. Solum, R.J. Pugmire, D.M. Grant, Carbon-13 solid-state NMR of argonne-premium coals, Energy Fuel 3 (1989) 187–193.
[46] R. Jovanovic, A. Milewska, B. Swiatkowski, A. Goanta, H. Spliethoff, Sensitivity analysis of different devolatilisation models on predicting ignition point position during pulverized coal combustion in $O_2/N_2$ and $O_2/CO_2$ atmospheres, Fuel 101 (2012) 23–37.
[47] L. Álvarez, M. Gharebaghi, J. Jones, M. Pourkashanian, A. Williams, J. Riaza, C. Pevida, J. Pis, F. Rubiera, CFD modeling of oxy-coal combustion: prediction of burnout, volatile and NO precursors release, Appl. Energy 104 (2013) 653–665.
[48] J. Zhang, W. Prationo, L. Zhang, Z. Zhang, Computational fluid dynamics modeling on the air-firing and oxy-fuel combustion of dried Victorian brown coal, Energy Fuel 27 (2013) 4258–4269.
[49] D.W. Shaw, X. Zhu, M.K. Misra, R.H. Essenhigh, Determination of global kinetics of coal volatiles combustion, Proceedings of the Combustion Institute, Elsevier 1991, pp. 1155–1162.
[50] L. Wang, Z. Liu, S. Chen, C. Zheng, Comparison of different global combustion mechanisms under hot and diluted oxidation conditions, Combust. Sci. Technol. 184 (2012) 259–276.
[51] B. Magnussen, On the structure of turbulence and a generalized eddy dissipation concept for chemical reaction in turbulent flow, Nineteenth AIAA Meeting, St. Louis, 1981.
[52] A. Williams, M. Pourkashanian, J. Jones, Combustion of pulverised coal and biomass, Prog. Energy Combust. Sci. 27 (2001) 587–610.
[53] S. Hill, L. Douglas Smoot, Modeling of nitrogen oxides formation and destruction in combustion systems, Prog. Energy Combust. Sci. 26 (2000) 417–458.
[54] Y. Zeldovich, D. Frank-Kamenetskii, P. Sadovnikov, Oxidation of Nitrogen in Combustion, Publishing House of the Acad of Sciences of USSR, 1947.
[55] B. Alganash, M.C. Paul, I.A. Watson, Numerical investigation of the heterogeneous combustion processes of solid fuels, Fuel 141 (2015) 236–249.
[56] J. Derksen, S. Sundaresan, H. Van den Akker, Simulation of mass-loading effects in gas–solid cyclone separators, Powder Technol. 163 (2006) 59–68.
[57] A. Chinnici, M. Arjomandi, Z.F. Tian, Z. Lu, G.J. Nathan, A novel solar expanding-vortex particle reactor: influence of vortex structure on particle residence times and trajectories, Sol. Energy 122 (2015) 58–75.
[58] T.C. Lau, G.J. Nathan, Influence of Stokes number on the velocity and concentration distributions in particle-laden jets, J. Fluid Mech. 757 (2014) 432–457.

Please cite this article as: M. Saha, et al., Effect of particle size on the MILD combustion characteristics of pulverised brown coal, Fuel Processing Technology (2015), http://dx.doi.org/10.1016/j.fuproc.2016.04.003

# CHAPTER 6

# BURNING CHARACTERISTICS OF VICTORIAN BROWN COAL UNDER MILD COMBUSTION CONDITIONS

# Statement of Authorship

| | |
|---|---|
| Title of Paper | Burning Characteristics of Victorian Brown Coal in a MILD Combustion Furnace |
| Publication Status | ☐ Published ☐ Accepted for Publication<br>☑ Submitted for Publication ☐ Unpublished and Unsubmitted w ork w ritten in manuscript style |
| Publication Details | **M. Saha,** B. B. Dally, P. R. Medwell, and A. Chinnici, "Burning Characteristics of Victorian Brown Coal in a MILD Combustion Furnace", *Combustion and Flame,* paper CNF-D-16-00037, 2016 (*under review*). |

## Principal Author

| | | | |
|---|---|---|---|
| Name of Principal Author (Candidate) | Manabendra Saha | | |
| Contribution to the Paper | Designed, built and commissioned furnace. Conducted experiments, analysed data, wrote manuscript and acted as corresponding author. | | |
| Overall percentage (%) | 75% | | |
| Certification: | This paper reports on original research I conducted during the period of my Higher Degree by Research candidature and is not subject to any obligations or contractual agreements with a third party that would constrain its inclusion in this thesis. I am the primary author of this paper. | | |
| Signature | | Date | 6/04/2016 |

## Co-Author Contributions

By signing the Statement of Authorship, each author certifies that:

i. the candidate's stated contribution to the publication is accurate (as detailed above);

ii. permission is granted for the candidate in include the publication in the thesis; and

iii. the sum of all co-author contributions is equal to 100% less the candidate's stated contribution.

| | | | |
|---|---|---|---|
| Name of Co-Author | Bassam B. Dally | | |
| Contribution to the Paper | Supervised development of work, helped in developing ideas, data interpretation and manuscript evaluation. | | |
| Signature | | Date | 6-4-16 |

| | | | |
|---|---|---|---|
| Name of Co-Author | Paul R. Medwell | | |
| Contribution to the Paper | Supervised development of work, helped in developing ideas, data interpretation and manuscript evaluation. | | |
| Signature | | Date | 13-APR-2016 |

| | | | |
|---|---|---|---|
| Name of Co-Author | Alfonso Chinnici | | |
| Contribution to the Paper | Helped in performing CFD modelling, data interpretation and manuscript evaluation. | | |
| Signature | | Date | 7/04/2016 |

Elsevier Editorial System(tm) for Combustion and Flame

Manuscript Draft

Manuscript Number: CNF-D-16-00037R1

Title: Burning Characteristics of Victorian Brown Coal under MILD Combustion Conditions

Article Type: Full Length Article

Keywords: Pulverised fuel; Victorian brown coal; MILD combustion; Turbulent jet; Temperature.

Corresponding Author: Mr. Manabendra Saha, MSc, BSc in Mechanical Engineering

Corresponding Author's Institution: The University of Adelaide

First Author: Manabendra Saha, MSc, BSc in Mechanical Engineering

Order of Authors: Manabendra Saha, MSc, BSc in Mechanical Engineering; Bassam B Dally, Ph.D., B.Sc. in Mechanical Engineering; Paul R Medwell, Ph.D., B.E. in Mechanical Engineering; Alfonso Chinnici, Ph.D., B.Sc. in Chemical Engineering

Abstract: In this work a vertical furnace is used to investigate the MILD (Moderate or Intense Low-oxygen Dilution) combustion characteristics of pulverised Victorian brown coal. This paper reports the effect of turbulence on the volatiles' release and reactions under vitiated co-flow conditions as well as the impact on the pollutants' formation and emission. Loy-Yang brown coal from the Latrobe Valley, Victoria, Australia, with particle sizes in the range of 53-125 µm, is injected into the furnace using CO2 as a carrier gas through an insulated and water-cooled central jet. The bulk jet Reynolds number was varied from Rejet = 5,527 to Rejet = 20,000. The furnace walls as well as co-flow temperature and local oxygen concentrations are controlled by a secondary swirling burner using non-premixed natural gas combustion. The co-flow in the furnace was operated with an O2 concentration of 5.9% (db by volume). Detailed measurements of in-furnace temperatures and chemical species are presented and discussed, together with visual observations and CH chemiluminescence (CH*) imaging at the bottom, middle and top parts of the furnace. The CH* signal intensity is found to be significantly lower at the top part of the furnace which is an indication of slow rate of the heterogeneous combustion of char particles. The largest amount of CO concentrations are measured for the highest jet velocity (i.e., Rjet = 20,000) case which implies that with increasing turbulence there is a better mixing and a broad devolatilisation zone is formed which produces more CO. The measured NO emission for any case was less than 125 ppmv (db at 3% O2) which provides evidence to the potential benefits of MILD combustion application to Victorian brown coal towards reducing NO emission. Complementary CFD model helped in shedding light on the flow field, turbulence intensity, volatiles' release rate, combustion of volatile matters, and overall carbon consumption inside the furnace for the three cases. It was found that increasing the jet Reynolds number increases the volatiles release rates and decrease the rate of overall carbon consumption.

# Burning Characteristics of Victorian Brown Coal under MILD Combustion Conditions

Manabendra Saha*, Bassam B. Dally, Paul R. Medwell, and Alfonso Chinnici

Centre for Energy Technology, School of Mechanical Engineering,

The University of Adelaide, SA 5005, Australia

## ABSTRACT

In this work a vertical furnace is used to investigate the MILD (Moderate or Intense Low-oxygen Dilution) combustion characteristics of pulverised Victorian brown coal. This paper reports the effect of turbulence on the volatiles' release and reactions under vitiated co-flow conditions as well as the impact on the pollutants' formation and emission. Loy-Yang brown coal from the Latrobe Valley, Victoria, Australia, with particle sizes in the range of 53-125 μm, is injected into the furnace using $CO_2$ as a carrier gas through an insulated and water-cooled central jet. The bulk jet Reynolds number was varied from $Re_{jet}$ = 5,527 to $Re_{jet}$ = 20,000. The furnace walls as well as co-flow temperature and local oxygen concentrations are controlled by a secondary swirling burner using non-premixed natural gas combustion. The co-flow in the furnace was operated with an $O_2$ concentration of 5.9% (db by volume). Detailed measurements of in-furnace temperatures and chemical species are presented and discussed, together with visual observations and CH chemiluminescence ($CH^*$) imaging at the bottom, middle and top parts of the furnace. The $CH^*$ signal intensity is found to be significantly lower at the top part of the furnace which is an indication of slow rate of the heterogeneous combustion of char particles. The largest amount of CO concentrations

are measured for the highest jet velocity (i.e., $R_{jet}$ = 20,000) case which implies that with increasing turbulence there is a better mixing and a broad devolatilisation zone is formed which produces more CO. The measured NO emission for any case was less than 125 ppmv (db at 3% $O_2$) which provides evidence to the potential benefits of MILD combustion application to Victorian brown coal towards reducing NO emission. Complementary CFD model helped in shedding light on the flow field, turbulence intensity, volatiles' release rate, combustion of volatile matters, and overall carbon consumption inside the furnace for the three cases. It was found that increasing the jet Reynolds number increases the volatiles release rates and decrease the rate of overall carbon consumption.

**KEYWORDS:** Pulverised fuel, Victorian brown coal, MILD combustion, Turbulent jet, Temperature.

*Corresponding author.
E-mail: *manabendra.saha@adelaide.edu.au*
Phone: +61 (0)8 8313 5460

# 1. INTRODUCTION

Brown coal is among the lowest cost fuels for energy generation in the world [1]. Brown coal reserves in Victoria, Australia, represents a significant proportion of the world's brown coal reserve (24% of the world's total reserve), estimated at ~430 billion tonnes [2]. The Loy-Yang brown coal in Victoria is a low rank and tertiary aged coal which is called lignite [3]. Moreover, Victorian brown coal has a high volatile and oxygen content, and is low in ash, sulphur and heavy metals, making it unique when compared with other solid fuels such as biomass, peat, bituminous coal and anthracite [3]. However, Victorian brown coal has high moisture content (about 60 – 70 wt%) [4] which reduces the thermal efficiency when burned. In addition, the Victorian brown coal has a high content of iron, alkali and alkaline earth metallic species (mainly Na, Mg, and Ca) [5], which are largely responsible for slagging and fouling problems in the pulverised fuel combustion system. Typical Victorian brown coal-fired system plants are characterised by a high emission intensity (≈ 1.22 ton-$CO_2$/MWh) and $NO_x$ emissions (≈ 650 ppmv) [6, 7] that hampers the utilization of this coal. Thus the efficient use of Victorian brown coal and its impact on the environment remains a major challenge. Hence, the development of advanced coal combustion technologies motivated this research to reduce emission and improve efficiency, to develop accurate modelling and scaling tools and to optimize in order to improve viability and utilisation.

New combustion technologies are required in order to improve efficiency and reduce impact on the environment. Such technologies include Ultra Super Critical Combustion (USCC) [8], Oxy-coal combustion [9], and Integrated Gasification Combined Cycle (IGCC) [10].

One of the simplest approaches to improve thermal efficiency is to increase combustion temperature, usually by preheating the reactants [11] through exhaust heat

recovery; the immediate drawback of this technique is the rise in thermal $NO_x$ formation. In other words, the reduction of pollutants often comes at the price of efficiency losses. To overcome this dilemma of high efficiency with increasing $NO_x$ formation, flue or exhaust gas recirculation into the reaction zone is one of the most successful schemes [12, 13]. The recirculated exhaust gases or products of combustion contain low oxygen concentration that establishes high temperature and dilution rate inside the combustion chamber. The high rate of dilution results in the reactants (oxidiser and fuel) mixing with inert gases (i.e. flue gases) before they react [14]. The combination of high temperature and high dilution inside the combustion chamber is essential to the establishment of Moderate or Intense Low-oxygen Dilution (MILD) combustion. The high temperature of reactants and low oxygen concentration alter the reaction zone to be classified as "volumetric", leading to lower and more homogeneous temperatures which in turn achieve very low pollutant emissions and improved thermal efficiency of the combustion system [15]. These characteristics make this technology attractive in comparison to other abatement techniques. MILD combustion is often called "flameless combustion" or "flameless oxidation" [16] because, at optimised conditions, the flames are both invisible and inaudible. MILD combustion is a subset of the "high temperature air combustion" (HiTAC) regime because the combustion air is usually preheated to high temperatures [17]. The term "MILD combustion" will be used throughout this paper.

Many numerical and experimental investigations have been carried out to investigate the characteristics of MILD combustion using gaseous fuels [15, 18-20]. Although MILD combustion has been studied extensively for gaseous fuels, MILD combustion of particulate fuels has received much less attention and its burning characteristics are poorly understood [17, 21-40]. The first substantial effort to apply MILD combustion

technology on the burning of high volatile pulverised coal was led by Kiga et al. [17] in a drop tube furnace under the atmosphere of high-temperature preheated air. Their experimental measurements suggested that increasing the air preheat resulted in a significant elevation of the combustion efficiency, along with a substantial reduction of $NO_x$ emissions, when compared with conventional combustion. However, they concluded that "the use of high-temperature diluted air was not suitable for stable pulverised coal combustion" because of the slow combustion rate under low-oxygen combustion conditions. The MILD combustion behaviour of high volatile bituminous coal was conducted in a 0.58MW furnace by Weber et al. [26] at the International Flame Research Foundation (IFRF). The experimental findings of Weber et al. [26] are somewhat contradictory to the conclusions of Kiga et al. [17] in terms of stable pulverised coal MILD combustion. The results reported a high $NO_x$ reduction potential for the MILD combustion technology, where the $NO_x$ emissions in the exhaust were measured below 175 ppm (at 3% $O_2$). However, the fundamental mechanism of $NO_x$ formation/destruction was difficult to unravel from the experiments. Smart and Riley [36] conducted an experimental study to burn high volatile Russian bituminous coal under Oxy-MILD combustion conditions in a 500 kW furnace. They reported a marginally stable Oxy-MILD coal combustion occurred with their burner configuration, where there was a large separation between the pulverised coal and the oxidant. Weidmann et al. [37, 38] reported MILD combustion of highly volatile sub-bituminous Columbian coal in a 7 m long and 500 kW down-fired furnace with a 750 mm diameter cylindrical shape. The combustion air was preheated to 423 K before being introduced into the furnace for these experiments. The investigations were specially focussed on the impact of the carrier gas on the pollutant (e.g., CO and $NO_x$) emissions under coal-MILD combustion conditions. Other reported studies include previously reported

experimental and numerical results [31] of pulverised brown and black coal combustion under MILD mode in a recuperative furnace. This comprehensive study was aimed at better understanding the formation and destruction of pollutants, like $NO_x$ under MILD combustion conditions. It was found that due to lower temperatures, most of the $NO_x$ is produced by the fuel mechanism and that $NO_x$ reburning mechanism plays an important role in the total emission. Mei et al. [23, 41] numerically investigated the impacts of reactants' injection velocities and fuel injection angles on coal MILD combustion, using the experimental data of Weber et al. [26]. They reported that increasing the velocity of the primary air played a significant role in achieving local diluted conditions and decreasing the combustion temperature and overall $NO_x$ emissions. Vascellari and Cau [28] reported the influence of turbulence-chemistry interactions on the predictions of pulverised coal MILD combustion using the experimental case of Weber et al. [26]. They modelled gas phase reactions using either detailed kinetic mechanisms (consisting of 103 reactions) or global kinetic mechanisms (consisting of 2 reactions). Nevertheless, no substantial benefits were achieved for the prediction of coal MILD combustion using the detailed kinetic mechanisms, in comparison with those found for the global kinetic mechanisms. Global kinetic mechanisms require less computational time, without losing any major benefits. Therefore, the present study modelled the gas phase homogeneous reactions using global kinetics mechanisms. A numerical investigation focussed on the microscopic characteristics of pulverised coal MILD combustion was conducted by Jin and Zhou [42], using the eddy dissipation concept (EDC) and the eddy dissipation model (EDM), along with a simplified gas phase global reaction. The numerical results were validated using the experimental data from Weber et al. [26]. They concluded that the EDC model reproduces the experimental data more effectively. A numerical study [32] on the MILD combustion characteristics of Australian brown and black coal was

reported using a self-recuperative furnace. It was found that effective mixing between the product of combustion and the reactant jets plays a vital role in establishing the MILD combustion regime. In addition, it was found that the residence time of the coal particles has major impact on the pollutant formations and destructions under MILD combustion conditions. In general, a long residence time is essential for complete burning of coal particles under MILD combustion conditions in a recuperative furnace. This is because under MILD combustion conditions chemical reactions are slower and hence characteristic time of the reactions is longer than conventional combustion [18]. Razaei et al. [43] reported an experimental study on the flame stability and ignition of coal particles under coaxial oxy-coal turbulent diffusion combustion conditions. Using thermo-gravimetric analyses (TGA) and Nuclear Magnetic Resonance (NMR) analyses, the study concluded that the fundamental chemical structure of the coal has a major impact on the flame stability of oxy-coal combustion under complex turbulent diffusion conditions. However, they did not reveal any insight to understand the impact of the turbulence field and the surrounding flow on the volatiles' release and reaction from pulverised coals burning, under conditions relevant to practical combustion systems (i.e., a furnace environment).

Although the aforementioned experimental and numerical investigations have provided valuable insight into coal MILD combustion, there is a lack of experimental data to understand the influence of the turbulence field on the stability and pollutant formation and destruction of burning pulverised coal under MILD combustion conditions. Moreover, no study has been found in the literature that reports the impact of the surrounding flow (i.e., vitiated co-flow) and thermal fields on the volatiles' release and reaction from pulverised Loy-Yang brown coal burning under MILD conditions. Therefore, it is essential to develop the understanding of the effect of

turbulence mixing on the combustion stability and pollutant formation and emissions from the MILD combustion of pulverised coal to successfully utilise this technology in a wide range of industrial devices.

The main objective of the current work is to investigate the burning characteristics of pulverised Victorian brown coal under MILD combustion conditions. In particular, the present study experimentally and numerically investigates the influence of jet inlet velocities of Loy-Yang brown coal carried by $CO_2$ on the flame stability and pollutants' formation and destruction. The fuel jet bulk Reynolds number is varied from $Re_{jet}$ = 5,527 to $Re_{jet}$ = 20,000 to investigate the impact of turbulence on the devolatilisation as well as volatiles' reaction of the coal particles under MILD combustion conditions. Owing to the highly reactive nature of the Victorian brown coal, as a class of low rank coal, it deserves special attention to probe the devolatilisation zone during the combustion. Furthermore, it is well established that the devolatilisation step of pulverised coal combustion, and especially the volatiles release location and volatiles release rate, are the main controlling parameters, which regulate the flame shape and length [44].

A previous paper by the authors [45] examined the impact of particles' size on the MILD combustion of pulverised brown coal using a constant jet bulk Reynolds number (viz., $Re_{jet}$ = 20,000), whereas the current paper examines the effect of fuel jet Reynolds number on the burning of pulverised brown coal under MILD combustion conditions at fixed particles size range. Detailed measurements of in-furnace gas concentration (CO, $CO_2$, $O_2$, and $NO_x$) and in-furnace temperatures along with exhaust emissions are analysed and discussed. To augment the understanding of the experimental measurements, computational fluid dynamic (CFD) modelling is carried out. The numerical results are presented to shed light on the flow field structure, devolatilisation

zone as well as volatiles release rate, combustion of volatile matters, and overall carbon consumption inside the furnace for three different fuel jet Reynolds number cases.

## 2. EXPERIMENTAL SETUP AND METHODOLOGY

### 2.1 Furnace Detail

A schematic diagram of the MILD combustion furnace and supply system with secondary swirl burner arrangement, designed and built for this research study, is shown in Figure 1. The vertically-oriented furnace has an inner working length of 1200 mm and a cross-section of 260 × 260 $mm^2$. The furnace walls are well insulated, with 100-mm-thick high-temperature ceramic fibre-board refractory. This aids to reach steady-state operation of the furnace from the cold state with warm-up time of 2 hours and helps in the stability of the pulverised coal combustion under MILD conditions. It is measured that only around ~9% of total heat is lost through the furnace walls. The heat loss through the walls is calculated as a percentage of the total thermal input. The total thermal input of the furnace was 48 kW whereas 10 kW was added by the pulverised coal combustion and rest was supplied by the secondary burner. The total conduction heat losses through the walls were calculated to be ~4.3 kW. The furnace has equally spaced eight openings/windows (120 × 75 $mm^2$) along the vertical directions on three walls to allow full optical access. These openings can accommodate UV-grade clear quartz windows, when needed, or be insulated by window plugs. Worth noting to mention that the openings for optical access were insulated most of the time during the experiments, except the flame photo/CH* images were captured. The authors carefully considered the impact of radiation heat loss through the specific window opening for the short period of time required to capture the images and concluded that it is negligible. The maximum capacity of the furnace is 60 kW where 20 kW heat can be added by pulverised fuel combustion and 40 kW comes from the secondary burner with

a turndown ratio of 2:1. More details of the experimental set-up have been described previously [45].

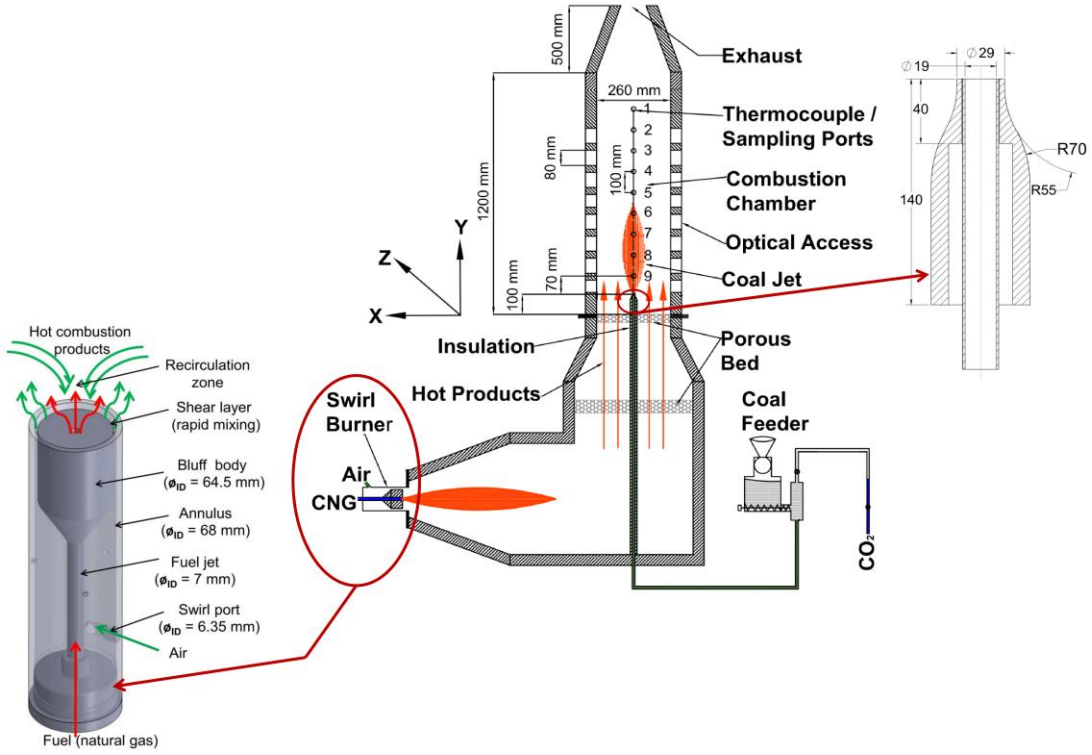


Figure 1. Schematic diagram of the MILD combustion furnace and supply system, co-flow swirl burner, and jet exit details.

An insulated duct configuration is built to transport the hot combustion products (co-flow) from the secondary burner to the furnace. Two porous beds filled with ceramic beads (mean bead diameter ~ 4mm) of 20 mm layers are used to help create a uniform co-flow. The water-cooled and well insulated central jet with an internal diameter ($D_{jet}$) of 19 mm is used to inject coal into the furnace carried with $CO_2$.

The secondary burner is a swirl burner which operates in a non-premixed mode that supplies hot combustion products under various fuel-lean conditions. A schematic of the swirling burner is shown in Figure 1. The swirling burner has a bluff-body of 64.5 mm diameter with a 7 mm central fuel jet. The bluff-body is surrounded by an annulus, 68 mm in diameter. The length of the annulus and the swirling burner together is 275

mm. The combustion air stream is introduced into the annulus through a 6.35 mm diameter tangential swirl port/inlet, which is positioned 45 mm downstream of the burner's bottom plane and inclined 30º upward to the radial/horizontal plane. The swirl burner can operate between the equivalence ratios of 0.5 and 1.0, with a stable and attached non-sooty flame, where commercial natural gas (NG) is used as a fuel.

## 2.2. Furnace Operating Conditions

Three different experimental conditions were used in this study. For all cases, stable steady-state combustion was achieved and thermal equilibrium was reached before data collection started. A summary of the experimental conditions on the stable operation of Loy-Yang brown coal MILD combustion is shown in Table 1.

The temperature of the co-flow, and the furnace wall as well as $O_2$ concentrations in the co-flow was controlled through the secondary swirling burner. Air at room temperature was used as oxidant and commercial natural gas was used as fuel. The secondary swirling burner operated with an equivalence ratio of $\Phi = 0.7$ (excess $O_2$ of 5.9% db by volume). A summary of the operating conditions and measured gas concentrations in the co-flow, at the exit plane of the coal jet, is shown in Table 2.

When the thermocouple temperature at the exit plane of the jet, exceeded a set threshold (≈ 1100 K) well above the self-ignition temperature of pulverised coal, the coal particles were introduced into the furnace through the water-cooled fuel jet using carbon dioxide ($CO_2$) as a carrier gas. It is worth noting that $CO_2$ was selected as a carrier gas for the current experiments based on previous work [31, 37]. Previously, the authors investigated the effect of carrier gas (using either $CO_2$ or $N_2$) on the MILD combustion characteristics of pulverised coal [31] and results only showed minor differences associated the type of an inert carrier gas. Another experimental study [46]

was conducted to burn biomass fuel under MILD combustion conditions using the same furnace [31] where pulverised biomass fuel was carried using either air, $CO_2$, or $N_2$ as a carrier gas. It was found that the case with air as the carrier gas gave the worst results, in terms of CO and $NO_x$ emissions and resulted in faint flame sheets appearing inside the furnace. However, the case with $CO_2$ as a carrier gas gave the best results in terms of pollutant emissions. Weidmann et al. [37] reported a similar observation for MILD combustion of pulverised coal. They found a significant increase in CO and $NO_x$ emissions when $CO_2$ was replaced by air as a carrier gas of the coal particles. In addition, the use of an inert simulates the circulating of exhaust gasses through the fuel stream to ensure sufficient dilution before reaction can start. This is a pre-requisite for the establishment of MILD combustion.

**Table 1:** Furnace operating parameters for the stable combustion of Loy-Yang brown coal

| **Parameters** | **Case 1** | **Case 2** | **Case 3** |
|---|---|---|---|
| Fuel jet inlet temperature (K) | 325 | 325 | 325 |
| Fuel jet velocity (m/s) | 8.84 | 4.88 | 2.44 |
| Jet Reynolds number | 20000 | 11054 | 5527 |
| Furnace wall temperature (K) | 1112 - 1236 | 1112 - 1236 | 1112 - 1236 |
| Particle sizes (μm) | 53 - 125 | 53 - 125 | 53 - 125 |
| Global equivalence ratio, Φ | 0.96 ± 0.02 | 0.95 ± 0.01 | 0.93 ± 0.02 |
| Co-flow velocity (m/s) | 1.56 | 1.56 | 1.56 |
| Co-flow temperature (K) | 1284 | 1284 | 1284 |
| Co-flow $O_2$ ( v/v % db) | 5.9 | 5.9 | 5.9 |
| Co-flow Reynolds number | 2385 | 2385 | 2385 |

**Table 2:** Operating parameters of secondary (swirl) burner and measured gas concentrations of co-flow

| **Parameters** | **Co-flow** |
|---|---|
| Fuel | Natural gas* |
| Equivalence ratio, Φ | 0.7 |
| Velocity (m/s) | 1.56 |
| Temperature (K) | 1284 |
| Excess $O_2$ ( v/v % db) | 5.9 |
| CO (ppmv dry) | 19 |
| $CO_2$ (v/v % db) | 8.9 |
| $NO_x$ (ppmv dry) | 98 |

* Natural gas properties [mole% (v/v)]: $CH_4$ 92%, $C_2H_6$ 4.28%, Other inerts 3.72%. *Moomba Natural gas analysis, SA, Australia.*

## 2.3. Coal Characteristics

A Victorian brown coal, Loy-Yang, was milled and sieved into the range 53<d<125 micron. The coal particles were pulverised using an electrical grinder. The pulverised coal was dried in an electric oven at 105 ºC for 4-5 hours to remove moisture and then stored in a sealed container under ambient condition. Proximate and ultimate analyses of the coals are presented in Table 3. The gross dry calorific value of Loy-Yang brown coal is measured to be 24.5 MJ/kg.

A twin-screw volumetric coal feeder was specially built for this project to decouple the carrier gas flow rate from the solid particle supply rate. Volumetric feeding produces an accurate and controllable discharge rate for continuous operation, especially when the bulk density of the fed material is consistent [47]. On the other hand, a gravimetric feeder is more expensive, more difficult to control, and are mainly used for high precision applications such as the pharmaceutical industry [48]. From, our previous experience [31] and the other researchers' [49] experimental observation encouraged us to select a

volumetric feeder for discharging carbonaceous solid particles at a constant and consistent flow rate. A twin-screw feeding system is used because it is specifically useful for discharging sticky, non-compliant solid fuels, such as pulverised brown coal. A screw feeder at the bottom of the hopper gradually moves the pulverised coal particles to the large throat and then into the discharge screws. The coal feeder is slightly pressurized to prevent outside air penetration and all joints are sealed by using leak-proof gaskets to avoid any moisture addition in the coal. The coal feeding rate was constant and set to 1.47 kg/hr for ≈10 kW heat input by the pulverised coal for all the experiments. It is worth noting that the absolute error of the coal mass flowrate was measured to be $\pm$ 1.5%, whereas the absolute error of the gas flowrate measurements was $\pm$ 2%, according to the manufacturer's specifications.

**Table 3.** Loy-Yang brown coal analyses

| Ultimate analysis (wt % dry ash free) | |
|---|---|
| C | 66.8 |
| H | 4.8 |
| O (by difference) | 28.0 |
| N | 0.4 |
| S | - |
| Proximate analysis (wt % dry basis) | |
| Fixed carbon | 47.3 |
| Volatile matter | 51.3 |
| Ash | 1.4 |

## 2.4 Measurement Techniques

The temperature inside the furnace was measured using 6-mm-diameter sheathed Pt/Pt 13% Rh (R-Type) thermocouples. The temperature measurements were corrected to account for thermocouples' radiation. All temperature measurements are logged

continuously using a PC and USB-TC data logger. The measurements were conducted at 27 different locations along the furnace height at locations Y= 70, 170, 270, 370, 470, 570, 670, 770, and 870 mm from the fuel jet exit plane and for three horizontal locations starting from the centreline Z=0, and at locations Z=50mm and Z=100mm.

A steady-state energy balance equation is used on the thermocouples' bead surface for radiation temperature corrections. The corrected furnace temperature ($T_f$) was calculated from the measured thermocouples' temperature ($T_m$) and net radiation energy between diffuse-gray surfaces in an enclosure according to Howell et al [50] as follows:

$$T_f = T_m + \frac{A_b \varepsilon_b \sum_{w=1}^{N} \sigma G_{1w} (T_m^4 - T_w^4)}{h} \quad (1)$$

Where $A_b$ and $\varepsilon_b$ represents the cross-sectional area and emissivity of thermocouple's bead surface respectively, $N$ represents the total number of walls in the enclosure (i.e., furnace), $\sigma$ represents the Stefan–Boltzmann constant, $G_{1w}$ represents the emitted radiation fraction of the thermocouple bead which is absorbed by a specific wall surface $W$ in the enclosure (i.e., furnace) [50], $T_w$ represents the wall surface temperature of the furnace and $h$ is the convective heat transfer coefficient for a sphere (i.e., thermocouple's bead surface). The calculations show that the maximum radiation correction is 4.5% while most correction is less than 2% between actual furnace temperatures and thermocouples measurement. It is worth mentioning that the conductive heat transfer through the ceramic sheath as well as any catalytic and oxidation effects of the thermocouple were neglected and are believed to be negligible.

A water-cooled sampling probe [31] is used and introduced through the sampling/thermocouple ports to measure in-furnace $O_2$, CO, $CO_2$ and $NO_x$ mole fraction using a portable gas analyser, TESTO Model 350XL. The gas analyser cools

and filters the gases before the sensing cells. The absolute errors of these measurements, according to the manufacturer's specifications, are ±0.8% (by volume) for $O_2$, ±10 ppmv for CO, and ±5 ppmv for NO of measured value. In addition to the in-furnace measurements, global emissions were also recorded at the exit of the furnace using the same gas analyser.

## 3. BRIEF DESCRIPTION OF THE NUMERICAL MODEL

The numerical study is conducted to deepen understanding on the experimental observations and in particular to shed light on the flow field structure, turbulence intensity, devolatilisation zone and volatile reaction rate. This study uses a two-dimensional, structured, hexahedral mesh of 1 million cells, and models half of the furnace geometry. The commercial CFD software ANSYS Fluent version 14.5 is used for the implicit and steady state simulation. The mesh of the geometry was created using ANSYS Meshing. A grid independence study was conducted and the current mesh density was found to be adequate. All models solved the Reynolds-Averaged Navier-Stokes (RANS) equations. The pressure-velocity coupling is solved using the Semi-Implicit Method for Pressure Linked Equations (SIMPLE) algorithm method. The two-equation realisable k-ε turbulence model [51] is used for simulating gas-phase turbulent flow characteristics, which is different from the standard k-ε model in the fields of the ε equation and eddy viscosity constant Cμ [42] . The modified source term of the ε equation is used to solve the spreading rate of round jets, and the constant Cμ can guarantee the realisability effect, which is relative to mean strain and rotation rates [42]. The model has been widely adopted to predict turbulent flow performance for different kinds of flows, such as rotational flow and strong recirculation flow to better reproduce the experimental results [23, 28, 32, 41, 42]. The Rosin-Rammler distribution is used to

describe particle size distribution, with particle size range from 53 to 125 μm. Discrete Ordinates (DO) [52] radiation model, considering the directional nature of the radiation, is used to solve the radiation heat transfer equation because the DO radiation model is considered to be more suitable than weighted-sum of grey-gases (WSGG) model for the laboratory-scale furnace [53, 54].

The Discrete Phase Model (DPM) was implemented to calculate the particle trajectories relative to the fluid phase. The two-way coupling of a deterministic Lagrangian approach [55] was adopted to describe the fluid particle interactions. The dispersion of particles due to turbulence in the continuous fluid phase was calculated using a stochastic tracking model with a discrete random walk that includes the effects of instantaneous turbulent velocity fluctuations on particle trajectories. The iteration frequency parameter of the particle phase was set to 20, meaning that following every 20 iterations of the gas phase calculation, the particle trajectories were calculated and updated. The second-order upwind scheme is employed for all spatial discretisations. The simulations were run with 48 cores on the Tizard supercomputer facilities of eResearch SA.

The coal devolatilisation process is modelled using a single-step reaction model where the kinetic rate is calculated on the assumption that the devolatilization process is first-order dependent on the coal volatile matters. The pre-exponent factor and activation energy of Arrhenius equation of this study used for the specific Loy-Yang brown coal following Zhang et al. [56]. A previous study [32] concluded that the single-step reaction model is comparable with an advanced devolatilisation model (viz., Chemical Percolation Devolatilization, CPD) to predict the coal combustion process. Noteworthy is that there is no kinetic data available for an advanced devolatilisation model except for the single-step reaction devolatilisation model as

reported in [56]. A global volatile combustion mechanism is used to describe volatile oxidation reaction as follows:

$$C_pH_qO_rN_sS_t + \left(\frac{p}{2} + \frac{q}{2} - \frac{r}{2} + t\right)O_2 \longrightarrow pCO + \frac{q}{2}H_2O + \frac{s}{2}N_2 + tSO_2 \quad \text{(R1)}$$

The values of the variables *p, q, r, s*, and *t* are found from the ultimate analysis of the coal (refer to Table 3). Two-step homogeneous reactions are used to describe gas-phase chemistry:

$$CO + 0.5O_2 + H_2O \rightleftharpoons CO_2 + H_2O \quad \text{(R2)}$$

$$H_2 + 0.5O_2 \rightleftharpoons H_2O \quad \text{(R3)}$$

The three step heterogeneous reactions are used to describe char-particle surface reactions which is the combination of oxidation (R4), Boudouard (R5) and gasification (R6) reactions:

$$C_{char} + \frac{1}{2}O_2 \longrightarrow CO \quad \text{(R4)}$$

$$C_{char} + CO_2 \longrightarrow 2CO \quad \text{(R5)}$$

$$C_{char} + H_2O \longrightarrow H_2 + CO \quad \text{(R6)}$$

In Table 4, the kinetic constants are listed for the equations (R1) – (R6). In this study, Eddy Dissipation Concept (EDC) model [57] with finite-rate chemistry is used to describe turbulence–chemistry interaction.

Table 4: Kinetic constants for reactions (R1)-(R6)

| Reaction | $A$ | $E_a$ (J/kg mol) | Reference |
|---|---|---|---|
| (R1) | $4.84\times10^{7}$ | $5.1\times10^{7}$ | [58] |
| (R2) Forward | $2.24\times10^{6}$ | $4.18\times10^{7}$ | [59] |
| Backward | $1.1\times10^{13}$ | $3.28\times10^{8}$ | |
| (R3) Forward | $7.9\times10^{10}$ | $1.46\times10^{8}$ | [59] |
| Backward | $3.48\times10^{13}$ | $3.98\times10^{8}$ | |
| (R4) | $2.4\times10^{-3}$ | $6.906\times10^{1}$ | [56] |
| (R5) | $5.3\times10^{-3}$ | $1.255\times10^{3}$ | [56] |
| (R6) | $6.35\times10^{-3}$ | $1.62\times10^{2}$ | [56] |

# 4. RESULTS AND DISCUSSION

Three different experiments and modelling cases were conducted with different fuel jet bulk Reynolds numbers, namely; $Re_{jet}$ = 5,527, $Re_{jet}$ = 11,054, and $Re_{jet}$ = 20,000. For all cases, the co-flow conditions (see Table 2) and the mass flow rate of pulverised coal were kept constant. Only the flow rate of the carrier gas, $CO_2$, is changed. This section is a mix of computational and experimental results that describe the flow, thermal and scalar fields for the three cases.

## 4.1. In-furnace appearances of coal-MILD combustion

Figure 2 shows photographs taken from a side window close to the bottom (Y = 80 mm), middle (Y = 500 mm), and top (Y = 995 mm) of the furnace for the three jet Reynolds number cases. These instantaneous images were captured with the same camera settings (F/4.6 – 16 ms – ISO 250) for all cases. The bottom photographs imply that no flame is visible at the jet exit. The coal particles would have been subjected to radiation heating from the walls and started to mix with the hot vitiated co-flow. No

apparent flames can be seen but it is expected that the devolatilisation process would have started. Figure 2 shows that a luminous flame in the middle and top parts of the furnace for case 1. The appearance of faint yellowish flames in case 1 are believed to be associated with the poor mixing of volatile matter with the surrounding hot products of combustion. Similar findings regarding the existence of ghost flames or sparks are reported by Li et al. [30], Weber et al. [26] and Smart et al. [36] for the MILD combustion of pulverised coal. On the other hand, no visible flame is found in the middle and top parts of the furnace for cases 2 and 3, suggesting that in these regions the combustion can be described as stable flameless or MILD combustion. On the fundamental side, the different ignition delay and burnout times of coal particles under three dissimilar turbulence levels (viz. $Re_{jet}$ = 5,527, $Re_{jet}$ = 11,054, and $Re_{jet}$ = 20,000) impacted on the furnace's flame appearance. However, the location of flame ignition is very difficult to determine from these images alone and the existence of MILD combustion will be further supported by the subsequent results presented in this paper.

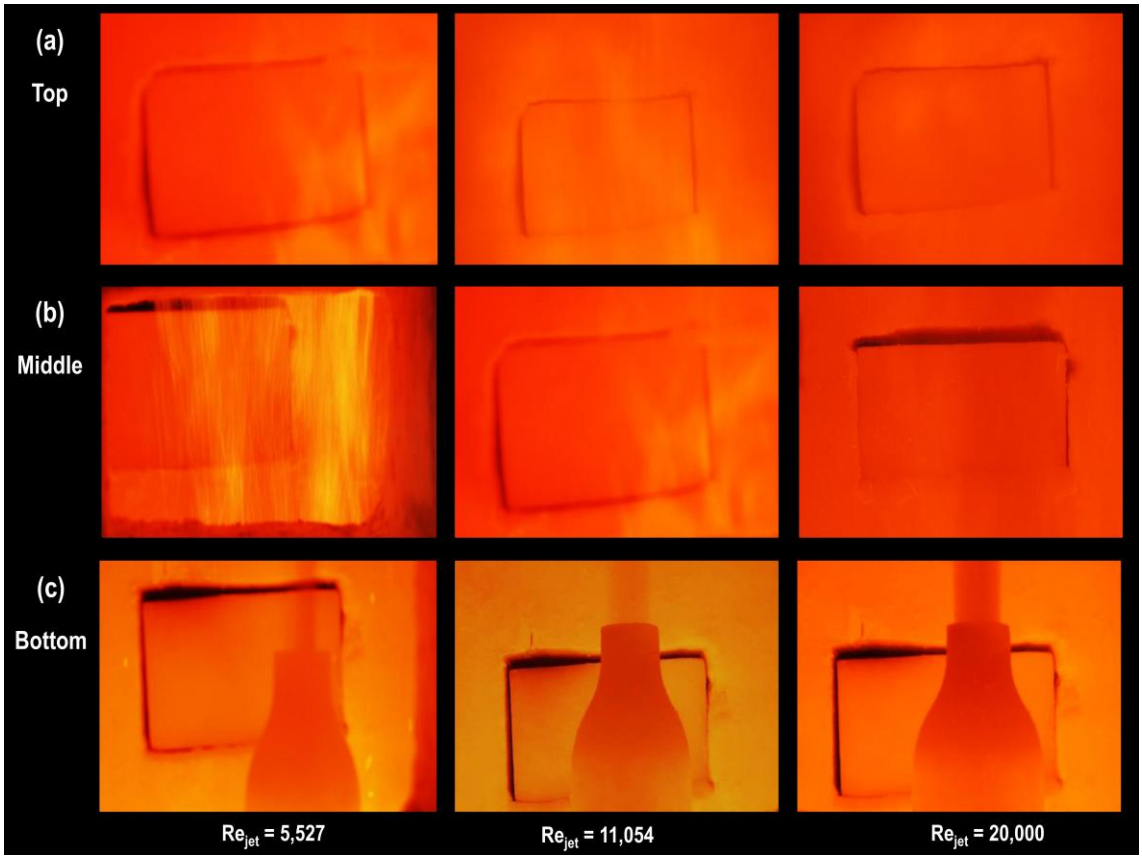


Figure 2. Photographs of the furnace for different jet Reynolds number cases; (a) top (Y = 995 mm), (b) middle (Y = 500 mm), and (c) bottom (Y = 80 mm) part of the furnace

## 4.2. Flow fields

To understand the mixing pattern of fuel jet and surrounding vitiated co-flow gases, it is essential to probe the aerodynamics inside the furnace. Figure 3 demonstrates the flow path-lines as well as velocity magnitudes for the three jet Reynolds number cases. The velocity contours show substantial differences in terms of flow recirculation pattern between the three cases. No recirculation is observed for the $Re_{jet}$ = 5,527 case, which shows signs of conventional combustion, with a visible flame owing to the poor mixing of volatile matter with the hot vitiated co-flow. This observation is consistent with visual experimental observation (see Figure 2). For cases 2 and 3, a strong recirculation is predicted half way along the furnace. This recirculation zone is more intense and broad for the highest Reynolds number case. In addition, the recirculation zone is

shifted upstream of the fuel jet by increasing the jet Reynolds number. Simply, higher jet Reynolds numbers lead to enhance mixing of the fuel jet with the vitiated co-flow.

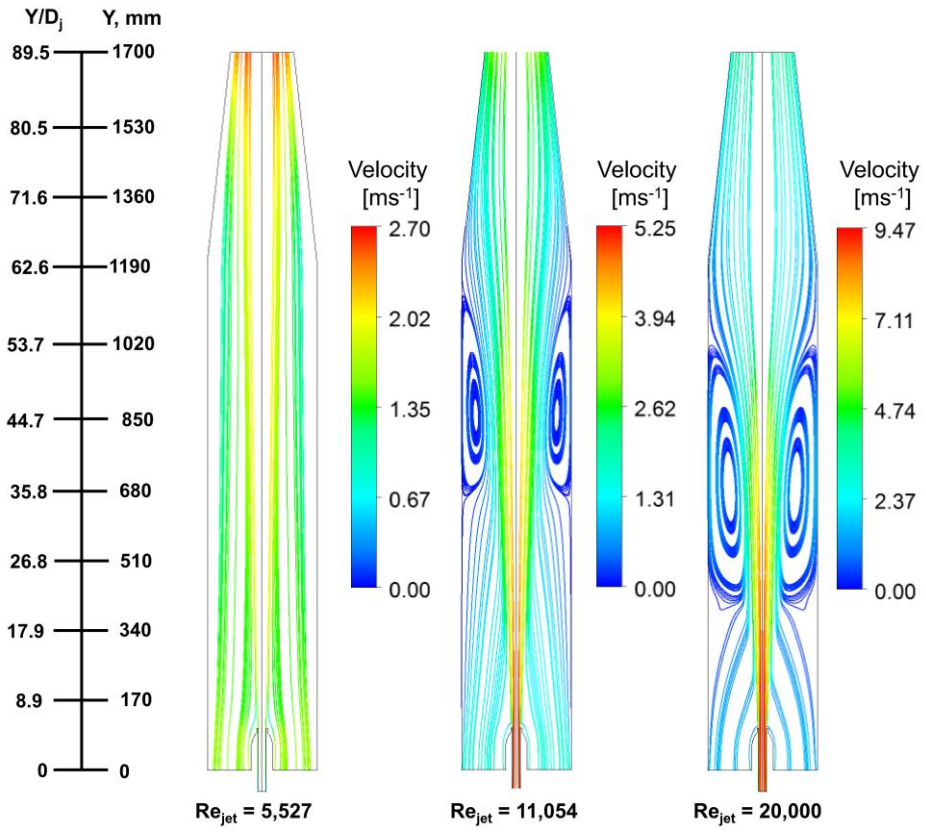


Figure 3. Predicted velocity distribution of Loy-Yang brown coal MILD combustion for cases 1-3

## 4.3. Turbulence intensity

Figure 4 shows the comparison of turbulence intensity for cases 1-3. The plot depicts that the turbulence intensity rises with increasing jet Reynolds number, as expected. Low turbulence intensity, up to 5% is found for case 1; while for case 2 the turbulence intensity is calculated to be 15%; and the maximum turbulence intensity is calculated to be more than 20% for case 3. The high-turbulence intensity for case 3 is centred on the stronger recirculation vortex in the middle of the furnace. The recirculation vortex impacts on the particle dispersion and mixing with volatile matters and surrounding hot co-flow gases.

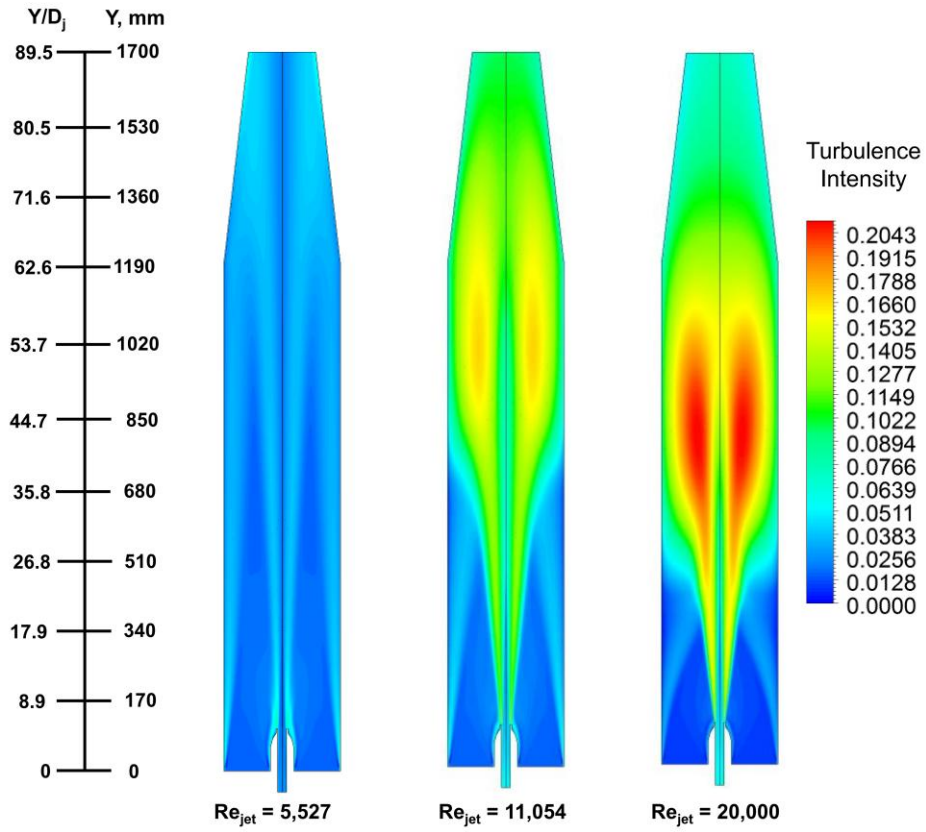


Figure 4. Calculated contours of turbulence intensity for all three cases

Figure 5 illustrates the distributions of coal particles' concentration in terms of velocity for cases 1-3. The plot further points to the dependency of particles' path-line on the turbulence intensity. For the low turbulence intensity case (case 1), the particle trajectory follows a straight path-line. While for case 3, the particles are found to be entrained into the furnace volume, particularly in the recirculation vortex of the flow. The intense recirculation of the particles for case 3 influence on the devolatilisation process and chemical species formation as described later in section 4.7

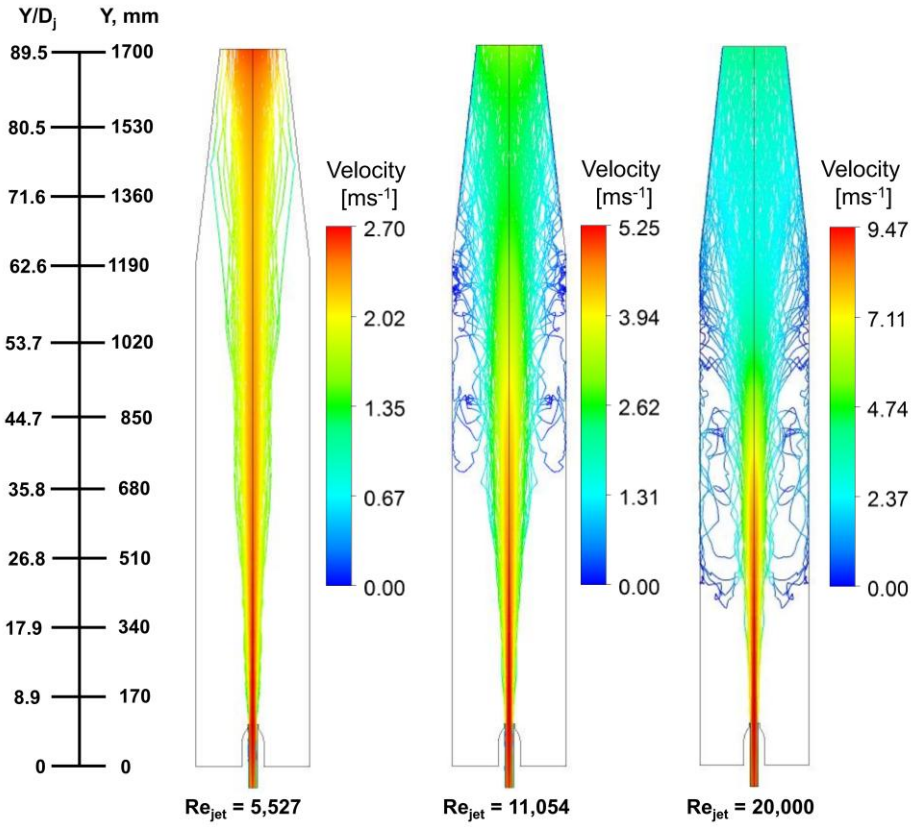


Figure 5. Computed coal particles' velocity and path-line for cases 1-3

## 4.4. Thermal fields

The comparisons between the model predictions and the measured, mean temperatures for the three cases are shown in Figure 6. The temperature difference at various locations of the furnace is less than 100 K which implies that a homogeneous temperature distribution is achieved for each of the studied cases. However, a clear distinction exists between those measured temperatures for different jet Reynolds numbers along the furnace centreline (X= 0, Z = 0). The furnace temperature for $Re_{jet}$ = 20,000 case is ~150K lower than $Re_{jet}$ = 5,527 case. The difference is attributed to the carrier gas stream, which adds 3.6 times more $CO_2$ to the system for the $Re_{jet}$ = 20,000, as compared with the $Re_{jet}$ = 5,527 case. The thermal mass of the additional $CO_2$ accounts for the heat sink and most of the resultant reduction in temperature. Worth

noting is that the fuel heat input for all cases remained constant and only the carrier gas flow rate is changed to increase the bulk jet Reynolds number.

The axial temperature profiles at Z = 50mm and Z =100mm show consistent results for the three cases with minor variation related to the location of heat release.

In Figure 6, no substantial difference between the model predictions and the measurements can be seen, with the exception of the fuel jet at the centreline (X = 0 mm, Z = 0 mm) position in the furnace. The numerical model underestimated the flame temperature for the prediction of centreline temperature profiles. However, the temperature predictions by the model and the measurements are quite reasonable at the top part of the furnace centreline, in particular at location $Y/D_j > 28$. This discrepancy can be explained by the presence of a cold zone that corresponds to the central fuel jet of the model, which is not found by experimental measurements. A similar cold zone has been reported by Vascellari et al. [28] for the simulations of pulverised coal MILD combustion using a detailed chemistry mechanism. Nevertheless, the trends of the temperature levels and the temperature peaks are reproduced well by the model for all cases at the position of Z = 50 mm and Z = 100 mm. It is noteworthy that the temperature profiles are flat from the middle to top of the furnace, pointing to a homogenous combustion and a slow reaction. This feature is well reproduced by the numerical model.

Figure 7 presents comparison of the measured mean temperature contours, for half of the furnace, between the three jet Reynolds numbers' cases. The contour plots depict the trend of decreasing temperature with increasing coal injection velocities, leading to a large temperature difference at the bottom of the furnace, in particular close to the jet exit. This expected trend relates to volatiles' release and reaction which is extended

further downstream with increasing jet velocity and furthermore, the high velocity cold jet penetrates further downstream for the largest Reynolds number case (i.e., $Re_{jet}$ = 20,000). The increased penetration of the jet extends the volatiles' release zone, enhances mixing with the surrounding flow and delays ignition and start of the reaction. Such effects lead to a significant impact on the suppression of the temperature. A similar thermal boundary layer seems to develop next to the wall for all three cases.

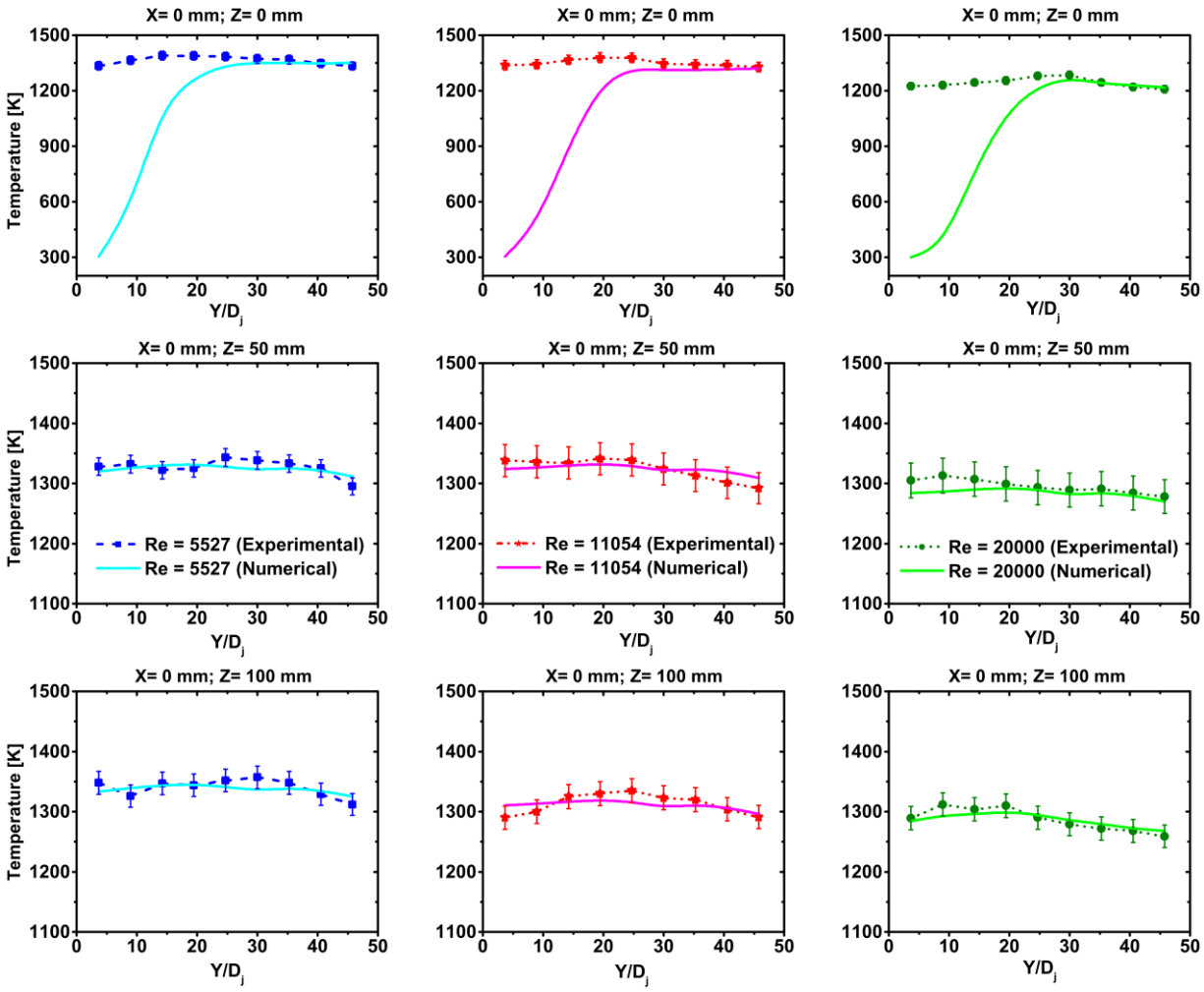


Figure 6. Measured and computed temperature profiles of Loy-Yang brown coal under MILD combustion for cases 1-3

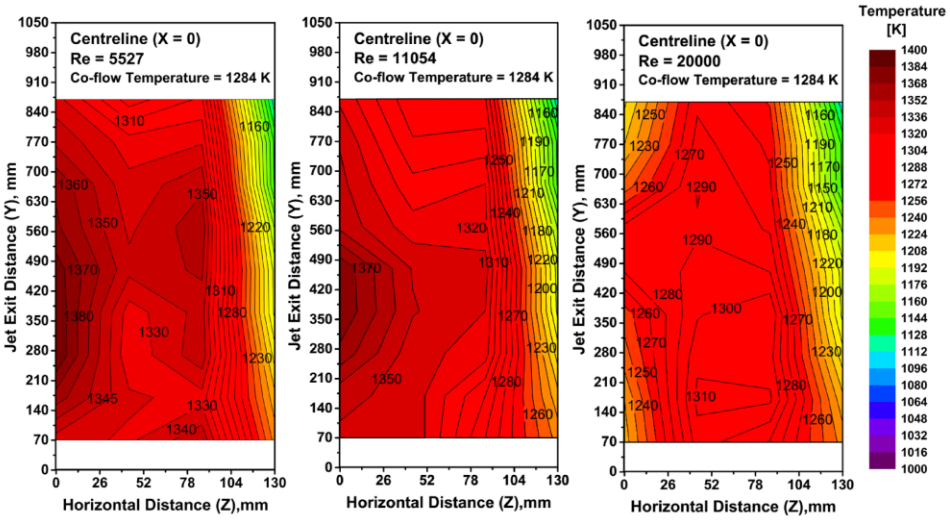


Figure 7. Measured mean temperature distribution for one half in the middle of the furnace for cases 1-3.

## 4.5. Release of volatiles

Figure 8 shows the contours of volatiles' mole fraction for cases 1-3. The CFD model assumes the volatile matter is composed of C, H, O, N, and S elements that are released as a combustible gas after the devolatilisation process. The volatile composition was obtained employing the coal calculator in ANSYS Fluent, based on the proximate and ultimate analysis of Victorian brown coal (as shown in Table 3). The volatile mole fraction was computed as the ratio of released gaseous volatiles from the coal particles to the total moles of gas in the furnace. The two-dimensional contours of gas-phase volatiles' mole fraction were directly computed by the ANSYS Fluent software employing a post-processing approach. Figure 8 illustrates that the release of volatiles is influenced by the turbulence level and mixing pattern in the furnace, while the mass flow rate of fuel was constant for all cases. Nonetheless, the maximum volatiles mole fraction was produced for the $Re_{jet}$ = 5,027 case due to the lower flow rate of carrier gas into the furnace. Considering the shape of volatiles' mole fraction zone, the volatile gases are released through a wide region away from jet exit plane for the $Re_{jet}$ = 20,000 case, which is due to the better mixing and higher level of dilution by

$CO_2$ carrier gas stream. Whilst, for the cases of $Re_{jet}$ = 5,027 and $Re_{jet}$ = 11,054 the volatiles are released along the centreline of the furnace.

Figure 9 displays the relationship between the computed mean particle residence time and normalised maximum volatiles mole fraction along the furnace centreline for all cases. The mean particles residence time for the case of $Re_{jet}$ = 5,027 is calculated to be ≈ 690 ms, whereas for the case of $Re_{jet}$ = 11,054 the value is ≈ 470 ms and for the highest Reynolds number ($Re_{jet}$ = 20,000) case the mean particle residence time is ≈ 370 ms. The residence time of each injected particles was recorded at the furnace outlet when it exited from the furnace, employing a sampling method. This approach is called "residence time distribution (RTD) by particle tracking method" [60, 61]. The mean particle residence time in this work was directly calculated from the RTD method. Noteworthy, is that despite this difference, the normalised values of maximum volatiles mole fraction indicate that volatiles release rates are independent of particles residence time. Nonetheless, the rate of volatile gases release is predominantly related to mixing pattern (and hence heating rate and mass transport) and the level of turbulence as shown in Figure 4. For all cases, larger values of jet Reynolds number indicate higher release rates of volatiles.

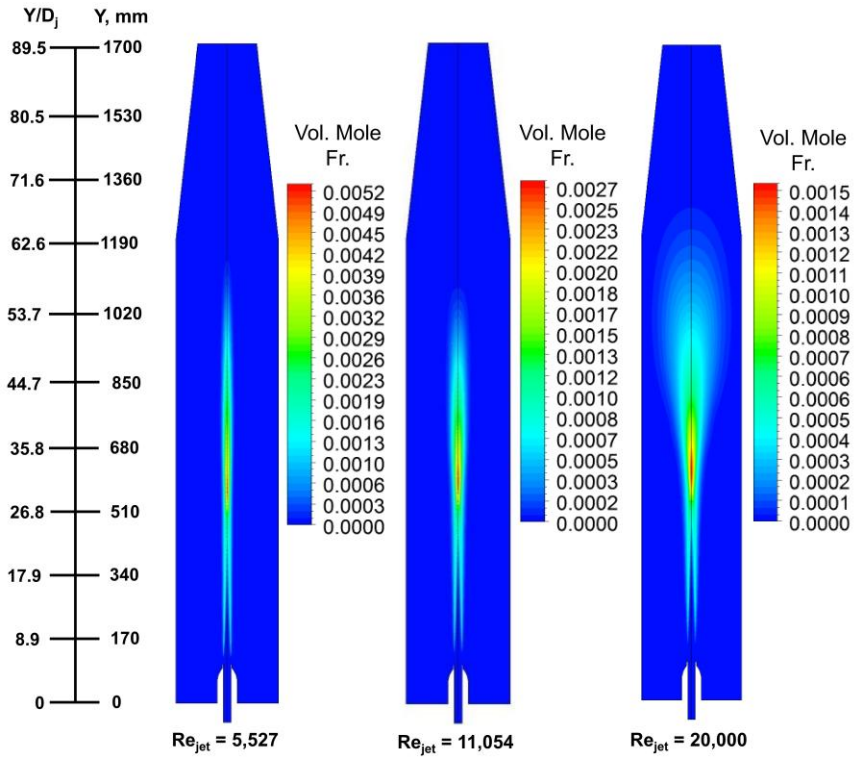


Figure 8. Computed contours of volatiles' mole fraction

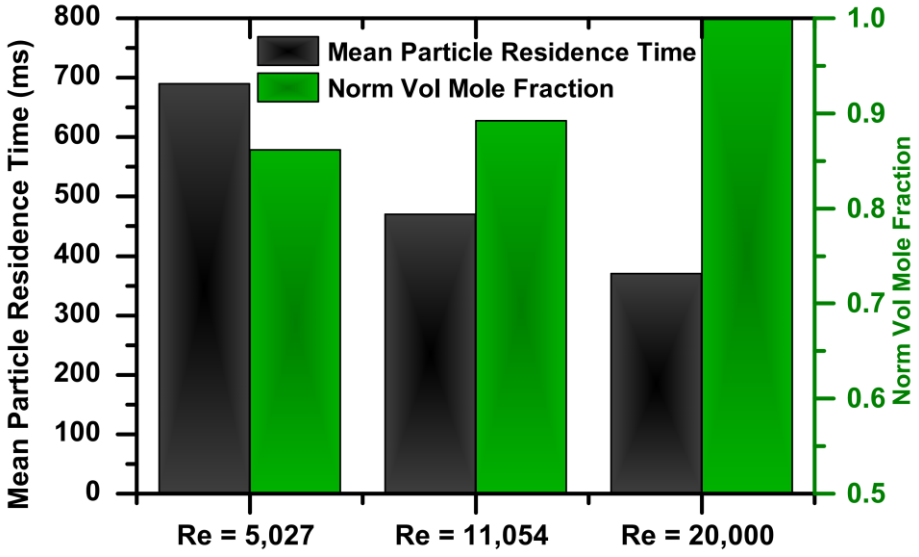


Figure 9. Calculated mean particle residence time and normalised maximum volatiles mole fraction for case 1-3

## 4.4. Volatiles' combustion

In Figure 10, the predicted volatiles' reaction rate, (reaction (R1)) for the three cases is presented. It is clear that volatile reaction rate increases significantly with increasing the jet Reynolds number. The highest level of volatiles' combustion rate is observed for the largest jet Reynolds number case. These results are in good agreement with experimental observations that will be presented later (see Figure 11). In the experiments, the largest amount of in-furnace CO concentration is measured for the $Re_{jet}$ = 20,000 case which is consistent with the model prediction. As seen in Figure 6, increasing the fuel injection velocity into the furnace increases the volatile combustion rates, which is due to the increased circulation and better mixing of fuel jet stream with surrounding hot oxidant stream.

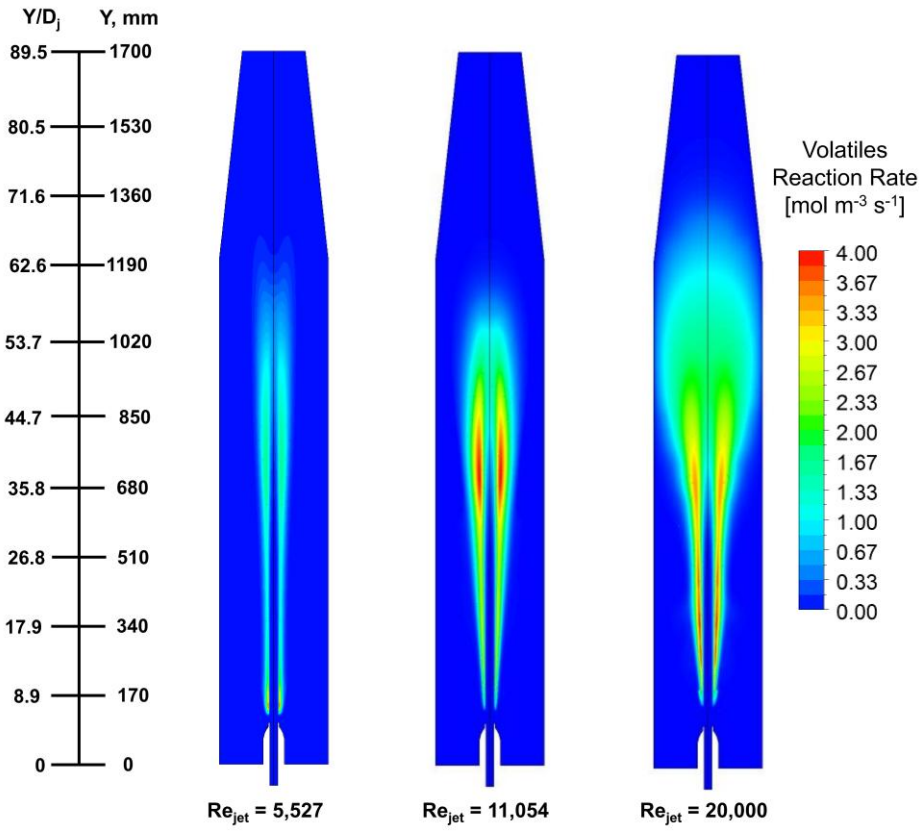


Figure 10. Calculated contours of volatiles reaction (R1) rate for all three cases

## 4.7. In-furnace Gas Composition

Figure 11 represents a comparison of in-furnace CO dry mole fraction between three different jet velocities along the centreline of the furnace. The measured in-furnace CO levels for the $Re_{jet}$ = 20,000 case were generally higher in these experiments than the other two cases (lower jet Reynolds numbers). The increase in Reynolds number leads to a better mixing of the volatiles and the co-flow and hence producing more CO. In addition, the formation of CO might also be influenced by the delayed diffusion rate of coal volatiles under the conditions of higher $CO_2$ concentration. In the top part of the furnace, CO levels are found at their lowest concentration, suggesting that the gaseous volatiles are almost burned by then. Furthermore, for the case of $Re_{jet}$ = 5527 the highest level of volatiles are released at the Y = 270 mm (Y/D = 14.2) position along the centreline of the furnace because of relatively longer residence time of coal particles. Although the position of highest concentration of CO are measured to be similar at the Y = 570 mm (Y/D = 30) position along the furnace centreline for the cases 2 and 3, the total CO concentration at this position for case 3 is about 48% higher than that for case 2.

A comparison between the measured and computed CO dry mole fraction is depicted in Figure 11. In general, the numerical simulation predicts a lower concentration of CO, with respect to the experimental results. This disagreement could be influenced by several factors. A sequential number of reactions are involved in CO production. The coal devolatilisation process releases CO as a volatile matter. In addition, CO is formed by the oxidation of the volatile contents and char. Moreover, the water gas shift reaction ($CO + H_2O \rightarrow CO_2 + H_2$) alters the CO concentrations. None of these processes were considered in the numerical model, other than volatile oxidation and char combustion.

Nonetheless, the numerical prediction of a lower CO mole fraction is quite similar to previous works [23, 28, 31, 32] for the MILD combustion of pulverised coal.

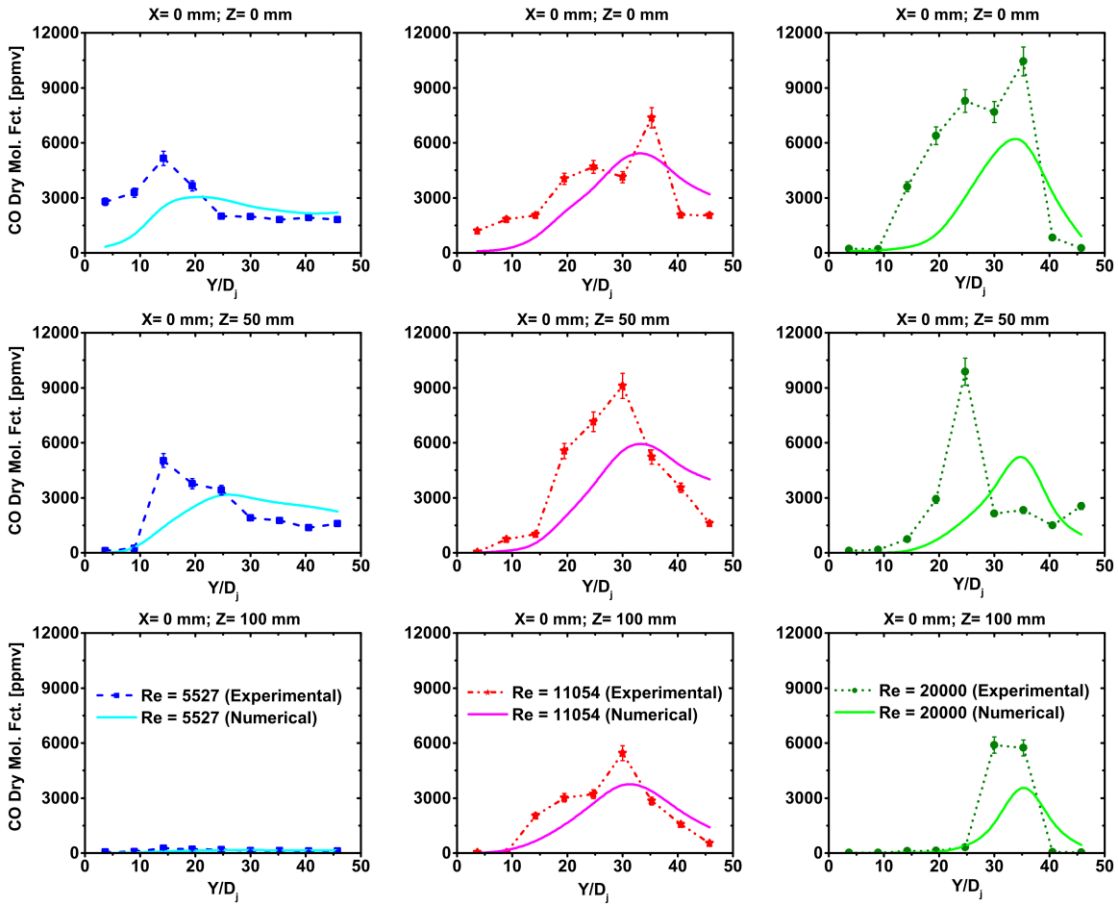


Figure 11. Measured and computed profiles of in-furnace CO molar fraction (db) for cases 1-3

The numerical results and measured axial (X = 0 mm) in-furnace $CO_2$ mole fraction (db) for cases 1-3 are shown in Figure 12. The maximum values of $CO_2$ mole fraction are found to be closer to the jet exit position (X = 0 mm, Z= 0 mm) which are measured to be ≈ 61.7 % for the $Re_{jet}$ = 20,000 case, whereas for the case of $Re_{jet}$ = 11,054 the value is ≈ 46.3 % and for the lowest Reynolds number ($Re_{jet}$ = 5,527) case the value is ≈ 22.6 %. It is not surprising that the highest level of $CO_2$ was found for the largest Reynolds number case, because the largest volume of $CO_2$ concentration was introduced into the furnace as a carrier gas for this case. On the other hand, the $CO_2$

concentrations values are found to be lowest and almost similar for different cases at the location of 70 mm above the jet exit plane for 50 mm (X = 0 mm, Z= 50 mm) and 100 mm (X = 0 mm, Z= 100 mm) away from the furnace centreline suggesting that the combustion reaction started slowly due to the high dilution of reactants and consequently extended the ignition delay.

The numerical model predicts a similar trend of $CO_2$ concentrations to those obtained experimentally at locations Z = 50 mm and Z = 100 mm. However, the model overestimated the $CO_2$ concentration along the centreline (X = 0 mm, Y = 0 mm) of the furnace. The high $CO_2$ concentration at the centreline of the furnace is mainly associated with the $CO_2$ injected into the furnace as a carrier gas. Nonetheless, the discrepancy between the model predictions and the measurements can be explained by the poor mixing of the carrier gas ($CO_2$) with the combustion products.

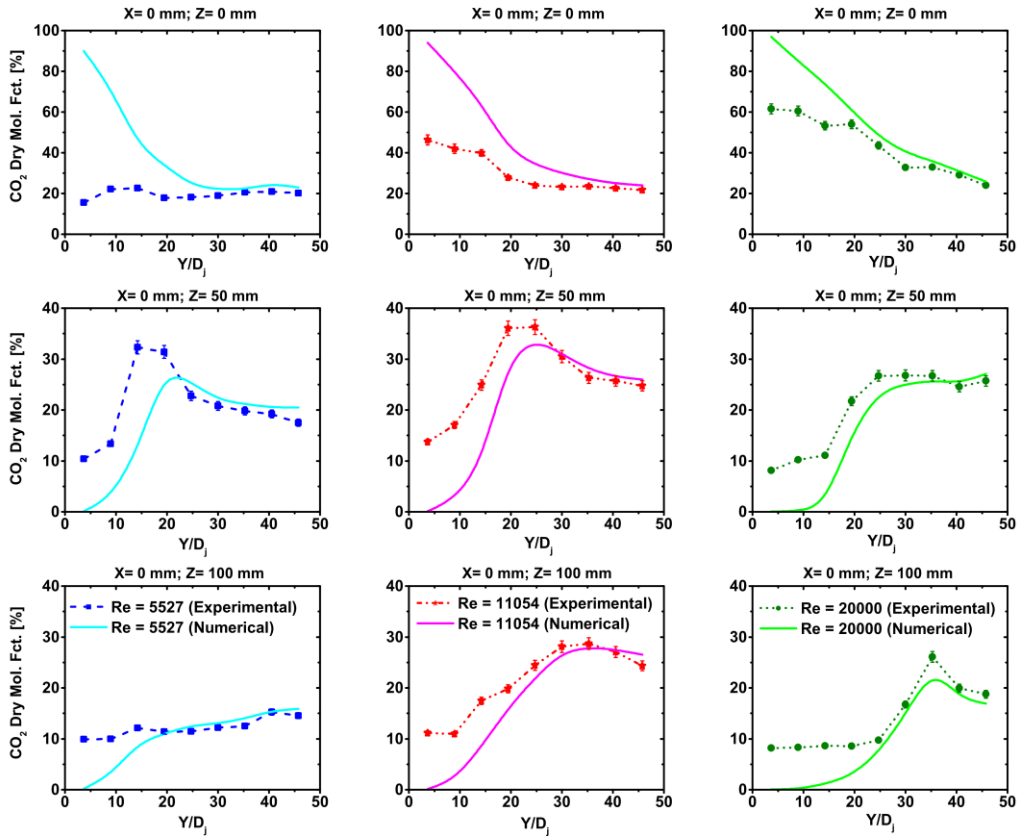


Figure 12. Measured and computed profiles of in-furnace $CO_2$ dry molar fraction for cases 1-3

Figure 13 illustrates the comparison of measured in-furnace $O_2$ dry molar fraction, for cases 1-3, along the centreline (X = 0 mm, Z= 0 mm) of the furnace; and 50 mm (X = 0 mm, Z= 50 mm) and 100 mm (X = 0 mm, Z= 100 mm) away from the furnace centreline. The $O_2$ concentration near (around 70 mm above) the jet exit point of the furnace centreline (X = 0 mm, Z= 0 mm) is measured to be 2.63% for $Re_{jet}$ = 20,000 while the co-flow $O_2$ concentration was 5.9%. The lower value of $O_2$ concentration is obtained because of high level of dilution with incoming $CO_2$ concentration as a carrier gas for the largest Reynolds number. This could also be associated with the delayed ignition of the flame for high level of turbulence. On the other hand, the measured $O_2$ concentration near to the jet exit point are found to be similar (≈4.6% - 4.8%) for cases 1 and 2. Considering the same vertical position (Y/D = 3.7) for 50 mm (X = 0 mm, Z= 50 mm) and 100 mm (X = 0 mm, Z= 100 mm) away from the furnace centreline, the measured $O_2$ concentration is found to be similar to the co-flow $O_2$ concentration (≈5.7%), for all cases. The lowest values of $O_2$ concentration were found at the top of the furnace, which are at levels similar to the exhaust, indicating that almost all of the volatile matters are consumed before reaching this region.

No major discrepancy between the numerical predictions and measured $O_2$ concentration can be found for the three cases at locations Z = 50 mm and Z = 100 mm. However, the $O_2$ concentrations are underestimated along the centreline of the furnace; particularly for locations downstream from the fuel jet exit. This discrepancy is not well understood and, speculatively, it is associated with inaccurate calculations of the fuel jet entrainment.

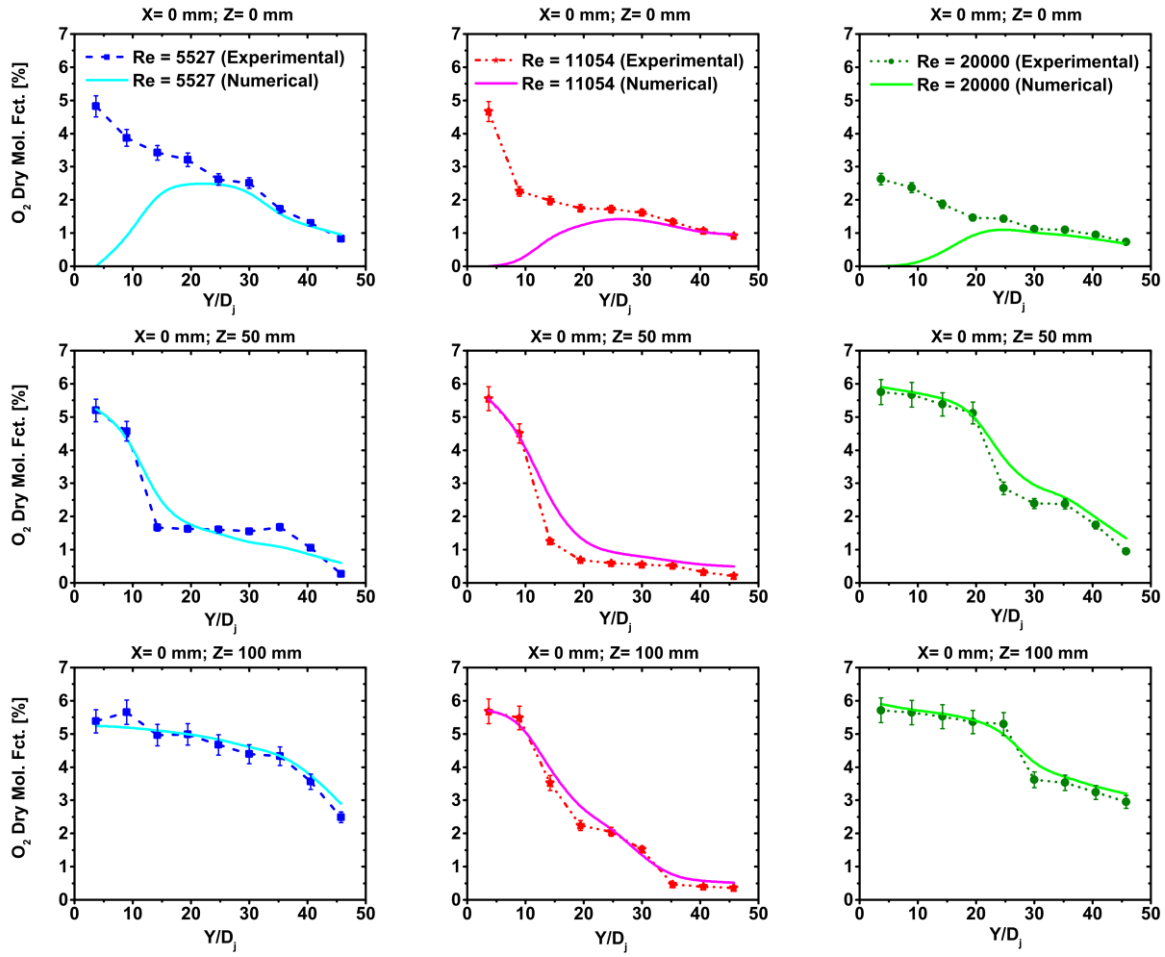


Figure 13. Measured and computed profiles of in-furnace $O_2$ dry molar fraction for cases 1-3

## 4.8. NO Distribution

It is well established that nitric oxides ($NO_x$, i.e., combination of NO and $NO_2$) are produced through three different formation routes during the combustion of pulverised solid fuels (e.g., coal) as follows:

1. Thermal $NO_x$: The formation of thermal-$NO_x$ corresponds to the immediate oxidation of molecular nitrogen ($N_2$) from the combustion air which is favoured by high combustion temperature. However, thermal-$NO_x$ formation is insignificant when the local temperatures are below 1800 K [23, 35]. Indeed, the highest mean temperature of the present experiments is measured to be lower than 1400 K, and thus the contribution of thermal-$NO_x$ is expected to be negligible.

2. Prompt $NO_x$: The prompt-$NO_x$ production generally occurs in the fuel-rich medium by the reaction of atmospheric $N_2$ with hydrocarbon fuels. In general, prompt-$NO_x$ has a minor effect on the overall $NO_x$ formation under MILD combustion conditions because of the strong diluted mixture of reactants with large amounts of products.

3. Fuel $NO_x$: Fuel $NO_x$ is generated by the oxidation reaction of the nitrogen (N) incorporated in the solid particles. It is assumed that the nitrogen (N) bound into the particle is entirely discharged throughout the devolatilization process and diffused into the volatile matters and the char. Thus, the fuel-$NO_x$ is produced by two evolution paths such as oxidation reaction of volatile-nitrogen and char-nitrogen. It is noteworthy to mention that $NO_2$ level was below the detection limits of the gas analyser in all the measurements and thus only NO is reported in this paper. Nevertheless, it is well-known that NO accounts of more than 95% of total $NO_x$ formation in most coal combustion process [44, 62]. This mechanism is known to be responsible for the majority of NO formation under coal MILD combustion.

Finally, the turbulent mixing of coal particles with hot product of combustion from secondary burner within the furnace develops a strong reburning reaction of NO and consequently leads to minimize overall NO emission.

Figure 14 compares the measured in-furnace NO dry molar fraction between the three jet Reynolds number cases and for all measurement locations. The highest value of in-furnace NO mole fraction for the $Re_{jet}$ = 20,000 case is found to be ≈170 ppm at 570 mm (Y/D = 30) above the jet exit which decreases to ≈157 ppm at the exit. This

indicates that NO is consumed through the reburning reactions. It is interesting to note that the largest NO concentration peaks for the cases of $Re_{jet}$ = 11,054 and $Re_{jet}$ = 5,527 are observed at the position of Y/D = 24.7 and Y/D = 19.5 along the furnace centreline (X = 0 mm, Z= 0 mm) which can be explained by the early devolatilisation of coal particles for the lowest Reynolds number case. Those results re-confirm that NO is predominantly formed by the volatile matter oxidation through the fuel-NO path.

Considering the NO profiles at 50 mm (X = 0 mm, Z= 50 mm) and 100 mm (X = 0 mm, Z= 100 mm) away from the furnace centreline, minor differences between the three cases can be observed from Figure 14, although for $Re_{jet}$ = 5,527 case, the NO mole fraction in the middle part of the furnace is measured to be higher than the other two cases. This can be explained by the higher residence time of coal particles for the lowest jet Reynolds number. The long particle residence time allows the production of higher fuel-NO from the oxidation reaction of the incorporated nitrogen (N) in the coal particles. It is presumed that the nitrogen (N) in the coal particle is entirely released during the devolatilization process. In comparing the cases between $Re_{jet}$ = 20,000 and $Re_{jet}$ = 5,527, it is clear that the particles' residence time is significantly higher for the $Re_{jet}$ = 5,527 case and thus it is speculated that for this case (i) a share of nitrogen bound in the coal is converted into fuel-NO by the volatile-N oxidation; and (ii) a share of the remaining nitrogen is converted into fuel-NO by the char-N oxidation reaction. Furthermore, higher in-furnace temperature for the case of $Re_{jet}$ = 5,527 contributes to generate relatively higher NO through the thermal-NO route, although this impact is believed to be minor under MILD combustion conditions [28, 32].

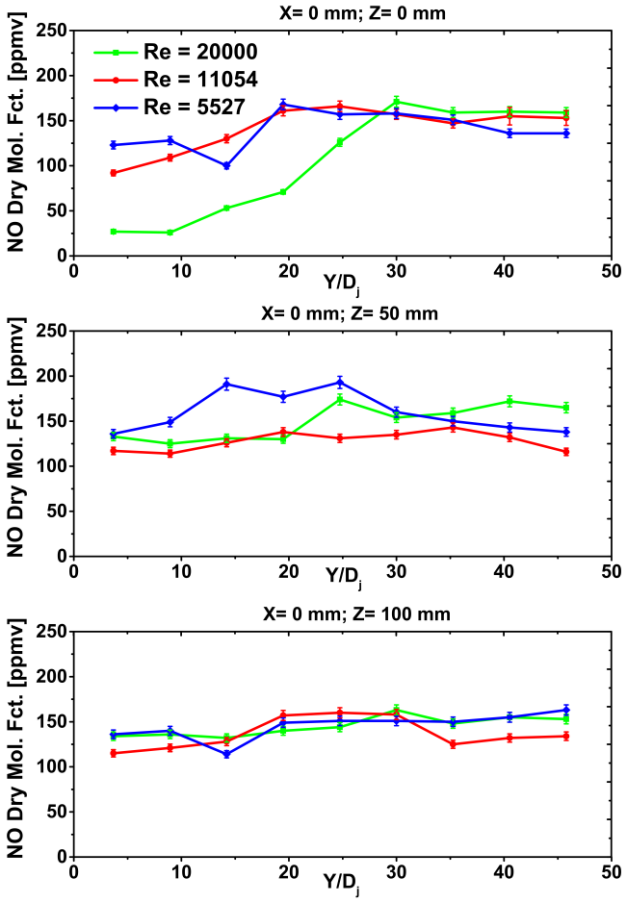


Figure 14. Measured axial profiles of in-furnace NO dry molar fraction of cases 1-3

## 4.9. $CH^*$ chemiluminescence

The $CH^*$ chemiluminescence is a natural light emission by excited CH molecules from an upper/excited state of energy to a lower state of energy. Schefer [63] reported $CH^*$ chemiluminescence as a simple but effective tool to describe ignition zone in the combustion reaction regions where $CH^*$ is formed by one of the following reactions:

$$C_2 + OH \longrightarrow CO + CH^*$$

$$C_2H + O \longrightarrow CO + CH^*$$

Delabroya et al. [64] used $CH^*$ chemiluminescence to visualise the location and temporal evolution of an actively pulsed flame. Many other researchers [63-67] have shown that $CH^*$ chemiluminescence can be used as a qualitative and/or quantitative

combustion diagnostic tool. In the current work, $CH^*$ chemiluminescence is presented to better understand the effect of turbulence on volatiles' reaction intensity by providing more qualitative information on the reaction zone during coal MILD combustion.

The time-averaged $CH^*$ emission was captured using a digital camera. The camera lens was positioned and focused at a right angle to the upward flow direction of the fuel jet, while a 430 nm centred interference filter was mounted to the camera lens. To capture the maximum signal intensity of $CH^*$ chemiluminescence, a long exposure time (~ 2.5 seconds) was selected for the experiments. Figure 15 displays example of instantaneous $CH^*$ chemiluminescence images for case 1 at the locations close to the bottom (Y = 80 mm), middle (Y = 500 mm), and top (Y = 995 mm) of the furnace. From Figure 9 it is clear that $CH^*$ is below detection limits at the bottom of the furnace suggesting no ignition is initiated at this location, while at the middle of the furnace, a bright zone was highlighted with the largest intensity $CH^*$ suggesting that the reaction of volatile matters with the surrounding co-flow occurs in this region. Low intensity $CH^*$ chemiluminescence signals are observed at the top of the furnace. The low intensity $CH^*$ signals indicate that most volatiles have burned and char particles combustion is taking place. Moreover, Figure 15 suggests that homogeneous chemical reactions of volatile matters ignition occur more rapidly than the heterogeneous combustion of char particles. This observation agrees with that Molina and Shaddix [65] for single particle bituminous pulverised coal ignition in an entrained-flow reactor.

Figure 16 plots the corrected and normalised total $CH^*$ signal in the averaged images (averaged from 27 instantaneous images of $CH^*$ chemiluminescence), against the horizontal distance from the jet exit plane along the furnace centreline for cases 1-3. The standard deviation of the $CH^*$ signal was found between $\pm$ 6.8% and $\pm$ 9.4% in the

bottom, ± 1.6% and ± 6.4% in the middle and ± 0.6% and ± 8.9% in the top of the furnace, for the different cases. Total $CH^*$ signal here refers to radially integrated $CH^*$ across the whole width of the reaction zone which is exposed through the optical access of the furnace. For the same co-flow condition, the higher intensity of $CH^*$ signal is measured for case 1 among all the cases. In addition, the peak of $CH^*$ emission is found at the middle of the furnace for the same case. Both are the indication of strong $CH^*$ radical emissions from the lowest Reynolds number case and generally responsible for the visible flame produced by the non-premixed combustion of coal particles.

The spatial gradient of total $CH^*$ signal intensity is significantly lower for the higher jet Reynolds number cases. The weak $CH^*$ chemiluminescence for the $Re_{jet}$ = 11,054 and $Re_{jet}$ = 20,000 cases indicate the presence of an invisible flame and homogeneous reaction regime inside the furnace. Furthermore, no peak intensity of $CH^*$ signal in the middle and top of the furnace is observed for the case of $Re_{jet}$ = 20,000, which suggests a more uniform temperature distribution with high level of turbulence.

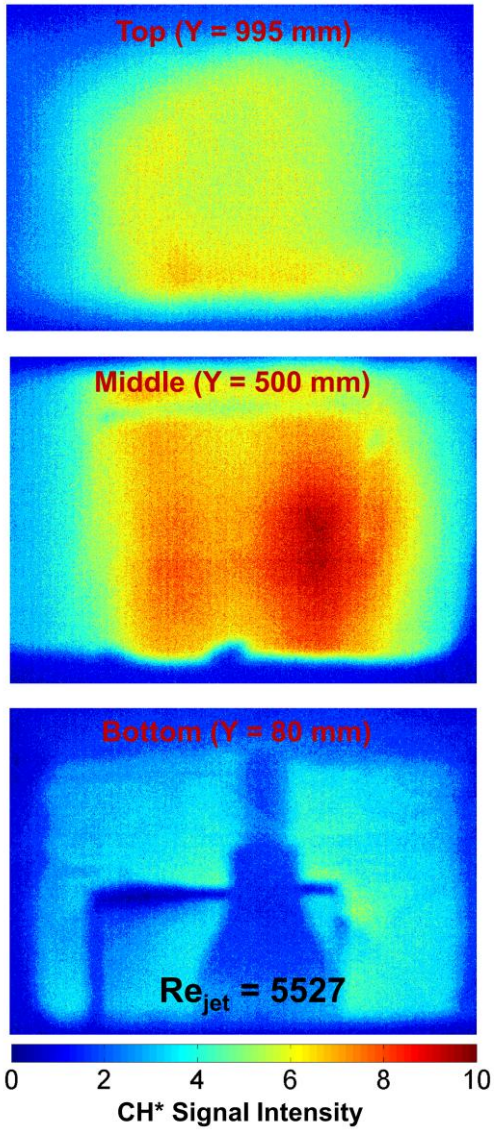


Figure 15. Example of instantaneous CH* images of different locations of the furnace for the case of $Re_{jet}$ = 5527 with 5.9% $O_2$ of co-flow

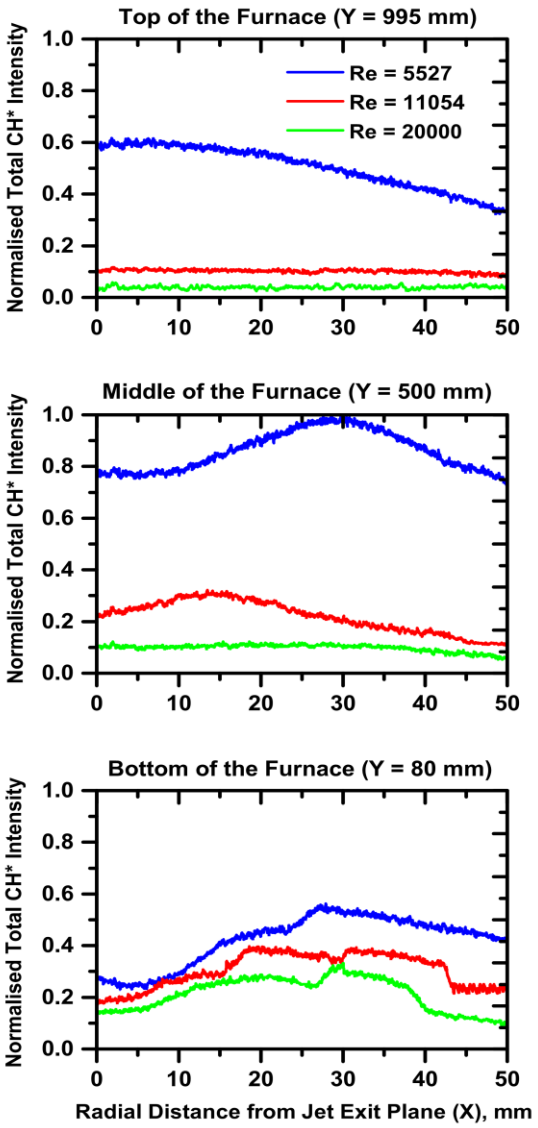


Figure 16. Normalised radially integrated total intensity of CH* signal as a function of horizontal distance from the jet exit plane (X) along the furnace centreline for cases 1-3

## 4.10. Exhaust emissions

Figure 17 illustrates the comparison of measured concentrations of exhaust gases including; NO (measured value of $NO_2$ was negligible in this experimental campaign), CO, $O_2$, and $CO_2$ for all three cases.

The largest NO emission was measured for the $Re_{jet}$ = 5,527 case which is ≤ 147 ppm, whilst for the case of $Re_{jet}$ = 11,054 the value is ≤ 118 ppm and for the highest Reynolds number ($Re_{jet}$ = 20,000) case the value is ≤ 106 ppm. The overall NO formation is impacted by the dilution of the flows with additional $CO_2$ volume flow rate into the mixture for the higher jet Reynolds number. The additional $CO_2$ volume flow rate of the mixture increases about 72% for the $Re_{jet}$ = 20,000 case when compared with $Re_{jet}$ = 5,527 case and consequently the overall NO emission decreased by 34% for the $Re_{jet}$ = 20,000 case. It is worth noting that for all the cases, the value of NO in the exhaust is lower than that measured in the furnace. This lower NO emission rate was attributed to the strong mixing of hot co-flow combustion products with coal volatiles or light hydrocarbons that allowed for NO reburning in the combustion zone. This phenomenon can be explained by the NO-reburning mechanism which depends primarily on the NO recombination with hydrocarbons according to reaction ($C_xH_y + NO \rightarrow HCN + product$) and therefore diminishes the overall NO emission. Moreover, the NO-reburning reaction is increased with increasing fuel jet Reynolds numbers, owing to the higher jet turbulence and better mixing. These results suggest that overall $NO_x$ emission of pulverised coal combustion can be successfully reduced by increasing the jet turbulence under MILD conditions.

The exhaust CO level was measured to be 2410~2500 ppmv for the $Re_{jet}$ = 5,527 case while for the highest Reynolds number ($Re_{jet}$ = 20,000) case the CO level was 1650~1780 ppmv. It is noticeable that the exhaust CO emission for the lowest Reynolds number ($Re_{jet}$ = 5,527) case is considerably higher than that of larger Reynolds number cases ($Re_{jet}$ = 11,054 and $Re_{jet}$ = 20,000), however the in-furnace CO concentration (see Figure 5) was found to be substantially lower for the lowest Reynolds number ($Re_{jet}$ = 5,527). The reason of higher CO emission for the lowest Reynolds number case is most likely related to the more eminent char burnout by the heterogeneous reactions between char ($C_{(s)}$) and gaseous products ($C_{(s)} + 1/2O_2 \rightarrow CO$, $C_{(s)} + CO_2 \rightarrow 2CO$, $C_{(s)} + H_2O \rightarrow CO + H_2$) of the combustion reaction. It is believed that coal particles have a sufficient time to burn char for the $Re_{jet}$ = 5527 case due to the higher residence time. On the contrary, the residence time of the coal particles for the higher jet Reynolds number cases was distinctly insufficient when compared with $Re_{jet}$ = 5527 case.

Similar values of oxygen concentration at the furnace outlet were measured for all cases. This confirms that the overall equivalence ratio was almost same for each case (refer Table 1). The concentration of $CO_2$ emission was measured to be higher for the highest Reynolds number case which is related to the largest volume of incoming $CO_2$ concentration as a carrier gas.

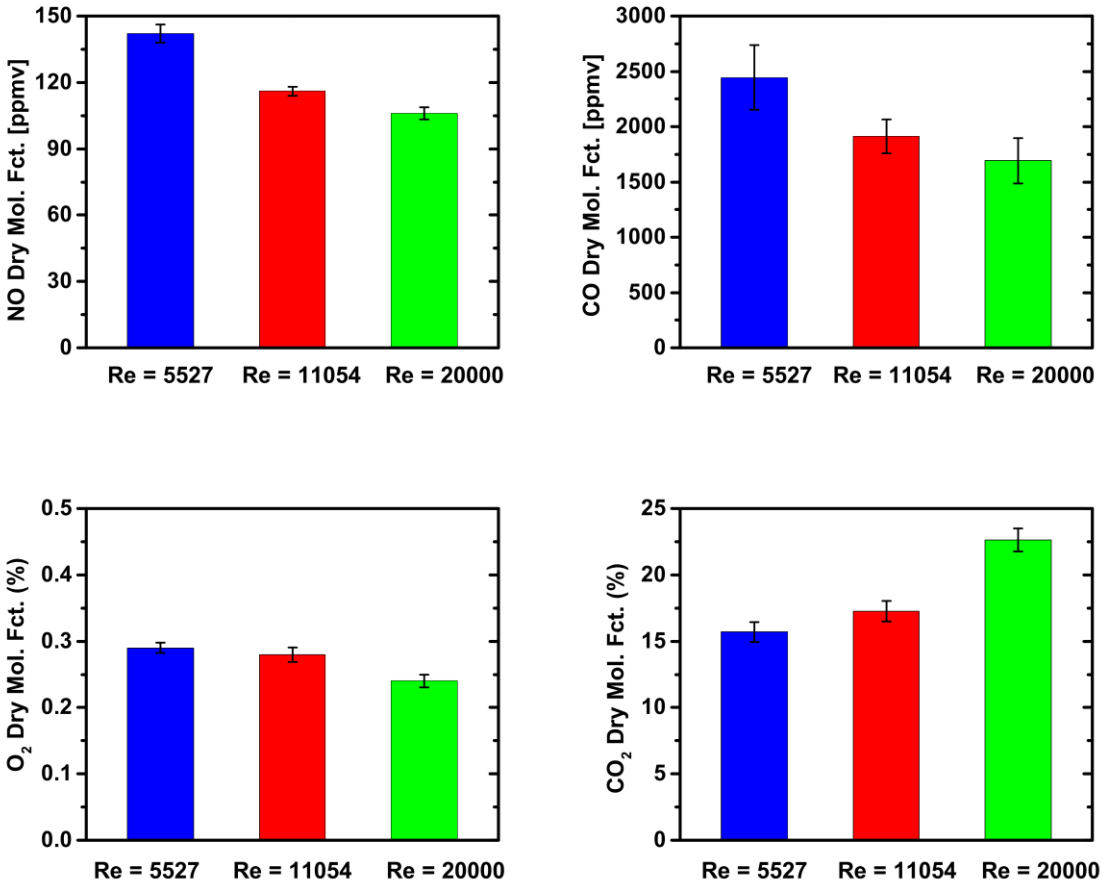


Figure 17. Measured exhaust gas concentrations at the furnace exit of Loy-Yang brown coal MILD combustion for cases 1-3

## 4.11. Overall Carbon Consumption

Figure 18 shows the comparison of overall calculated carbon consumption for all cases. The overall carbon consumption (OCC) was calculated by a simple carbon balance between the inlet and outlet of the furnace following Schaffel et al. [27]. The initial carbon content (%) and coal ash (%) coming into the furnace can be found from the ultimate and proximate analysis of coal. The carbon content (%) in the furnace outlet can be directly obtained from the numerical simulations employing post-processing approach. The overall carbon consumption (OCC) was calculated as:

$$\text{Overall carbon consumption (OCC)} = 1 - \frac{Amount\ of\ carbon\ \ coming\ into\ the\ furnace}{Amount\ of\ carbon\ in\ the\ furnace\ outlet}$$

The bar graph implies that almost all carbon content (around 95%) of inlet fuel was burnt for the case of $Re_{jet}$ = 5,027, whereas for the case of $Re_{jet}$ = 11,054 the value is calculated to be ≈ 83% and for the highest Reynolds number ($Re_{jet}$ = 20,000) case the carbon consumption value is around 71%. The carbon burning rate is significantly affected by the particle residence time. It is quite understandable that the particle residence time for the lowest Reynolds number case was significantly higher than the highest Reynolds number case. The comparatively short residence time is impacted on the lower rate of carbon consumption for case 3.

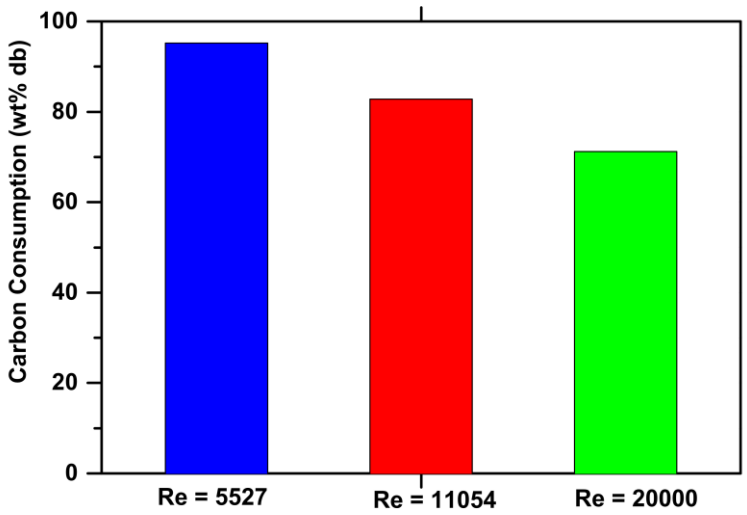


Figure 18. Calculated overall carbon consumption for cases 1-3

## 5. CONCLUSIONS

This study was conducted to explore the effect of jet Reynolds number on the burning characteristics of pulverised Victorian brown coal in a vertical furnace operating under MILD combustion conditions. The coal is carried by $CO_2$ and injected into the furnace via an insulated and cooled jet surrounded by a hot and diluted co-flow. The interaction of the volatiles with the vitiated co-flow and its impact on the formation and emission of soot, $NO_x$ and other pollutants have been investigated.

The key findings of this study are as follows:

1. Stable MILD combustion was established for experimental cases 2 and 3. No visible flame was found at the jet exit for all Reynolds number cases. A faint, yellowish, visible flame was observed at the middle and top part of the furnace for the lower jet velocity ($R_{jet}$ = 5,527) case, while no visible flame was found in the furnace for the other cases. The appearance of the flames for the lower jet velocity case is related to the longer particle residence time and poor mixing;

2. Higher Reynolds number leads to the establishment of a recirculation zone leading an increase in the volatiles combustion rate and contributes to more uniform reaction zone;

3. Increasing the jet Reynolds number increases the volatiles' release rates. This predominantly depends on the better mixing, however it is independent of the particles' residence time;

4. The particle residence time significantly affects the overall carbon consumption rate. The comparatively longer residence time for lower jet velocity ($R_{jet}$ = 5,527) case is accountable for higher rate of carbon consumption.

5. The CH chemiluminescence ($CH^*$) imaging indicates that the jet turbulence (jet Reynolds number) has a significant impact on the MILD combustion characteristics of pulverised Victorian brown coal. In particular, the $CH^*$ signal intensity is found to be significantly lower at the top part of the furnace where heterogeneous combustion of char particles occur. Moreover, no peak intensity of $CH^*$ signal in the middle and top

of the furnace is observed for the largest jet velocity case (i.e., $R_{jet}$ = 20,000), which suggests the presence of a more uniform temperature distribution and homogeneous combustion reactions for higher level of turbulence;

6. Minor differences associated with the carrier gas velocities on furnace temperatures and $NO_x$ formation, whilst a major difference is found regarding CO production;

7. The temperature distribution inside the furnace is quite uniform with less than 100 K difference from top to bottom of the furnace for all cases;

8. The largest amount of CO concentrations are measured for the highest jet velocity ($R_{jet}$ = 20,000) case which implies that an increase of the turbulence level (i.e., at higher jet Reynolds number) leads to better mixing and hence better reaction of the volatiles that produces more CO;

9. In general, higher NO is measured in the middle part of the furnace for the $R_{jet}$ = 5,527 case. This is attributed to the flame sheets observed in this part of the furnace, which is likely to exhibit higher local temperatures commonly associated with higher thermal $NO_x$ formation. Nevertheless, it is worth noting that very low NO emission (not more than 125 ppmv db at 3% $O_2$) was measured at the furnace outlet for all of the investigated cases, providing strong evidence of the potential benefits of MILD combustion application to Victorian brown coal.

10. The numerical model reproduced the experimental data well. However, the numerical simulation somewhat underestimates the CO and $O_2$ formation. This

discrepancy between the simulations and measurements indicates that the simplified devolatilisation model, the reduction mechanism of the gaseous species, and the simplistic char combustion reactions, which play such an important role, are as yet incapable of replicating the experimental results completely.

## ACKNOWLEDGMENTS

The support of the University of Adelaide is gratefully acknowledged; in particular M. Saha acknowledges the Adelaide Scholarship International (ASI) of The University of Adelaide and Brown Coal Innovation Australia (BCIA) Top-Up scholarship for financial support. The authors would like to thank Mr Marc Simpson, Manager, Thebarton Laboratory, for his help throughout the experiments. The authors would also like to acknowledge eResearch SA for the use of their computational facilities.

## REFERENCES

[1] U.S. Energy Information Administration. International Energy Outlook 2015; U.S. Department of Energy (DOE): Washington, DC, 2015.

[2] Department of Economic Development, Transport and Resources, Victoria, Australia Energy and Earth Resources. Available: http://www.energyandresources.vic.gov.au/earth-resources/victorias-earth-resources/coal (accessed 25/01/2016).

[3] C.-Z. Li, Some recent advances in the understanding of the pyrolysis and gasification behaviour of Victorian brown coal, Fuel 86 (2007) 1664-1683.

[4] E. Binner, L. Zhang, C.-Z. Li, S. Bhattacharya, In-situ observation of the combustion of air-dried and wet Victorian brown coal, Proc. Combust. Inst. 33 (2011) 1739-1746.

[5] D.M. Quyn, H. Wu, C.-Z. Li, Volatilisation and catalytic effects of alkali and alkaline earth metallic species during the pyrolysis and gasification of Victorian brown coal. Part I. Volatilisation of Na and Cl from a set of NaCl-loaded samples, Fuel 81 (2002) 143-149.

[6] A.H. Al-Abbas, J. Naser, D. Dodds, CFD modelling of air-fired and oxy-fuel combustion in a large-scale furnace at Loy Yang A brown coal power station, Fuel 102 (2012) 646-665.

[7] Z.F. Tian, P.J. Witt, M.P. Schwarz, W. Yang, Numerical modelling of Victorian brown coal combustion in a tangentially fired furnace, Energy Fuels 24 (2010) 4971-4979.

[8] K. Stępczyńska-Drygas, H. Łukowicz, S. Dykas, Calculation of an advanced ultra-supercritical power unit with CO2 capture installation, Energy Convers. Manage. 74 (2013) 201-208.

[9] L. Chen, S.Z. Yong, A.F. Ghoniem, Oxy-fuel combustion of pulverized coal: Characterization, fundamentals, stabilization and CFD modeling, Prog. Energy Combust. Sci. 38 (2012) 156-214.

[10] B.S. Hoffmann, A. Szklo, Integrated gasification combined cycle and carbon capture: A risky option to mitigate $CO_2$ emissions of coal-fired power plants, Appl. Energy 88 (2011) 3917-3929.

[11] I.B. Özdemir, N. Peters, Characteristics of the reaction zone in a combustor operating at mild combustion, Exp. Fluids 30 (2001) 683-695.

[12] S. Orsino, R. Weber, U. Bollettini, Numerical simulation of combustion of natural gas with high-temperature air, Combust. Sci. Technol. 170 (2001) 1-34.

[13] E. Mastorakos, A. Taylor, J. Whitelaw, Extinction of turbulent counter flow flames with reactants diluted by hot products, Combust. Flame 102 (1995) 101-114.

[14] A. Milani, A. Saponaro, Diluted combustion technologies, IFRF Combust. J. (2001) 1-32.

[15] A. Cavaliere, M. de Joannon, Mild combustion, Prog. Energy Combust. Sci. 30 (2004) 329-366.

[16] J. Wünning, J. Wünning, Flameless oxidation to reduce thermal NO-formation, Prog. Energy Combust. Sci. 23 (1997) 81-94.

[17] T. Kiga, K. Yoshikawa, M. Sakai, S. Mochida, Characteristics of pulverized coal combustion in high-temperature preheated air, J. Propul. Power 16 (2000) 601-605.

[18] P. Sabia, G. Sorrentino, A. Chinnici, A. Cavaliere, R. Ragucci, Dynamic behaviors in methane MILD and oxy-fuel combustion. Chemical effect of $CO_2$, Energy Fuels 29 (2015) 1978-1986.

[19] A. Parente, J.C. Sutherland, B.B. Dally, L. Tognotti, P.J. Smith, Investigation of the MILD combustion regime via Principal Component Analysis, Proc. Combust. Inst. 33 (2011) 3333-3341.

[20] A. Effuggi, D. Gelosa, M. Derudi, R. Rota, Mild combustion of methane-derived fuel mixtures: Natural gas and biogas, Combust. Sci. Technol. 180 (2008) 481-493.

[21] T. Suda, M. Takafuji, T. Hirata, M. Yoshino, J. Sato, A study of combustion behavior of pulverized coal in high-temperature air, Proc. Combust. Inst. 29 (2002) 503-509.

[22] R. He, T. Suda, M. Takafuji, T. Hirata, J. Sato, Analysis of low NO emission in high temperature air combustion for pulverized coal, Fuel 83 (2004) 1133-1141.

[23] Z. Mei, P. Li, F. Wang, J. Zhang, J. Mi, Influences of reactant injection velocities on moderate or intense low-oxygen dilution coal combustion, Energy Fuels 28 (2013) 369-384.

[24] Y. Tu, H. Liu, K. Su, S. Chen, Z. Liu, C. Zheng, W. Li, Numerical study of $H_2O$ addition effects on pulverized coal oxy-MILD combustion, Fuel Process. Technol. 138 (2015) 252-262.

[25] Y. Tu, H. Liu, S. Chen, Z. Liu, H. Zhao, C. Zheng, Numerical study of combustion characteristics for pulverized coal under oxy-MILD operation, Fuel Process. Technol. 135 (2015) 80-90.

[26] R. Weber, J.P. Smart, W. Kamp, On the (MILD) combustion of gaseous, liquid, and solid fuels in high temperature preheated air, Proc. Combust. Inst. 30 (2005) 2623-2629.

[27] N. Schaffel, M. Mancini, A. Szlek, R. Weber, Mathematical modeling of MILD combustion of pulverized coal, Combust. Flame 156 (2009) 1771-1784.

[28] M. Vascellari, G. Cau, Influence of turbulence–chemical interaction on CFD pulverized coal MILD combustion modeling, Fuel 101 (2012) 90-101.

[29] M. Tamura, S. Watanabe, K. Komaba, K. Okazaki, Combustion behaviour of pulverised coal in high temperature air condition for utility boilers, Appl. Therm. Eng. 75 (2015) 445-450.

[30] P. Li, F. Wang, Y. Tu, Z. Mei, J. Zhang, Y. Zheng, H. Liu, Z. Liu, J. Mi, C. Zheng, Moderate or Intense Low-Oxygen Dilution Oxy-combustion characteristics of light oil and pulverized coal in a pilot-scale furnace, Energy Fuels 28 (2014) 1524-1535.

[31] M. Saha, B.B. Dally, P.R. Medwell, E.M. Cleary, Moderate or Intense Low Oxygen Dilution (MILD) combustion characteristics of pulverized coal in a self-recuperative furnace, Energy Fuels 28 (2014) 6046-6057.

[32] M. Saha, A. Chinnici, B.B. Dally, P.R. Medwell, Numerical study of pulverized coal MILD combustion in a self-recuperative furnace, Energy Fuels 29 (2015) 7650- 7669.

[33] H. Zhang, G. Yue, J. Lu, Z. Jia, J. Mao, T. Fujimori, T. Suko, T. Kiga, Development of high temperature air combustion technology in pulverized fossil fuel fired boilers, Proc. Combust. Inst. 31 (2007) 2779-2785.

[34] H. Stadler, D. Toporov, M. Förster, R. Kneer, On the influence of the char gasification reactions on NO formation in flameless coal combustion, Combust. Flame 156 (2009) 1755-1763.

[35] H. Stadler, D. Ristic, M. Förster, A. Schuster, R. Kneer, G. Scheffknecht, $NO_x$-emissions from flameless coal combustion in air, $Ar/O_2$ and $CO_2/O_2$, Proc. Combust. Inst. 32 (2009) 3131-3138.

[36] J.P. Smart, G.S. Riley, Combustion of coal in a flameless oxidation environment under oxyfuel firing conditions: the reality, J. Energy Inst. 85 (2012) 131-134.

[37] M. Weidmann, D. Honoré, V. Verbaere, G. Boutin, S. Grathwohl, G. Godard, C. Gobin, R. Kneer, G. Scheffknecht, Experimental characterization of pulverized coal MILD flameless combustion from detailed measurements in a pilot-scale facility, Combust. Flame (2016), doi:10.1016/j.combustflame.2016.01.029.

[38] M. Weidmann, V. Verbaere, G. Boutin, D. Honoré, S. Grathwohl, G. Goddard, C. Gobin, H. Dieter, R. Kneer, G. Scheffknecht, Detailed investigation of flameless oxidation of pulverized coal at pilot-scale (230 $kW_{th}$), Appl. Therm. Eng. 74 (2015) 96 - 101.

[39] D. Ristic, M. Schneider, A. Schuster, G. Scheffknecht, J. Wünning. Investigation of $NO_x$ formation for flameless coal combustion. 7th High Temperature Air Combustion and Gasification International Symposium (2008); paper 08, Phuket, Thailand.

[40] D. Ristic, A. Schuster, G. Scheffknecht, H. Stadler, M. Foerster, R. Kneer, J. Wunning, Experimental study on flameless oxidation of pulverised coal in bench and pilot scale, Proceedings of the 23th German Flame day (2007) paper 45, Berlin, Germany.

[41] Z. Mei, P. Li, J. Mi, F. Wang, J. Zhang, Diffusion MILD combustion of firing pulverized-coal at a pilot furnace, Flow Turbul. Combust. 95 (2015) 803-829.

[42] X. Jin, Y. Zhou, numerical analysis on microscopic characteristics of pulverized coal Moderate and Intense Low-Oxygen Dilution combustion, Energy Fuels 29 (2015) 3456-3466.

[43] D. Rezaei, Y. Zhou, J. Zhang, K.E. Kelly, E.G. Eddings, R.J. Pugmire, M.S. Solum, J.O. Wendt, The effect of coal composition on ignition and flame stability in coaxial oxy-fuel turbulent diffusion flames, Energy Fuels 27 (2013) 4935-4945.

[44] A. Williams, M. Pourkashanian, J. Jones, Combustion of pulverised coal and biomass, Prog. Energy Combust. Sci. 27 (2001) 587-610.

[45] M. Saha, B.B. Dally, P.R. Medwell, A. Chinnici, Effect of particle size on the MILD combustion characteristics of pulverised brown coal, Fuel Process. Technol. (2016), doi:10.1016/j.fuproc.2016.04.003.

[46] B.B. Dally, S.H. Shim, R.A. Craig, P.J. Ashman, G.G. Szegö, On the burning of sawdust in a MILD combustion furnace, Energy Fuels 24 (2010) 3462-3470.

[47] Feeder selection guide, K-Tron feeder, US, available: http://www.ktron.com/process-equipment/feeders/feeder-selection.cfm (accessed on 12/11/2014).

[48] M. Thompson, S. Weatherley, R. Pukadyil, P. Sheskey, Foam granulation: new developments in pharmaceutical solid oral dosage forms using twin screw extrusion machinery, Drug Dev. Ind. Pharm. 38 (2012) 771-784.

[49] T. Kupka, M. Mancini, M. Irmer, R. Weber, Investigation of ash deposit formation during co-firing of coal with sewage sludge, saw-dust and refuse derived fuel, Fuel 87 (2008) 2824-2837.

[50] J.R. Howell, R. Siegel, M.P. Menguc, Thermal Radiation Heat Transfer, fifth ed., CRC press, New York, 2010.

[51] T.-H. Shih, W.W. Liou, A. Shabbir, Z. Yang, J. Zhu, A new $k$-$\epsilon$ eddy viscosity model for high reynolds number turbulent flows, Comput. Fluids 24 (1995) 227-238.

[52] E. Chui, G. Raithby, Computation of radiant heat transfer on a nonorthogonal mesh using the finite-volume method, Numer. Heat Transfer 23 (1993) 269-288.

[53] C. Sheng, B. Moghtaderi, R. Gupta, T.F. Wall, A computational fluid dynamics based study of the combustion characteristics of coal blends in pulverised coal-fired furnace, Fuel 83 (2004) 1543-1552.

[54] M.A. Rajhi, R. Ben-Mansour, M.A. Habib, M.A. Nemitallah, K. Andersson, Evaluation of gas radiation models in CFD modeling of oxy-combustion, Energy Convers. Manage. 81 (2014) 83-97.

[55] B. Popoff, M. Braun. A Lagrangian approach to dense particulate flows. International Conference on Multiphase Flow (2007), paper 06, Leipzig, Germany; 2007.

[56] J. Zhang, W. Prationo, L. Zhang, Z. Zhang, Computational fluid dynamics modeling on the air-firing and oxy-fuel combustion of dried Victorian brown coal, Energy Fuels 27 (2013) 4258-4269.

[57] B. Magnussen, On the structure of turbulence and a generalized eddy dissipation concept for chemical reaction in turbulent flow, Nineteenth AIAA Meeting (1981), pp. 1-6.

[58] D.W. Shaw, X. Zhu, M.K. Misra, R.H. Essenhigh. Determination of global kinetics of coal volatiles combustion, Symp. (Int.) Combust. 23 (1991) 1155-1162.

[59] L. Wang, Z. Liu, S. Chen, C. Zheng, Comparison of different global combustion mechanisms under hot and diluted oxidation conditions, Combust. Sci. Technol. 184 (2012) 259-276.

[60] V. Shilapuram, D.J. Krishna, N. Ozalp, Residence time distribution and flow field study of aero-shielded solar cyclone reactor for emission-free generation of hydrogen, Int. J. Hydrogen Energy 36 (2011) 13488-13500.

[61] A. Chinnici, M. Arjomandi, Z.F. Tian, Z. Lu, G.J. Nathan, A Novel Solar Expanding-Vortex Particle Reactor: Influence of Vortex Structure on Particle Residence Times and Trajectories, Sol. Energy 122 (2015) 58-75.

[62] S. Hill, L. Douglas Smoot, Modeling of nitrogen oxides formation and destruction in combustion systems, Prog. Energy Combust. Sci. 26 (2000) 417-458.

[63] R. Schefer, Flame sheet imaging using CH chemiluminescence, Combust. Sci. Technol. 126 (1997) 255-279.

[64] O. Delabroy, E. Haile, F. Lacas, S. Candel, A. Pollard, A. Sobiesiak, H. Becker, Passive and active control of $NO_x$ in industrial burners, Exp. Therm Fluid Sci. 16 (1998) 64-75.

[65] A. Molina, C.R. Shaddix, Ignition and devolatilization of pulverized bituminous coal particles during oxygen/carbon dioxide coal combustion, Proc. Combust. Inst. 31 (2007) 1905-1912.

[66] L.G. Blevins, M.W. Renfro, K.H. Lyle, N.M. Laurendeau, J.P. Gore, Experimental study of temperature and CH radical location in partially premixed $CH_4$/air coflow flames, Combust. Flame 118 (1999) pp. 684-696.

[67] A. Yoshida, M. Narisawa, H. Tsuji, T. Hirose, Chemiluminescence Emission of C2, CH and OH Radicals from Opposed Jet Burner Flames, JSME Int J. 38 (1995) 222-229.

# CHAPTER 7

# SUMMARY, CONCLUSIONS AND RECOMMENDATIONS

# Chapter 7 Summary, Conclusions and Recommendations

## 7.1. Summary

The results and discussions generated through experimental and computational investigations, as presented in Chapters 3, 4, 5, and 6, have revealed new knowledge and insights that helped to deepen our understanding of the burning characteristics of pulverised coals under the MILD combustion regime. This section provides a summary of these findings.

### 7.1.1. Effect of Coal Rank and Carrier Gas

Coal rank is one of the key parameters in pulverised coal combustion under MILD mode, due to its impact on the reaction zone structure and pollutant emissions. Although previous research has reported results from the combustion of differently ranked coals under MILD conditions, no study has been reported on Australian coal burning under these conditions, in particular low-volatile black coal and high-volatile brown coal. A detail description of the MILD combustion characteristics of high-volatile Kingston brown coal and low-volatile Bowen basin black coal with particle sizes in the range of 38-180 μm in a self-recuperative furnace was presented in

Chapter 3. The experimental study investigated the effect of the carrier gas (either $CO_2$ or $N_2$), fuel rank (either low or high volatile coal) and the operating parameters on the characteristics of MILD combustion. The in-furnace gas concentrations and temperature, as well as pollutant emissions in the exhaust stream were discussed and analysed. No visible flame was found inside the furnace. The temperature difference across the furnace was less than 100 K with minimal fluctuation. The semi-uniform furnace temperature implies that a homogeneous temperature distribution is achieved in coal-MILD combustion using a simple burner design. A major difference was found between the two ranked coals in temperature and chemical species formation and pollutant emissions, while the variation of the carrier gas has a minor impact. The measured CO level for brown coal cases (≈ 5000 ppmv) was around ten times higher than that for black coal cases (≈ 530 ppmv). The higher CO emissions for brown coal are related to the more significant char burnout of brown coal, as was confirmed by the ash content analysis. The ash content analysis reveals that the unburnt carbon in the ash for the black coal (≈ 61%) is significantly higher than for brown coal (≈ 17%) which points to insufficient residence time in the furnace. The overall NO emission for brown coal (≈ 230 ppmv) was only 37% of that measured for black coal (≈ 366 ppmv) at a global equivalence ratio of $\Phi$ = 0.88. The reason behind the higher NO emissions for black coal combustion is not clearly understood from this study, however it is speculated that the high N contents of fuel (where the value of N contents in black coal is around 64% higher than that of brown coal) lead to higher NO emissions that are produced through the fuel-NO formation path.

A complementary numerical study was presented in order to shed light on the flow and thermal fields' structure inside the furnace, along with the investigations of the effects of inlet air momentum on furnace flow dynamics and global CO emissions. In all cases, volatiles are released in the fuel jet and carried by a strong vortex induced by the air jets in a manner not dissimilar to gaseous MILD combustion in the self-recuperative furnace. The most significant impact of increasing the air jet momentum, either by raising the temperature or by raising the mass flow rate, is an increased air jet penetration distance. The modelling results reveal that increasing the air jet momentum broadens the reaction zone, but also lowers reaction rates and increases CO emissions.

### 7.1.2. Suitability of Devolatilisation Models

To understand the influence of devolatilisation models on the prediction accuracy of pulverised coal combustion under MILD mode, a comprehensive numerical study was conducted (the details were reported in Chapter 4). Three devolatilisation models were analysed, namely: a conventional single-rate model, a two competing-rates model, and an advanced chemical percolation devolatilization (CPD) model, based on structural networks of the coal with a global kinetics mechanism. Moreover, a new simplified numerical model was developed for Australian black and brown coal and optimised for MILD combustion conditions. The modelling cases are validated with the experimental results of Australian brown and black coal MILD combustion in a self-recuperative furnace. From the comparison, the advanced CPD devolatilization model with a three-step global kinetic mechanism gives, as expected, the best agreement (e.g., within 3% of temperature, 7.8% of CO, 5.3% of NO, 2.5%

of $CO_2$) with the experimental measurements for the brown coal case, while all the models tested provide similar results for the black coal case.

The numerical investigation was also carried out to advance our understanding of $NO_x$ formation and destruction mechanisms of these combustion cases. The results reveal that the sum of contributions from the thermal-NO and prompt-NO routes account for less than 3.8% to the total NO emissions, whilst the fuel-NO route dominates the NO emissions with more than 96% of the total NO is produced through this route. It is also found that the total of the NO emissions is reduced by up to 47% in the case of brown coal case and up to 39% in the case of black coal, via the reburning mechanism.

The effects of heterogeneous reactions on the char burnout rate for pulverised coal MILD combustion are also tested in this study. The calculated results reveal that only ≈ 39% of the total carbon was consumed for black coal and the rest is not combusted, which points to incomplete char burnout of black coal combustion, while around ≈ 90% of the total carbon was consumed in the case of brown coal combustion. The overall carbon consumption predictions are in very good agreement with the experimental values, i.e. 38.9% for black coal and 91.7% in the case of brown coal. However, this agreement may be coincidental because a simplified char reaction model alone was used in the present study.

### 7.1.3. Effect of Turbulence

An insulated jet of 19 mm diameter with a hot and diluted co-flow inside an enclosed and insulated vertical furnace, 1200 mm long with a cross-section of

260 × 260 $mm^2$, were also used in this project. Such geometry helped to decouple the surrounding temperature and composition from the fuel jet conditions, and therefore facilitated a systematic study, varying parameters such as jet momentum and turbulence, particle size and carrier gas, and examining their effect on the devolatilisation and burning of pulverised coal. The furnace walls, as well as co-flow temperatures and local oxygen concentrations, are controlled by a secondary swirling burner, using non-premixed natural gas combustion. The coal is carried to the jet exit plane using $CO_2$, which allowed the control of the gaseous flowrate at constant coal particle mass loading.

In Chapter 5, the effect of turbulence on the volatiles' release and reactions under vitiated co-flow conditions, as well as the impact on the pollutants' formation and emissions, are presented for brown coal MILD combustion. Loy-Yang brown coal from the Latrobe Valley, Victoria, Australia, with particle sizes in the range of 53-125 μm, was injected into the furnace, using $CO_2$ as a carrier gas, through an insulated and water-cooled central jet. The bulk jet Reynolds number was varied from $Re_{jet}$ = 5,527 to $Re_{jet}$ = 20,000. The co-flow in the furnace was operated with an $O_2$ concentration of 5.9% (db by volume).

Stable MILD combustion was established for all experimental cases. However, a faint yellowish flame is observed at the middle and in the top part of the furnace in the case of lower jet velocity ($R_{jet}$ = 5,527). The appearance of flames for the lower jet velocity case is related to longer particle residence time, low strain rate, and poor mixing.

CH chemiluminescence ($CH^*$) imaging indicates that the jet turbulence (jet Reynolds number) has a significant impact on the MILD combustion characteristics of pulverised coal. In particular, the $CH^*$ signal intensity is found to be significantly lower at the top part of the furnace, where heterogeneous combustion of char particles occurs. Moreover, no peak intensity of $CH^*$ signal in the middle and top of the furnace is observed for the highest jet velocity case (i.e., $R_{jet}$ = 20,000), which suggests the presence of a homogeneous combustion reactions for a higher level of turbulence.

The largest CO concentrations are measured for the highest jet velocity (i.e., $R_{jet}$ = 20,000) case, which implies that with increasing turbulence there is a better mixing and a broad devolatilisation zone is formed which produces more CO. The measured NO emissions for any case was less than 125 ppmv (db at 3% $O_2$), which provides evidence of the potential benefits of MILD combustion applications of Victorian brown coal towards reducing NO emissions.

Complementary CFD modelling helped in shedding light on the flow field, turbulence intensity, volatiles' release rate, combustion of volatile matters, and overall carbon consumption inside the furnace for the three cases. It was found that increasing the jet Reynolds number increases the volatiles' release rates and decreases the rate of overall carbon consumption. This predominantly depends on better mixing of fuel jet stream with surrounding vitiated co-flow gases; however it is independent of the particles' residence time.

### 7.1.4. Effect of Particle Size

To probe the effect of particle size on the MILD combustion characteristics of pulverised brown coal, a combined experimental and numerical investigation has been conducted (details are reported in Chapter 6). The specific investigation focused on the devolatilisation and volatiles combustion from the different sized coal particles with a vitiated co-flow and its impact on the formation and emission of CO, $CO_2$, and $NO_x$. Highly volatile Victorian brown coal with particle sizes in the range of 53-125 μm and 250-355 μm is injected into the furnace using $CO_2$ as a carrier gas. In addition, this work investigates the particle size impact on the NO formation/destruction, along with volatile combustion rates and heterogeneous reactions on char burnout.

Stable MILD combustion is established with a similar large recirculation vortex around the centre of the furnace for both particle cases. Devolatilisation starts earlier for the smaller particles and is completed at the end of the recirculation vortex, while for the larger particles, the devolatilisation happened at positions downstream of the recirculation vortex. The difference is related to the particle dispersion within the jet and differences in Stokes number. The particle flow path and the difference in residence time had an influence on char burn-out and emission levels. The formation/destruction of NO is measured to be subtly varied by the combination of the physical and chemical nature of the MILD combustion characteristics related to both particle sizes. The measured NO emissions of the larger particles are 15% higher than that of the smaller particles. The model calculated about 95.5% of the total NO is produced via the fuel-NO route. A strong NO-reburning mechanism is

found in both cases, where ≈ 55% of total NO is reduced in the case of small particles and ≈ 39% of total NO is reduced in the case of large particles.

## 7.2. Conclusions

This thesis has deepened the understanding of MILD combustion of pulverised fuels through a set of numerical and experimental investigations using both a self-recuperative laboratory-scale furnace and a vertical furnace with a vitiated co-flow arrangement. The key findings from these investigations are as follows:

1. A semi-uniform temperature distribution inside a self-recuperative laboratory-scale MILD combustion furnace was achieved with no visible flame for all experimental cases using low rank Kingston brown coal and high rank Bowen basin black coal, carried by either $CO_2$ or $N_2$ and without any external air preheating. Computed and measured temperature results indicate that a large recirculation zone, similar to gaseous fuel MILD combustion, is established halfway along the furnace, suggesting there is a rapid devolatilisation of the pulverised fuels in the self-recuperative furnace.

2. No major difference was found regarding chemical species formation and pollutant emissions when varying the carrier gas; while the variations in the coal types changed the results significantly. It was found that for brown coal, the exhaust NO emissions dropped to 37% of that measured for black coal at a constant equivalence ratio of $\Phi = 0.88$ and same heat input.

3. A high level of unburnt carbon (more than 50%) was found at the furnace outlet for the black coal combustion cases, which highlights the insufficient residence time of the black coal particles in the small recuperative furnace. The measured level of CO emissions from brown coal was around ten times higher than that for black coal cases. The higher CO emissions are related to the more substantial char burnout of brown coal, which is confirmed by the carbon content analysis of the ash.

4. The numerical investigation of coal MILD combustion using a parallel jet self-recuperative MILD combustion furnace is conducted to probe the impact of devolatilisation models on the prediction accuracy of pulverised coal combustion. In addition, the study analysed the effect of increasing the air jet momentum on furnace dynamics and global emissions for the present furnace. The study also advances the understanding of $NO_x$ formation and destruction mechanisms, flow-field characteristics, and the effect of heterogeneous reactions on char burnout. The results reveal that the CPD devolatilisation model better replicates the temperature and species concentrations, in comparison with the simplified models tested in this study, for brown coal. Meanwhile, the single-rate, two-competing rates, and the CPD model show similar accuracy in reproducing the experimental data for black coal. It is worth noting that all the models fail to predict the rate of devolatilisation and reaction close to the jet exit.

5. The modelling results indicate that the NO emissions are predominantly formed by the fuel-NO path, whereas the sum of the contribution of the total NO emissions from the thermal-NO and prompt-NO is less than 3.8% for any of the cases. Moreover, a strong NO reburning reaction exists inside the furnace, which leads to relatively low NO emissions in the exhaust. It is also found that the total NO emission are reduced by up to 47% for brown coal and up to 39% for black coal, via the reburning mechanism.

6. In all the modelling cases, volatiles are released from the fuel jet and carried by a strong vortex induced by the air jets in a manner not dissimilar to gaseous MILD combustion in this furnace. The most significant impact of increasing the air jet momentum, either by raising the temperature or by raising the mass flow rate, is an increased air jet penetration distance. This facilitates the reaction of the volatiles with vitiated mixtures and leads to volumetric reaction zones.

7. The effect of turbulence on the volatiles' release and the interaction of the volatiles with the vitiated co-flow and its impact on the formation and emission of soot, $NO_x$ and other pollutants of pulverised brown coal have been investigated using a vertical MILD combustion furnace. Stable MILD combustion was established for all experimental cases with no visible flame. Increasing the jet Reynolds number increases the volatiles' release rates and leads to the establishment of a recirculation zone that contributes to the establishment of the volumetric reaction zone. This mostly depends on the

better level of mixing, however it is independent of the particles' residence time.

8. The particles' residence time significantly affects the overall carbon consumption rate. The comparatively longer residence time for the lower jet velocity ($R_{jet}$ = 5,527) case is accountable for a higher rate of carbon consumption.

9. Minor differences associated with the carrier gas velocities are found on furnace temperatures and $NO_x$ formation, whilst a major difference is found regarding CO production. It is worth noting that low NO emissions (not more than 125 ppmv db at 3% $O_2$) were measured at the furnace outlet for all of the investigated cases, providing strong evidence of the potential benefits of MILD combustion applications in terms of Victorian brown coal.

10. The impact of particle size on the MILD combustion characteristics of pulverised brown coal was investigated through a combined experimental and numerical investigation. No visible flame is found in the furnace for any particle sizes. However, higher luminosity and interior furnace radiation are observed for the small particles, rather than the large particles. The small particles' case produces a higher furnace temperature than the large particle case. The high temperature production is influenced by more intense volatile combustion of the smaller particles. More importantly, the increasing Stokes

number of the larger particles has a negative impact on any mixing with the hot vitiated co-flow, as well as on the volatile release rate and reactions and consequently decreases the combustion temperature.

11. The NO formation rate is measured to be considerably higher for smaller particles than for bigger particles. The small size particles release volatiles earlier and combustion is also initiated early. As a consequence, the NO production is high. On the other hand, the large particles take a longer time to dissociate for volatile evolution and volatile combustion takes a longer combustion time to initiate. While the CO emission for the large particles is substantially, around 52%, lower than for the small particles. This indicates that the volatiles' release rate is significantly lower for the large particles in comparison with the small particles.

12. The numerical models predict similar flow path-lines in the furnace for both small and large particles. The flow pattern inside the furnace is dominated by the carrier gas injection velocity rather than the coal particle size. The smaller particles are circulated and mixed with the hot vitiated co-flow following the flow pattern, while the larger particles did not follow the flow path-line. The modelling results reveal that NO formation through the fuel-NO route is significantly higher for the small particles than the large particles. However, it is calculated that for the small particles' case a reduction of ≈55% in the total NO while for the large particles' case a decrease of ≈39% in the total NO

through the NO-reburning mechanism. As a consequence, the overall NO emission is measured as being higher at the furnace exit for the large particles.

## 7.3. Recommendations for Future Work

The present research demonstrates significant progress towards a fundamental understanding of MILD combustion of solid fuels. As always, some issues remain and either warrant future investigation or further improvement. The following recommendations are made to advance this field beyond this thesis:

1. To apply advanced non-intrusive laser based techniques for simultaneous imaging of temperature and key species (viz. formaldehyde ($CH_2O$) and hydroxyl radical (OH)) for investigating the impact of turbulence, surrounding composition and temperature on the interaction of volatiles released from pulverised solid fuels. Those data will provide valuable information on the structure of the reaction zone under MILD combustion conditions. In particular, the temporally and spatially resolved data will lead to breakthroughs in model development and validation and accelerate the adoption of new technology. Worth noting is that the newly designed and built vertical MILD combustion furnace has optical access to allow for laser diagnostic techniques.

2. Collecting and analysing ash from the furnace exit for different experimental conditions will help to understand either unburnt char contents or the carbon consumption of the MILD combustion of pulverised fuel. In addition, that

information will improve the data base for the validation of CFD simulation results.

3. Extending this work to biomass fuels under MILD combustion conditions will also be desirable. It will be worthwhile to utilise different types of biomass fuels, in particular, grape marc and almond husk, as both are readily available in Australia and currently used as a waste material for landfill.

4. It would be interesting to conduct a further study with a combination of MILD combustion technology and oxy-fuel combustion technology for pulverised solid fuels. In particular, a comprehensive study is required to predict optimum $CO_2/O_2$ ratios for high volatile coal combustion, in order to establish stable MILD-oxy combustion.

5. The improvement of CFD modelling is required to better replicate the experimental data for pulverised fuel combustion under MILD mode. In particular, further study is recommended with more elaborated char reaction models, considering the complex deactivation mechanisms during char combustion in order to highlight the effect of heterogeneous reactions on char oxidation.